Theoretical Astroparticle Physics

Contents

1. Topics

- Electron-positron plasma
  - Relativistic degeneracy in nonequilibrium electron-positron plasma
- Thermal emission from relativistic plasma and GRBs
  - Thermal emission in early afterglow from the GRB-SNR interaction
- Ultra high energy particles
  - Cosmic absorption of ultra high energy particles
  - Interaction of high energy photons with the background radiation in the Universe
- Neutrinos in cosmology
- Self-gravitating systems of Dark Matter particles
  - A regular and relativistic Einstein cluster within the S2 orbit centered in SgrA*
  - Semidegenerate self-gravitating system of fermion as Dark Matter on galaxies I: Universality laws
  - On the core-halo distribution of dark matter in galaxies
  - Dark matter massive fermions and Einasto profiles in galactic halos

2. Participants

2.1. ICRANet participants

- Carlo Luciano Bianco
- Jorge Rueda
- Remo Ruffini
- Gregory Vereshchagin
- She-Sheng Xue

2.2. Past collaborators

- Marco Valerio Arbolino (DUNE s.r.l., Italy)
- Andrea Bianconi (INFN Pavia, Italy)
- Neta A. Bahcall (Princeton University, USA)
- Damien Begue (KTH, Sweden)
- Alberto Benedetti (Max Planck Institute for Nuclear Physics, Heidelberg)
- Micol Benetti (Observatório Nacional, Rio de Janeiro, Brazil)
- Daniella Calzetti (University of Massachusets, USA)
- Valeri Chechetkin (Keldysh Institute, Russia)
- Gustavo de Barros (former IRAP PhD, Brazil)
- Jaan Einasto (Tartu Observatory, Estonia)

- Roberto Fabbri (University of Firenze, Italy)
- Long-Long Feng (University of Science and Technology of China, China)
- Jiang Gong Gao (Xinjiang Institute of Technology, China)
- Andrea Geralico (ICRA, Rome, Italy)
- Mauro Giavalisco (University of Massachusets, USA)
- Gabriele Ingrosso (INFN, University of Lecce, Italy)
- Yi-peng Jing (Shanghai Astronomical Observatory, China)
- Wien Biao Han (Shanghai Astronomical Observatory, Chinese Academy of Science, China)
- Massimiliano Lattanzi (University of Ferrara, Italy)
- Hyung-Won Lee (Inje University, South Korea)
- Nikolaos Mavromatos (King's College London, University of London, UK)
- Alessandro Melchiorri (Univ. "Sapienza" di Roma, Italy)
- Marco Merafina (University of Rome "Sapienza", Italy)
- Houjun Mo (University of Massachusetts, USA)
- Enn Saar (Tartu Observatory, Estonia)
- Jay D. Salmonson (Livermore Lab, USA)
- Luis Alberto Sanchez (National University Medellin, Colombia)
- Costantino Sigismondi (ICRA and University of Rome "La Sapienza", Italy)
- Doo Jong Song (Korea Astronomy Observatory, South Korea)
- Luigi Stella (Astronomical Observatory of Rome, Italy)

- William Stoeger (Vatican Observatory, University of Arizona USA)
- Sergio Taraglio (ENEA, Italy)
- Gerda Wiedenmann (MPE Garching, Germany)
- Jim Wilson (Livermore Lab, USA)
- Urbano França (Instituto de Física Corpuscular, Valencia, Spain)
- Julien Lesgourgues (CERN, Theory Division, Geneva, Switzerland)
- Lidia Pieri (Institute d'Astrophysique, Paris, France)
- Sergio Pastor (Instituto de Física Corpuscolar, Valencia, Spain)
- Joseph Silk (Oxford University, UK)
- Roustam Zalaletdinov (Tashkent University, Uzbekistan)

2.3. Ongoing collaborations

- Carlos Arguelles (ICRANet, Pescara, Italy)
- Alexey Aksenov (ICAD, RAS, Russia)
- Bernardo Fraga (ICRANet, Rome, Italy)
- Ivan Siutsou (ICRANet-Rio, Brazil)
- Wang Yu (ICRANet, Pescara, Italy)

3. Brief description

Astroparticle physics is a new field of research emerging at the intersection of particle physics, astrophysics and cosmology. Theoretical development in these fields is mainly triggered by the growing amount of experimental data of unprecedented accuracy, coming both from the ground based laboratories and from the dedicated space missions.

3.1. Electron-positron plasma

Electron-positron plasma is of interest in many fields of physics and astrophysics, e.g. in the early universe, active galactic nuclei, the center of our Galaxy, compact astrophysical objects such as hypothetical quark stars, neutron stars and gamma-ray bursts sources. It is also relevant for the physics of ultraintense lasers and thermonuclear reactions. We study physical properties of dense and hot electron-positron plasmas. In particular, we are interested in the issues of its creation and relaxation, its kinetic properties and hydrodynamic description, baryon loading and radiation from such plasmas.

Two different states exist for electron-positron plasma: optically thin and optically thick. Optically thin pair plasma may exist in active galactic nuclei and in X-ray binaries. The theory of relativistic optically thin nonmagnetic plasma and especially its equilibrium configurations was established in the 80s by Svensson, Lightman, Gould and others. It was shown that relaxation of the plasma to some equilibrium state is determined by a dominant reaction, e.g. Compton scattering or bremsstrahlung.

Developments in the theory of gamma ray bursts from one side, and observational data from the other side, unambiguously point out on existence of optically thick pair dominated non-steady phase in the beginning of formation of GRBs. The spectrum of radiation from optically thick plasma is usually assumed to be thermal.

These months we have been focusing on effects of relativistic degeneracy. In doing so we have generalized the numerical schemes for solution of Boltzmann equations for pairs and photons, used in previous works. As the outcome, we have developed a computer code which has been extensively tested. All two-particle interactions are taken into account. From three-particle interactions the double Compton process is tested.

Then, in a broader context, we consider the appearance of thermal emission from relativistic plasma, focusing on several topics. In what follows all this work is discussed in details, while in Appendix all relevant papers can be found.

3.1.1. Relativistic degeneracy in the pair plasma

It is well known that at relativistic temperatures plasma becomes degenerate Landau and Lifshitz (1980). In order to study relativistic degeneracy we have introduced the Bose enhancement and Pauli blocking factors in the Boltzmann equation that allows us to follow the relaxation of the pair plasma to Planck spectrum of photons and Fermi-Dirac distribution of electrons and positrons. This improvement allows us to study higher energy densities with respect to those treated before in Aksenov et al. (2007, 2009). However, for such high energy densities the assumption adopted in these works, namely that three-particle interactions operate on longer timescale with respect to two-particle ones, does not hold any longer. For this reason we had to introduce the collisional integrals for three-particle interactions based on the exact QED matrix elements, in full analogy with previously treated two-particle interactions.

Thus in this work we consider relaxation of nonequilibrium optically thick pair plasma to complete thermal equilibrium by integrating numerically relativistic Boltzmann equations with collisional integrals computed from the first principles, namely from the QED matrix elements both for two-particle and three-particle interactions.

We point out that unlike classical Boltzmann equation for binary interactions such as scattering, more general interactions are typically described by four collisional integrals for each particle that appears both among incoming and outgoing particles.

Our numerical results indicate that the rates of three-particle interactions become comparable to those of two-particle ones for temperatures exceeding the electron rest-mass energy. Thus three particle interactions such as relativistic bremsstrahlung, double Compton scattering and radiative pair creation become essential not only for establishment of thermal equilibrium, but also for correct evaluation of interaction rates, energy losses etc. Our results on this topic are reported in Appendix A.

3.2. Thermal emission from relativistic plasma and GRBs

Emission from optically thick stationary plasma is an important topic in astrophysics. Such plasma confined by the gravitational field constitutes stars, accretion disks and other objects. The light from these systems is coming from the so called photosphere defined as a region where the optical depth computed from the interior of the optically thick plasma outwards reaches unity.

There are also dynamical sources where bulk velocities of plasma reach ultrarelativistic values such as microquasars, active galactic nuclei and gamma-ray bursts (GRBs). While in the former two objects there is clear evidence for jets which contain optically thin plasma, in the latter objects the issue of jets is controversial, and the source is required to be optically thick. This observational fact poses a new problem: the emission from (spherically) expanding plasma which initially is optically thick. Such plasma eventually becomes optically thin during its expansion, and initially trapped photons should be released.

Recently, thermal components were found in spectra of GRBs not only in the prompt emission, but also in the early afterglow. This motivated us to extend the study of thermal emission previously focused on ultrarelativistic photosphere into a more broad context of thermal emission from relativistic plasma in GRBs.

3.2.1. Thermal emission in early afterglow from the GRB-SNR interaction

The interaction between the GRB ejecta and a baryonic shell is considered in the context of the binary driven hypernova model of GRBs. The kinematic and observational properties of the shell after the interaction are derived. In particular, the temperature and the duration of the thermal emission are obtained. The model is then applied to GRB 090618 and other sources, and the observed characteristics of the thermal component are reproduced. For details see Appendix B.

3.3. Relativistic kinetic theory and its applications

We pay particular attention to presenting our results in relativistic kinetic theory in a systematic and pedagogic manner. This approach resulted in a lecture course created by G.V. Vereshchagin for the students of the IRAP PhD Erasmus Mundus Joint Doctorate program. This lecture course was also delivered at the XV Brazilian School of Cosmology and Gravitation in Mangaratiba, Brazil in 2012. The lecture notes are published in Cambridge Scientific Publishers this year and are presented in Appendix C.

3.4. Ultra high energy particles

This year we started a new research field on propagation of ultra high energy particles on cosmological distances. We consider cosmic limits on the propagation distance, or *cosmic horizon* due to interactions of such particles with known cosmological backgrounds, such as cosmic microwave background of photons, extragalactic background light, and cosmic neutrino background. We examine the mean free path and mean energy losss distances due to various interactions such as Breit-Wheeler process, photon-photon scattering, photopion process, Bethe-Heitler process, neutrino-neutrino scattering etc.

3.4.1. Cosmic absorption of ultra high energy particles

This work summarizes the limits on propagation of ultra high energy particles in the Universe, set up by their interactions with cosmic background of photons and neutrinos. By taking into account cosmic evolution of these backgrounds and considering appropriate interactions we derive the mean free path for ultra high energy photons, protons and neutrinos. For photons the relevant processes are the Breit-Wheeler process as well as the double pair production process. For protons the relevant reactions are the photopion production and the Bethe-Heitler process. We discuss the interplay between the energy loss length and mean free path for the Bethe-Heitler process. Neutrino opacity is determined by its scattering off the cosmic background neutrino.

We compute for the first time the high energy neutrino horizon as a function of its energy. For details see Appendix D.

3.4.2. Interaction of high energy photons with the background radiation in the Universe

We compare and contrast cosmic limits on propagation of very high energy photons set by their interactions with cosmic microwave background and extragalactic background light with data on very high energy photons detected from gamma-ray bursts and blazars. We calculate the optical depth due to the Breit-Wheeler pair creation and Euler-Heisenberg photon-photon scattering, taking into account cosmic evolution of the background photons, as well as particle energy redshift. We confirm, that pair production at TeV energy and higher impose dominant constraint on transparency of high energy cosmic photons and the photon-photon scattering at energy less than 1 TeV impose almost the same constrain as Breit-Wheeler on transparency of high energy cosmic photons. For details see Appendix E.

3.5. Neutrinos in cosmology

Many observational facts make it clear that luminous matter alone cannot account for the whole matter content of the Universe. Among them there is the cosmic background radiation anisotropy spectrum, that is well fitted by a cosmological model in which just a small fraction of the total density is supported by baryons.

In particular, the best fit to the observed spectrum is given by a flat ΛCDM model, namely a model in which the main contribution to the energy density of the Universe comes from vacuum energy and cold dark matter. This result is confirmed by other observational data, like the power spectrum of large scale structures.

Another strong evidence for the presence of dark matter is given by the rotation curves of galaxies. In fact, if we assume a spherical or ellipsoidal mass distribution inside the galaxy, the orbital velocity at a radius r is given by Newton's equation of motion. The peculiar velocity of stars beyond the visible edge of the galaxy should then decrease as $1/r$. What is instead observed is that the velocity stays nearly constant with r. This requires a halo of invisible, dark, matter to be present outside the edge. Galactic size should then be extended beyond the visible edge. From observations is follows that the halo radius is at least 10 times larger than the radius of visible part of the galaxy. Then it follows that a halo is at least 10 times more massive than all stars in a galaxy.

Neutrinos were considered as the best candidate for dark matter about twenty years ago. Indeed, it was shown that if these particles have a small mass $m_\nu \sim 30\,\mathrm{eV}$, they provide a large energy density contribution up to critical density. Tremaine and Gunn (1979) have claimed, however, that massive neutrinos cannot be considered as dark matter. Their paper was very influential and turned most of cosmologists away from neutrinos as cosmologically important particles.

Tremaine and Gunn paper was based on estimation of lower and upper bounds for neutrino mass; when contradiction with these bounds was found, the conclusion was made that neutrinos cannot supply dark matter. The upper bound was given by cosmological considerations, but compared with the energy density of clustered matter. It is possible, however, that a fraction of neutrinos lays outside galaxies.

Moreover, their lower bound was found on the basis of considerations of galactic halos and derived on the ground of the classical Maxwell-Boltzmann statistics. Gao and Ruffini (1980) established a lower limit on the neutrino mass by the assumption that galactic halos are composed by degenerate neutrinos. Subsequent development of their approach Arbolino and Ruffini (1988) has shown that contradiction with two limits can be avoided.

At the same time, in 1977 the paper by Lee and Weinberg (1977) appeared, in which authors turned their attention to massive neutrinos with $m_\nu >> 2\,\mathrm{GeV}$. Such particles could also provide a large contribution into the energy density of the Universe, in spite of much smaller value of number density.

Recent experimental results from laboratory (see Dolgov (2002) for a review) rule out massive neutrinos with $m_\nu > 2\,\mathrm{GeV}$. However, the paper by Lee and Weinberg was among the first where very massive particles were considered as candidates for dark matter. This can be considered as the first of cold dark matter models.

Today the interest toward neutrinos as a candidate for dark matter came down, since from one side, the laboratory limit on its mass do not allow for significant contribution to the density of the Universe, and from other side, conventional neutrino dominated models have problems with formation of structure on small scales. However, in these scenarios the role of the chemical potential of neutrinos was overlooked, while it could help solving both problems.

3.5.1. Massive neutrino and structure formation

Lattanzi et al. (2003) have studied the possible role of massive neutrinos in the large scale structure formation. Although now it is clear, that massive light neutrinos cannot be the dominant part of the dark matter, their influence on the large scale structure formation should not be underestimated. In particular, large lepton asymmetry, still allowed by observations, can affect cosmological constraints on neutrino mass.

3.5.2. Cellular structure of the Universe

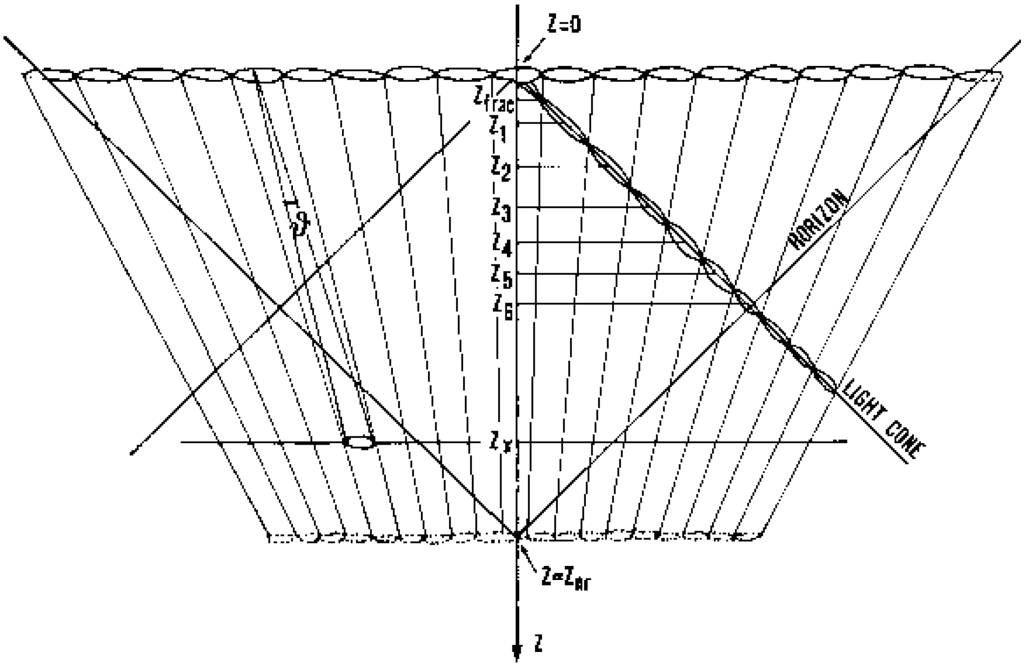

Figure 3.1.: Cellular structure of the Universe.

One of the interesting possibilities, from a conceptual point of view, is the change from the description of the physical properties by a continuous function, to a new picture by introducing a self-similar fractal structure. This approach has been relevant, since the concept of homogeneity and isotropy formerly apply to any geometrical point in space and leads to the concept of a Universe observer-homogeneous (Ruffini (1989)). Calzetti et al. (1987), Giavalisco (1992), Calzetti et al. (1988) have defined the correlation length of a fractal

$$r_0 = \left(1 - \frac{\gamma}{3}\right)^{1/\gamma} R_S, \tag{3.5.1}$$

where R_S is the sample size, $\gamma = 3 - D$, and D is the Hausdorff dimension of the fractal. Most challenging was the merging of the concepts of fractal, Jeans mass of dark matter and the cellular structure in the Universe, advanced by Ruffini et al. (1988). The cellular structure emerging from this study is represented in Figure 3.1. There the upper cutoff in the fractal structure $R_{\rm cutoff} \approx 100$ Mpc, was associated to the Jeans mass of the "ino" $M_{\rm cell} = \left(\frac{m_{pl}}{m_{ino}}\right)^2 m_{pl}$.

3.5.3. Lepton asymmetry of the Universe

Lattanzi et al. (2005), Lattanzi et al. (2006) studied how the cosmological constraints on neutrino mass are affected by the presence of a lepton asymmetry. The main conclusion is that while constraints on neutrino mass do not change by the inclusion into the cosmological model the dimensional chemical potential of neutrino, as an additional parameter, the value of lepton asymmetry allowed by the present cosmological data is surprisingly large, being

$$L = \sum_\nu \frac{n_\nu - n_{\bar\nu}}{n_\gamma} \lesssim 0.9. \tag{3.5.2}$$

Therefore, large lepton asymmetry is not ruled out by the current cosmological data.

3.6. Self-gravitating systems of Dark Matter particles

A general study of Dark Matter (DM) within the particle DM paradigm requires the interconnection between particle Physics (Standard Model (SM) and beyond SM Physics), together with a fully general relativistic treatment.

The study of the Physics must be always guided by the many different known astrophysical scenarios where DM plays certainly a role, i.e.: the interaction nature within the primordial plasma in the early universe, leptogenesis, baryogenesis, the large structure of the Universe, structure formation, gravitational lensing in clusters of galaxies, galaxy rotation curves and the overall galaxy density profiles. The current attention of research within our group is focused in the Physics and astrophysics of DM particles in the early Universe, its effects in the mass and neutrino species number constraints, and mainly, the role of DM in galaxies at all scales.

The study of all these issues are in part a natural continuation of the pioneering works developed in the past by former members of the ICRA group and collaborators, all headed by the director of the institute, Prof. R. Ruffini (see Ruffini et al. (1983, 1988); Ruffini and Stella (1983); Arbolino and Ruffini (1988); Merafina and Ruffini (1989); Gao et al. (1990); Ingrosso et al. (1992); Bisnovatyj-Kogan et al. (1993); Bisnovatyi-Kogan et al. (1998)).

The nature of the DM particle interactions for the recently proposed sterile neutrino in the context of the so called neutrino Minimal Standard Model (νMSM, see Boyarsky et al. (2009b) and references therein), in compatibility with the early cosmology and further constrained with data coming form the center of the galaxies, is being studied by the Ph.D student C. R. Argüelles under the tutorship of the Prof. J. A. Rueda and Prof. R. Ruffini, in collaboration with N. Mavromatos. Some correlated aspects of the role of sterile ν in the early Universe, as neutrino species number constraints is currently being studied by the Ph.D student B. Fraga, guided by the professors J. A. Rueda and Prof. R. Ruffini.

The actual main topic of research respecting the role of fermionic DM particles in halos as well as in the centers of the galaxies together with its possible interaction regime is studied by the Ph.D students C. R. Argüelles and B. Fraga, with the collaboration of the ICRANet colleagues I. Siutsou, J. A. Rueda, and the external collaboration of the Prof. N. Mavromatos, headed by Prof. R. Ruffini.

Below we present an introduction for each topic of research together with a more detailed description through the links to actual results and ongoing papers.

The problem of the distribution of DM in galaxies as generally studied in the literature, is mainly focused in the halo regions and associated with the galactic rotation curves, where the major amount of data is available. The most common actual mathematical techniques used to deal with this problem are phenomenological fits (See e.g. Burkert (1995)) as well as best fits resulting from numerical N-body simulations centered in the ΛCDM paradigm (See Navarro et al. (1997), Navarro et al. (2004)).

We propose here a new approach for this problem based on the following main assumptions:

1) that the problem of the galactic core and the halo have to be addressed unitarily;

2) for definiteness we study the simplest problem of 'bare' neutrinos in thermodynamic equilibrium fulfilling only the Fermi Dirac statistical distribution

$$f = \frac{1}{\exp\frac{\epsilon-\mu}{kT}+1} = \frac{1}{\exp\left(\frac{\epsilon}{\beta mc^2}-\theta\right)+1}, \tag{3.6.1}$$

where ϵ is kinetic energy of the particles, μ is chemical potential, T is the temperature, k is Boltzmann constant, m is the mass of 'ino', c is the speed of light, $\beta = kT/mc^2$, $\theta = \mu/kT$, without consider either Fermi weak interactions or alternative interactions;

3) we consider zero total angular momentum and also we neglect any effect of Baryonic matter.

The equilibrium configurations of a self-gravitating semi-degenerate system of fermions were first studied in Newtonian gravity by Ruffini and Stella (1983) and then generalized in general relativity by Gao et al. (1990). It is shown that in any such system the density at large radii scales as r^{-2} quite independently of the values of the central density, always providing a flat rotation curve. These solutions were extended to an energy and angular momentum cut-off in the distribution function Ingrosso et al. (1992).

A typical mass density profile solution from the model, contrasted with a Navarro-Frenk-White (NFW) profile Navarro et al. (1997), as well as a Boltzmannian Isothermal sphere model is shown in Fig. 3.2,

It is interesting that the quantum and relativistic treatment of the configurations considered here are characterized by the presence of central cored structures unlike the typical cuspy configurations obtained from a classic non-relativistic approximation, such as the ones of numerical N-body simulations in Navarro et al. (1997). This naturally leads to a possible solution to the well-known core-cusp discrepancy de Blok et al. (2001).

We have recently returned to the Gao et. al. work, and propose a completely different way for solving the boundary condition problem for the system of non-linear first order differential equations, in order to fulfill the

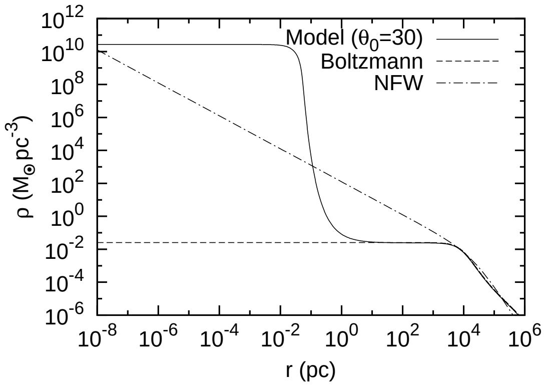

Figure 3.2.: The cored behaviour of the dark matter density profiles from our model is contrasted with the cuspy NFW density profile. The free parameters of the model are fixed as $\beta_0 = 1.251 \times 10^{-7}$, $\theta_0 = 30$ and $m = 10.54\mathrm{keV}/c^2$, while the corresponding free parameters in the NFW formula $\rho_{NFW}(r) = \rho_0 r_0/(r(1+r/r_0)^2)$ are chosen as $\rho_0 = 5 \times 10^{-3} M_\odot \mathrm{pc}^{-3}$ and $r_0 = 25$ Kpc (i.e. typical of spiral galaxies according to de Blok et al. (2008)).

observationally inferred values of typical dark matter halos in spiral galaxies as given in de Blok et al. (2008). Namely, for a given initial condition for the total mass $M(0) = 0$ (consistent with no singularity at the center), arbitrary fixed θ_0 (depending on the chosen central degeneracy), and defining the halo radius r_h at the onset of the flat rotation curve, we solve an eigenvalue problem for the central temperature parameter β_0, until the *observed* halo circular velocity v_h is obtained. After this, we solve a second eigenvalue problem for the particle mass m until the *observed* halo mass M_h is reached at the radius r_h.

The quest has been to use all these information in order to put a novel lower constraints on the mass of the 'ino' in galactic halos by introducing the above mentioned observational properties. This bound is for typical spiral galaxies:

$$m \geq 0.42 keV/c^2. \tag{3.6.2}$$

The novel density profile solutions as well as the rotation curves in agreement with the *observed* halo properties are plotted in Fig. 3.3 for different values of the central degeneracy parameter θ_0 in correspondence with the particle mass m,

Another relevant observational aspect on galactic halos is the so called *Uni-*

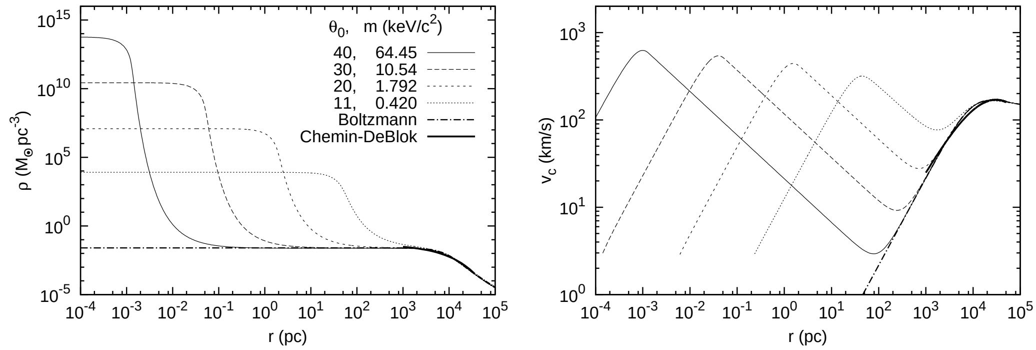

Figure 3.3.: Mass density profiles and rotation curves for specific ino masses m and central degeneracies θ_0 fulfilling the observational constraints $M_h = 1.6 \times 10^{11} M_\odot$ at $r_h = 25$ Kpc. All the quantum configurations have a dark matter halo circular velocity $v_h = 168$ km/s in correspondence with $\beta_0 = 1.251 \times 10^{-7}$. These solutions are contrasted with a Boltzmannian isothermal sphere and the observationally inferred dark matter profile of typical spirals (see Chemin et al. (2011), de Blok et al. (2008)).

versality laws. Donato et al. (2009), fitting DM halos with Burkert profiles, found out that the surface density $\mu_{0D} = r_B \rho_0$ of galaxy dark matter halos, where r_B and ρ_0 are the burkert radius and central halo density, is nearly constant for a wide number of galaxies with different total masses and absolute magnitudes. This further implies a constant acceleration due to DM at the Burkert radius $a_{DM} G M_B / r_B^2 = 3.2 \times 10^{-9}$ cm/s^2. The fact that from our model we obtain scaling formulas for the magnitudes r_B and M_B with respect the free parameters of the model m, β_0 and θ_0, it allow us to show that always exist a definite range of the θ_0 as well as β_0 parameter for a given particle mass above the limit found in (3.6.2), which is in agreement with the observational universal result.

In these months the group was focused on the following issues.

3.6.1. A regular and relativistic Einstein cluster within the S2 orbit centered in SgrA*

In 1939 Einstein provided a model of self-gravitating masses, each moving along geodesic circular orbits under the influence of the gravitational field of the rest of the particle's system. This model allowed him to argue that

'Schwarzschild singularities' do not exist in physical reality because a cluster with a given number of masses cannot be arbitrarily concentrated. And this is due to the fact that otherwise the particles constituting the cluster would reach the speed of light. Of course, actually this model can only be considered as an interesting possibility to try to provide a counterexample of a singularity within gravity Einstein's theory, being nonetheless the Black Holes, a physical reality within the theory of General Relativity.

In this work we first present the theoretical formalism of Einstein Clusters (EC), and secondly we use the model under the special assumption of a constant density distribution to model the central (sub-miliparsec) region of our galaxy, in order to provide an alternative for the SMBH of $M = 4.4 \times 10^6 M_\odot$ thought to be hosted at very center. The matter content will be treated as dark matter, i.e. we assume a dark EC composed by dark matter particles of mass m (regardless of its nature), and therefore no contribution to the pressure in form of radiation is assured as the cluster shrinks till relativistic regimes. We first analyze the stability condition in the specific case of a regular and relativistic energy density EC, contained marginally inside the S2 star peri-center $r_{p(S2)}$ as observed in the literature. Secondly, and for an EC with fixed particle number $\mathcal{N}$, we will explicitly show through the R vs. M relation, and for particle velocities ranging from zero up to the speed of light, up to which point an EC can be contracted before losing its global stability. For details see Appendix F.

3.6.2. Semidegenerate self-gravitating system of fermion as Dark Matter on galaxies I: Universality laws

We compare and contrast the RAR model against an observational and Universal empirical correlation between the surface density of DM halos and their one-halo scale-lengths as observed and recently presented in the literature. Specifically speaking, the so-called 'central' surface density of galaxy DM halos $\Sigma_{0D} = r_0/\rho_{0h}$, where r_0 and ρ_{0h} are the core radius of the halo (or halo-scale-length) and central (halo) density respectively, was found to be roughly a constant independently of the galaxy luminosity. This significant result, involved a sample of several hundreds of rotation curves allowing for mass models in a very wide range of galaxy types from dwarf to elliptical galaxies, and was analyzed under the assumption that each DM halo follows a Burkert profile $\rho_B(r)$. We demonstrate here that the self-gravitating systems of keV fermions (RAR model), when applied to a wide range of galaxies, is able to reproduce the Universality law of constant surface density of DM halos. It is further shown how these Universal laws can be used to put constraints the free parameters (β_0 and θ_0) within a definite range, as well as to provide an approximate correlation between these both free parameters in that range of validity. As a consequence of this phenomenological approach, the range of validity of θ_0 can be used now to study the density behaviour of the central degenerate core regions. When this is done appears the remarkable conclusion that the fulfillment of the DM Universality law, valid for dwarf up to big spirals, is at the same time consistent with dense compact DM objects (below sub-parsec scales) with masses 10^4 and 10^7 $M_\odot$ respectively. For details see Appendix G.

3.6.3. On the core-halo distribution of dark matter in galaxies

Within the realm of non-baryonic DM in the form of collisionless massive fermions, we present a model of self-gravitating and semi-degenerate fermions including relativistic effects, and named as the Ruffini - Arguelles - Rueda (RAR) model. The integration of the system under study will allow to deal with distance-scales well below mpc up to Mpc, being able to segregate different marked physical regimes: a degenerate quantum regime in the central part of the configurations, and a classical Boltzmannian one in the outermost part. We further show the mean features of the equilibrium configurations in terms of the free parameters, and most important, how sensitive is the particle mass when the model is asked to fulfill all the accessible observables at galaxy scales. With the different applications of this model to galaxies, ranging from dwarf to big elliptical, it will be clear the central role of an underlying Fermi-Dirac late-time phase-space density $g/h^3 f(r,p)$ of DM in a virialized halo. It is shown in particular, a natural and novel way to constraint the DM content in the very central part of dwarf spheroidal and spiral galaxies. More interestingly, it is analyzed in some detail up to which extents this central DM content can be interpreted as an alternative to the central BH paradigm, and how, when equilibrium solutions allows for it, the keV fermionic DM particle appears as a natural candidate. For details see Appendix H.

3.6.4. Dark matter massive fermions and Einasto profiles in galactic halos

In 2008, a sample of 34 nearby (closer than 15 Mpc) spiral and irregular galaxies (Sb to Im) were observed with The HI Nearby Galaxy Survey (THINGS). These observations allowed to obtain the highest quality rotation curves available to date due to the high spatial and velocity resolution of THINGS. Then a sub-sample of these rotation curves, corresponding to 19 rotationally dominated and undisturbed galaxies, were combined with information on the distribution of gas and stars to construct mass models for the dark matter component of the sample. After that, using these rotation curves from THINGS, the Einasto dark matter halo mode has been proposed as the standard model for dark matter halos as it provides both cored and cusped distributions for different values of model

parameters when compared with other models of the literature. Here we fit rotation curves of the THINGS sample with the RAR model based on semi-degenerate self-gravitating system of fermions, to further compare and contrast the results of the fitting procedures with different dark matter phenomenological models used in the literature. In particular we compare the best-fitting results with respect to the Navarro–Frenk–White (NFW) 2-parameter model, and with respect to the Einasto 3-parameter model. As it is shown here, the comparison among different models shows that the fermionic structures can present a better fit when contrasted with the rotation curve data of THINGS. More relevant is the fact that the overall fermionic model solutions, in contrast with the other models analyzed here, are associated with important predicting power regarding the innermost dark matter distribution due to the quantum nature of their sub-parsec cores. For details see Appendix I.

4. Publications

4.1. Publications before 2005

1. R. Ruffini, D. J. Song, and L. Stella, "On the statistical distribution of massive fermions and bosons in a Friedmann universe" Astronomy and Astrophysics, Vol. 125, (1983) pp. 265-270.

   The distribution function of massive Fermi and Bose particles in an expanding universe is considered as well as some associated thermodynamic quantities, pressure and energy density. These considerations are then applied to cosmological neutrinos. A new limit is derived for the degeneracy of a cosmological gas of massive neutrinos.

2. R. Ruffini and D. J. Song, "On the Jeans mass of weakly interacting neutral massive leptons", in Gamow cosmology, eds. F. Melchiorri and R. Ruffini, (1986) pp. 370–385.

   The cosmological limits on the abundances and masses of weakly interacting neutral particles are strongly affected by the nonzero chemical potentials of these leptons. For heavy leptons ($m_x > \mathrm{GeV}$), the value of the chemical potential must be much smaller than unity in order not to give very high values of the cosmological density parameter and the mass of heavy leptons, or they will be unstable. The Jeans' mass of weakly interacting neutral particles could give the scale of cosmological structure and the masses of astrophysical objects. For a mass of the order 10 eV, the Jeans' mass could give the scenario of galaxy formation, the supercluster forming first and then the smaller scales, such as clusters and galaxies, could form inside the large supercluster.

3. D. Calzetti, M. Giavalisco, R. Ruffini, J. Einasto, and E. Saar, "The correlation function of galaxies in the direction of the Coma cluster", Astrophysics and Space Science, Vol. 137 (1987) pp. 101-106.

   Data obtained by Einasto et al. (1986) on the amplitude of the correlation function of galaxies in the direction of the Coma cluster are compared with theoretical predictions of a model derived for a self-similar observer-homogeneous structure. The observational samples can be approximated by cones of angular width alpha of about 77 deg. Eliminating sources of large observational error, and by making a specified correction, the observational data are found to agree very well with the theoretical predictions of Calzetti et al. (1987).

4. R. Ruffini, D. J. Song, and S. Taraglio, “The ’ino’ mass and the cellular large-scale structure of the universe”, Astronomy and Astrophysics, Vol. 190, (1988) pp. 1-9.

   Within the theoretical framework of a Gamow cosmology with massive ”inos”, the authors show how the observed correlation functions between galaxies and between clusters of galaxies naturally lead to a ”cellular” structure for the Universe. From the size of the ”elementary cells” they derive constraints on the value of the masses and chemical potentials of the cosmological ”inos”. They outline a procedure to estimate the ”effective” average mass density of the Universe. They also predict the angular size of the inhomogeneities to be expected in the cosmological black body radiation as remnants of this cellular structure. A possible relationship between the model and a fractal structure is indicated.

5. D. Calzetti, M. Giavalisco, and R. Ruffini, “The normalization of the correlation functions for extragalactic structures”, Astronomy and Astrophysics, Vol. 198 (1988), pp. 1-15.

   It is shown that the spatial two-point correlation functions for galaxies, clusters and superclusters depend explicitly on the spatial volume of the statistical sample considered. Rules for the normalization of the correlation functions are given and the traditional classification of galaxies into field galaxies, clusters and superclusters is replaced by the introduction of a single fractal structure, with a lower cut-off at galactic scales. The roles played by random and stochastic fractal components in the galaxy distribution are discussed in detail.

6. M. V. Arbolino and R. Ruffini, “The ratio between the mass of the halo and visible matter in spiral galaxies and limits on the neutrino mass”, Astronomy and Astrophysics, Vol. 192, (1988) pp. 107-116.

   Observed rotation curves for galaxies with values of the visible mass ranging over three orders of magnitude together with considerations involving equilibrium configurations of massive neutrinos, impose constraints on the ratio between the masses of visible and dark halo comporents in spiral galaxies.

Upper and lower limits are derived for the mass of the particles making up the dark matter.

7. A. Bianconi, H. W. Lee, and R. Ruffini, "Limits from cosmological nucleosynthesis on the leptonic numbers of the universe", Astronomy and Astrophysics, Vol. 241 (1991) pp. 343-357.

   Constraints on chemical potentials and masses of 'inos' are calculated using cosmological standard nucleosynthesis processes. It is shown that the electron neutrino chemical potential (ENCP) should not be greater than a value of the order of 1, and that the possible effective chemical potential of the other neutrino species should be about 10 times the ENCP in order not to conflict with observational data. The allowed region (consistent with the He-4 abundance observations) is insensitive to the baryon to proton ratio η, while those imposed by other light elements strongly depend on η.

8. R. Ruffini, J. D. Salmonson, J. R. Wilson, and S.-S. Xue, "On the pair electromagnetic pulse of a black hole with electromagnetic structure", Astronomy and Astrophysics, Vol. 350 (1999) pp. 334-343.

   We study the relativistically expanding electron-positron pair plasma formed by the process of vacuum polarization around an electromagnetic black hole (EMBH). Such processes can occur for EMBH's with mass all the way up to $6 \cdot 10^5 M_\odot$. Beginning with a idealized model of a Reissner-Nordstrom EMBH with charge to mass ratio $\xi = 0.1$, numerical hydrodynamic calculations are made to model the expansion of the pair-electromagnetic pulse (PEM pulse) to the point that the system is transparent to photons. Three idealized special relativistic models have been compared and contrasted with the results of the numerically integrated general relativistic hydrodynamic equations. One of the three models has been validated: a PEM pulse of constant thickness in the laboratory frame is shown to be in excellent agreement with results of the general relativistic hydrodynamic code. It is remarkable that this precise model, starting from the fundamental parameters of the EMBH, leads uniquely to the explicit evaluation of the parameters of the PEM pulse, including the energy spectrum and the astrophysically unprecedented large Lorentz factors (up to $6 \cdot 10^3$ for a 10^3 $M_\odot$ EMBH). The observed photon energy at the peak of the photon spectrum at the moment of photon decoupling is shown to range from 0.1 MeV to 4 MeV as a function of the EMBH mass. Correspondingly the total energy in photons is in the range of 10^{52} to 10^{54} ergs, consistent with observed gamma-ray bursts. In these computations we neglect the presence of baryonic matter which will be the subject of forthcoming publications.

9. R. Ruffini, J. D. Salmonson, J. R. Wilson, and S.-S. Xue, "On the pair-electromagnetic pulse from an electromagnetic black hole surrounded by a baryonic remnant", Astronomy and Astrophysics, Vol. 359 (2000) pp. 855-864.

   The interaction of an expanding Pair-Electromagnetic pulse (PEM pulse) with a shell of baryonic matter surrounding a Black Hole with electromagnetic structure (EMBH) is analyzed for selected values of the baryonic mass at selected distances well outside the dyadosphere of an EMBH. The dyadosphere, the region in which a super critical field exists for the creation of e^+e^- pairs, is here considered in the special case of a Reissner-Nordstrom geometry. The interaction of the PEM pulse with the baryonic matter is described using a simplified model of a slab of constant thickness in the laboratory frame (constant-thickness approximation) as well as performing the integration of the general relativistic hydrodynamical equations. Te validation of the constant-thickness approximation, already presented in a previous paper Ruffini et al. (1999) for a PEM pulse in vacuum, is here generalized to the presence of baryonic matter. It is found that for a baryonic shell of mass-energy less than 1% of the total energy of the dyadosphere, the constant-thickness approximation is in excellent agreement with full general relativistic computations. The approximation breaks down for larger values of the baryonic shell mass, however such cases are of less interest for observed Gamma Ray Bursts (GRBs). On the basis of numerical computations of the slab model for PEM pulses, we describe (i) the properties of relativistic evolution of a PEM pulse colliding with a baryonic shell; (ii) the details of the expected emission energy and observed temperature of the associated GRBs for a given value of the EMBH mass; $10^3 M_\odot$, and for baryonic mass-energies in the range 10^{-8} to 10^{-2} the total energy of the dyadosphere.

10. M. Lattanzi, R. Ruffini, and G. Vereshchagin, "On the possible role of massive neutrinos in cosmological structure formation", in Cosmology and Gravitation, eds. M. Novello and S. E. Perez Bergliaffa, Vol. 668 of AIP Conference Series, (2003) pp. 263–287.

    In addition to the problem of galaxy formation, one of the greatest open questions of cosmology is represented by the existence of an asymmetry between matter and antimatter in the baryonic component of the Universe. We believe that a net lepton number for the three neutrino species can be used to understand this asymmetry. This also implies an asymmetry in the matter-antimatter component of the leptons. The existence of a nonnull lepton number for the neutrinos can easily explain a cosmological abundance of neutrinos consistent with the one needed to explain both the rotation curves of galaxies and the flatness of the Universe. Some propedeutic results are presented in order to attack this problem.

4.2. Publications (2005 – 2014)

1. D. Begue and G.V. Vereshchagin, "Transparency of an instantaneously created electron-positron-photon plasma", MNRAS, Vol. 439 (2014), pp. 924-928.

   The problem of the expansion of a relativistic plasma generated when a large amount of energy is released in a small volume has been considered by many authors. We use the analytical solution of Bisnovatyi-Kogan and Murzina for the spherically symmetric relativistic expansion. The light curves and the spectra from transparency of an electron-positron-photon plasma are obtained. We compare our results with the work of Goodman.

2. I.A. Siutsou and G.V. Vereshchagin, "Relativistic spotlight ", Physics Letters B, Volume 730 (2014), pp. 190â€"192.

   Relativistic motion gives rise to a large number of interesting and sometimes counterintuitive effects. In this work we consider an example of such effects, which we term relativistic spotlight. When an isotropic source of soft photons with proper intensity I_0 is placed at rest between a distant observer and photosphere of relativistic wind, its intensity as seen by the observer gets enhanced up to $\sim \Gamma^4 I_0$, where Γ is bulk Lorentz factor of the wind. In addition, these photons may extract a large part of the wind kinetic energy. We speculate that such effect may be relevant for the physics of GRBs.

3. G.V. Vereshchagin, "Physics of non-dissipative ultrarelativistic photospheres ", International Journal of Modern Physics D Vol. 23, No. 1 (2014) 1430003.

   Recent observations, especially by the Fermi satellite, point out the importance of the thermal component in GRB spectra. This fact revives strong interest in photospheric emission from relativistic outflows. Early studies already suggested that the observed spectrum of photospheric emission from relativistically moving objects differs in shape from the Planck spectrum. However, this component appears to be subdominant in many GRBs and the origin of the dominant component is still unclear. One of the popular ideas is that energy dissipation near the photosphere may produce a nonthermal spectrum and account for such emission. Before considering such models, though, one has to determine precise spectral and timing characteristics of the photospheric emission in the simplest possible case. Hence this paper focuses on various physical effects which make the photospheric emission spectrum different from the black body spectrum and quantifies them.

4. I.A. Siutsou, R. Ruffini and G.V. Vereshchagin, "Spreading of ultrarelativistically expanding shell: an application to GRBs", New Astronomy, Vol. 27 (2014), pp. 30-33.

   Optically thick energy dominated plasma created in the source of Gamma-Ray Bursts (GRBs) expands radially with acceleration and forms a shell with constant width measured in the laboratory frame. When strong Lorentz factor gradients are present within the shell it is supposed to spread at sufficiently large radii. There are two possible mechanisms of spreading: hydrodynamical and thermal ones. We consider both mechanisms evaluating the amount of spreading that occurs during expansion up to the moment when the expanding shell becomes transparent for photons. We compute the hydrodynamical spreading of an ultrarelativistically expanding shell. In the case of thermal spreading we compute the velocity spread as a function of two parameters: comoving temperature and bulk Lorentz factor of relativistic Maxwellian distribution. Based on this result we determine the value of thermal spreading of relativistically expanding shell. We found that thermal spreading is negligible for typical GRB parameters. Instead hydrodynamical spreading appears to be significant, with the shell width reaching $\sim 10^{10}$ cm for total energy $E = 10^{54}$ erg and baryonic loading $B = 10^{-2}$. Within the fireshell model such spreading will result in the duration of Proper Gamma-Ray Bursts up to several seconds.

5. G.V.Vereshchagin, "Relativistic Kinetic Theory with some Applications", in: Cosmology and Gravitation: XVth Brazilian School of Cosmology and Gravitation, eds. Mario Novello and Santiago E.Perez Bergliaffa, Cambridge Scientific Publishers, 2014, pp 1-40.

A brief introduction into relativistic kinetic theory is given. Some applications of this theory in plasma physics, astrophysics and cosmology are reviewed.

6. A. Benedetti, R. Ruffini and G.V. Vereshchagin, "Evolution of the pair plasma generated by a strong electric field", Physics Letters A, Volume 377 (2013), Issue 3-4, p. 206-215.

   We study the process of energy conversion from overcritical electric field into electron-positron-photon plasma. We solve numerically Vlasov-Boltzmann equations for pairs and photons assuming the system to be homogeneous and anisotropic. All the 2-particle QED interactions between pairs and photons are described by collision terms. We evidence several epochs of this energy conversion, each of them associated to a specific physical process. Firstly pair creation occurs, secondly back reaction results in plasma oscillations. Thirdly photons are produced by electron-positron annihilation. Finally particle interactions lead to completely equilibrated thermal electron-positron-photon plasma.

7. D. Begue, I. A. Siutsou and G. V. Vereshchagin, "Monte Carlo simulations of the photospheric emission in GRBs", the Astrophysical Journal Volume 767 (2013), Issue 2, article id. 139.

   We studied the decoupling of photons from ultra-relativistic spherically symmetric outflows expanding with constant velocity by means of Monte Carlo simulations. For outflows with finite widths we confirm the existence of two regimes: photon-thick and photon-thin, introduced recently by Ruffini et al. (RSV). The probability density function of the last scattering of photons is shown to be very different in these two cases. We also obtained spectra as well as light curves. In the photon-thick case, the time-integrated spectrum is much broader than the Planck function and its shape is well described by the fuzzy photosphere approximation introduced by RSV. In the photon-thin case, we confirm the crucial role of photon diffusion, hence the probability density of decoupling has a maximum near the diffusion radius well below the photosphere. The time-integrated spectrum of the photon-thin case has a Band shape that is produced when the outflow is optically thick and its peak is formed at the diffusion radius.

8. R. Ruffni, I. A. Siutsou and G. V. Vereshchagin, "Theory of photospheric emission from relativistic outflows" , the Astrophysical Journal, Vol. 772, Issue 1 (2013) article id. 11.

We derive the optical depth and photospheric radius of relativistic outflow using the model of relativistic wind with finite duration. We also discuss the role of radiative diffusion in such outflow. We solve numerically radiative transfer equation and obtain light curves and observed spectra of photospheric emission. The obtained spectra are nonthermal and in some cases have Band shape.

9. R. Ruffini and G.V. Vereshchagin, "Electron-positron plasma in GRBs and in cosmology", Il Nuovo Cimento C 36 (2013) 255.

   Electron-positron plasma is believed to play imporant role both in the early Universe and in sources of Gamma-Ray Bursts (GRBs). We focus on analogy and difference between physical conditions of electron-positron plasma in the early Universe and in sources of GRBs. We discuss a) dynamical differences, namely thermal acceleration of the outflow in GRB sources vs cosmological deceleration; b) nuclear composition differences as synthesis of light elements in the early Universe and possible destruction of heavy elements in GRB plasma; c) different physical conditions during last scattering of photons by electrons. Only during the acceleration phase of the optically thick electron-positron plasma comoving observer may find it similar to the early Universe. This similarity breaks down during the coasting phase. Reprocessing of nuclear abundances may likely take place in GRB sources. Heavy nuclear elements are then destroyed, resulting mainly in protons with small admixture of helium. Unlike the primordial plasma which recombines to form neutral hydrogen, and emits the Cosmic Microwave Background Radiation, GRB plasma does not cool down enough to recombine.

10. A.G. Aksenov, R. Ruffni and G. V. Vereshchagin, "Comptonization of photons near the photosphere of relativistic outflows", MNRAS Letters, Vol. 436, Issue 1 (2013) pp. L54-L58.

    We consider the formation of photon spectrum at the photosphere of ultra-relativistically expanding outflow. We use the Fokker–Planck approximation to the Boltzmann equation, and obtain the generalized Kompaneets equation which takes into account anisotropic distribution of photons developed near the photosphere. This equation is solved numerically for relativistic steady wind and the observed spectrum is found in agreement with previous studies. We also study the photospheric emission for different temperature dependences on radius in such outflows. In particular, we found that for $T \propto r^{-2}$ the

Band low-energy photon index of the observed spectrum is $\simeq -1$, as typically observed in Gamma-Ray Bursts.

11. R. Ruffini, C. R. Argüelles, B. M. O. Fraga, A. Geralico, H. Quevedo, J. A. Rueda, I. Siutsou, ”Black Holes in Gamma Ray Bursts and Galactic Nuclei”, IJMPD 22 No. 11, 1360008, 2013.

    Current research marks a clear success in identifying the moment of formation of a Black Hole of $10M_{\odot}$, with the emission of a Gamma Ray Burst. This explains in terms of the 'Blackholic Energy' the source of the energy of these astrophysical systems. Their energetics up to 10^{54} erg, make them detectable all over our Universe. Concurrently a new problematic has been arising related to: (a) The evidence of Dark Matter in galactic halos; (b) The origin of the Super Massive Black Holes in active galactic nuclei and Quasars and (c) The purported existence of a Black Hole in the Center of our Galaxy. These three aspects of this new problematic have been traditionally approached independently. We propose an unified approach to all three of them based on a system of massive self-gravitating neutrinos in General Relativity. Perspectives of future research are presented.

12. C. R. Argüelles, I. Siutsou, R. Ruffini, J. A. Rueda, B. Machado, ”On the core-halo constituents of a semi-degenerate gas of massive fermions” AAS, Probes of Dark Matter on Galaxy Scales, 45, 30204, 2013.

    We propose a model of self-gravitating bare fermions at finite temperature in General Relativity to describe the dark matter (DM) in galaxies. We obtain a universal density profile composed by a flat and fully degenerate core for small radii, a low-degenerate plateau and a Newtonian tail that scales with r^{-2} for the outer halo region. The free parameters of the model are fitted using galactic observables such as the constant rotation velocity, mass of the central object and the halo radius, concluding that the particle mass should be in the keV range. We further show that thighter constraints of a few keV for the mass of the fermions are obtained when using typical smallest dwarf galaxies.

13. B. M. O. Fraga, C. R. Argüelles, R. Ruffini, ”Self-Gravitating System of Semidegenerated Fermions as Central Objects and Dark Matter Halos in Galaxies”, IJMPS 23, 357-362, 2013.

    We propose a unified model for dark matter haloes and central galactic objects as a self-gravitating system of semidegenerated fermions in thermal equilibrium. We consider spherical symmetry and then we solve the equations of gravitational equilibrium using the Fermi integrals in a dimensionless manner, obtaining the density profile and velocity curve. We also obtain scaling laws for the observables of the system and show that, for a wide range of our parameters, our model is consistent with the so called universality of the surface density of dark matter.

14. Micol Benetti, S. Pandolfi, M. Lattanzi, M.Martinelli, A. Melchiorri. "Featuring the primordial power spectrum: new constraints on interrupted slow-roll from CMB and LRG data ", Physical Review D (2013) vol. 87, Issue 2, id. 023519

    Using the most recent data from the WMAP, ACT and SPT experiments, we update the constraints on models with oscillatory features in the primordial power spectrum of scalar perturbations. This kind of features can appear in models of inflation where slow-roll is interrupted, like multifield models. We also derive constraints for the case in which, in addition to cosmic microwave observations, we also consider the data on the spectrum of luminous red galaxies from the 7th SDSS catalog, and the SNIa Union Compilation 2 data. We have found that: (i) considering a model with features in the primordial power spectrum increases the agreement with data with the respect of the featureless "vanilla" ΛCDM model by $\Delta\chi^2 \simeq 7$; (ii) the uncertainty on the determination of the standard parameters is not degraded when features are included; (iii) the best fit for the features model locates the step in the primordial spectrum at a scale $k \simeq 0.005$ Mpc^{-1}, corresponding to the scale where the outliers in the WMAP7 data at $\ell = 22$ and $\ell = 40$ are located.; (iv) a distinct, albeit less statistically significant peak is present in the likelihood at smaller scales, with a $\Delta\chi^2 \simeq 3.5$, whose presence might be related to the WMAP7 preference for a negative value of the running of the scalar spectral index parameter; (v) the inclusion of the LRG-7 data do not change significantly the best fit model, but allows to better constrain the amplitude of the oscillations.

15. M. Benetti, M. Gerbino, W. H. Kinney, E. W. Kolb, M. Lattanzi, A. Melchiorri, L. Pagano, A. Riotto. "Cosmological data and indications for new physics", Journal of Cosmology and Astroparticle Physics, 10 (2013) 030.

    Data from the Atacama Cosmology Telescope (ACT) and the South Pole Telescope (SPT), combined with the nine-year data release from the WMAP satellite, provide very precise measurements of the cosmic microwave background (CMB) angular anisotropies down to very small angular scales. Augmented with measurements from Baryonic Acoustic Oscillations surveys and determinations of the Hubble constant, we investigate whether there are indications for new physics beyond a Harrison-Zel'dovich model for primordial perturbations and the standard number of relativistic degrees of freedom at primordial recombination. All combinations of datasets point to physics beyond the minimal Harrison-Zel'dovich model in the form of either a scalar spectral index different from unity or additional relativistic degrees of freedom at recombination (e.g., additional light neutrinos). Beyond that, the extended datasets including either ACT or SPT provide very different indications: while the extended-ACT (eACT) dataset is perfectly consistent with the predictions of standard slow-roll inflation, the extended-SPT (eSPT) dataset prefers a non-power-law scalar spectral index with a very large variation with scale of the spectral index. Both eACT and eSPT favor additional light degrees of freedom. eACT is consistent with zero neutrino masses, while eSPT favors nonzero neutrino masses at more than 95% confidence.

16. M. Benetti. "Updating constraints by Planck data on inlationary features model", Physical Review D 88 (2013) 087302.

    We present new constraints on possible features in the primordial inflationary density perturbations power spectrum in light of the recent Cosmic Microwave Background Anisotropies measurements from the Planck satellite. We found that the Planck data hints for the presence of features in two different ranges of angular scales, corresponding to multipoles $10 < l < 60$ and $150 < l < 300$, with a decrease in the best fit χ^2 value with respect to the featureless "vanilla" LCDM model of $\Delta\chi^2$ around 9 in both cases.

17. B. Patricelli, M.G. Bernardini, C.L. Bianco, L. Caito, G. de Barros, L. Izzo, R. Ruffini and G.V. Vereshchagin, "Analysis of GRB 080319B and GRB 050904 within the Fireshell Model: Evidence for a Broader Spectral Energy Distribution", The Astrophysical Journal, Volume 756, Issue 1, article id. 16 (2012).

    The observation of GRB 080319B, with an isotropic energy $E_{iso}= 1.32 \cdot 10^{54}$ erg, and GRB 050904, with $E_{iso}= 1.04 \cdot 10^{54}$ erg, offers the possibility of studying the spectral properties of the prompt radiation of two of the most energetic gamma-ray bursts (GRBs). This allows us to probe the validity of the fireshell model for GRBs beyond 10^{54} erg, well outside the energy range where it has been successfully tested up to now (10^{49}-10^{53}erg). We find that in the low-energy region, the prompt emission spectra observed by Swift Burst Alert

Telescope (BAT) reveals more power than theoretically predicted. The opportunities offered by these observations to improve the fireshell model are outlined in this paper. One of the distinguishing features of the fireshell model is that it relates the observed GRB spectra to the spectrum in the comoving frame of the fireshell. Originally, a fully radiative condition and a comoving thermal spectrum were adopted. An additional power law in the comoving thermal spectrum is required due to the discrepancy of the theoretical and observed light curves and spectra in the fireshell model for GRBs 080319B and 050904. A new phenomenological parameter α is correspondingly introduced in the model. We perform numerical simulations of the prompt emission in the Swift BAT bandpass by assuming different values of within the fireshell model. We compare them with the GRB 080319B and GRB 050904 observed time-resolved spectra, as well as with their time-integrated spectra and light curves. Although GRB 080319B and GRB 050904 are at very different redshifts ($z = 0.937$ and $z = 6.29$, respectively), a value of $\alpha = -1.8$ for both of them leads to a good agreement between the numerical simulations and the observed BAT light curves, time-resolved and time-integrated spectra. Such a modified spectrum is also consistent with the observations of previously analyzed less energetic GRBs and reasons for this additional agreement are given. Perspectives for future low-energy missions are outlined.

18. A.G. Aksenov, R. Ruffni, I. A. Siutsou and G. V. Vereshchagin, "Dynamics and emission of mildly relativistic plasma", International Journal of Modern Physics: Conference Series, Vol. 12, Issue 01, (2012) pp. 1-9.

    Initially optically thick (with $\tau = 3 \cdot 10^7$) spherically symmetric outflow consisting of electron-positron pairs and photons is considered. We do not assume thermal equilibrium, and include the two-body processes that occur in such plasma: Moller and Bhaba scattering of pairs, Compton scattering, two-photon pair annihilation, two-photon pair production, together with their radiative three-body variants: bremsstrahlung, double Compton scattering, and three-photon pair annihilation, with their inverse processes. We solve numerically the relativistic Boltzmann equations in spherically symmetric case for distribution functions of pairs and photons. Three epochs are considered in details: a) the thermalization, which brings initially nonequilibrium plasma to thermal equilibrium; b) the self-accelerated expansion, which we find in agreement with previous hydrodynamic studies and c) decoupling of photons from the expanding electron-positron plasma. Photon spectra are computed, and appear to be non thermal near the peak of the luminosity. In particular, the low energy part of the spectrum contain more power with respect to the black body one.

19. A. Benedetti, W.-B. Han, R. Ruffini and G.V. Vereshchagin, "On the frequency of oscillations in the pair plasma generated by a strong electric field", Physics Letters B, Vol. 698 (2011) 75-79.

    We study the frequency of the plasma oscillations of electron-positron pairs created by the vacuum polarization in a uniform electric field with strength E in the range $0.2E_c < E < 10E_c$. Following the approach adopted in Ruffini et al. (2007) we work out one second order ordinary differential equation for a variable related to the velocity from which we can recover the classical plasma oscillation equation when E→0. Thereby, we focus our attention on its evolution in time studying how this oscillation frequency approaches the plasma frequency. The time-scale needed to approach to the plasma frequency and the power spectrum of these oscillations are computed. The characteristic frequency of the power spectrum is determined uniquely from the initial value of the electric field strength. The effects of plasma degeneracy and pair annihilation are discussed.

20. B. Patricelli, M.G. Bernardini, C.L. Bianco, L. Caito, L. Izzo, R. Ruffini and G.V. Vereshchagin, "A New Spectral Energy Distribution of Photons in the Fireshell Model of GRBs", International Journal of Modern Physics D, Vol. 20 (2011) 1983-1987.

    The analysis of various Gamma-Ray Bursts (GRBs) having a low energetics within the fireshell model has shown how the N(E) spectrum of their prompt emission can be reproduced in a satisfactory way by a convolution of thermal spectra. Nevertheless, from the study of very energetic bursts such as, for example, GRB 080319B, some discrepancies between the numerical simulations and the observational data have been observed. We investigate a different spectrum of photons in the comoving frame of the fireshell in order to better reproduce the spectral properties of GRB prompt emission within the fireshell model. We introduce a phenomenologically modified thermal spectrum: a thermal spectrum characterized by a different asymptotic power-law index in the low energy region. Such an index depends on a free parameter α, so that the pure thermal spectrum corresponds to the case $\alpha = 0$. We test this spectrum by comparing the numerical simulations with the observed prompt emission spectra of various GRBs. From this analysis it has emerged that the observational data can be correctly reproduced by assuming a modified thermal spectrum with $\alpha = -1.8$.

21. Elena Giusarma, Martina Corsi, Maria Archidiacono, Roland de Putter, Alessandro Melchiorri, Olga Mena, Stefania Pandolfi. "Constraints on massive sterile neutrino species from current and future cosmological data", Phys.Rev. D83, 115023 (2011)

    Sterile massive neutrinos are a natural extension of the standard model of elementary particles. The energy density of the extra sterile massive states affects cosmological measurements in an analogous way to that of active neutrino species. We perform here an analysis of current cosmological data and derive bounds on the masses of the active and the sterile neutrino states, as well as on the number of sterile states. The so-called (3+2) models, with three sub-eV active massive neutrinos plus two sub-eV massive sterile species, is well within the 95% CL allowed regions when considering cosmological data only. If the two extra sterile states have thermal abundances at decoupling, big bang nucleosynthesis bounds compromise the viability of (3+2) models. Forecasts from future cosmological data on the active and sterile neutrino parameters are also presented. Independent measurements of the neutrino mass from tritium beta-decay experiments and of the Hubble constant could shed light on sub-eV massive sterile neutrino scenarios.

22. M. Archidiacono, A. Melchiorri, S. Pandolfi, "The impact of Reionization modelling on CMB Neutrino Mass Bounds", Nuclear Physics B, Proceedings Supplements, Volume 217, Issue 1, p. 65-67. (2011)

    We investigate the bounds on the neutrino mass in a general reionization scenario based on a principal component approach. We found the constraint on the sum of the neutrino masses from CMB data can be relaxed by a ~ 40 % in a generalized reionization scenario.

23. Erminia Calabrese, Eloisa Menegoni, C. J. A. P. Martins, Alessandro Melchiorri, and Graca Rocha, "Constraining variations in the fine structure constant in the presence of early dark energy", Phys.Rev. D84 (2011) 023518.

    We discuss present and future cosmological constraints on variations of the fine structure constant α induced by an early dark energy component having the simplest allowed (linear) coupling to electromagnetism. We find that current cosmological data show no variation of the fine structure constant at recombination respect to the present-day value, with $\alpha/\alpha_0 = 0.975 \pm 0.020$ at 95% c.l., constraining the energy density in early dark energy to $\Omega_e < 0.060$ at 95% c.l. Moreover, we consider constraints on the parameter quantifying the strength of the coupling by the scalar field. We find that current cosmological constraints on the coupling are about 20 times weaker than those obtainable locally (which come from Equivalence Principle tests). However forthcoming or future missions, such as Planck Surveyor and CMBPol, can match and possibly even surpass the sensitivity of current local tests.

24. Micol Benetti, Massimiliano Lattanzi, Erminia Calabrese, Alessandro Melchiorri, "Features in the primordial spectrum: new constraints from WMAP7+ACT data and prospects for Planck", Phys. Rev. D 84, 063509 (2011)

    We update the constraints on possible features in the primordial inflationary density perturbation spectrum by using the latest data from the WMAP7 and ACT Cosmic Microwave Background experiments. The inclusion of new data significantly improves the constraints with respect to older work, especially to smaller angular scales. While we found no clear statistical evidence in the data for extensions to the simplest, featureless, inflationary model, models with a step provide a significantly better fit than standard featureless power-law spectra. We show that the possibility of a step in the inflationary potential like the one preferred by current data will soon be tested by the forthcoming temperature and polarization data from the Planck satellite mission.

25. Stefania Pandolfi, Elena Giusarma, Edward W. Kolb, Massimiliano Lattanzi, Alessandro Melchiorri, Olga Mena, Manuel Pena, Asantha Cooray, Paolo Serra, "Impact of general reionization scenarios on extraction of inflationary parameters", Phys.Rev. D82, 123527, (2010).

    Determination of whether the Harrison–Zel'dovich spectrum for primordial scalar perturbations is consistent with observations is sensitive to assumptions about the reionization scenario. In light of this result, we revisit constraints on inflationary models using more general reionization scenarios. While the bounds on the tensor-to-scalar ratio are largely unmodified, when different reionization schemes are addressed, hybrid models are back into the inflationary game. In the general reionization picture, we reconstruct both the shape and amplitude of the inflaton potential. We find a broader spectrum of potential shapes when relaxing the simple reionization restriction. An upper limit of

10^{16} GeV to the amplitude of the potential is found, regardless of the assumptions on the reionization history.

26. A.G. Aksenov, R. Ruffini and G.V. Vereshchagin, "Pair plasma relaxation time scales", Physical Review E, Vol. 81 (2010) 046401.

    By numerically solving the relativistic Boltzmann equations, we compute the time scale for relaxation to thermal equilibrium for an optically thick electron-positron plasma with baryon loading. We focus on the time scales of electromagnetic interactions. The collisional integrals are obtained directly from the corresponding QED matrix elements. Thermalization time scales are computed for a wide range of values of both the total energy density (over 10 orders of magnitude) and of the baryonic loading parameter (over 6 orders of magnitude). This also allows us to study such interesting limiting cases as the almost purely electron-positron plasma or electron-proton plasma as well as intermediate cases. These results appear to be important both for laboratory experiments aimed at generating optically thick pair plasmas as well as for astrophysical models in which electron-positron pair plasmas play a relevant role.

27. R. Ruffini, G.V. Vereshchagin and S.-S. Xue, "Electron-positron pairs in physics and astrophysics: from heavy nuclei to black holes" Physics Reports, Vol. 487 (2010) No 1-4, pp. 1-140.

    From the interaction of physics and astrophysics we are witnessing in these years a splendid synthesis of theoretical, experimental and observational results originating from three fundametal physical processes. They were originally proposed by Dirac, by Breit and Wheeler and by Sauter, Heisenberg, Euler and Schwinger. For almost seventy years they have all three been followed by a continued effort of experimental verification on Earth-based experiments. The Dirac process, $e^+e^- \to 2\gamma$, has been by far the most successful. It has obtained extremely accurate experimental verification and has led as well to an enormous number of new physics in possibly one of the most fruitful experimental avenue by introduction of storage rings in Frascati and followed by the largest accelerators worldwide: DESY, SLAC etc. The Breit-Wheeler process, $2\gamma \to e^+e^-$, although conceptually simple, being the inverse process of the Dirac one, has been by far one of the most difficult to be verified experimentally. Only recently, through the technology based on free electron X-ray laser and its numerous applications in Earth-based experiments, some first indications of its possible verification have been reached. The vacuum polarization process in strong electromagnetic field, pioneered by Sauter, Heisenberg, Euler and Schwinger, introduced the concept of critical electric field $E_c = m_e^2c^3/e\hbar$. It has been searched without success for more than forty years by heavy-ion collisions in many of the leading particle accelerators worldwide. The novel situation today is that these same processes can be studied on a much more grandiose scale during the gravitational collapse leading to the formation of a black hole being observed in Gamma Ray Bursts (GRBs). This report is dedicated to the scientific race in act. The theoretical and experimental work developed in Earth-based laboratories is confronted with the theoretical interpretation of space-based observations of phenomena originating on cosmological scales. What has become clear in the last ten years is that all the three above mentioned processes, duly extended in the general relativistic framework, are necessary for the understanding of the physics of the gravitational collapse to a black hole. Vice versa, the natural arena where these processes can be observed in mutual interaction and on an unprecedented scale, is indeed the realm of relativistic astrophysics. We systematically analyze the conceptual developments which have followed the basic work of Dirac and Breit-Wheeler. We also recall how the seminal work of Born and Infeld inspired the work by Sauter, Heisenberg and Euler on effective Lagrangian leading to the estimate of the rate for the process of electron-positron production in a constant electric field. In addition of reviewing the intuitive semi-classical treatment of quantum mechanical tunneling for describing the process of electron-positron production, we recall the calculations in *Quantum Electro-Dynamics* of the Schwinger rate and effective Lagrangian for constant electromagnetic fields. We also review the electron-positron production in both time-alternating electromagnetic fields, studied by Brezin, Itzykson, Popov, Nikishov and Narozhny, and the corresponding processes relevant for pair production at the focus of coherent laser beams as well as electron beam-laser collision. We finally report some current developments based on the general JWKB approach which allows to compute the Schwinger rate in spatially varying and time varying electromagnetic fields. We also recall the pioneering work of Landau and Lifshitz, and Racah on the collision of charged particles as well as experimental success of AdA and ADONE in the production of electron-positron pairs. We then turn to the possible experimental verification of these phenomena. We review: A) the experimental verification of the $e^+e^- \to 2\gamma$ process studied by Dirac. We also briefly recall the very successful experiments of e^+e^- annihilation to hadronic channels, in addition to the Dirac electromagnetic channel; B) ongoing Earth based experiments to detect electron-positron production in strong fields by focusing coherent laser beams and by electron beam-laser collisions; and C) the multiyear attempts to detect electron-positron production in Coulomb fields for a large atomic number $Z > 137$ in heavy ion collisions. These attempts follow the classical theoretical work of Popov and Zeldovich, and Greiner and their schools. We then turn to astrophysics. We first review the basic work on the energetics and electrodynamical properties of an electromagnetic black hole and the application of the Schwinger formula around Kerr-Newman black holes as pioneered by Damour and Ruffini. We only focus on black hole masses larger than the critical mass of neutron stars, for convenience assumed to coincide with the Rhoades and Ruffini upper limit of $3.2M_{\odot}$. In this case the electron Compton wavelength is much smaller than the spacetime curvature and all previous results invariantly expressed can be applied following well established rules of the equivalence principle. We derive the corresponding rate of electron-positron pair production and the introduction of the concept of Dyadosphere. We review recent progress in describing the evolution of optically thick electron-positron plasma in presence of supercritical electric field, which is relevant both in astrophysics as well as ongoing laser beam experiments. In particular we review recent progress based on the Vlasov-Boltzmann-Maxwell equations to study the feedback of the created electron-positron pairs on the original constant electric field. We evidence the existence of plasma oscillations and its interaction with photons leading to energy and number equipartition of photons, electrons and positrons. We finally review the recent progress obtained by using the Boltzmann equations to study the evolution of an electron-positron-photon plasma towards thermal equilibrium and determination of its characteristic timescales. The crucial difference introduced by the correct evaluation of the role of two and three body collisions, direct and inverse, is especially evidenced. We then present some general conclusions. The results reviewed in this report are going to be submitted to decisive tests in the forthcoming years both in physics and astrophysics. To mention only a few of the fundamental steps in testing in physics we recall the starting of experimental facilities at the National Ignition Facility at the Lawrence Livermore National Laboratory as well as corresponding French Laser the Mega Joule project. In astrophysics these results will be tested in galactic and extragalactic black holes observed in binary X-ray sources, active galactic nuclei, microquasars and in the process of gravitational collapse to a neutron star and also of two neutron stars to a black hole giving origin to GRBs. The astrophysical description of the stellar precursors and the initial physical conditions leading to a gravitational collapse process will be the subject of a forthcoming report. As of today no theoretical description has yet been found to explain either the emission of the remnant for supernova or the formation of a charged black hole for GRBs. Important current progress toward the understanding of such phenomena as well as of the electrodynamical structure of neutron stars, the supernova explosion and the theories of GRBs will be discussed in the above mentioned forthcoming report. What is important to recall at this stage is only that both the supernovae and GRBs processes are among the most energetic and transient phenomena ever observed in the Universe: a supernova can reach energy of ˜10^{54} ergs on a time scale of a few months and GRBs can have emission of up to ˜10^{54} ergs in a time scale as short as of a few seconds. The central role of neutron stars in the description of supernovae, as well as of black holes and the electron-positron plasma, in the description of GRBs, pioneered by one of us (RR) in 1975, are widely recognized. Only the theoretical basis to address these topics are discussed in the present report.

28. A. G. Aksenov, R. Ruffini, and G. V. Vereshchagin, "Kinetics of the Mildly Relativistic Plasma and GRBs" in the Proceedings of "The Sun, the stars, the Universe and General Relativity" meeting in honor of 95th Anniversary of Ya. B. Zeldovich in Minsk, AIP Conference Proceedings 1205 (2010) 11-16.

    We consider optically thick photon-pair-proton plasma in the framework of Boltzmann equations. For the sake of simplicity we consider the uniform and isotropic plasma. It has been shown that arbitrary initial distribution functions evolve to the thermal equilibrium state through so called kinetic equilibrium state with common temperature of all particles and nonzero chemical potentials. For the plasma temperature $0.1 - 10$ MeV relevant for GRB (Gamma-Ray Burst) sources we evaluate the thermalization time scale as function of total energy density and baryonic loading parameter.

29. E. Menegoni, S. Pandolfi, S. Galli, M. Lattanzi, A. Melchiorri "Constraints on the dark energy equation of state in presence of a varying fine structure constant" in Int. J. Mod. Phys D19, 507 (2010).

    We discuss the cosmological constraints on the dark energy equation of state in the pres- ence of primordial variations in the fine structure constant. We find that the constraints from CMB data alone on w and the Hubble constant are much weaker when variations in the fine structure constant are permitted. Vice versa, constraints on the fine struc- ture constant are relaxed by more than 50% when dark energy models different from a cosmological constant are considered.

30. C.J.A.P. Martins, E. Menegoni, S. Galli and A. Melchiorri, "Varying couplings in the early universe: correlated variations of α and G, Physical Review D 82 023532 (2010)

    The cosmic microwave background anisotropies provide a unique opportunity to constrain simultaneous variations of the fine-structure constant α and Newton's gravitational constant G. Those correlated variations are possible in a wide class of theoretical models. In this brief paper we show that the current data, assuming that particle masses are constant, give no clear indication for such variations, but already prefer that any relative variations in α should be of the same sign of those of G for variations of 1%. We also show that a cosmic complementarity is present with big bang nucleosynthesis and that a combination of current CMB and big bang nucleosynthesis data strongly constraints simultaneous variations in α and G. We finally discuss the future bounds achievable by the Planck satellite mission.

31. E. Menegoni, "New Constraints on Variations of Fine Structure Constant from Cosmic Microwave Background Anisotropies", GRAVITATIONAL PHYSICS: TESTING GRAVITY FROM SUBMILLIMETER TO COSMIC: Proceedings of the VIII Mexican School on Gravitation and Mathematical Physics. AIP Conference Proceedings, Volume 1256, pp. 288-292 (2010).

    The recent measurements of Cosmic Microwave Background temperature and polarization anisotropy made by the ACBAR, QUAD and BICEP experiments substantially improve the cosmological constraints on possible variations of the fine structure constant in the early universe. In this work I analyze this recent data obtaining the constraint $\alpha/\alpha 0$ = 0.987+/-0.012 at 68% c.l.. The inclusion of the new HST constraints on the Hubble constant further increases the bound to $\alpha/\alpha 0$ = 1.001+/-0.007 at 68% c.l., bringing possible deviations from the current value below the 1% level.

32. A. Melchiorri, F. De Bernardis, E. Menegoni, "Limits on the neutrino mass from cosmology". GRAVITATIONAL PHYSICS: TESTING GRAVITY FROM SUBMILLIMETER TO COSMIC: Proceedings of the VIII Mexican School on Gravitation and Mathematical Physics. AIP Conference Proceedings, Volume 1256, pp. 96-106 (2010).

We use measurements of luminosity-dependent galaxy bias at several different redshifts, SDSS at z = 0.05, DEEP2 at z = 1 and LBGs at z = 3.8, combined with WMAP five-year cosmic microwave background anisotropy data and SDSS Red Luminous Galaxy survey three-dimensional clustering power spectrum to put constraints on cosmological parameters.

33. A.G. Aksenov, R. Ruffini and G.V. Vereshchagin, "Thermalization of the mildly relativistic plasma", Physical Review D, Vol. 79 (2009) 043008.

    In the recent Letter Aksenov et al. (2007) we considered the approach of nonequilibrium pair plasma towards thermal equilibrium state adopting a kinetic treatment and solving numerically the relativistic Boltzmann equations. It was shown that plasma in the energy range 0.1-10 MeV first reaches kinetic equilibrium, on a timescale $t_{\rm k} \lesssim 10^{-14}$ sec, with detailed balance between binary interactions such as Compton, Bhabha and Møller scattering, and pair production and annihilation. Later the electron-positron-photon plasma approaches thermal equilibrium on a timescale $t_{\rm th} \lesssim 10^{-12}$ sec, with detailed balance for all direct and inverse reactions. In the present paper we systematically present details of the computational scheme used in Aksenov et al. (2007), as well as generalize our treatment, considering proton loading of the pair plasma. When proton loading is large, protons thermalize first by proton-proton scattering, and then with the electron-positron-photon plasma by proton-electron scattering. In the opposite case of small proton loading proton-electron scattering dominates over proton-proton one. Thus in all cases the plasma, even with proton admixture, reaches thermal equilibrium configuration on a timescale $t_{\rm th} \lesssim 10^{-11}$ sec. We show that it is crucial to account for not only binary but also triple direct and inverse interactions between electrons, positrons, photons and protons. Several explicit examples are given and the corresponding timescales for reaching kinetic and thermal equilibria are determined.

34. A. G. Aksenov, R. Ruffini, and G. V. Vereshchagin, "Thermalization of pair plasma with proton loading" in the Proceedings of "PROBING STELLAR POPULATIONS OUT TO THE DISTANT UNIVERSE" meeting, AIP Conference Proceedings 1111 (2009) 344-350.

    We study kinetic evolution of nonequilibrium optically thick electron-positron plasma towards thermal equilibrium solving numerically relativistic Boltzmann equations with energy per particle ranging from 0.1 to 10 MeV. We generalize our results presented in Aksenov et al. (2007), considering proton loading of the pair plasma. Proton loading introduces new characteristic timescales essentially due to proton-proton and proton-electron Coulomb collisions. Taking into account not only binary but also triple direct and inverse interactions between electrons, positrons, photons and protons we show that thermal equilibrium is reached on a timescale $t_{\rm th} \simeq 10^{-11}$ sec.

35. A.G. Aksenov, R. Ruffini and G.V. Vereshchagin, "Thermalization of nonequilibrium electron-positron-photon plasmas", Physical Review Letters, Vol. 99 (2007) No 12, 125003.

    Starting from a nonequilibrium configuration we analyze the role of the direct and the inverse binary and triple interactions in reaching thermal equilibrium in a homogeneous isotropic pair plasma. We focus on energies in the range $0.1 - 10$ MeV. We numerically integrate the relativistic Boltzmann equation with the exact QED collisional integrals taking into account all binary and triple interactions. We show that first, when a detailed balance is reached for all binary interactions on a time scale $t_k < 10^{-14}$ sec, photons and electron-positron pairs establish kinetic equilibrium. Subsequently, when triple interactions satisfy the detailed balance on a time scale $t_{eq} < 10^{-12}$ sec, the plasma reaches thermal equilibrium. It is shown that neglecting the inverse triple interactions prevents reaching thermal equilibrium. Our results obtained in the theoretical physics domain also find application in astrophysics and cosmology.

36. C.L. Bianco, R. Ruffini, G.V. Vereshchagin and S.-S. Xue, "Equations of Motion and Initial and Boundary Conditions for Gamma-ray Burst", Journal of the Korean Physical Society, Vol. 49 (2006) No. 2, pp. 722-731.

    We compare and contrast the different approaches to the optically thick adiabatic phase of GRB all the way to the transparency. Special attention is given to the role of the rate equation to be self consistently solved with the relativistic hydrodynamic equations. The works of Shemi and Piran (1990), Piran, Shemi and Narayan (1993), Meszaros, Laguna and Rees (1993) and Ruffini, Salmonson, Wilson and Xue (1999,2000) are compared and contrasted. The role of the baryonic loading in these three treatments is pointed out. Constraints on initial conditions for the fireball produced by electro-magnetic black hole are obtained.

37. P. Singh, K. Vandersloot and G.V. Vereshchagin, "Nonsingular bouncing

universes in loop quantum cosmology", Physical Review D, Vol. 74 (2006) 043510.

Nonperturbative quantum geometric effects in loop quantum cosmology (LQC) predict a ρ^2 modification to the Friedmann equation at high energies. The quadratic term is negative definite and can lead to generic bounces when the matter energy density becomes equal to a critical value of the order of the Planck density. The nonsingular bounce is achieved for arbitrary matter without violation of positive energy conditions. By performing a qualitative analysis we explore the nature of the bounce for inflationary and cyclic model potentials. For the former we show that inflationary trajectories are attractors of the dynamics after the bounce implying that inflation can be harmoniously embedded in LQC. For the latter difficulties associated with singularities in cyclic models can be overcome. We show that nonsingular cyclic models can be constructed with a small variation in the original cyclic model potential by making it slightly positive in the regime where scalar field is negative.

38. M. Lattanzi, R. Ruffini and G.V. Vereshchagin, "Joint constraints on the lepton asymmetry of the Universe and neutrino mass from the Wilkinson Microwave Anisotropy Probe", Physical Review D, Vol. 72 (2005) 063003.

We use the Wilkinson Microwave Anisotropy Probe (WMAP) data on the spectrum of cosmic microwave background anisotropies to put constraints on the present amount of lepton asymmetry L, parametrized by the dimensionless chemical potential (also called degeneracy parameter) xi and on the effective number of relativistic particle species. We assume a flat cosmological model with three thermally distributed neutrino species having all the same mass and chemical potential, plus an additional amount of effectively massless exotic particle species. The extra energy density associated to these species is parametrized through an effective number of additional species $\Delta N_{others}{}^{eff}$. We find that $0 < |\xi| < 1.1$ and correspondingly $0 < |L| < 0.9$ at 2σ, so that WMAP data alone cannot firmly rule out scenarios with a large lepton number; moreover, a small preference for this kind of scenarios is actually found. We also discuss the effect of the asymmetry on the estimation of other parameters and, in particular, of the neutrino mass. In the case of perfect lepton symmetry, we obtain the standard results. When the amount of asymmetry is left free, we find at 2sigma. Finally we study how the determination of $|L|$ is affected by the assumptions on ΔN^{eff}_{others}. We find that lower values of the extra energy density allow for larger values of the lepton asymmetry, effectively ruling out, at 2sigma level, lepton symmetric models with $\Delta N_{others}^{eff} \simeq 0$.

39. G.V. Vereshchagin, "Gauge Theories of Gravity with the Scalar Field in Cosmology", in "Frontiers in Field Theory", edited by O. Kovras, Nova Science Publishers, New York, (2005), pp. 213-255 (ISBN: 1-59454-127-2).

    Brief introduction into gauge theories of gravity is presented. The most general gravitational lagrangian including quadratic on curvature, torsion and nonmetricity invariants for metric-affine gravity is given. Cosmological implications of gauge gravity are considered. The problem of cosmological singularity is discussed within the framework of general relativity as well as gauge theories of gravity. We consider the role of scalar field in connection to this problem. Initial conditions for nonsingular homogeneous isotropic Universe filled by single scalar field are discussed within the framework of gauge theories of gravity. Homogeneous isotropic cosmological models including ultrarelativistic matter and scalar field with gravitational coupling are investigated. We consider different symmetry states of effective potential of the scalar field, in particular restored symmetry at high temperatures and broken symmetry. Obtained bouncing solutions can be divided in two groups, namely nonsingular inflationary and
    oscillating solutions. It is shown that inflationary solutions exist for quite general initial conditions like in the case of general relativity. However, the phase space of the dynamical system, corresponding to the cosmological equations is bounded. Violation of the uniqueness of solutions on the boundaries of the phase space takes place. As a result, it is impossible to define either the past or the future for a given solution. However, definitely there are singular solutions and therefore the problem of cosmological singularity cannot be solved in models with the scalar field within gauge theories of gravity.

40. R. Ruffini, M. G. Bernardini, C. L. Bianco, L. Caito, P. Chardonnet, M. G. Dainotti, F. Fraschetti, R. Guida, M. Rotondo, G. Vereshchagin, L. Vitagliano, S.-S. Xue,
    "The Blackholic energy and the canonical Gamma-Ray Burst" in Cosmology and Gravitation: XIIth Brazilian School of Cosmology and Gravitation, edited by M. Novello and S.E. Perez Bergliaffa, AIP Conference Proceedings, Vol. 910, Melville, New York, 2007, pp. 55-217.

Gamma-Ray Bursts (GRBs) represent very likely "the" most extensive computational, theoretical and observational effort ever carried out successfully in physics and astrophysics. The extensive campaign of observation from space based X-ray and γ-ray observatory, such as the Vela, CGRO, BeppoSAX, HETE-II, INTEGRAL, Swift, R-XTE, Chandra, XMM satellites, have been matched by complementary observations in the radio wavelength (e.g. by the VLA) and in the optical band (e.g. by VLT, Keck, ROSAT). The net result is unprecedented accuracy in the received data allowing the determination of the energetics, the time variability and the spectral properties of these GRB sources. The very fortunate situation occurs that these data can be confronted with a mature theoretical development. Theoretical interpretation of the above data allows progress in three different frontiers of knowledge: a) the ultrarelativistic regimes of a macroscopic source moving at Lorentz gamma factors up to ~ 400; b) the occurrence of vacuum polarization process verifying some of the yet untested regimes of ultrarelativistic quantum field theories; and c) the first evidence for extracting, during the process of gravitational collapse leading to the formation of a black hole, amounts of energies up to 10^{55} ergs of blackholic energy — a new form of energy in physics and astrophysics. We outline how this progress leads to the confirmation of three interpretation paradigms for GRBs proposed in July 2001. Thanks mainly to the observations by Swift and the optical observations by VLT, the outcome of this analysis points to the existence of a "canonical" GRB, originating from a variety of different initial astrophysical scenarios. The communality of these GRBs appears to be that they all are emitted in the process of formation of a black hole with a negligible value of its angular momentum. The following sequence of events appears to be canonical: the vacuum polarization process in the dyadosphere with the creation of the optically thick self accelerating electron-positron plasma; the engulfment of baryonic mass during the plasma expansion; adiabatic expansion of the optically thick "fireshell" of electron-positron-baryon plasma up to the transparency; the interaction of the accelerated baryonic matter with the interstellar medium (ISM). This leads to the canonical GRB composed of a proper GRB (P-GRB), emitted at the moment of transparency, followed by an extended afterglow. The sole parameters in this scenario are the total energy of the dyadosphere E_{dya}, the fireshell baryon loading M_B defined by the dimensionless parameter $B = M_B c^2 / E_{dya}$, and the ISM filamentary distribution around the source. In the limit $B \longrightarrow 0$ the total energy is radiated in the P-GRB with a vanishing contribution in the afterglow.

In this limit, the canonical GRBs explain as well the short GRBs. In these lecture notes we systematically outline the main results of our model comparing and contrasting them with the ones in the current literature. In both cases, we have limited ourselves to review already published results in refereed publications. We emphasize as well the role of GRBs in testing yet unexplored grounds in the foundations of general relativity and relativistic field theories.

41. M. Lattanzi, R. Ruffini and G.V. Vereshchagin, "Do WMAP data constraint the lepton asymmetry of the Universe to be zero?" in Albert Einstein Century International Conference, edited by J.-M. Alimi, and A. Füzfa, AIP Conference Proceedings, Vol. 861, Melville, New York, 2006, pp.912-919.

    It is shown that extended flat ΛCDM models with massive neutrinos, a sizeable lepton asymmetry and an additional contribution to the radiation content of the Universe, are not excluded by the Wilkinson Microwave Anisotropy Probe (WMAP) first year data. We assume a flat cosmological model with three thermally distributed neutrino species having all the same mass and chemical potential, plus an additional amount of effectively massless exotic particle species X. After maximizing over seven other cosmological parameters, we derive from WMAP first year data the following constraints for the lepton asymmetry L of the Universe (95% CL): $0 < |L| < 0.9$, so that WMAP data alone cannot firmly rule out scenarios with a large lepton number; moreover, a small preference for this kind of scenarios is actually found. We also find for the neutrino mass $m_\nu < 1.2eV$ and for the effective number of relativistic particle species $-0.45 < \Delta N^{eff} < 2.10$, both at 95% CL. The limit on ΔN^{eff} is more restrictive man others found in the literature, but we argue that this is due to our choice of priors.

42. R. Ruffini, C.L. Bianco, G.V. Vereshchagin, S.-S. Xue "Baryonic loading and e^+e^- rate equation in GRB sources" to appear in the proceedings of "Relativistic Astrophysics and Cosmology - Einstein's Legacy" Meeting, November 7-11, 2005, Munich, Germany.

    The expansion of the electron-positron plasma in the GRB phenomenon is compared and contrasted in the treatments of Meszaros, Laguna and Rees, of Shemi, Piran and Narayan, and of Ruffini et al. The role of the correct numerical integration of the hydrodynamical equations, as well as of the rate equation for the electron-positron plasma loaded with a baryonic mass, are outlined and confronted for crucial differences.

43. G.V. Vereshchagin, M. Lattanzi, H.W. Lee, R. Ruffini, "Cosmological massive neutrinos with nonzero chemical potential: I. Perturbations in cosmological models with neutrino in ideal fluid approximation", in proceedings of the Xth Marcel Grossmann Meeting on Recent Developments in Theoretical and Experimental General Relativity, World Scientific: Singapore, 2005, vol. 2, pp. 1246-1248.

    Recent constraints on neutrino mass and chemical potential are discussed with application to large scale structure formation. Power spectra in cosmological model with hot and cold dark matter, baryons and cosmological term are calculated in newtonian approximation using linear perturbation theory. All components are considered to be ideal fluids. Dissipative processes are taken into account by initial spectrum of perturbations so the problem is reduced to a simple system of equations. Our results are in good agreement with those obtained before using more complicated treatments.

44. M. Lattanzi, H.W. Lee, R. Ruffini, G.V. Vereshchagin, "Cosmological massive neutrinos with nonzero chemical potential: II. Effect on the estimation of cosmological parameters", in proceedings of the Xth Marcel Grossmann Meeting on Recent Developments in Theoretical and Experimental General Relativity, World Scientific: Singapore, 2005, vol. 2, pp. 1255-1257.

    The recent analysis of the cosmic microwave background data carried out by the WMAP team seems to show that the sum of the neutrino mass is ¡0.7 eV. However, this result is not model-independent, depending on precise assumptions on the cosmological model. We study how this result is modified when the assumption of perfect lepton symmetry is dropped out.

45. R. Ruffini, M. Lattanzi and G. Vereshchagin, "On the possible role of massive neutrinos in cosmological structure formation" in Cosmology and Gravitation: Xth Brazilian School of Cosmology and Gravitation, edited by M. Novello and S.E. Perez Bergliaffa, AIP Conference Proceedings, Vol. 668, Melville, New York, 2003, pp.263-287.

    In addition to the problem of galaxy formation, one of the greatest open questions of cosmology is represented by the existence of an asymmetry between matter and antimatter in the baryonic component of the Universe. We believe that a net lepton number for the three neutrino species can be used to understand this asymmetry. This also implies an asymmetry in the matter-antimatter component of the leptons. The existence of a nonnull lepton number for the neutrinos can easily explain a cosmological abundance of neutrinos consistent with the one needed to explain both the rotation curves of galaxies and the flatness of the Universe. Some propedeutic results are presented in order to attack this problem.

46. A.G. Aksenov, C.L. Bianco, R. Ruffini and G.V. Vereshchagin, "GRBs and the thermalization process of electron-positron plasmas" in the Proceedings of the "Gamma Ray Bursts 2007" meeting, AIP Conf.Proc. 1000 (2008) 309-312.

    We discuss temporal evolution of the pair plasma, created in Gamma-Ray Bursts sources. A particular attention is paid to the relaxation of plasma into thermal equilibrium. We also discuss the connection between the dynamics of expansion and spatial geometry of plasma. The role of the baryonic loading parameter is emphasized.

47. A. G. Aksenov, R. Ruffini, and G. V. Vereshchagin, "Thermalization of Electron-Positron-Photon Plasmas with an Application to GRB" in RELATIVISTIC ASTROPHYSICS: 4th Italian-Sino Workshop, AIP Conference Proceedings, Vol. 966, Melville, New York, 2008, pp. 191-196.

    The pair plasma with photon energies in the range $0.1 - 10$MeV is believed to play crucial role in cosmic Gamma-Ray Bursts. Starting from a nonequilibrium configuration we analyze the role of the direct and the inverse binary and triple interactions in reaching thermal equilibrium in a homogeneous isotropic pair plasma.We numerically integrate the relativistic Boltzmann equation with the exact QED collisional integrals taking into account all binary and triple interactions. We show that first, when a detailed balance is reached for all binary interactions on a time scale $t_k = 10^{-14}$sec , photons and electronpositron pairs establish kinetic equilibrium. Subsequently, when triple interactions satisfy the detailed balance on a time scale $t_{eq} = 10^{-12}$sec , the plasma reaches thermal equilibrium. It is shown that neglecting the inverse triple interactions prevents reaching thermal equilibrium. Our results obtained in the theoretical physics domain also find application in astrophysics and cosmology.

48. R. Ruffini, G. V. Vereshchagin and S.-S. Xue, "Vacuum Polarization and Electron-Positron Plasma Oscillations" in RELATIVISTIC ASTROPHYSICS: 4th Italian-Sino Workshop, AIP Conference Proceedings, Vol. 966, Melville, New York, 2008, pp. 207-212.

We study plasma oscillations of electrons-positron pairs created by the vacuum polarization in an uniform electric field. Our treatment, encompassing the case of $E > E_c$, shows also in the case $E < E_c$the existence of a maximum Lorentz factor acquired by electrons and positrons and allows determination of the a maximal length of oscillation. We quantitatively estimate how plasma oscillations reduce the rate of pair creation and increase the time scale of the pair production.

4.3. Publications (2015)

1. G.V. Vereshchagin, "Relativistic Kinetic Theory with some Applications", in: Cosmology and Gravitation: XVth Brazilian School of Cosmology and Gravitation, eds. Mario Novello and Santiago E.Perez Bergliaffa, Cambridge Scientific Publishers, 2015, pp 1-40.

2. A. G. Aksenov, R. Ruffini, and G. V. Vereshchagin, "Radiative transfer in relativistic plasma outflows and comptonization of photons near the photosphere", Astronomy Reports, Vol. 59, No. 6, (2015) pp. 418–424.

3. G. V. Vereshchagin, "Physics of Non-Dissipative Ultrarelativistic Photospheres", in Proceedings of the MG13 Meeting on General Relativity, eds. Rosquist et al., WSPC (2015) pp. 708-728.

4. R. Ruffini, I.A. Siutsou and G.V. Vereshchagin, "Photon Thick and Photon Thin Relativistic Outflows and GRBs", in Proceedings of the MG13 Meeting on General Relativity, eds. Rosquist et al., WSPC (2015) pp. 1748-1750.

5. A.G. Aksenov, R. Ruffini and G.V. Vereshchagin, "Radiative Transfer Near the Photosphere of Mildly and Ultrarelativistic Outflows", in Proceedings of the MG13 Meeting on General Relativity, eds. Rosquist et al., WSPC (2015) pp. 1754-1756.

6. D. Bégué, I.A. Siutsou and G.V. Vereshchagin, "On the Decoupling of Photons from Relativistically Expanding Outflows", in Proceedings of the MG13 Meeting on General Relativity, eds. Rosquist et al., WSPC (2015) pp. 1760-1761.

7. R. Ruffini, G. V. Vereshchagin and S.-S. Xue, “Cosmic absorption of ultra high energy particles”, submitted to Astrophys. Space Sci. (2015).
8. R. Ruffini G. V. Vereshchagin Yu Wang, “Thermal emission in the early afterglow of GRBs from their interaction with supernova ejecta”, submitted to A&A (2015).
9. I. A. Siutsou, A. G. Aksenov and G. V. Vereshchagin, “On Thermalization of Electron-Positron-Photon Plasma”, to appear in proceedings of the Second César Lattes Meeting, AIP Conf. Proc. (2015).
10. S. Tizchang, S. Batebi, G.V. Vereshchagin, R. Mohammadi, S.-S. Xue and R. Ruffini, “Interaction of high energy photons with the background radiation in the Universe”, in preparation (2015).
11. R. Ruffini, C. R. Argüelles and J. A. Rueda, ”On the core-halo distribution of dark matter in galaxies” MNRAS, 451 (2015) 622.
12. I. Siutsou, C. R. Argüelles and R. Ruffini, ”Dark matter massive fermions and Einasto profiles in galactic halos”, Astron. Rep. 59 No. 7 (2015) 656.
13. C. R. Argüelles and R. Ruffini, ”A regular and relativistic Einstein cluster within the S2 orbit centered in SgrA*” The Thirteenth Marcel Grossmann Meeting Book, Vol. B (2015) 1734.
14. B. M. O. Fraga, C. R. Argüelles, R. Ruffini and I. Siutsou, ”Semidegenerate self-gravitating system of fermion as Dark Matter on galaxies I: Universality laws”, The Thirteenth Marcel Grossmann Meeting Book, Vol. B (2015) 1730.

4.4. Invited talks at international conferences

1. “Thermal emission in the early afterglow”, 1st Scientific ICRANet Meeting in Armenia, Yerevan, Armenia, 30 June - 4 July 2014.

   (G.V. Vereshchagin)

2. “Photospheric emission from relativistic outflows”, Zeldovich-100 International Conference, Space Research Institute (IKI), Moscow, Russia, 16-20 June, 2014

(G.V. Vereshchagin)

3. “Dark matter massive fermions and Einasto profiles in galactic haloes “

   (Ivan Siutsou)

   Subatomic particles, Nucleons, Atoms, Universe: Processes and Structure International conference in honor of Ya. B. Zeldovich 100th Anniversary, March 10-14, 2014, Minsk, Belarus

4. “DM halos and super massive dark objects at sub-parsec scales:the nature of the DM particle “

   (Carlos R. Argüelles)

   Subatomic particles, Nucleons, Atoms, Universe: Processes and Structure International conference in honor of Ya. B. Zeldovich 100th Anniversary, March 10-14, 2014, Minsk, Belarus

5. “Physics of non-dissipative ultrarelativistic photospheres“

   (G.V. Vereshchagin)

   On recent developments in theoretical and experimental general relativity, gravitation and relativistic field theories: XIII Marcel Grossmann Meeting, Stockholm, 1-7 July 2012.

6. ”Photon thick and photon thin relativistic outflows and GRBs”

   (I.A. Siutsou, R. Ruffini and G.V. Vereshchagin)

   On recent developments in theoretical and experimental general relativity, gravitation and relativistic field theories: XIII Marcel Grossmann Meeting, Stockholm, 1-7 July 2012.

7. ”Monte Carlo simulations of the photospheric emission in GRBs”

   (D. Begue, I.A. Siutsou and G.V. Vereshchagin)

   On recent developments in theoretical and experimental general relativity, gravitation and relativistic field theories: XIII Marcel Grossmann Meeting, Stockholm, 1-7 July 2012.

8. ”Phase space evolution of pairs created in strong electric fields” (A. Benedetti, R. Ruffini and G.V. Vereshchagin) On recent developments

in theoretical and experimental general relativity, gravitation and relativistic field theories: XIII Marcel Grossmann Meeting, Stockholm, 1-7 July 2012.

9. "Applications of the Boltzmann equation: from an interacting plasma toward the photospheric emission of a GRB" (A. Benedetti, R. Ruffini and G.V. Vereshchagin) Erasmus Mundus School, Nice, France, 3rd – 19th September, 2012.

10. "Photospheric emission from thermally accelerated relativistic outflows"

    GRBs, their progenitors and the role of thermal emission, Les Houches, France, 2-7 October, 2011

    (G.V. Vereshchagin, R. Ruffini and I.A. Siutsou)

11. "Thermalization of the pair plasma"

    (G.V. Vereshchagin, A.G. Aksenov and R. Ruffini)

    From Nuclei to White Dwarfs and Neutron Stars, Les Houches, France, 3-8 April, 2011

12. "Photospheric emission from relativistic outflows: 1DHD"

    (G.V. Vereshchagin, R. Ruffini and I.A. Siutsou)

    Recent News from the MeV, GeV and TeV Gamma-Ray Domains, Pescara, Italy, 21-26 March, 2011

13. "Thermalization of degenerate electron-positron plasma"

    I.A. Siutsou, A.G. Aksenov, R. Ruffini and G.V. Vereshchagin

    IRAP Ph.D. Erasmus Mundus School—May 27, 2011, Nice, France

14. "Semidegenerate self-gravitating systems of fermions as central objects and dark matter halos in galaxies"

    (I. A. Siutsou, A. Geralico and R. Ruffini)

    Recent News from the MeV, GeV and TeV Gamma-Ray Domains, March 24, 2011, Pescara, Italy

15. ”Thermalization of degenerate electron-positron plasma”

    (I.A. Siutsou, A.G. Aksenov, G.V. Vereshchagin and R. Ruffini)

    3rd Galileo-Xu Guangqi Meeting—October 12, 2011, Beijing, China

16. ”Photospheric emission of relativistically expanding outflows”

    (I.A. Siutsou, G.V. Vereshchagin and R. Ruffini)

    12th Italian-Korean Symposium on Relativistic Astrophysics—July 5, 2011, Pescara, Italy

17. On the frequency of oscillations in the pair plasma generated by a strong electric field.

    (Alberto Benedetti, W.-B. Han, R. Ruffini, G.V. Vereshchagin)
    IRAP Ph.D. Erasmus Mundus Workshop, April 5, 2011, Pescara (Italy)

18. Oscillations in the pair plasma generated by a strong electric field

    (Alberto Benedetti, W.-B. Han, R. Ruffini, G.V. Vereshchagin)
    Italian-Korean Meeting, July 4-9, 2011, Pescara (Italy)

19. Electron-Positron plasma oscillations: hydro-electrodynamic and kinetic approaches

    (Alberto Benedetti, R. Ruffini, G.V. Vereshchagin)
    IRAP Ph.D. Erasmus Mundus School, September 7, 2011, Nice (France)

20. Boltzmann equation: from an interacting plasma toward the photospheric emission of a GRB

    (Alberto Benedetti, A. Aksenov, R. Ruffini, I. Siotsou, G.V. Vereshchagin)
    IRAP Ph.D. Erasmus Mundus Workshop, October 6, 2011, Les Houches (France)

21. Electron-Positron plasma oscillations: hydro-electrodynamic and kinetic approaches.

    (Alberto Benedetti, A. Aksenov, R. Ruffini, I. Siutsou, G.V. Vereshchagin)
    Galileo-Xu Guanqui Meeting, October 12, 2011, Beijing (China)

22. "Inflation in a general reionization scenario "

    (S. Pandolfi)

    Essential Cosmology for the Next Generation, Puerto Vallarta, Mexico, January 10-14, 2011

23. "Constraints on Inflation in extended cosmological scenarios "

    (S. Pandolfi)

    28 January 2011, Dark Cosmlogy Center, Copenhagen, Denmark.

24. "Theoretical Development toward the Planck mission "

    (S. Pandolfi)

    IRAP PhD and Erasmus MundusWorkshop: Workshop on Recent News from the GeV and TeV Gamma-Ray Domains: Results and Interpretations,21-26 March 2011, ICRANet (Pescara), Italy.

25. "Joint Astrophysical and Cosmological constrains on reionization "

    (S. Pandolfi)

    DAVID WORKSHOP VI, Scuola Normale Superiore, Pisa, October 18-20 2011

26. "New constraints on features in the primordial spectrum "

    (M. Benetti)

    3rd Galileo- Xu Guangqi meeting, Beijing (China), October 11-15, 2011.

27. "Thermalization of the pair plasma"

    (G.V. Vereshchagin with A.G. Aksenov and R. Ruffini)

    Korean Physical Society 2010 Fall Meeting, Pyeong-chang, Korea, 20-22 October, 2010.

28. "The spatial structure of expanding optically thick relativistic plasma and the onset of GRBs"

    (G.V. Vereshchagin with A.G. Aksenov, G. de Barros and R. Ruffini)

    GRB 2010 / Dall'eV al TeV tutti i colori dei GRB, Secondo Congresso Italiano sui Gamma-ray Burst, Cefalu' 15-18 June 2010.

29. “From thermalization mechanisms to emission processes in GRBs”

    (G.V. Vereshchagin)

    XII Marcel Grossmann Meeting, Paris, 12-18 July 2009.

30. “Kinetics of the mildly relativistic plasma and GRBs”

    (A.G. Aksenov R. Ruffini, and G.V. Vereshchagin)

    “The Sun, the Stars, the Universe, and General Relativity” - International conference in honor of Ya. B. Zeldovich 95th Anniversary, Minsk, Belarus, April 19-23, 2009.

31. “Pair plasma around compact astrophysical sources: kinetics, electrodynamics and hydrodynamics”

    (G.V. Vereshchagin and R. Ruffini)

    Invited seminar at RMKI, Budapest, February 24, 2009.

32. “Thermalization of the pair plasma with proton loading”

    (G.V. Vereshchagin, R. Ruffini, and A.G. Aksenov)

    Probing Stellar Populations out to the Distant Universe, Cefalu’, Italy, September 7-19, 2008.

33. “Thermalization of the pair plasma with proton loading”

    (G.V. Vereshchagin, R. Ruffini, and A.G. Aksenov)

    3rd Stueckelberg Workshop, Pescara, Italy, 8-18 July, 2008.

34. “Thermalization of the pair plasma”

    (G.V. Vereshchagin, R. Ruffini, and A.G. Aksenov)

35. “Non-singular solutions in Loop Quantum Cosmology”

    (G.V. Vereshchagin)

    2nd Stueckelberg Workshop, Pescara, Italy, 3-7 September, 2007.

36. “(From) massive neutrinos and inos and the upper cutoff to the fractal structure of the Universe (to recent progress in theoretical cosmology)”

    (G.V. Vereshchagin, M. Lattanzi and R. Ruffini)

    A Century of Cosmology, San Servolo, Venice, Italy, 27-31 August, 2007.

37. "Pair creation and plasma oscillations"

    (G.V. Vereshchagin, R. Ruffini, and S.-S. Xue)
    4th Italian-Sino Workshop on Relativistic Astrophysics, Pescara, Italy, 20-29 July, 2007.

38. "Thermalization of electron-positron plasma in GRB sources"

    (G.V. Vereshchagin, R. Ruffini, and A.G. Aksenov)
    Xth Italian-Korean Symposium on Relativistic Astrophysics, Pescara, Italy, 25-30 June, 2007.

39. "Kinetics and hydrodynamics of the pair plasma"

    (G.V. Vereshchagin, R. Ruffini, C.L. Bianco, A.G. Aksenov)

40. "Pair creation and plasma oscillations"

    (G.V. Vereshchagin, R. Ruffini and S.-S. Xue)
    Cesare Lattes Meeting on GRBs, Black Holes and Supernovae, Mangaratiba-Portobello, Brazil, 26 February - 3 March 2007.

41. "Cavallo-Rees classification revisited"

    (G.V. Vereshchagin, R.Ruffini and S.-S. Xue)

    On recent developments in theoretical and experimental general relativity, gravitation and relativistic field theories: XIth Marcel Grossmann Meeting, Berlin, Germany, 23-29 July, 2006.

42. "Kinetic and thermal equilibria in the pair plasma"

    (G.V. Vereshchagin)

    The 1st Bego scientific rencontre, Nice, 5-16 February 2006.

43. "From semi-classical LQC to Friedmann Universe"

    (G.V. Vereshchagin)

    Loops '05, Potsdam, Golm, Max-Plank Institut für Gravitationsphysik (Albert-Einstein-Institut), 10-14 October 2005.

44. "Equations of motion, initial and boundary conditions for GRBs"

    (G.V. Vereshchagin, R. Ruffini and S.-S. Xue)

    IXth Italian-Korean Symposium on Relativistic Astrophysics, Seoul, Mt. Kumgang, Korea, 19-24 July 2005.

45. “On the Cavallo-Rees classification and GRBs”

    (G.V. Vereshchagin, R. Ruffini and S.-S. Xue)

    II Italian-Sino Workshop on Relativistic Astrophysics, Pescara, Italy, 10-20 June, 2005.

46. “New constraints on features in the primordial spectrum ”

    (M. Benetti)

    Essential Cosmology for the Next Generation Ph.D School, January 16-21 2012, Cancun, Mexico

47. “New constraints on features in the primordial spectrum ”

    (M. Benetti)

    XIth School of Cosmology, Gravitational Lenses: their impact in the study of galaxies and Cosmology, Ph.D School, September 17-22 2012, Cargese, France

48. “New Horizons for Observational Cosmology ”

    (M. Benetti)

    Ph.D School, June 30th-July 6th 2013, Varenna, Italy

49. “BLACK HOLES IN GAMMA RAY-BURSTS AND GALACTIC NUCLEI ”

    (R. Ruffini, C.R. Arguelles, B.M.O. Fraga, A. Geralico, H. Quevedo and J.A. Rueda, and I. Siutsou)

    3rd Galileo–Xuguangqi Meeting, Beijing, China, 11–15 October 2011

4.5. Lecture courses

1. “Relativistic kinetic theory and its applications in astrophysics and cosmology”, 4 lectures

   (G.V. Vereshchagin)

   IRAP Ph.D. Erasmus Mundus September school, Nice, 2 – 20 September, 2013.

2. “Relativistic Boltzmann equations”, 2 lectures

   (G.V. Vereshchagin)

   Second Bego Rencontre, IRAP Ph.D. Erasmus Mundus school, Nice, 16 – 31 May, 2013.

3. “First light from Gamma Ray Bursts”, 3 lectures

   (G.V. Vereshchagin)

   IRAP Ph.D. Erasmus Mundus September school, Nice, 3 – 21 September, 2012.

4. “Relativistic kinetic theory and its applications in astrophysics and cosmology”, 5 lectures

   (G.V. Vereshchagin)

   XV Brazilian School of Cosmology and Gravitation, Mangaratiba - Rio de Janeiro – Brazil, August 19 - September 1, 2012.

5. ”Pair plasma in GRBs and cosmology”

   (G.V. Vereshchagin)

   2 lectures, IRAP Ph.D. Erasmus Mundus September school, 12 – 23 September, 2011, University of Nice Sophia Antipolis, Nice, France.

6. “Relativistic kinetic theory and its applications in astrophysics and cosmology”

   (G.V. Vereshchagin)

   Lecture course for International Relativistic Astrophysics PhD, Erasmus Mundus Joint Doctorate Program from the

   European Commission, September 6-24, 2010, University of Nice Sophia Antipolis, Nice, France.

7. “Relativistic kinetic theory and its applications”, IRAP Ph.D. lectures

   (G.V. Vereshchagin)

   February 1-19, 2010, Observatoire de la Cote d’Azur, Nice, France.

8. Inflationary Constraints and reionization

   (S. Pandolfi)

   IRAP Ph.D. Lectures in Nice, Observatoire de la Cote d'Azur, 12-16 February 2010

5. APPENDICES

A. On Thermalization of Electron-Positron-Photon Plasma

A.1. INTRODUCTION

Degenerate relativistic plasmas are common is astrophysics. For instance, white dwarfs are supported by pressure of degenerate electron gas, while pressure in neutron stars is dominated by degenerate neutrons. Photon gas in thermal equilibrium is a classical example of a quantum system, where occupation numbers of energy levels are infinitely increasing towards lower energies Landau and Lifshitz (1980). Kinetic description of such systems out of equilibrium necessary include Bose enhancement and Pauli blocking, see Landau and Lifshitz (1981).

Relaxation of optically thick electron-positron plasma to thermal equilibrium has been considered in Aksenov et al. (2007, 2009). There relativistic Boltzmann equations with exact QED collision integrals taking into account all relevant two-particle (Bhabha scattering, Møller scattering, Compton scattering, pair creation and annihilation) and three-particle (relativistic bremsstrahlung, three photon annihilation, double Compton scattering, and radiative pair production) interactions were solved numerically. It was confirmed that a metastable state called *"kinetic equilibrium"* (Pilla and Shaham, 1997) exists in such plasma, which is characterized by the same temperature of all particles, but nonnull chemical potentials. Such state occurs when the detailed balance of all two-particle reactions is established. It was pointed out that direct and inverse three-particle interactions become relevant when kinetic equilibrium has been reached. These three-particle interactions are shown to be essential Aksenov et al. (2007) in bringing electron-positron plasma to thermal equilibrium, as they are particle non-conserving processes. This work was extended considering creation of electron-positron pairs out of the vacuum in external electric field in Benedetti et al. (2013).

In Aksenov et al. (2010) relaxation timescales for optically thick electron-positron plasma in a wide range of temperatures and proton loadings were computed numerically using the kinetic code developed in Aksenov et al. (2007, 2009). These timescales were previously estimated in the literature by order of magnitude arguments using the reaction rates of the dominant processes (Gould, 1981; Stepney, 1983). It was shown that these numerically obtained timescales differ from previous estimations by several orders of magnitude.

In all these works Boltzmann statistics of particles was adopted. However, it is well known that electrons, positrons and photons fulfill quantum Fermi-Dirac and Bose-Einstein statistics, respectively. Accounting for correct particle statistics is essential at relativistic temperatures since even thermal relativistic plasma has non negligible degree of degeneracy. Indeed, the average occupation number can characterize the degree of degeneracy in relativistic plasma. In ultrarelativistic limit in thermal equilibrium this averaged occupation numbers are equal to 0.368 for photons, and 0.087 for electrons and positrons. In plasma out of equilibrium degeneracy can be much higer. This requires the change of reaction rates considered firstly in Uehling and Uhlenbeck (1933); Uehling (1934).

The role of relativistic degeneracy in electron-positron plasma was studied in Avetisian et al. (1988) for the process of one-photon pair creation and annihilation. This process is possible in ultradense plasmas due to collective effects leading to effective refraction index n in dispersion relation for photons. The problem of propagation of electromagnetic perturbations in highly degenerate nonrelativistic and relativistic plasmas was addressed in a number of papers El-Taibany and Mamun (2012); Sadiq et al. (2014) by application of quantum magnetohydrodynamic approach. Possible formation of solitons was found and their properties investigated. However, to the best of our knowledge, the role of relativistic degeneracy in pair plasma in establishing thermal equilibrium has never been studied from kinetic point of view. In this paper we bridge this gap.

In this paper we consider relaxation of nonequilibrium optically thick pair plasma to complete thermal equilibrium by integrating numerically relativistic Boltzmann equations with exact QED two-particle and three-particle collision integrals. Quantum nature of particle statistics is accounted for in collision integrals by the corresponding Bose enhancement and Pauli blocking factors.

We point out that unlike classical Boltzmann equation for binary interactions such as scattering, more general interactions are typically described by four collision integrals for each particle that appears both among incoming and outgoing particles.

We generalize previous works on thermalization of uniform isotropic neutral pair plasma. In addition to collision integrals for two-particle interactions expressed through QED matrix elements we take into account also three-particle interactions in the same way. Plasma degeneracy is accounted for by quantum corrections to collision integrals with the corresponding Pauli blocking and Bose enhancement factors. We describe our numerical scheme and provide some preliminary results. Conclusions follow.

A.2. DEGENERACY OF PLASMA AND ITS INFLUENCE ON THE KINETICS

As it was already mentioned, both fermion and boson presence in the plasma provide corrections to the rates of processes involving these particles. Its relative importance can be estimated by the degeneracy parameter (Groot et al., 1980, p. 352) defined as $D = \frac{1}{n\lambda_{th}^3}$, where n is number density of particles, $\lambda_{th} = \frac{c\hbar}{kT}$ is the thermal wave-length, k is Boltzmann constant, T is temperature, $\hbar = h/(2\pi)$, h is Planck constant. In Fig. A.1 on the number density–energy density diagram for relativistic electron-positron plasma we show nondegenerate ($D > 1$) and degenerate ($D < 1$) regions. It is clear then that plasma near thermal equilibrium can be degenerate and inclusion of Bose enhancement and Pauli blocking coefficients is important in studying its kinetics.

A.2.1. Interactions and Equilibrium

Kinetic equilibrium Rybicki and Lightman (1979); Pilla and Shaham (1997) is defined as the state with vanishing difference between the rates of direct and inverse interactions for each of the two-particle processes. Such state is characterized by two parameters: common temperature of all particles T and non-null chemical potential μ. Combining detailed balance conditions in

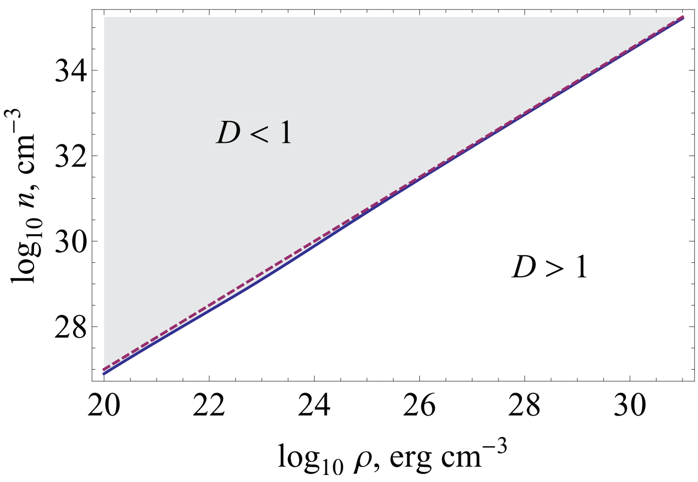

Figure A.1.: Number density-energy density diagram of relativistic electron-positron plasma. Solid curve shows critical particle density $n_{cr}(\rho)$ in thermal equilibrium with chemical potential $\xi = 0$. Dashed line corresponds to transition from nondegenerate $D > 1$ to degenerate $D < 1$ plasma.

two-particle interactions, we arrive to Aksenov et al. (2009)

$$\theta = \theta_+ = \theta_- = \theta_\gamma, \qquad \xi = \xi_\gamma = \xi_+ = \xi_-, \tag{A.2.1}$$

where $\theta = \dfrac{kT}{m_e c^2}$ is dimensionless temperature and $\xi = \dfrac{\mu}{kT}$ is dimensionless chemical potential of components.

In fact, the chemical potential in kinetic equilibrium is constrained by the condition $\xi \leq 0$. The equality in this relation implies that there is a critical number density n_{cr} given by $\xi = 0$. Since in two-particle processes the total number of particles (number density) is conserved, for $n > n_{cr}$ Bose condensation of photons is expected. However, in reality three-particle interactions do change the number of particles bringing the system to thermal equilibrium with $\xi = 0$ Khatri et al. (2012).

Thermal equilibrium is defined as the state with vanishing difference between the rates of direct and inverse interactions of all processes. It was shown in Aksenov et al. (2007) that in electron-positron plasma two-particle processes are insufficient to bring the non-equilibrium system to thermal equilibrium. The necessary condition for reaching thermal equilibrium is detailed balance in three-particle processes. Provided that kinetic equilibrium is

Table A.1.: Particle interactions in the pair plasma.

Two-particle processes	**Three-particle processes**
Compton scattering	Double Compton
$e^{\pm}\gamma \longrightarrow e^{\pm\prime}\gamma'$	$e^{\pm}\gamma \longleftrightarrow e^{\pm\prime}\gamma'\gamma''$
Coulomb, Møller and Bhabha scattering	Bremmstrahlung
$e_1^{\pm}e_2^{\pm} \longrightarrow e_1^{\pm\prime}e_2^{\pm\prime}$	$e_1^{\pm}e_2^{\pm} \longleftrightarrow e_1^{\pm\prime}e_2^{\pm\prime}\gamma$
$e^{+}e^{-} \longrightarrow e^{+\prime}e^{-\prime}$	$e^{+}e^{-} \longleftrightarrow e^{+\prime}e^{-\prime}\gamma$
Creation/annihilation	Three-photon annihilation
$e^{+}e^{-} \longleftrightarrow \gamma_1\gamma_2$	$e^{+}e^{-} \longleftrightarrow \gamma_1\gamma_2\gamma_3$
	Pair creation/annihilation
	$\gamma_1\gamma_2 \longleftrightarrow e^{+}e^{-}\gamma'$
	$e^{\pm}\gamma \longleftrightarrow e^{\pm\prime}e^{+}e^{-}$

established, this condition constrains the chemical potential to vanish, $\xi = 0$. This state is the state of complete thermal equilibrium, and it is characterized by temperature θ only.

A.3. BOLTZMANN EQUATIONS

In uniform electron-positron plasma relativistic Boltzmann equations for distribution functions f_α have the following form (Aksenov et al., 2007):

$$\frac{d}{dt} f_\alpha(\mathbf{p}, t) = \sum_q \left(\eta_\alpha^q - \chi_\alpha^q f_\alpha(\mathbf{p}, t) \right), \tag{A.3.1}$$

where $f_\alpha(\varepsilon)$ are distribution functions of particle species α, normalized as $n_\alpha(t) = \int f_\alpha(\vec{p}, t) d^3\vec{p}$, n_α are the corresponding number densities, the sum enumerated by index q is taken over all two- and three-particle processes q listed in Table A.1, η_α^q and χ_α^q are, respectively, emission and absorption coefficients.

Not coming into details of calculations of two-particle collision integral, that can be found in textbooks, for example Groot et al. (1980), we just mention the important property of three-particle interactions. As the same particle specie can appear in both sides of of three-particle reaction, collision integrals appear to have *four* different terms corresponding to absorption and emission of the particle in a given quantum state in both direct and inverse reaction. Generally speaking, *such four terms should be present in collision integral of any reaction for a particle specie which is present both among incoming and outgoing particles, unless the process is a scattering* (in such a case direct and inverse reaction are the same reaction from quantum point of view and it should not be taken twice). This statement is valid for arbitrary number of incoming and outgoing particles. It is not limited to QED but applies to any quantum field theory in general.

All three-particle QED processes listed in Table A.1, with exception of three-photon annihilation, are indeed represented by four terms in collision integrals. Such four terms for double Compton scattering with corresponding symmetrization factors were considered by Chluba Chluba (2005). It should be noted, that the detailed balance conditions may be obtained Lightman (1981); Thorne (1981) with only two terms in collision integrals. However, the structure of all four coefficients is different, and their presence in collision integral is essential.

The rates of reactions can be expressed from QED matrix elements squared, that for double Compton scattering is given by Eqs. (3), (9), (10) of Mandl and Skyrme (1952). For relativistic bremsstrahlung it can be found in Appendix B of Haug and Nakel (2004). Matrix elements for all other processes of Tab. A.1 were obtained from the ones of double Compton scattering and of relativistic bremsstrahlung by the substitution law, given in (Jauch and Rohrlich, 1976, Sec. 8.5). For inverse three-particle interaction we use the detailed balance condition to find the rates of reactions from direct ones. Then collision integral of any of three-particle processes is a seven-dimensional integral in momentum space. In the next Section we show how such integral is computed numerically on finite grid.

A.4. THE NUMERICAL SCHEME

The main difficulty arising in computation of collision integrals in comparison with previous works Aksenov et al. (2007, 2009, 2010) is that particle emission and absorbtion coefficients contain not only distribution functions of incoming particles, but also those of outgoing particles. Therefore we adopt a different approach which we refer to as "*reaction-oriented*" instead of "particle-oriented" one used earlier.

The phase space is divided in zones. Introducing variables "kinetic energy" ε–"cosine of polar angle" μ–"azimuthal angle" ϕ, corresponding to spherical symmetry of the problem, we define zones as spherical layers corresponding to intervals in energy with arbitrary angles. Emission and absorption coefficients in the interaction of particles from different zones are obtained by integration of corresponding collision integrals over them. The corresponding integrals are replaced by sums on the grid of angles. When energies of incoming particles are fixed on the grid, the energies of outgoing particles are generally not on the grid. Hence redistribution of two final particles is adopted, each over two adjacent zones. It enforces the exact number of particles and energy conservation in each two-particle process, as well as corresponding change of particle number and energy conservation in each three-particle process.

The redistribution of final particles should also satisfy requirements of quantum statistics. Therefore if a process occurs for fermion, when final particle should be distributed over the quantum states which are fully occupied, such process is forbidden. Thus we introduce the Bose enhancement/Pauli blocking coefficients in the reaction rates as minimum of the two values corresponding to zones where the final particles are redistributed to.

The sums over angles in collisional integrals can be found once and for all at the beginning of the calculations. We then store in the program for each set of the incoming and outgoing particles the corresponding terms and redistribution coefficients.

Representation of discretized collisional integral for number density Y_a^I of particle I in energy zone a in two- and three-particle processes $I + II \rightleftarrows III + IV$ and $I + II \rightleftarrows III + IV + V$ is then

$$\begin{aligned}\frac{dY_a^I}{dt} = -\sum A \times Y_a^I Y_b^{II} \times \left[1 \pm \frac{Y_c^{III}}{\bar{Y}_c^{III}}\right]\left[1 \pm \frac{Y_d^{IV}}{\bar{Y}_d^{IV}}\right] + \\ \sum B \times Y_c^{III} Y_d^{IV} \times \left[1 \pm \frac{Y_a^{I}}{\bar{Y}_a^{I}}\right]\left[1 \pm \frac{Y_b^{II}}{\bar{Y}_b^{II}}\right] \\ -\sum C \times Y_a^I Y_b^{II} \times \left[1 \pm \frac{Y_c^{III}}{\bar{Y}_c^{III}}\right]\left[1 \pm \frac{Y_d^{IV}}{\bar{Y}_d^{IV}}\right]\left[1 \pm \frac{Y_f^{V}}{\bar{Y}_f^{V}}\right] + \\ \sum D \times Y_c^{III} Y_d^{IV} Y_f^{V} \times \left[1 \pm \frac{Y_a^{I}}{\bar{Y}_a^{I}}\right]\left[1 \pm \frac{Y_b^{II}}{\bar{Y}_b^{II}}\right],\end{aligned} \tag{A.4.1}$$

where $\bar{Y}_a^I$ are the number density corresponding to occupation numbers for quantum states equals unity over the zone, and constant coefficients A, B, C, D are obtained from the summation over angles in the corresponding sums representing integrated collision integrals. The full Boltzmann equation contains similar sums for all processes from Tab. A.1. Each individual term in these sums appears in the system of discretized Boltzmann equations four or five times in emission and absorption coefficients for each particle entering a given process. Then each term can be computed only once and added to all corresponding sums, that is the essence of our *"reaction-oriented" approach*.

In our method exact energy and number of particles conservation laws are satisfied. The number of energy intervals is typically 40, while internal grid of angles has 16 points in μ and 32 in ϕ. The system under consideration has several characteristic times for different processes, and therefore the resulting system of ordinary differential equations is stiff. We use Gear's method Hall and Watt (1976) to integrate the system numerically.

A.5. PRELIMINARY RESULTS AND CONCLUSIONS

To test our approach we calculate first the final state of evolution given by two-particle interactions only. Starting with total energy density $\rho = 10^{25}$ erg/cm^3 and corresponding thermal particle density, we obtain numerical equilibrium that reproduces thermal spectra for Plank and Fermi-Dirac distributions, see Figure A.2. Two discrepancies are present: small deviation in the lowest energy interval for photons and high-energy "tails" for both distributions. However, maxima of thermal distributions are reproduced very well, as well as Plank low-energy power law.

Given that result we continue the testing by introducing double Compton scattering. Switching off two-particle interactions and taking into account only double Compton scattering we obtain final numerical equilibrium spectra shown in Figure A.3. Low-energy part of photon distribution falls down faster then corresponding Plank spectrum. That can be attributed to higher effect of Bose enhancement realization in numerical scheme on three-particle interactions. Combined two-particle and double Compton reactions result in numerical equilibrium shown in Figure A.4. The picture of resulting spectra are somewhat in between of the two previous.

Detailed balance condition can be checked directly from the rates of re-

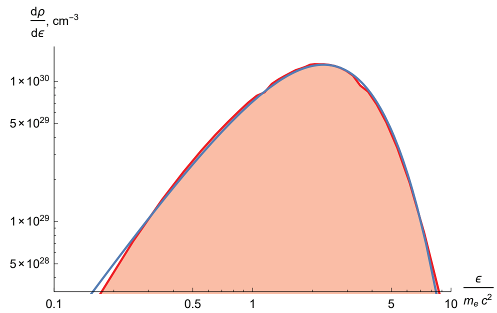

Figure A.2.: Numerical spectral energy densities of photons (left) and pairs (right) at numerical equilibrium in two-particle reactions for $\rho = 10^{25}$ erg/cm^3. Thick curves show the corresponding Plank and Fermi-Dirac distributions with the corresponding temperature.

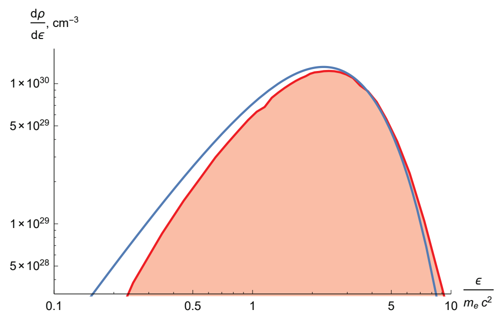

Figure A.3.: Numerical spectral energy densities of photons (left) and pairs (right) at numerical equilibrium in double Compton reaction for $\rho = 10^{25}$ erg/cm^3. Thick curves show the corresponding Plank and Fermi-Dirac distributions with the corresponding temperature.

action, illustrated by Figure A.5. Corresponding rates in direct and inverse reactions coincide in the low and middle energy parts of spectra, starting to deviate at high energy due to ”tails” mentioned above.

The partial summations over angles in three-particle processes appears to be the most time-consuming part of the numerical solution of Boltzmann equation. Typical number of points in calculations is 10^{12}.

Our preliminary numerical results indicate that the rates of three-particle interactions become comparable to those of two-particle ones for temperatures exceeding the electron rest-mass energy, see Figure A.5. Thus three particle interactions such as relativistic bremsstrahlung, double Compton scat-

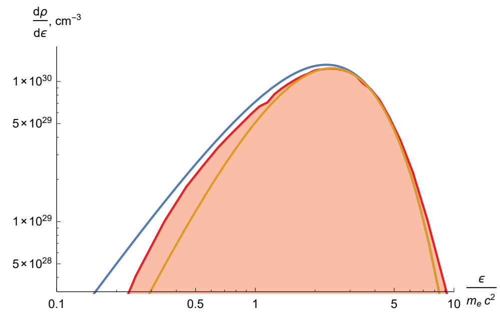

Figure A.4.: Numerical spectral energy densities of photons (left) and pairs (right) at numerical equilibrium in two-particle and double Compton reactions for $\rho = 10^{25}$ erg/cm^3. Thick blue curves show the corresponding Plank and Fermi-Dirac distributions with the corresponding temperature, and thick brown curves show the corresponding Wien and Boltzmann distributions for classical particles.

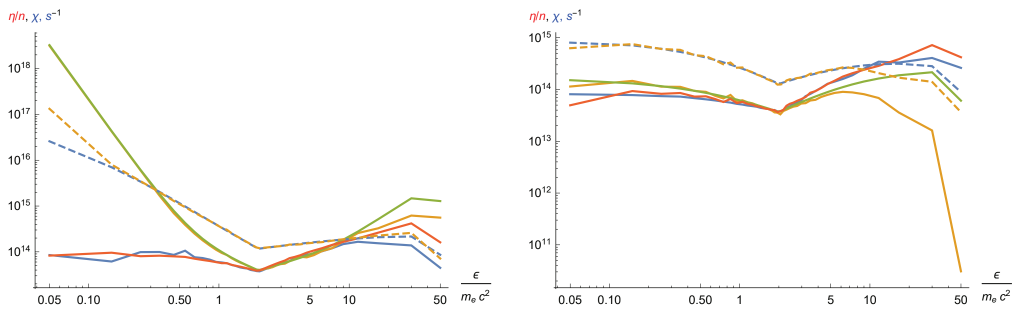

Figure A.5.: Numerical rates of double (solid line) and ordinary (dashed line) Compton scattering of photons (left) and pairs (right) at numerical equilibrium in two-particle and double Compton reactions for $\rho = 10^{25}$ erg/cm^3. Blue and brown lines denote χ and η/n in direct reaction, while green and red lines denote χ and η/n in inverse reaction, correspondingly.

tering, and radiative pair creation become essential not only for establishment of thermal equilibrium, but also for correct estimation of interaction rates, energy losses etc.

B. Thermal emission from the interaction of GRBs and supernova ejecta

B.1. Introduction

A thermal X-ray component, regularly coupled with a flare, is observed in the early afterglow of many gamma-ray bursts (GRBs), for instance, GRB 060729, 081007, 090618, 130427A, see more examples inPage et al. (2011); Sparre and Starling (2012); Starling et al. (2012); Ruffini et al. (2014a,b) . Some possible mechanisms were proposed, in the literature there is no consensus. The traditional shockwave breakout model has difficulties in generating the observed high luminosity in a distant radius Ghisellini et al. (2007); Starling et al. (2012). In ref. Friis and Watson (2013), the authors link the afterglow thermal radiation to the prompt phase via photospheric emission from the jet, but from the observation, the cooling of thermal components in the prompt phase and in the afterglow follows different trends, see an example in Fig.B.3. In ref.Pe'er et al. (2006), the thermal emission is interpreted as coming from a hot plasma "cocoon" heated by the GRB jet, but this model requires much higher Lorentz factors (on the order of 10) than the ones inferred from the observations.

In this paper, we attempt to explain the thermal component in the early afterglow by considering the interaction of GRB outflow with a baryonic shell encircling a GRB source. In the particular paradigm of induced gravitational collapse (IGC), see e.g. Ruffini et al. (2014a) and references therein, such shell is interpreted as a supernova (SN) ejecta. IGC delineates a missive star exploding as a SN in a close binary system, the companion neutron star accretes a partial SN ejecta and gravitationally collapses to a blackhole, GRB occurs simultaneously. The mechanisms of GRB energy engine and explosive dynamics in the prompt phase are described by fireshell model, see e.g.

Ruffini et al. (2010a, 2009) and references therein. Such a GRB then interacts with the rest of the supernova ejecta, accelerates and heats the supernova ejecta, as a consequence, the supernova ejecta expands mild-relativistically and emits the thermal radiation.

The content is organized as follows. In Section B.2 we solve the equations of relativistic energy-momentum conservation in order to recover the amount of thermal energy and velocity of the shell after the collision with the GRB ejecta, also the photon diffusion is considered. In Section B.3 we compute the resulting temperature and estimate the optical depth of the shell. We apply the model in Section B.4 and consider the cases of 6 GRBs, including the prototype GRB 090618. Conclusions follow.

B.2. Velocity and internal energy

Assuming the SN ejecta is a shell comprised of baryonic clumps with different sizes and thicknesses at radius R from the SN source, the clumps near the GRB are thinner than the more distant ones as a result of the accretion by the initial neutron star. The circumstances we deal with in this paper have $R > 10^{12}$ cm, two orders of magnitude larger than the distance ($< 10^{10}$ cm) between binary stars in the IGC paradigm, therefore R is also considered approximatively as the distance between the shell and the GRB Fryer et al. (2014). This shell interacts with the GRB ultra-relativistic outflow. Here we approximate the total energy of GRB outflow as the observed isotropic energy E_{iso}. In practice, the shell may not fully cover the sphere, also the GRB outflow may be jetted, so in the following computation, we only consider the interacting part, involving a portion of the shell with area $4\pi\epsilon R^2$ and the associated mass $M = \epsilon M_s$, the energy of GRB outflow interacting with this portion of shell $E = \epsilon E_{iso}$, where ϵ is a fractional factor and M_s is a mass of the spherical shell. For simplicity, in the following text, when we mention the shell, it means the interacting part of the shell.

B.2.1. Interaction

Interaction transfers energy and momentum from the GRB outflow to the clumps of the shell. Energy-momentum conservation reads

$$E + Mc^2 = \left(Mc^2 + W\right)\Gamma, \tag{B.2.1}$$
$$\frac{E}{c} = \left(M + \frac{W}{c^2}\right)\Gamma v, \tag{B.2.2}$$

where $\Gamma = \left[1 - (v/c)^2\right]^{-1/2}$ is the Lorentz factor of radial motion of the shell, c is the speed of light, W is internal energy. These equations can be used to find the internal energy and the velocity of the shell after the interaction. If the shell remains opaque, the internal energy of the shell is transformed into its kinetic energy resulting in acceleration. At the phase of acceleration the radial momentum is not conserved, and equation (B.2.2) in the above set cannot be used. The final velocity after the acceleration phase can be found from the energy conservation alone, namely from equation (B.2.1). For having concise expressions, we neglect the initial energy and momentum of the shell, which only affects less than 5% and 12% of the temperature and mass respectively for our cases.

In order to solve equations (B.2.1) and (B.2.2) we introduce the new variables

$$\eta = \frac{E}{Mc^2}, \qquad \omega = \frac{W}{Mc^2}, \qquad u = \Gamma\frac{v}{c} \tag{B.2.3}$$

we rewrite the energy-momentum conservation

$$\eta = (\omega + 1)\sqrt{u^2 + 1} - 1, \tag{B.2.4}$$
$$\eta = (\omega + 1)\, u. \tag{B.2.5}$$

The solution to this system reads

$$u = \frac{\eta}{\sqrt{1 + 2\eta}}, \qquad \frac{W}{E} = \frac{\omega}{\eta} = \frac{1}{u} - \frac{1}{\eta}. \tag{B.2.6}$$

In nonrelativistic and ultrarelativistic asymptotics, respectively, the solution

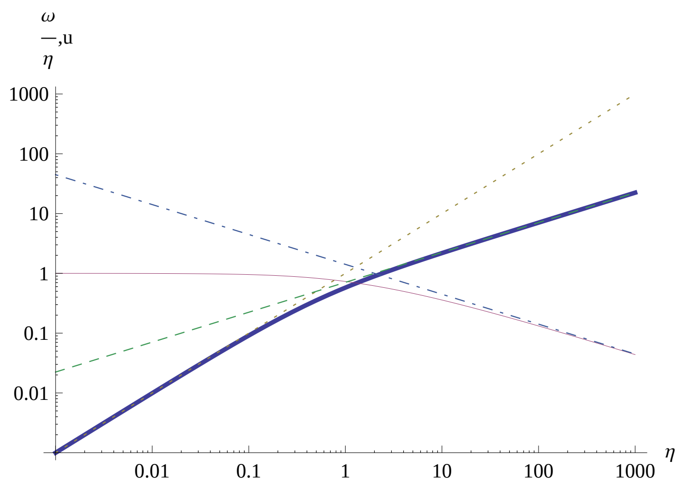

Figure B.1.: Two functions are shown: the dimensionless velocity parameter $u = \Gamma v/c$ of the shell after the interaction with photons (thick), as function of the parameter $\eta = E/(Mc^2)$, as well as the ratio between the internal energy and the initial energy in photons (thin), $\omega/\eta = W/E$, as function of the same parameter η. Dotted (dashed) line shows the nonrelativistic (ultrarelativistic) asymptotics for u, while the dash-dotted line shows the ultrarelativistic asymptotics for W/E.

becomes

$$u \simeq \frac{v}{c} \simeq \eta \ll 1, \qquad \omega \simeq \eta, \tag{B.2.7}$$

$$u \simeq \Gamma \simeq \sqrt{\frac{\eta}{2}} \gg 1, \qquad \frac{\omega}{\eta} \simeq \sqrt{\frac{2}{\eta}}. \tag{B.2.8}$$

This solution is illustrated in Figure B.1. These results imply the following. On the one hand, when the energy in photons is much less than the rest mass of the shell, $E \ll Mc^2$, most of the energy is transferred into internal energy $W \simeq E$, and the resulting velocity of the shell is nonrelativistic, $v/c \simeq E/(Mc^2)$. On the other hand, for $E \gg Mc^2$ the transfer of momentum is inefficient. We have $\Gamma \simeq \sqrt{E/(2Mc^2)}$ and $W/(Mc^2) \simeq \sqrt{2Mc^2/E}$. The shell is accelerated to ultrarelativistic velocity, but some energy goes into internal energy as well. This internal energy will then be transferred into kinetic one during the acceleration phase.

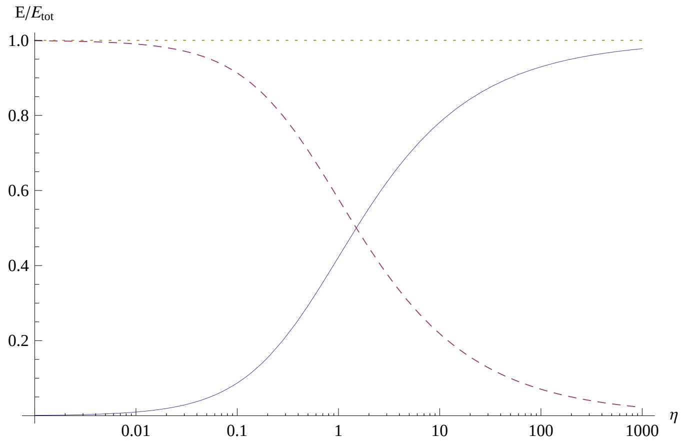

Figure B.2.: The ratio between internal (dashed) and kinetic (solid) energy to initial energy (dotted) after the interaction. In nonrelativistic case with $\eta \ll 1$ all the energy of the GRB ejecta is transformed into internal energy (heat) of the baryonic shell. In ultrarelativistic case with $\eta \gg 1$ the energy of the GRB ejecta is transformed mostly in kinetic energy of the shell.

In Figure B.2 we present the ratio between internal and kinetic energy of the shell to initial energy of the system, composed of the GRB ejecta and the baryonic shell, computed after the interaction. One can see that in the nonrelativistic case with $E \ll Mc^2$ all the energy of the GRB ejecta is transformed into internal energy of the baryonic shell. In contrast, in ultrarelativistic case with $E \gg Mc^2$ the energy of the GRB ejecta is transformed mostly in kinetic energy of the shell. Notice the striking similarity with the corresponding diagram for the energies emitted in the P-GRB and in the extended afterglow, in units of the total energy of the plasma within the fireshell model, see e.g. Figure 5 in Ruffini et al. (2009).

B.2.2. Acceleration

If the shell is spherically symmetric, assuming all energy is ultimately transferred into kinetic energy of the shell ($W \ll Mc^2$) from the energy conservation, equation (B.2.1), one has

$$\Gamma - 1 = \frac{E}{Mc^2} = \frac{E_{iso}}{M_s c^2} = \eta, \tag{B.2.9}$$

Again, in nonrelativistic and ultrarelativistic asymptotics, respectively, one finds

$$\frac{v}{c} \simeq \sqrt{2\eta}, \qquad \eta \ll 1, \tag{B.2.10}$$

$$\Gamma \simeq \eta, \qquad \eta \gg 1. \tag{B.2.11}$$

As a matter of fact, the values of velocity (Lorentz factor) after the interaction are always smaller than the final values, reached after the acceleration phase.

Note that in the derivation in this Section we never used the condition $W \ll Mc^2$. This condition is valid in GRBs context as baryons after collision never reach relativistic temperatures, $kT \ll m_p c^2$.

B.3. Temperature and optical depth

The comoving temperature of the shell T_c is found from the condition $W = 4\pi\epsilon a R^2 l T_c^4$. The observed temperature for the source with angle ϑ with respect to the line of sight is

$$T = \frac{T_c}{\Gamma\left(1 - \beta\cos\vartheta\right)} = \frac{\sqrt{1+2\eta}}{1+\eta-\eta\cos\vartheta}\left(\frac{\omega}{\eta}\frac{F}{al}\right)^{1/4}, \tag{B.3.1}$$

where $F = \epsilon E_{iso}/\left(4\pi\epsilon R^2\right) = E_{iso}/\left(4\pi R^2\right)$ is isotropic energy flux. This expression gives, respectively, in nonrelativistic and ultrarelativistic asymptotics

$$T \simeq \left(\frac{F}{al}\right)^{1/4}, \qquad E \ll Mc^2, \tag{B.3.2}$$

$$T \simeq 2\Gamma\left[\frac{F}{al}\left(\frac{2}{\eta}\right)^{1/2}\right]^{1/4}, \qquad E \gg Mc^2, \tag{B.3.3}$$

where in eq. (B.3.3) we assume that the source is on the line of sight.

The shell will emit photons from its photosphere. The case of ultrarelativistic photosphere with $\Gamma \gg 1$ is treated in Ruffini et al. (2013b), see also recent review Vereshchagin (2014). From now on assume that the photosphere is not ultrarelativistic. We still retain fully relativistic expression (B.3.1). The validity of the treatment in the previous section requires that the shell is opaque, namely its optical depth τ is large. The latter is given by

$$\tau = \sigma n l = \frac{\sigma M}{4\pi\epsilon R^2 Z m_p} \gg 1, \tag{B.3.4}$$

where σ is Thomson cross section m_p is proton mass, Z is atomic number. Further acceleration of the shell, considered above, is possible only of the shell is still opaque during the acceleration phase.

The emission from the photosphere occurs due to radiative diffusion from the interior of the shell. The emission lasts until all energy diffuses out from the shell. The characteristic diffusion time form a clump with a given thickness is

$$t_D = \frac{l^2}{D} = 3\tau\frac{l}{c}, \tag{B.3.5}$$

where $D = c/(3\sigma n)$ is the diffusion coefficient for photons. Since $\tau \gg 1$ we have $l \ll ct_D$. The density decrease in diffusion coefficient due to expansion of the shell can be neglected if the diffusion time is less than the dynamical time of expansion R/v, namely if

$$3\tau\frac{v}{c} \ll \frac{R}{l}. \tag{B.3.6}$$

In the opposite case one has to consider the effects of expansion and the thermal spreading of the baryonic shell after interaction with photons on the diffusion time. In any case, this effect reduces the diffusion time.

Note that equations (B.2.8) and especially (B.3.3) are relevant in the context of the fireshell model Ruffini et al. (2009) as they describe the values of the Lorentz factor of the PEMB pulse and its temperature at the moment after the collision of the PEM pulse with the baryonic remnant. The asymptotic expression (B.2.11) describes the Lorentz factor of the PEMB pulse under the condition $\eta < 10^4$.

B.4. Application

From the observation one can derive the isotropic energy via the observed flux and redshift, and by fitting the light curve and spectra, one can obtain the evolution of temperature from thermal emission, as well as the velocity of expansion. In practice, the satellites do not cover all the energy band, what we can have are only given temperatures with given duration. The *Swift*-XRT is the most widely used instrument on detecting the GRB afterglow, it covers $0.3 \sim 10$ KeV. In other words, by analyzing the data from *Swift*-XRT, we can only obtain the thermal temperature in soft X-ray band, and the corresponding duration. For example, in Fig.7 of Ruffini et al. (2014b), clearly the temperature of blackbody radiation from 196 s to 461 s is within the scope *Swift*-XRT, temperature cools along the time. Therefore here we adopt three parameters E_{iso}, t_D and u given by the observations, then we deduce the temperature using the above equations for the comparison with the observational one. It is convenient to rewrite equation (B.3.1) using equations (B.2.6) and (B.3.5) as

$$\begin{aligned} T &= X(u)F^{1/2}\left(a\frac{m_p c^2}{3\sigma}Zct_D\right)^{-1/4} \\ &\simeq 2.13X(u)E_{iso,52}^{1/2}R_{13}^{-1}t_{100}^{-1/4}Z_{10}^{-1/4}\text{keV}, \end{aligned} \tag{B.4.1}$$

where $E_{52} = E/10^{52}$erg, $R_{13} = R/10^{13}$cm, $t_{100} = t_D/100$s, $Z_{10} = Z/10$,

$$X = \frac{1}{\sqrt{u}}\frac{1}{\sqrt{1+u^2} - u\cos\vartheta}\left(\frac{u+\sqrt{1+u^2}-1}{2u^2+2u\sqrt{1+u^2}+1}\right)^{1/4} \tag{B.4.2}$$
$$= \begin{cases} u^{-1/4}, & u \ll 1, \\ 2^{3/4}u^{1/4}, & u \gg 1 \end{cases}$$

is a slowly varying function of u which decreases as $u^{-1/4}$ for $u < 1$ and increases as $u^{1/4}$ for $u > 1$, with $X(u = 1, \vartheta = 0) \approx 1.7$.

In fact, in most cases thermal component in soft X-ray contains small fraction of the GRB energy, see table B.1. The baryonic shell may not necessary be spherically symmetric as we assumed, clumps have different thickness. The thinner clumps have earlier emission with higher temperature, and vice versa. The small ratio between thermal energy in X-ray and GRB energy can be explained assuming small ratio of the total surface of relatively thin baryonic clumps to the total spherical area at that radius. Naturally in the IGC paradigm, these thin clumps are accumulated around the accreting source, the progenitor of GRB. Some similar ideas in treatment of thermal emission in GRBs are discussed in Badjin et al. (2013); Pe'er et al. (2006).

B.4.1. The case of GRB 090618

A thermal component has been inferred from observations of the early X-ray afterglow in GRB 090618. Following Izzo et al. (2012) and Ruffini et al. (2014a) we summarize the parameters:

- isotropic energy of GRB $E_{iso} = 2.9 \times 10^{53}$ erg,
- observed duration of the thermal component in Episode 3, $t = 150$ s,
- observed temperature T is decreasing from 1 keV to 0.3 keV.

Two alternative models were presented to explain this component: a relativistic wind model (e.g. Friis and Watson (2013)) and a mild-relativistic shell model Ruffini et al. (2014a). Here we focus on the second one. In the model described above we neglected the initial kinetic energy of the shell and assumed that the interaction between the GRB ejecta and the shell results in two effects: heating of the shell and its acceleration. The parameters of the shell were inferred from observations Ruffini et al. (2014a):

- radius $R = 10^{13}$ cm,
- velocity $0.75 < v/c < 0.89$.

These parameters are quite close to those discussed above. The observed trend of decreasing temperature can be explained by the expansion of the shell, neglected in our simplified treatment in Section B.3. Given relativistic velocities of the shell, neither nonrelativistic nor ultrarelativistic approximations can be used to infer the parameters of the clump. Instead, the full analytic solution (B.2.6) must be used. So from equation (B.2.6) we determine

$$3.0 < \eta < 8.1,$$

then knowing the energy in the thermal component the mass is

$$0.02 M_\odot < M_s < 0.05 M_\odot,$$

then the optical depth of the clump is found from equation (B.3.4), and it is

$$1.3 \times 10^4 < Z\tau < 3.4 \times 10^4,$$

then the length of the clump is obtained from equation (B.3.5) and it gives

$$4.4 \times 10^7 \text{cm} < \frac{l}{Z} < 1.2 \times 10^8 \text{cm}.$$

Again, with these parameters the constraint equation (B.3.6) is satisfied.

It is clear from Figure B.2, that with these parameters the energy of GRB ejecta is divided nearly equally between kinetic energy of the shell and its internal energy.

Assuming the shell is composed of hydrogen with $Z = 1$ the temperature of the shell is 8.62 keV, which is a factor 9 higher than the observed one. Instead, if the shell is composed of radioactive elements produced at the supernova explosion, the atomic number should be around $Z = 26$, which gives for the temperature a much closer value to the one observed, namely 3.8 keV. Clearly, in our simplified treatment this coincidence is remarkable. In fact, we assumed that the temperature and density distribution in the shell are uniform. However, realistic temperature and density profiles will give smaller temperature at the photosphere, compared to the temperature in the interior of the shell.

Our model predicts that in non-relativistic case ($\eta \lesssim 1$) practically all kinetic energy of the GRB outflow is transferred into internal energy of the baryonic shell, namely $W \simeq E$. In the case of GRB 090618 we have $W \simeq E/2$. However, the total energy in the thermal component is estimated to be only $E_{BB} = 2.1 \times 10^{49}$ erg. This can be explained if only a small fraction ($\epsilon \simeq 0.005$) of the GRB ejecta actually interacts with thin baryonic clumps. Recall that our model is also valid without imposing the spherical symmetry. It implies that the mass of thin baryonic material around the GRB source is $M \sim 10^{-4} M_{\odot}$. This is the lower limit to the total mass of baryonic material around the source. The rest of the material can be much more massive and thicker.

If the GRB ejecta is spherical, interaction of this ejecta with the main part of the SN remnant will increase the internal energy of the ejecta, thus contributing to the bolometric luminosity of the optical SN light curve. This effect can explain why the nickel mass inferred in GRB-SN systems is systematically higher than in other Ibc type SN.

In the IGC paradigm, accretion contributes to the emission of first seconds, while in the fireball model, photospheric emission could exist in the beginning. In both cases, as a result, thermal emission could be detected if its fluence is sufficient. For GRB 090618, a decreasing thermal temperature within

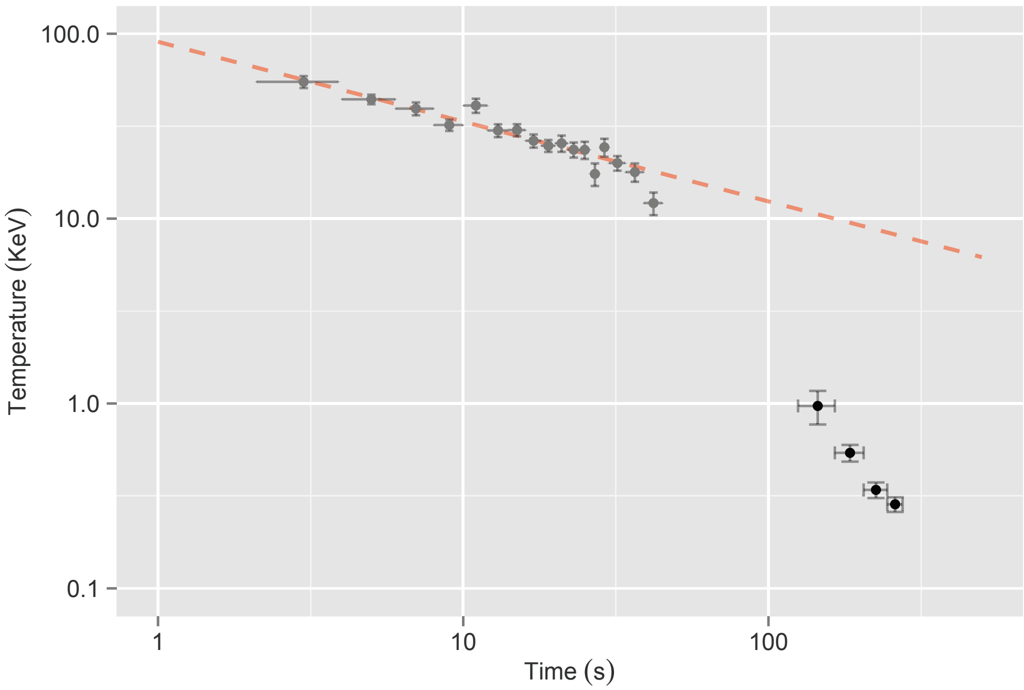

Figure B.3.: Temperature of the thermal component in the prompt emission (grey points) and in the afterglow (black points). The single power-law fitting of the temperature in the prompt emission clearly shows its extrapolation lays much higher than the temperature in the afterglow. The value of temperature comes from Ruffini et al. (2014a); Izzo et al. (2012).

the first 50 s is observed, and we extrapolate this temperature by a single power-law till hundreds of seconds and find that the extrapolated value is much higher than the observed one, as shown in Figure B.3. This consideration Begue (2014) supports that the thermal component in the afterglow has a different origin, as in this article we adopt the proposal from IGC paradigm, generated by the collision of GRB afterglow and a baryonic shell.

GRB	z	E_{iso} ($\times 10^{52}$ erg)	R_c ($\times 10^{13}$ cm)	$t_{d,c}$ ($\times$100s)	v ($\times 10^{10}$ cm/s)	$T_{obs,c}$ (KeV)	T (KeV)	E_{bb} ($\times 10^{50}$ erg)	ϵ	M (10^{-4} $M_{\odot}$)
060218	0.033	0.0053	0.039	25.40	0.040	0.18	5.18	0.063	0.12	2.6
100316D	0.070	0.0060	0.093	5.53	0.39	0.19	1.83	0.095	0.16	0.4
081007	0.53	0.15	0.13	0.45	2.15	0.47	5.45	0.42	0.028	0.1
060729	0.54	1.60	0.58	1.45	2.34	0.32	2.62	4.92	0.030	0.8
090618	0.54	41	1.00	0.98	2.45	0.97	4.85	24.00	0.006	1.2
130427A	0.34	140	1.20	2.65	2.40	0.50	9.77	28.68	0.002	4.0

Table B.1.: Observational parameters and deduced temperature of 5 supernova associated GRBs, subscript ′c′ presents the comoving frame. Observational data is taken from Ruffini et al. (2014a,b); Izzo et al. (2012); Starling et al. (2012).

B.4.2. More Examples

In order to have a more general comparison, we adopt 5 more GRBs with isotropic energy from 10^{49} erg to 10^{54} erg, all these GRBs show supernova signal either from the spectral aspect or a bump in the optical lightcurve is detected. To find a thermal component, two conditions are required due to the capacity of satellites, that the flux of thermal component is sufficient and the ratio of thermal flux versus total flux is prominent, the thermal flux within the observed duration t_D adopted in this article fulfills these two conditions. With this consideration, t_D should be shorter than the real thermal emission time, however, a great fraction of the total thermal energy is released during t_D, it's reasonable to employ the observed t_D as an approximation.

Table (B.1) shows the observational parameters and the temperature deduced from equation (B.4.1), and the ratio (defined as ϵ) of observed total thermal energy E_{bb} in Episode 3 versus isotropic energy, in Figure B.4, we demonstrate and fit the E_{iso} and E_{bb} relation, which shows approximately $E_{bb} \propto E_{iso}^{0.6}$. We notice that in reality, radius R and temperature T are not constants, common pattern are found as radius increases while temperature decreases within the duration t_D. But some GRBs in our sample do not provide

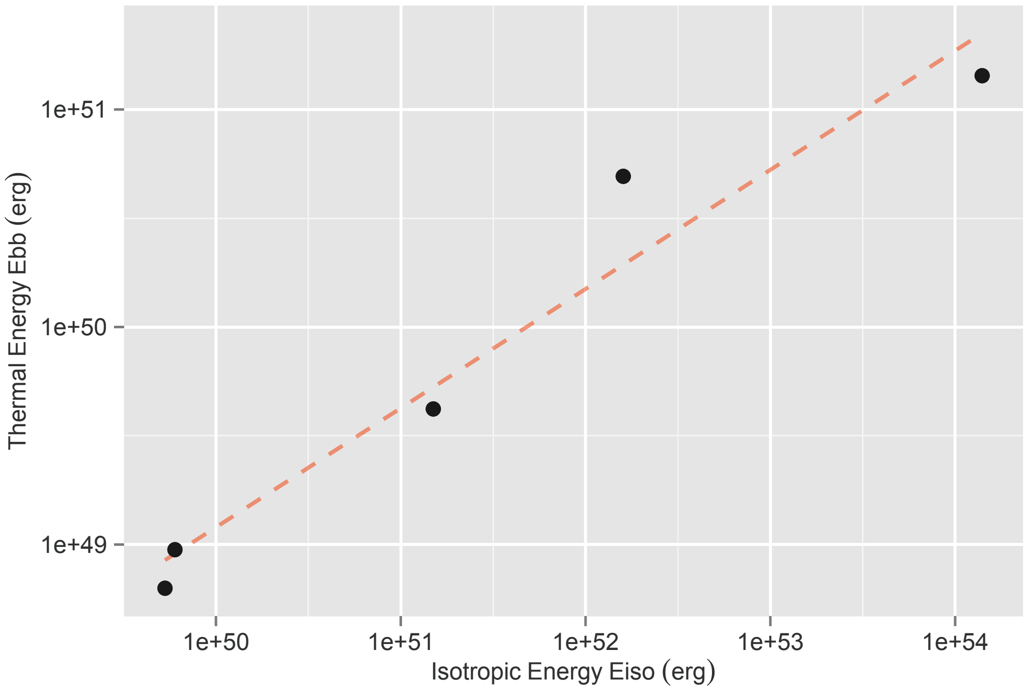

Figure B.4.: Isotropic energy versus thermal energy, dashed line displays a simple power-law fitting of the GRBs in Table B.1, the power-law index is 0.6, as $E_{\mathrm{bb}} \propto E_{\mathrm{iso}}^{0.6}$.

adequate data for having precise time resolved analysis, instead, averaged values are given for all the 5 GRBs.

The temperature deduced are universally higher than the observed ones, and a trend that the deduced temperature increases along with the observed temperature can be found. These results are within our expectation, because equation (B.4.1) depicts the average temperature, measured in the interior of the shell. In reality, a temperature distribution profile should be taken into consideration, and a steep gradient of temperature always exists at the outer edge which emits thermal photons. Detailed simulation will be given elsewhere.

B.5. Conclusions

The observed parameters of the thermal component in the Episode 3 of emission in GRB 090618 are reproduced by considering the interaction of the GRB outflow with the thin baryonic shell having mass of $10^{-4}M_{\odot}$ and thickness of 10^8 cm. In addition, thermal temperature of 5 more GRBs, namely 060218, 100316D, 081007, 060729, 130427A, with observed thermal emission in the early afteglow were analysed, and the parameters of associated baryonic shells are obtained.

Our results suggest an alternative explanation of the observed thermal signal in the early afterglow of some GRBs. While in Friis and Watson (2013) this signal is associated with the photospheric emission from relativistic wind, in our approach this emission is due to nonrelativistic photosphere of a thin baryonic shell, energized and accelerated by the associated GRB.

C. Relativistic kinetic theory and its applications

C.1. Introduction

Kinetic theory (KT) was born in the XIX century, the golden age of classical physics. Based on the atomic picture of a medium Boltzmann (2011) properties such as heat and electrical conductivity, as well as viscosity and diffusion found natural explanations. The term originates from the Greek where $\kappa\iota\nu\eta\sigma\iota\zeta$ means motion. In fact all these properties of the medium may be understood to be emerging from its microscopical structure and motion.

KT now has to be considered in a wider framework of statistical mechanics appearing at the end of XIX century essentially in the works of Maxwell, Boltzmann and Gibbs. It should be emphasized that the main ideas and principles of KT influenced the development of many other sciences, including the mathematics (probability theory, ergodic theory), biology (evolutionary biology, population genetics) and economics (financial markets, econophysics).

Within physics, KT is closely related to statistical physics, thermodynamics, hydro- and gasdynamics. Today one can say that the main task of kinetic theory is explanation of various macroscopic properties of a medium based on known microscopic properties and interactions. In a general context, KT is a microscopic theory of nonequilibrium systems. Indeed, all the above mentioned fields of physics such as e.g. thermodynamics assume that the medium is in its most probable microphysical state, called equilibrium. Clearly, any macroscopic manifestation of deviations from this microscopic equilibrium should be considered within KT.

The first classical applications of KT concerned gases. A successful description of ideal and nonideal gases has been reached within the framework of Newtonian mechanics. With the discovery of Special Relativity KT had to be reformulated in a Lorentz invariant fashion, to make it compatible with existence of a limiting velocity, the speed of light. Indeed, the generalization of Maxwell-Boltzmann equilibrium distributions to relativistic case was obtained already in 1911 Jüttner (1911). It soon became clear that there is another natural arena for application of KT which is plasma physics Landau (1936, 1937). The major difference between plasma and gas is the existence of long range forces, which has been accommodated by introduction of the mean field description Vlasov (1938). Formulation of relativistic KT has been completed in the 1960s and is presented in several monographs, see e.g. Synge (1957); Groot et al. (1980); Cercignani and Kremer (2002).

Since basic phenomena in the microworld are described on a quantum language, KT uses extensively quantum theory. In fact, basic principles and equations of KT may be derived from Quantum Field Theory, see Groot et al. (1980).

The purpose of these lecture notes is, however, not to review the foundations of KT that would require an entire dedicated monograph. In this paper I will only remind basic concepts of KT and introduce the necessary mathematical apparatus. The main goal is essentially to show a wide area of applications of KT, spanning from astrophysical compact objects to the whole Universe in its evolution.

C.2. Basic concepts

C.2.1. Distribution function

In classical (also relativistic) mechanics a complete description of a system composed of N interacting particles is given by their N equations of motion. In non-relativistic kinetic theory one deals with a space of positions and velocities of these particles, the configuration space. In relativistic kinetic theory it is replaced by the *phase space* $\mathcal{M}$ of positions and momenta. In principle, equivalent description of the system is given by a function $F(\Gamma)$ of $6N$ independent variables, defined on $\mathcal{M}$. An equation can be formulated for this function, called the Liouville equation, that can be written apparently in a very simple form

$$\frac{dF(\Gamma)}{ds} = 0, \tag{C.2.1}$$

where the derivative is over the proper time. However, its complexity is equivalent to the complexity of original N-body problem, and in majority of cases it cannot be addressed directly.

A tremendous simplification occurs for some systems, where N is very large. Under certain conditions, which will be discussed below in Sec. C.6, they can be described by a function defined on the 6-dimensional phase space $\mathcal{M}^6$. Such function depends only on 7 variables: 3 space coordinates, 3 momentum components, and time. In such a case the DF is called the *one particle distribution function* (DF) $f(x^\mu, p^\mu)$. This is the basic object used in statistical (probabilistic) description of a system composed of large number of particles. For brevity in what follows denote[1] the coordinates in momentum space as $x = x^\mu = (ct, \mathbf{x})$, $p = p^\mu = (p^0, \mathbf{p})$, where c is the speed of light. Notice that p^0 is not an independent variable and it satisfies the relativistic energy equation $p^0 = \sqrt{\mathbf{p}^2 + m^2c^2}$. The DF is defined such that the integral

$$N \equiv \int_{\mathcal{M}^6} f(\mathbf{p}, \mathbf{x}, t) d^3p d^3x, \tag{C.2.2}$$

gives the total number of particles. Notice that the integral is clearly Lorentz invariant. The invariance of the distribution function itself is not obvious from such a definition and will be demonstrated explicitly below in Sec. C.2.3. Then one observes that $f(x, p)d^3pd^3x$ is an average number of particles having momenta in the range $(\mathbf{p}, \mathbf{p}+d^3p)$ and coordinates in the range $(\mathbf{x}, \mathbf{x}+d^3x)$ at the moment t, and the integral (C.2.2) is taken in the whole phase space $\mathcal{M}^6$.

Notice that despite symmetrical form of $f(x, p)$ there is a conceptual difference between x and p. In particular, the integral

$$n(\mathbf{x}, t) \equiv \int_{-\infty}^{+\infty} f d^3p \tag{C.2.3}$$

is assumed to be finite, leading to certain restrictions on $f(p)$. In particular, when the DF is isotropic in momentum space, $p^2 f(|p|)$ should decrease with increasing momentum for $|p| \gg 1$ fast enough, at least faster than $1/\,|p|$; it also should not increase with decreasing momentum for $|p| \ll 1$ faster than $1/\,|p|$.

[1] In what follows Greek indices run from 0 to 3, while Latin ones run from 1 to 3. Einstein summation rule is adopted.

C.2.2. Averaging and macroscopic quantities

It is important to keep in mind that the DF defined by eq. (C.2.2) is not accessible directly to measurements. In any experiment or observation one has to deal with averaged quantities. While a microscopic state is defined on the phase space by the DF, it is useful to introduce a macroscopic quantity $A(x)$ as

$$A(x) \equiv \int_{-\infty}^{+\infty} A(x,p) d^3p. \tag{C.2.4}$$

Particle density (C.2.3) is the simplest example. By definition the macroscopic quantity does not depend on momentum, but only on coordinates and time. Such quantity may be further averaged in space or time as follows

$$\langle A \rangle_{\text{time}} (\mathbf{x}) \equiv \lim_{T\to\infty} \frac{1}{T} \int_0^T A(x)dt, \qquad \langle A \rangle_{\text{space}} (t) \equiv \lim_{V\to\infty} \frac{1}{V} \int_{\mathcal{V}} A(x) d^3x. \tag{C.2.5}$$

The averaging may also be made on finite time T and in finite volume V then the limits in front of integrals in eq. (C.2.5) are omitted.

In contrast to space and time averaging, statistical (or ensemble) averaging for a quantity $A(x,p)$ is defined as

$$\langle A \rangle_{\text{ens}} \equiv \frac{1}{N} \int_{\mathcal{M}^6} A(x,p) f(x,p) d^3p d^3x. \tag{C.2.6}$$

While experiments deal with space and time averaged quantities, theory usually works with ensemble averaged ones. The connection between macroscopic and microscopic quantities from the one hand, but also space-time averaged quantities and ensemble averaged ones from the other hand, is required. An important concept called *statistical equilibrium* requires that any macroscopically large part of the system has macroscopic physical quantities being equal to their statistical average values. For one particle DF this statement can be represented as follows

$$\frac{1}{V} \int_{\mathcal{V}} \int_{-\infty}^{+\infty} A(x,p) d^3p d^3x = \frac{\int_{\mathcal{V}} \int_{-\infty}^{+\infty} A(x,p) f(x,p) d^3p d^3x}{\int_{\mathcal{V}} \int_{-\infty}^{+\infty} f(x,p) d^3p d^3x}, \tag{C.2.7}$$

where $\mathcal{V}$ is an arbitrary macroscopic volume.

One of the most important theorems in statistical mechanics states that for *ergodic systems* the time averaged quantity should be equal to its ensemble average. In a specific case when the system is described by one particle DF it is reduced to

$$\lim_{T\to\infty} \frac{1}{T}\int_0^T A(x,p)dt = \frac{1}{N}\int_{\mathcal{M}^6} A(x,p)f(x,p)d^3pd^3x. \tag{C.2.8}$$

Note that it is difficult to prove ergodicity of a given physical system. Nevertheless, ergodicity is often assumed in practice.

C.2.3. Invariance of one particle DF

The one particle DF defined by (C.2.2) is not written in a Lorentz invariant way. However, it is an invariant, as demonstrated below following Ochelkov et al. (1979); Groot et al. (1980), see also Debbasch et al. (2001). Consider the system of particles of equal mass m with coordinates $\mathbf{x}_i(t)$ and momenta $\mathbf{p}_i(t)$. By definition, from the statistical point of view, the one particle DF is the averaged particle density in momentum space, see e.g. Debbasch and van Leeuwen (2009a), that is

$$f(\mathbf{p},\mathbf{x},t) = \left\langle \sum_i \delta^3\left[\mathbf{p}-\mathbf{p}_i(t)\right]\delta^3\left[\mathbf{x}-\mathbf{x}_i(t)\right]\right\rangle_{\text{ens}}. \tag{C.2.9}$$

In a relativistic context, it is natural to introduce an eight-dimensional one-particle phase space $\mathcal{M}^8$. In such phase space the variable p^0 is not necessarily related to $\mathbf{p}$, likewise t is not related to $\mathbf{x}$. At the end of any calculations involving $\mathcal{M}^8$ the physical results can be recovered by restricting every equation to the sub-manifold of the mass-shell where $p^0 > 0$. Introducing in this way a new quantity

$$\mathcal{F}(x,p) = 2\Theta(p^0)\delta(p^\mu p_\mu - m^2c^2)f(\mathbf{p},\mathbf{x},t), \tag{C.2.10}$$

where the term $\Theta(p^0)\delta(p^\mu p_\mu - m^2c^2)$ is Lorentz scalar, one has to show that this function is a Lorentz scalar. Recalling the identity

$$\delta\left(Z(x)\right) = \sum_i \left|\frac{dZ}{dx}\right|^{-1}\delta\left(x-x_i\right), \tag{C.2.11}$$

where x_i are the roots of the equation $Z(x) = 0$, rewrite eq. (C.2.10) using (C.2.9) as

$$\mathcal{F}(x,p) = \left\langle \sum_i \frac{1}{p_i^0(t)} \delta^3\left[\mathbf{p} - \mathbf{p}_i(t)\right] \delta\left[p - p_i^0(t)\right] \delta^3\left[\mathbf{x} - \mathbf{x}_i(t)\right] \right\rangle_{\text{ens}} . \tag{C.2.12}$$

Introducing additional integration over a delta function as

$$\mathcal{F}(x,p) = \int dt \left\langle \sum_i \frac{1}{p_i^0(t_i)} \delta\left[t - t_i\right] \delta^3\left[\mathbf{p} - \mathbf{p}_i(t_i)\right] \delta\left[p - p_i^0(t_i)\right] \delta^3\left[\mathbf{x} - \mathbf{x}_i(t_i)\right] \right\rangle_{\text{ens}} \tag{C.2.13}$$

and using the relation $ds_i = \frac{mc}{p_i^0(t_i)} dt_i$ one can show that $\mathcal{F}(x,p)$ is a scalar since

$$\mathcal{F}(x,p) = \frac{1}{mc} \int ds \left\langle \sum_i \delta^4\left[x - x_i(s)\right] \delta^4\left[p - p_i(s)\right] \right\rangle_{\text{ens}} , \tag{C.2.14}$$

where $x_i(s)$ and momenta $p_i(s)$ are trajectories in $\mathcal{M}^8$. The last expression can be understood as the ensemble averaged and time integrated Klimontovich one particle DF, see e.g. Zakharov (2000) and Sec. C.3.1 below.

C.2.4. Important macroscopic quantities

One can define an invariant quantity instead of eq. (C.2.3) as

$$j^\mu(\mathbf{x},t) \equiv c \int p^\mu f \frac{d^3p}{p^0} = c \int \mathcal{F}(x,p) p^\mu d^4p, \tag{C.2.15}$$

where both f and d^3p/p^0 are scalars. This *first moment* of the DF is the particle four-flux. Its spatial part represents usual three-vector flux $\mathbf{j}(\mathbf{x},t) \equiv c \int \mathbf{v} f d^3p$, where $\mathbf{v} = c\mathbf{p}/p^0$ is the velocity of a relativistic particle with momentum $\mathbf{p}$, $u^\mu = dx^\mu/ds$.

Analogously, the *second moment* can be constructed

$$T^{\mu\nu}(\mathbf{x},t) \equiv c \int p^\mu p^\nu f \frac{d^3p}{p^0}, \tag{C.2.16}$$

and so on. The quantity $T^{\mu\nu}$ is a symmetric tensor by construction. It represents an energy-momentum tensor of the system of particles. It should be noted that in eq. (C.2.16) only rest mass energy and kinetic energy of particles are taken into account, excluding their potential energy.

One more important quantity is entropy flux defined as

$$S^{\mu}(\mathbf{x}, t) \equiv -k_B c \int p^{\mu} f \frac{d^3 p}{p^0} \left[\log\left(h^3 f\right) - 1\right], \tag{C.2.17}$$

where two new constants appear: k_B is Boltzmann's constant and h is a dimensional parameter needed to make the argument of the logarithm dimensionless.

Unlike non-relativistic kinetic theory, in its relativistic counterpart macroscopic velocity can be defined in different ways. Two widespread definitions are due to Eckart Eckart (1940) and Landau and Lifshitz Landau and Lifshitz (1959):

$$U^{\mu}_{\mathrm{E}} \equiv \frac{c j^{\mu}}{\sqrt{j^{\mu} j_{\mu}}} \qquad \text{or} \qquad U^{\mu}_{\mathrm{LL}} \equiv \frac{c T^{\mu\nu} U_{\nu}}{\sqrt{U_{\rho} T^{\rho\sigma} T_{\sigma\tau} U^{\tau}}}. \tag{C.2.18}$$

While U^{μ}_{E} can be interpreted as the average velocity of particles, U^{μ}_{LL} can be understood as the average velocity of energy-momentum transfer.

C.3. Kinetic equation

This section follows the derivation presented in Groot et al. (1980). One can introduce a scalar quantity

$$\Delta J = \frac{1}{c} \int_{\Delta^3 \sigma} d^3 \sigma_{\mu} j^{\mu} = \int_{\Delta^3 \sigma} d^3 \sigma_{\mu} \int \frac{d^3 p}{p^0} p^{\mu} f, \tag{C.3.1}$$

where the time-like four-vector $d^3\sigma_\mu$ is an oriented three-surface element of a plane space-like surface σ, the quantity $\Delta^3\sigma$ is a small element and the last equality follows from eq. (C.2.15). In the Lorentz frame where $d^3\sigma_\mu$ is purely timelike it has components $(d^3 x, 0, 0, 0)$. In this frame

$$\Delta J = \int_{\Delta^3 \sigma} \int f\left(x, p\right) d^3 p d^3 x, \tag{C.3.2}$$

which is just an average number of world lines crossing the segment $\Delta^3\sigma$. Considering those world lines which have momenta in the range $\Delta^3 p$ around $\mathbf{p}$, one can get

$$\Delta J = \int_{\Delta^3\sigma} \int_{\Delta^3 p} f(x, p)\, d^3p d^3x. \tag{C.3.3}$$

Accepting this interpretation, consider world lines given by eq. (C.3.1) which later cross another segment $\Delta^3\hat{\sigma}$. Since there are no collisions it is possible to write

$$\int_{\Delta^3\hat{\sigma}} d^3\sigma_\mu \int_{\Delta^3 p} \frac{d^3p}{p^0} p^\mu f - \int_{\Delta^3\sigma} d^3\sigma_\mu \int_{\Delta^3 p} \frac{d^3p}{p^0} p^\mu f = 0, \tag{C.3.4}$$

or in other way

$$\int_{\Delta^3 x} d^3\sigma_\mu \int_{\Delta^3 p} \frac{d^3p}{p^0} p^\mu f = 0, \tag{C.3.5}$$

where $\Delta^3 x$ is the surface of Minkowski space element $\Delta^4 x$. Applying Gauss' theorem one gets

$$\int_{\Delta^4 x} d^4x \int_{\Delta^3 p} \frac{d^3p}{p^0} p^\mu \partial_\mu f = 0, \tag{C.3.6}$$

where $\partial_\mu = \left(c^{-1}\partial/\partial t, \nabla\right)$, $\Delta^3 x$ and $\Delta^3 p$ are some arbitrary hypersurfaces in the phase space.

The basic equation represents *time evolution* of the DF due to microscopic interactions in the system. In absence of any interactions between particles it represents continuity of the four-vector $p^\mu f$ and it follows from eq. (C.3.6) as

$$p^\mu \partial_\mu f = 0. \tag{C.3.7}$$

Written in the vector notation

$$\frac{\partial f}{\partial t} + \mathbf{v} \cdot \nabla f = 0. \tag{C.3.8}$$

In general case both collisions and external forces alter eq. (C.3.7) and the kinetic equation becomes

$$p^\mu \partial_\mu f + mF^\mu \frac{\partial f}{\partial p^\mu} = \mathrm{St}\, f, \tag{C.3.9}$$

where F^μ represents an external four-force, $\operatorname{St} f$ is the collision integral. This is the *relativistic transport equation*.

One of the main goals of KT is to establish the form of the collision integral. Consider an elastic collision

$$1 + 2 \longrightarrow 1' + 2', \tag{C.3.10}$$

where particles 1 and 2 have masses m_1 and m_2, momenta p^μ and k^μ which changed after the collision to p'^μ and k'^μ respectively. Energy-momentum conservation gives

$$p^\mu + k^\mu = p'^\mu + k'^\mu. \tag{C.3.11}$$

The average number of such collisions is proportional to 1) the number of particles per unit volume with momenta p^μ in the range d^3p, 2) the number of particles per unit volume with momenta k^μ in the range d^3k and 3) the intervals $d^3p'^\mu$, $d^3k'^\mu$ and d^4x. The proportionality coefficients, depending only on four-momenta before and after the collision are represented as $W(p,k \mid p',k') / \left(p^0 k^0 p'^0 k'^0\right)$. The quantity $W(p,k \mid p',k')$ is called the transition rate and it is a scalar. By this process particles leave the phase volume d^3p around p^μ. Collisions also bring particles back into this volume by the inverse process with the corresponding rate $W(p',k' \mid p,k)$.

Then Boltzmann equation can be written as

$$\begin{aligned}\int_{\mathcal{V}}\int_{\mathcal{P}} p^\mu \partial_\mu f \frac{d^3p}{p^0} d^4x = \frac{1}{2}\int_{\mathcal{V}}\int_{\mathcal{P}}\int \frac{d^3p}{p^0}\frac{d^3p'}{p'^0}\frac{d^3k}{k^0}\frac{d^3k'}{k'^0}\times \\ \times \left[f\left(x,p'\right) f\left(x,k'\right) W\left(p',k' \mid p,k\right) - f\left(x,p\right) f\left(x,k\right) W\left(p,k \mid p',k'\right)\right] d^4x,\end{aligned} \tag{C.3.12}$$

or in differential form

$$\begin{aligned}p^\mu \partial_\mu f = \frac{1}{2}\int \frac{d^3p'}{p'^0}\frac{d^3k}{k^0}\frac{d^3k'}{k'^0}\times \\ \times \left[f\left(x,p'\right) f\left(x,k'\right) W\left(p',k' \mid p,k\right) - f\left(x,p\right) f\left(x,k\right) W\left(p,k \mid p',k'\right)\right].\end{aligned} \tag{C.3.13}$$

The same equation in vector notation becomes

$$\frac{\partial f}{\partial t} + \mathbf{v}\cdot\nabla f = \frac{1}{2}\int d^3p' d^3k^3k' \left[f\left(x,p'\right) f\left(x,k'\right) w_{p'k';pk} - f\left(x,p\right) f\left(x,k\right) w_{pk;p'k'}\right], \tag{C.3.14}$$

where $w_{pk;p'k'} = cW(p,k \mid p',k') / \left(p^0 k^0 p'^0 k'^0\right)$. If in this expression particle momenta are substituted by their velocities, this equation will coincide with the one derived first by Boltzmann Boltzmann (2011). Notice that the factor 1/2 in front of collision integral is due to indistinguishability of particles.

C.3.1. Boltzmann equation in General Relativity

The derivation of Boltzmann equation in General Relativity is presented here following Zakharov (2000), for more details see Chernikov (1962, 1963b); Debbasch and van Leeuwen (2009a,b).

Let us start by introducing the 8-dimensional phase space $\mathcal{M}^8$. The distribution function $\mathcal{F}^K(x,p)$ in this phase space is defined Beliaev and Budker (1956) such that

$$j^\mu = \int u^\mu \mathcal{F}^K(x,p)\, d^4 p \tag{C.3.15}$$

is the usual particle-current four-vector (C.2.15). Define the Klimontovich DF Klimontovich (1960a)

$$\mathcal{F}^K(x,p) = \frac{1}{mc}\sum_i \int ds \delta^4\left[x - x_i(s)\right]\delta^4\left[p - p_i(s)\right], \tag{C.3.16}$$

where $ds = \left(g_{\mu\nu}dx^\mu dx^\nu\right)^{1/2}$ is the proper time. Notice that eq. (C.2.14) defined above is nothing but the ensemble averaged function (C.3.16). The equations of motion for each particle in the gravitational field are

$$mc\frac{dx^\mu}{ds} = p^\mu, \qquad mc\frac{dp^\mu}{ds} = -\Gamma^\mu_{\nu\lambda}p^\nu p^\lambda, \tag{C.3.17}$$

where the $\Gamma^\mu_{\nu\lambda}$ are the Christoffel symbols. Using the property

$$\frac{d}{ds}\delta\left[x - g(s)\right] = -\frac{d}{dx}\delta\left[x - g(s)\right]\frac{dg}{ds} \tag{C.3.18}$$

from the identity

$$\int ds \frac{d}{ds}\left\{\delta^4\left[x - x_i(s)\right]\delta^4\left[p - p_i(s)\right]\right\} = 0 \tag{C.3.19}$$

one can obtain
$$\frac{\partial\left(p^{\mu}\mathcal{F}^{K}\right)}{\partial x^{\mu}}-\frac{\partial}{\partial p^{\mu}}\left(\Gamma^{\mu}_{\nu\lambda}p^{\nu}p^{\lambda}\mathcal{F}^{K}\right)=0. \tag{C.3.20}$$

Using another identity

$$\frac{\partial p^{\mu}}{\partial x^{\mu}}-\frac{\partial}{\partial p^{\mu}}\left(\Gamma^{\mu}_{\nu\lambda}p^{\nu}p^{\lambda}\right)=0, \tag{C.3.21}$$

see Zakharov (2000), and applying to eq. (C.3.20) the averaging procedure with $\mathcal{F}=\left\langle\mathcal{F}^{K}(x,p)\right\rangle_{\text{ens}}$ one finally gets

$$p^{\mu}\frac{\partial\mathcal{F}}{\partial x^{\mu}}-\Gamma^{\mu}_{\nu\lambda}p^{\nu}p^{\lambda}\frac{\partial\mathcal{F}}{\partial p^{\mu}}=0. \tag{C.3.22}$$

This is the collisionless kinetic equation for the distribution function defined in $\mathcal{M}^{8}$. As for the DF $f(\mathbf{p},\mathbf{x},t)$ defined in $\mathcal{M}^{6}$ the corresponding equation can be obtained using eq. (C.2.10) and integrating eq. (C.3.22) over p^{0}. As the result one has
$$p^{\mu}\frac{\partial f}{\partial x^{\mu}}-\Gamma^{i}_{\nu\lambda}p^{\nu}p^{\lambda}\frac{\partial f}{\partial p^{i}}=0. \tag{C.3.23}$$

Finally, assuming that it is possible to introduce a local Lorentz frame and define the expressions for $\mathrm{St}\,f$ in that frame, one can write by analogy with eq. (C.3.9) the general expression for the Boltzmann equation as

$$p^{\mu}\frac{\partial f}{\partial x^{\mu}}-\Gamma^{i}_{\nu\lambda}p^{\nu}p^{\lambda}\frac{\partial f}{\partial p^{i}}=\mathrm{St}\,f. \tag{C.3.24}$$

This equation has to be compared with eq. (C.3.9): in General Relativity the curved nature of space-time results in a term similar to the external force in eq. (C.3.9). Another form of Boltzmann equation can be written in a different form, similar to eq. (C.3.13) by introducing the Cartan covariant derivative

$$\nabla_{\mu}\Phi(x,p)\equiv\frac{\partial\Phi}{\partial x^{\mu}}+\Gamma^{\lambda}_{\mu\nu}p_{\lambda}\frac{\partial\Phi}{\partial p_{\nu}}. \tag{C.3.25}$$

Then for the ensemble averaged DF one has

$$p^{\mu}\nabla_{\mu}f(x,p)=\mathrm{St}\,f. \tag{C.3.26}$$

Comparing this last expression with eq. (C.3.13) one can see that, as often occurs in General Relativity, usual derivative in eq. (C.3.13) is substituted with the covariant derivative in eq. (C.3.26).

C.3.2. Uehling-Uhlenbeck collision integral

In this section the collision integral of eq. (C.3.13) is obtained for the case of elastic collision between two classical particles. When particles follow quantum statistics it is still possible to use the collision integral Uehling and Uhlenbeck (1933); Uehling (1934) which is phenomenologically modified as follows

$$\begin{aligned} \mathrm{St}\, f = \frac{1}{2} \int \frac{d^3p'}{p'^0} \frac{d^3k}{k^0} \frac{d^3k'}{k'^0} \times \\ \times \left\{ f\left(x,p'\right) f\left(x,k'\right) \left[1+\theta\varphi\left(x,p\right)\right] \left[1+\theta\varphi\left(x,k\right)\right] W\left(p',k' \mid p,k\right) - \right. \\ \left. - f\left(x,p\right) f\left(x,k\right) \left[1+\theta\varphi\left(x,p'\right)\right] \left[1+\theta\varphi\left(x,k'\right)\right] W\left(p,k \mid p',k'\right) \right\}, \end{aligned} \tag{C.3.27}$$

where $f\left(x,p\right) = g\varphi\left(x,p\right) / \left(2\pi\hbar\right)^3$, g is the degeneracy factor, $\theta = \pm 1, 0$ for respectively Bose-Einstein, Fermi-Dirac and Boltzmann statistics. Comparing this expression to eq. (C.3.13) one finds additional multipliers $1 \pm \left(2\pi\hbar\right)^3 f\left(x,p\right)/g$, which guarantee that equilibrium distribution functions are indeed Bose-Einstein and Fermi-Dirac ones, respectively, see e.g. Chernikov (1964a); Ehlers (1973).

C.3.3. Cross-section

An important concept describing the strength of particle interactions is the cross-section. It plays an important role in the case of two particle collisions, which is the most simple and hence the most studied case. This concept will be illustrated for the process of scattering (C.3.10).

It is possible to introduce Mandelstam (1958) the following invariant variables

$$s = \left(p^\mu + k^\mu\right)^2, \qquad t = \left(p^\mu - p'^\mu\right)^2. \tag{C.3.28}$$

They prove technically useful, but they also possess a physical interpretation: sc^2 is the square of the energy in the center of mass reference system, t is related to the scattering angle in this system: $\cos\vartheta - 1 = 2t/\left(s - 4m_1m_2c^2\right)$.

Then one may rewrite

$$W\left(p,k \mid p',k'\right) = s\sigma\left(s,\vartheta\right)\delta^4\left(p^\mu + k^\mu - p'^\mu - k'^\mu\right), \tag{C.3.29}$$

where $\sigma\left(s,\vartheta\right)$ is the differential cross-section for a given process. Remind Berestetskii et al. (1982) that the cross-section is defined through

$$dw = jd\sigma, \tag{C.3.30}$$

where dw is the probability of the process per unit time and unit volume and

$$j = \left[\left(p^\mu k_\mu\right)^2 - \left(m_1 m_2 c^2\right)^2\right]^{1/2} \tag{C.3.31}$$

is invariant flux of particles in initial state. It is possible to show Groot et al. (1980) that

$$\int \frac{d^3p'}{p'^0}\frac{d^3k'}{k'^0}\frac{1}{j}W\left(p,k \mid p',k'\right) = \int \sigma d\Omega = \int d\sigma. \tag{C.3.32}$$

Then, using the detailed balance condition

$$W\left(p,k \mid p',k'\right) = W\left(p',k' \mid p,k\right) \tag{C.3.33}$$

one may write Boltzmann equation as

$$p^\mu\partial_\mu f = \frac{1}{2}\int \frac{d^3k}{k^0}\sigma\left[f\left(x,p'\right)f\left(x,k'\right) - f\left(x,p\right)f\left(x,k\right)\right]d\Omega, \tag{C.3.34}$$

or in vector notation as

$$\frac{\partial f}{\partial t} + \mathbf{v}\cdot\nabla f = \frac{1}{2}\int d^3k\sigma v\left[f\left(x,p'\right)f\left(x,k'\right) - f\left(x,p\right)f\left(x,k\right)\right]d\Omega, \tag{C.3.35}$$

where $v = cj/\left(p^0k^0\right)$ is the particles relative velocity.

C.4. Conservation laws and relativistic hydrodynamics

In this Section following Groot et al. (1980) the conservation laws fulfilled by the macroscopic quantities are derived, namely the *particle number* conservation, the *entropy* conservation and the *energy-momentum* conservation, see also Chernikov (1963a, 1964b).

Consider a mixture of D components whose particles may interact by elastic and inelastic collisions, conserving their total number. Boltzmann equations for each DF $f_k\left(x, p_k\right)$ then read

$$p_k^\mu \partial_\mu f_k = \sum_{l=1}^{D} C_{kl}\left(x, p_k\right), \tag{C.4.1}$$

where Latin indices now denote the species kind (not to be confused with tensor indices) and

$$C_{kl}\left(x, p_k\right) = \frac{1}{2}\sum_{i,j=1}^{D}\int \frac{d^3 p_l}{p_l^0}\frac{d^3 p_i}{p_i^0}\frac{d^3 p_j}{p_j^0}\left(f_i f_j W_{ij|kl} - f_k f_l W_{kl|ij}\right). \tag{C.4.2}$$

An important property of collision integrals follows from the microscopic conservation laws fulfilled at each interaction, namely

$$F = \sum_{k,l=1}^{D}\int \frac{d^3 p_k}{p_k^0}\psi_k(x) C_{kl}(x, p_k) = 0, \tag{C.4.3}$$

where $\psi_k(x)$ are so called summational invariants

$$\psi_k(x) = a_k(x) + p_k^\mu b_\mu(x), \tag{C.4.4}$$

they are arbitrary functions, except for the constraint that $a_k(x)$ is additively conserved in all reactions, i.e.

$$a_i(x) + a_j(x) = a_k(x) + a_l(x), \tag{C.4.5}$$

and $b_\mu(x)$ is an arbitrary vector. The proof of eq. (C.4.3) is based on eq. (C.4.5) and on energy-momentum conservation in a binary reaction $p_i^\mu + p_j^\mu = p_k^\mu +$

p_l^μ. In particular, for elastic scattering

$$\int \frac{d^3 p_k}{p_k^0} C_{kl}(x, p_k) = 0. \tag{C.4.6}$$

Now it is possible to show how the basic equations of relativistic hydrodynamics, namely the particle number conservation (continuity) equation and the energy-momentum conservation equations arise from Boltzmann equation.

Consider the case when in eq. (C.4.4) $b_\mu(x) = 0$ and $a_k(x) = q_k a(x)$, where $a(x)$ is an arbitrary function. Then from eqs. (C.4.1) and (C.4.2) one has

$$\sum_{k=1}^{D} q_k \int \frac{d^3 p_k}{p_k^0} p_k^\mu \partial_\mu f_k = 0. \tag{C.4.7}$$

Recalling the definition (C.2.15) for each component

$$j_k^\mu = c \int \frac{d^3 p_k}{p_k^0} p_k^\mu f_k, \tag{C.4.8}$$

one gets

$$\partial_\mu J^\mu = 0, \quad J^\mu = \sum_{k=1}^{D} q_k j_k^\mu, \tag{C.4.9}$$

where q_k is a charge (e.g. electric, leptonic, baryonic). In particular, with $q = 1$ this is just particle number conservation. Similarly the conservation law for the total particle number can be obtained. In particular, for elastic scattering using eq. (C.4.6) one finds

$$\partial_\mu j_k^\mu = 0. \tag{C.4.10}$$

Consider now the case $a_k(x) = 0$. Then from eq. (C.4.3) one finds

$$\sum_{k,l=1}^{D} \int \frac{d^3 p_k}{p_k^0} p_k^\mu C_{kl} = 0. \tag{C.4.11}$$

Substituting this into eqs. (C.4.1) and (C.4.2) and recalling the definition (C.2.16) one gets

$$\partial_\nu T^{\mu\nu} = 0, \tag{C.4.12}$$

where

$$T^{\mu\nu} = c\sum_{k=1}^{D}\int \frac{d^3p_k}{p_k^0} p_k^\mu p_k^\nu f_k, \tag{C.4.13}$$

is the energy-momentum tensor of the mixture. Equations (C.4.9) and (C.4.11) represent basic equations of relativistic hydrodynamics, see e.g. Mihalas and Mihalas (1984).

C.5. Entropy and equilibrium

In this Section the concept of thermodynamic equilibrium will be discussed from the point of view of kinetic theory.

C.5.1. $\mathcal{H}$-theorem

First let us show, following Groot et al. (1980), that the quantity defined as divergence of four-vector (C.2.17) as

$$\sigma(x) \equiv \partial_\mu S^\mu, \tag{C.5.1}$$

can never decrease. For alternative derivation see Chernikov (1963b). From eqs. (C.2.17) and (C.5.1) it follows

$$\sigma = -k_B c\int \frac{d^3p}{p^0}\left[\log\left(h^3 f\right)\right] p^\mu \partial_\mu f. \tag{C.5.2}$$

Substituting Boltzmann equation (C.3.9) into this expression one get

$$\sigma = -k_B c\int \frac{d^3p}{p^0}\left[\log\left(h^3 f\right)\right] Stf + k_B c\int \frac{d^3p}{p^0}\left[\log\left(h^3 f\right)\right] F^\mu \frac{\partial f}{\partial p^\mu}. \tag{C.5.3}$$

Assume that the force satisfies the following properties: $p^\mu F_\mu = 0$ and $\frac{\partial F^\mu}{\partial p^\mu} = 0$. The former condition means that the force is mechanical and does not alter particle rest mass. Then the second contribution in eq. (C.5.3) can be written as

$$2k_B c\int d^4p \frac{\partial}{\partial p^\mu}\left\{\Theta(p^0)\delta(p^\mu p_\mu - m^2c^2) f\left[\log\left(h^3 f\right) - 1\right] F^\mu\right\}, \tag{C.5.4}$$

and it vanishes, provided that the integrand is decreasing fast enough for large momenta in the sense defined above.

The first contribution can be rewritten as

$$\sigma = -\frac{1}{4} k_B c \sum_{i,j,k,l} \int \frac{d^3 p_i}{p_i^0} \frac{d^3 p_j}{p_j^0} \frac{d^3 p_k}{p_k^0} \frac{d^3 p_l}{p_l^0} \left[\log \left(\frac{f_k f_l}{f_i f_j} \right) \right] f_i f_j W_{ij|kl}. \tag{C.5.5}$$

Now using the property

$$\sum_{i,j,k,l} \int \frac{d^3 p_i}{p_i^0} \frac{d^3 p_j}{p_j^0} \frac{d^3 p_k}{p_k^0} \frac{d^3 p_l}{p_l^0} \left(f_k f_l - f_i f_j \right) W_{ij|kl} = 0, \tag{C.5.6}$$

which follows from the bilateral normalization condition Groot et al. (1980) one finally gets

$$\sigma = \frac{1}{4} k_B c \sum_{i,j,k,l} \int \frac{d^3 p_i}{p_i^0} \frac{d^3 p_j}{p_j^0} \frac{d^3 p_k}{p_k^0} \frac{d^3 p_l}{p_l^0} A\left(y\right) f_i f_j W_{ij|kl}, \tag{C.5.7}$$

where

$$A\left(y\right) = y - \log y - 1 \geq 0, \qquad y = \frac{f_k f_l}{f_i f_j}. \tag{C.5.8}$$

Since $A\left(y\right)$ is a non-negative function, eq. (C.5.7) implies that $\sigma \geq 0$. This completes the proof of the Boltzmann $\mathcal{H}$-theorem.

Notice that $\sigma = 0$ holds if and only if

$$f_i\left(x, p_i\right) f_j\left(x, p_j\right) = f_k\left(x, p_k\right) f_l\left(x, p_l\right). \tag{C.5.9}$$

This condition is satisfied, as can be seen from eq. (C.3.34) when collision integral in the RHS of Boltzmann equation vanishes. This case is identified as *local equilibrium*. In fact, the equilibrium DF is characterized by the following macroscopic quantities as parameters: density, temperature, 4-velocity. It is possible to show this by turning to a simple system with binary collisions and rewrite the condition (C.5.9) as

$$\log\left(h^3 f_1\right) + \log\left(h^3 f_2\right) = \log\left(h^3 f_1'\right) + \log\left(h^3 f_2'\right). \tag{C.5.10}$$

It is clear that the quantity $\log\left(h^3 f\right)$ is a summational invariant. The most general summational invariant, as discussed above, is a linear combination of a constant and p^μ. Then one particle distribution function in equilibrium is

$$f^{eq} = \frac{1}{h^3} \exp\left[a(x) + b_\mu(x) p^\mu\right] \tag{C.5.11}$$

with arbitrary space- and time-dependent parameters $a(x)$ and $b_\mu(x)$.

However, DF f^{eq} will be a solution of the Boltzmann equation only if it turns to zero also its LHS. Then the parameters of eq. (C.5.11) should satisfy

$$p^\mu \partial_\mu a(x) + p^\mu p^\nu \partial_\mu b_\nu(x) + m b_\mu(x) F^\mu(x, p) = 0, \tag{C.5.12}$$

which should be an identity for arbitrary p^μ. When the DF satisfies eq. (C.5.12) it is called *global equilibrium* DF f^{EQ}.

In the absence of external field f^{EQ} reduces to the Jüttner Jüttner (1911) momentum distribution

$$f^{EQ}(p) = \frac{1}{h^3} \exp\left[\frac{\phi - p^\mu U_\mu}{k_B T}\right], \tag{C.5.13}$$

where ϕ, T and U_μ are parameters, $U^\mu U_\mu = c^2$, h and k_B are Planck's and Boltzmann's constants.

It is possible now to compute such important macroscopic quantities as the number density, the energy density and the pressure of a system in local equilibrium. Using the definition (C.2.15) and $j^\mu = nU^\mu$ one has

$$n = \frac{j^\mu U_\mu}{c^2} = \frac{1}{ch^3} \exp\left(\frac{\phi}{k_B T}\right) \int \frac{d^3 p}{p^0} p^\mu U_\mu \exp\left(\frac{-p^\nu U_\nu}{k_B T}\right). \tag{C.5.14}$$

The integral, being a scalar, can be evaluated in the rest frame, where $U^\mu = (c, 0, 0, 0)$ by introducing polar coordinates and dimensionless variables $\theta = k_B T / \left(mc^2\right)$, $\nu = \phi / \left(mc^2\right)$ and $y = c\sqrt{\mathbf{p}^2 + m^2 c^2} / \left(k_B T\right)$. The result is

$$n = \frac{4\pi}{\lambda_C^3} \exp\left(\frac{\nu}{\theta}\right) K_2\left(\theta^{-1}\right), \tag{C.5.15}$$

where $\lambda_C = \frac{\hbar}{mc}$ and

$$K_n\left(\theta^{-1}\right) = \frac{2^{n-1}(n-1)!}{(2n-2)!} z^{-n} \int_z^\infty dy \left(y^2 - \theta^{-2}\right)^{n-\frac{3}{2}} y \exp(-y) \tag{C.5.16}$$

is the modified Bessel function of the second kind.

In full analogy, using the definition of the energy-momentum tensor and $T^{\mu\nu} = c^{-2}\rho U^\mu U^\nu - p\Delta^{\mu\nu}$, where $\Delta^{\mu\nu} = g^{\mu\nu} - c^{-2}U^\mu U^\nu$, one can compute the energy density ρ and pressure p as follows

$$\rho = \frac{T^{\mu\nu}U_\mu U_\nu}{c^2} = \frac{1}{c}\int \frac{d^3p}{p^0}\left(p^\mu U_\mu\right)^2 f^{EQ}, \tag{C.5.17}$$

$$p = -\frac{1}{3}T^{\mu\nu}\Delta_{\mu\nu} = -\frac{c}{3}\int \frac{d^3p}{p^0} p^\mu p^\nu \Delta_{\mu\nu} f^{EQ}. \tag{C.5.18}$$

Performing the integrals one finally gets

$$\rho = 4\pi\frac{mc^2}{\lambda_C^3}\exp\left(\frac{\nu}{\theta}\right)\left[3\theta^2 K_2\left(\theta^{-1}\right) + \theta K_1\left(\theta^{-1}\right)\right], \tag{C.5.19}$$

$$p = 4\pi\frac{mc^2}{\lambda_C^3}\exp\left(\frac{\nu}{\theta}\right)\theta^2 K_2\left(\theta^{-1}\right). \tag{C.5.20}$$

Introducing the enthalpy as $h_e = (\rho + p)/n$ one obtains

$$h_e = mc^2\frac{K_3\left(\theta^{-1}\right)}{K_2\left(\theta^{-1}\right)}. \tag{C.5.21}$$

Finally, the entropy density is given by

$$s = \frac{S^\mu U_\mu}{c^2} = -\frac{k_B}{c}\exp\left(\frac{\phi}{k_B T}\right)\int \frac{d^3p}{p^0} p^\mu U_\mu\left(\frac{\varphi - p^\nu U_\nu}{k_B T} - 1\right)\exp\left(\frac{-p^\nu U_\nu}{k_B T}\right). \tag{C.5.22}$$

Taking into account eqs. (C.5.15) and (C.5.19) this integral gives

$$s = \frac{1}{T}\left(\rho - \phi n\right) + k_B n. \tag{C.5.23}$$

Finally, for the thermal index $\Gamma = c_p/c_v$, which is the ratio of specific heat capacities

$$c_p = \left(\frac{\partial h_e}{\partial T}\right)_p, \quad c_v = \left(\frac{\partial\left(\rho/n\right)}{\partial T}\right)_v, \tag{C.5.24}$$

one has

$$\frac{\Gamma}{\Gamma - 1} = \theta^{-2} + 5\left(\frac{h_e}{\theta}\right) - \left(\frac{h_e}{\theta}\right)^2, \tag{C.5.25}$$

and the limiting cases are

$$\Gamma \to \begin{cases} \frac{5}{3}, & \theta \to 0, \\ \\ \frac{4}{3}, & \theta \to \infty. \end{cases} \tag{C.5.26}$$

In Fig. C.1 the dependence $\Gamma(\theta)$ computed using eqs. (C.5.25) and (C.5.21) is shown. Non-relativistic and ultra-relativistic asymptotics are clearly visible. Interestingly, at temperatures $k_B T \sim mc^2$ usually considered mildly relativistic this function is already close to its ultra-relativistic value.

Combining expressions (C.5.15), (C.5.19), (C.5.20), (C.5.23) and (C.5.21) above one find the perfect gas laws

$$\begin{aligned} p &= n k_B T, \\ p &= (\Gamma - 1)\,\rho, \\ \phi &= h_e - Ts. \end{aligned} \tag{C.5.27}$$

Note that the traditional scheme of thermodynamics is recovered if we identify T as temperature, ϕ as the chemical (Gibbs) potential.

C.5.2. Relativistic Maxwellian distribution

It is instructive to consider relativistic Maxwell distribution of particles with somewhat more attention. Considering eq. (C.5.13) in the local rest frame

$$f^{LEQ} = \frac{1}{h^3}\exp\left(\frac{\nu}{\theta}\right)\exp\left(-\frac{\gamma}{\theta}\right), \tag{C.5.28}$$

where $\gamma = p^0/\,(mc)$, using eq. (C.2.3) and comparing it with eq. (C.5.15) one gets

$$f = \frac{dn}{d\gamma} = \frac{4\pi}{\lambda_C^3 \theta K_2\left(\theta^{-1}\right)}\exp\left(\frac{\nu}{\theta}\right)\gamma\sqrt{\gamma^2 - 1}\exp\left(-\frac{\gamma}{\theta}\right). \tag{C.5.29}$$

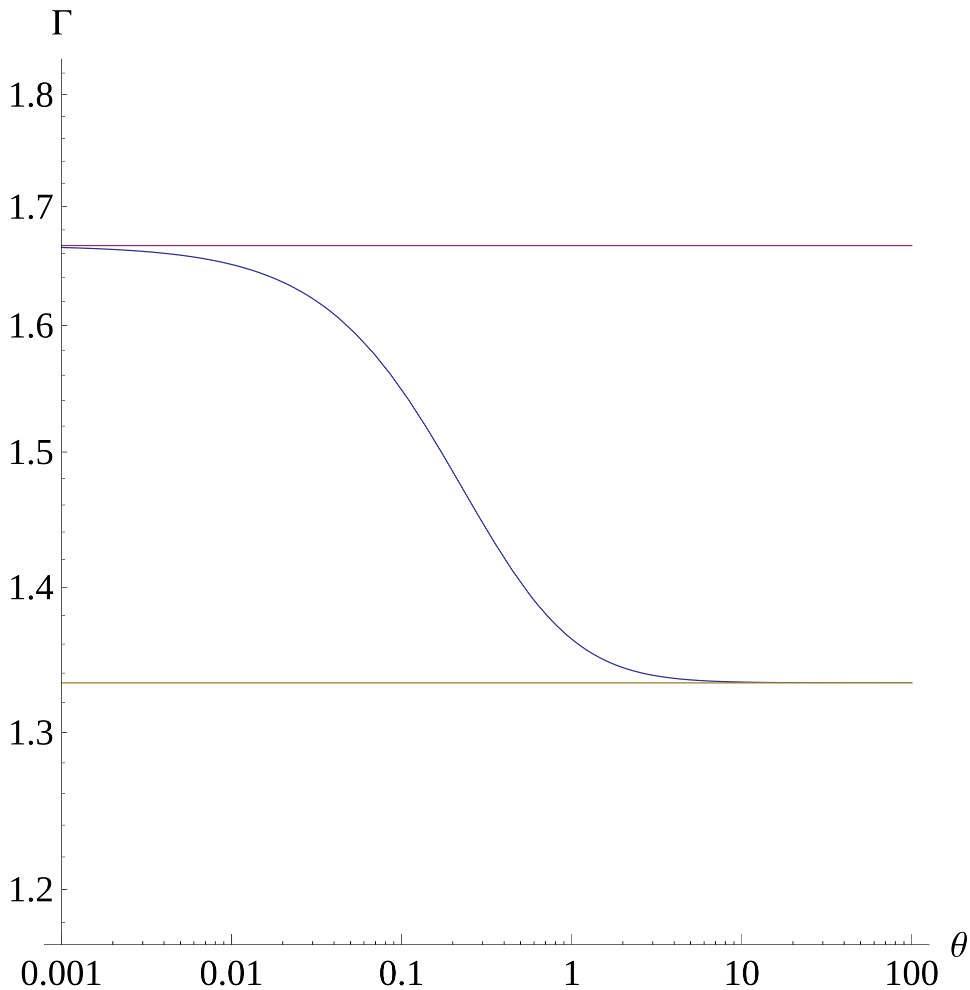

Figure C.1.: The thermal index of relativistic gas as function of dimensionless temperature.

The function $f(\beta)$ with $\beta = |\mathbf{v}|/c$ is shown in Fig. C.2 for selected values of the dimensionless temperature, each curve is normalized to unity. While the distribution function with the lowest temperature $\theta = 0.02$ reminds a classical Maxwellian, the one with the highest temperature $\theta = 1.78$ it is already far from it: the effect of limiting velocity is clearly visible.

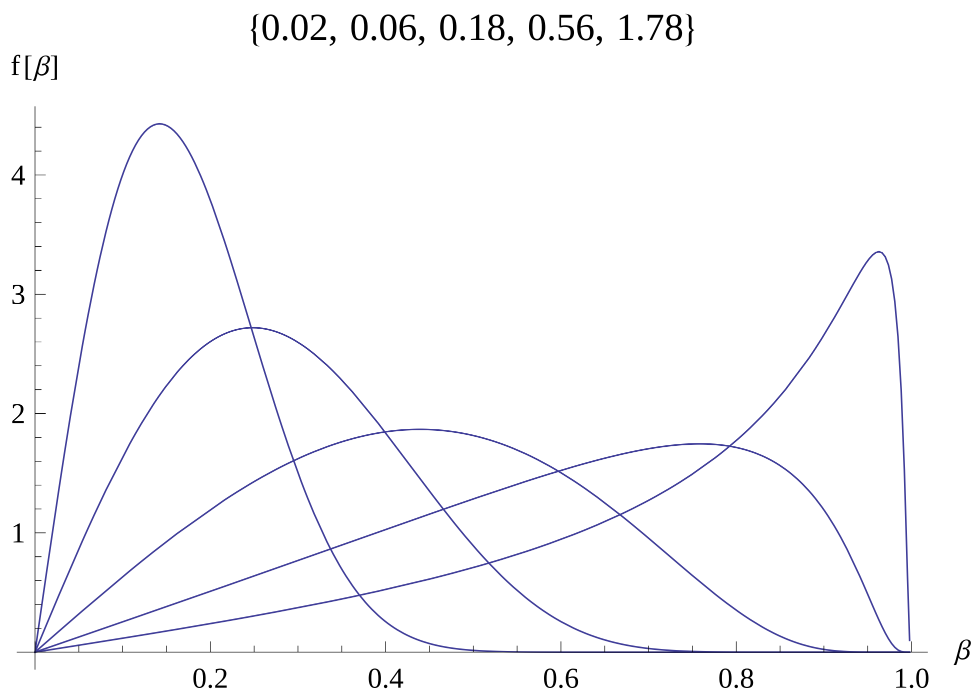

Figure C.2.: Relativistic Maxwellian distribution function for selected values of dimensionless temperature.

C.5.3. Generalized continuity equation

Up to now only such interactions where particle conservation is satisfied were discussed. An obvious example is scattering. However, there are processes where particle conservation does not hold. The simplest example annihilation of particles-antiparticle pair in two photons and the inverse process of pair creation from two photons. Even if total number of particles (both pairs and photons) is conserved, individual number of particles in each component can change. Consider this process in more details

$$e^+ + e^- \longleftrightarrow \gamma_1 + \gamma_2, \tag{C.5.30}$$

with the corresponding energy-momentum conservation $p_- + p_+ = k_1 + k_2$. For positron (electron) from eq. (C.3.13) one has[2]

$$p^\mu \partial_\mu f_\pm = \int \frac{d^3 p_\mp}{p^0_\mp} \frac{d^3 k_1}{k^0_1} \frac{d^3 k_2}{k^0_2} \left[f_1 f_2 W\left(k_1, k_2 \mid p_\pm, p_\mp\right) - f_\pm f_\mp W\left(p_\pm, p_\mp \mid k_1, k_2\right) \right], \tag{C.5.31}$$

where $f_\pm = f(x, p_\pm)$, etc. From eqs. (C.3.30) and (C.3.31) one gets

$$\frac{d^3 k_1}{k^0_1} \frac{d^3 k_2}{k^0_2} W\left(p_\pm, p_\mp \mid k_1, k_2\right) = j d\sigma, \tag{C.5.32}$$

$$v_{\mathrm{rel}} = \sqrt{\left(\mathbf{v}_- - \mathbf{v}_+\right)^2 - \left(\mathbf{v}_- \times \mathbf{v}_+\right)^2} = j \frac{c}{p^0_\pm p_{0\mp}},$$

where v_{rel} is the relative velocity between electron and positron. Then integrating eq. (C.5.31) over $\frac{d^3 p_\pm}{p^0_\pm}$ and using eq. (C.5.32) one obtains

$$\partial_\mu \int \frac{d^3 p_\pm}{p^0_\pm} p^\mu f_\pm = \int \frac{d^3 p_\pm}{p^0_\pm} \frac{d^3 p_\mp}{p^0_\mp} \frac{d^3 k_1}{k^0_1} \frac{d^3 k_2}{k^0_2} f_1 f_2 W\left(k_1, k_2 \mid p_\pm, p_\mp\right) - \tag{C.5.33}$$
$$- \int \frac{d^3 p_\pm}{p^0_\pm} \frac{d^3 p_\mp}{p^0_\mp} f_\pm f_\mp j d\sigma.$$

In view of eq. (C.2.3) and second equation in (C.5.32) the annihilation rate is defined as

$$n_\pm n_\mp \left\langle \sigma v \right\rangle_{ann} \equiv c \int \frac{d^3 p_\pm}{p^0_\pm} \frac{d^3 p_\mp}{p^0_\mp} f_\pm f_\mp j d\sigma. \tag{C.5.34}$$

This is an invariant quantity, as can be seen from analysis of the RHS. Notice, that the LHS in eq. (C.5.33) is nothing but derivative of the particle four-flux (C.2.15). In equilibrium this quantity is conserved, see eq. (C.4.10). So that in equilibrium

$$c \int \frac{d^3 p_\pm}{p^0_\pm} \frac{d^3 p_\mp}{p^0_\mp} \frac{d^3 k_1}{k^0_1} \frac{d^3 k_2}{k^0_2} f_1 f_2 W\left(k_1, k_2 \mid p_\pm, p_\mp\right) = n^{eq}_\pm n^{eq}_\mp \left\langle \sigma v \right\rangle_{ann}. \tag{C.5.35}$$

[2] Electrons and positrons are distinguishable particles and hence there is no factor $1/2$ in front of the collision integral.

Thus one can write

$$\partial_\mu j^\mu_\pm = \langle \sigma v \rangle_{ann} \left(n_+^{eq} n_-^{eq} - n_+ n_- \right), \tag{C.5.36}$$

and it reduces to eq. (C.4.10) in thermal equilibrium, since in equilibrium particle non conserving interactions balance each other. This equation finds numerous applications, especially in cosmology, since it is much easier to solve compared to integro-differential eq. (C.3.13).

C.6. Relativistic BBGKY hierarchy

In this section following de Jagher and Sluijter (1988), the derivation of relativistic Bogoliubov–Born–Green–Kirkwood–Yvon hierarchy is briefly illustrated, see also Klimontovich (1960a),Kuz'menkov (1978),Naumov (1981),Polyakov (1988) and Hakim (2011). The basic idea in this approach is that any many-body system can be characterized by the set of equations of motion under given interaction. Applying averaging to Klimontovich distribution functions one can derive the infinite chain of equations (hierarchy) for many particle distribution functions.

For definiteness let us discuss a system of charged particles of equal mass with the corresponding electromagnetic interaction. In that case it is convenient to use for the four-momentum $p^\mu \longrightarrow p^\mu - \frac{q}{c} A^\mu$, where A^μ is the vector potential of the electromagnetic field. The equations of motion are

$$\frac{dp^\mu}{ds} = -\frac{q}{c} F^{\mu\nu} u_\nu, \quad p^\mu = m u^\mu, \quad u^\mu = \frac{dx^\mu}{ds}, \tag{C.6.1}$$

where $F^{\mu\nu}$ is the electromagnetic field tensor, u^μ is the particle four-velocity. For the point particle the four-current is

$$j^\mu = q \int u^\mu \delta^4 \left[x^\nu - x^\nu(s) \right] ds. \tag{C.6.2}$$

Recalling the definition (C.3.16) of the Klimontovich DF one may proceed in analogy with Sec. C.3.1. Using eq. (C.6.1) one arrives to the Klimontovich equation

$$p^\mu \partial_\mu \mathcal{F}^K - \frac{q}{c} p_\mu F^{\mu\nu} \frac{\partial \mathcal{F}^K}{\partial p^\nu} = 0. \tag{C.6.3}$$

This equation has to be supplemented by the Maxwell field equations

$$\partial_\mu F^{\mu\nu} = 4\pi J^\nu, \quad \varepsilon_{\mu\nu\sigma\rho}\partial^\nu F^{\sigma\rho} = 0. \tag{C.6.4}$$

These equations are the basis for derivation of the hierarchy. Notice that these equations are used in numerical simulations (particle-in-cell algorithms). Solutions of eqs. (C.6.3), (C.6.4) are approximate solutions to the Vlasov-Maxwell system with the accuracy $\mathcal{O}(\mu)$, where $\mu = \left(n\lambda_D^3\right)^{-1}$, see e.g. Sigov (2001) is the plasma parameter, λ_D is the Debye length, see eq. (C.7.8) below, n is density.

The usual approach in statistical physics of a many-body system is to start with the Liouville theorem for ensemble density. In order to generalize the treatment to include fields with infinite degrees of freedom one has to consider linear spaces. Assume that relativistic Hamilton equations are valid (in symbolic form)

$$\frac{dX}{ds} = G\left[X\left(s\right), s\right], \tag{C.6.5}$$

and they are supplied with initial conditions $X(s = s_0) = X_0$. Introducing the N-particle phase space with coordinates X being the element of the linear space and probability density $F\left(X, s\right)$ in this phase space, after rather lengthy derivation one can show that Liouville's theorem holds

$$\frac{\partial}{\partial s}F\left(X,s\right) + F\left(X,s\right)\frac{\partial}{\partial X}\cdot G\left(X,s\right) + G\left(X,s\right)\cdot\frac{\partial}{\partial X}F\left(X,s\right) = 0. \tag{C.6.6}$$

Then one has to apply statistical averaging to eqs. (C.6.3) and (C.6.4), which have to be rewritten in the Hamiltonian form. This can be done by introducing a hypersurface S on which initial conditions are given and which determines a scalar that can be used as a time parameter. Then a linear space is constructed in which a point can be interpreted as a state vector for the system at the surface S. Assume that fields $F^{\mu\nu}$ restricted on S can be regarded as an element of a Hilbert space with a set of orthonormal coordinates denoted by $|\Psi_i\rangle$.

It is possible to show that statistical averaging and differentiation with respect to s commute, i.e.

$$\left\langle \frac{d}{ds}A\left(X,s\right)\right\rangle_{\text{ens}} = \frac{d}{ds}\left\langle A\left(X,s\right)\right\rangle_{\text{ens}}. \tag{C.6.7}$$

Introducing the one-particle DF (C.2.14) as $\mathcal{F}(x,p) = \left\langle \mathcal{F}^K(x,p)\right\rangle_{\text{ens}}$, averaged fields $\langle \sum_i F^{\mu\nu}(s)\,|\Psi_i\rangle\rangle_{\text{ens}}$ and currents $\left\langle q\int p^{\mu}\mathcal{F}^K(x,p)\,d^4p\right\rangle_{\text{ens}}$ it is possible to write down the hierarchy

$$\begin{aligned}
u^{\mu}\partial_{\mu}\mathcal{F}(x,p) &= \frac{1}{p_{\sigma}u^{\sigma}}\left\{\Delta_{\mu\nu}p^{\mu}\partial^{\nu}f + \frac{q}{c}p_{\mu}F^{\mu\nu}\frac{\partial f}{\partial p^{\nu}} + \frac{q}{c}p_{\mu}\frac{\partial I^{\mu\nu}}{\partial p^{\nu}}\right\},\\
u^{\sigma}\partial_{\sigma}F^{\mu\nu}(x) &= 4\pi\Delta^{\mu\nu}_{\lambda}\left(J^{\lambda} - \Delta_{\eta\sigma}\partial^{\eta}F^{\sigma\lambda}\right) + \Delta^{\mu\nu}_{\sigma\lambda\rho}\partial^{\sigma}F^{\lambda\rho},\\
u^{\mu}\partial_{\mu}I^{\mu\nu}(x,p) &= ...
\end{aligned}\tag{C.6.8}$$

where

$$I^{\mu\nu}(x,p) = \left\langle\left[F^{\mu\nu}(x) - \langle F^{\mu\nu}\rangle_{\text{ens}}\right]\left[\mathcal{F}^K(x,p) - \mathcal{F}(x,p)\right]\right\rangle_{\text{ens}}\tag{C.6.9}$$

is the particle-field correlation, $\Delta^{\mu\nu} = g^{\mu\nu} + U^{\mu}U^{\nu}$ is a projection operator and

$$\Delta^{\mu\nu}_{\lambda} = u^{\mu}\Delta^{\nu}_{\lambda} - u^{\nu}\Delta^{\mu}_{\lambda},\quad \Delta^{\mu\nu}_{\sigma\lambda\rho} = \left(\Delta^{\mu}_{\sigma}\Delta^{\nu}_{\rho} - \Delta^{\nu}_{\sigma}\Delta^{\mu}_{\rho}\right)u_{\lambda}.\tag{C.6.10}$$

Dynamical equation for $I^{\mu\nu}(x,p)$ contains particle variance, field variance

$$\begin{aligned}
g_{12}(x,p_1,p_2) &= \left\langle\left[\mathcal{F}^K(x,p_1) - f(x,p_1)\right]\left[\mathcal{F}^K(x,p_2) - f(x,p_2)\right]\right\rangle_{\text{ens}},\\
G^{\mu\nu\rho\sigma}(x) &= \langle\left[F^{\mu\nu}(x) - \langle F^{\mu\nu}\rangle_{\text{ens}}\right]\left[F^{\rho\sigma}(x) - \langle F^{\rho\sigma}\rangle_{\text{ens}}\right]\rangle_{\text{ens}},
\end{aligned}\tag{C.6.11}$$

as well as triple correlations and so on, for details see de Jagher and Sluijter (1988). The system (C.6.8) is the relativistic Bogoliubov–Born–Green–Kirkwood–Yvon hierarchy. Like in non-relativistic theory this hierarchy is infinite.

Notice that Klimontovich in his original derivation Klimontovich (1960b) of relativistic kinetic equation neglecting radiation used solution of Maxwell equations for the four-potential A_{μ}. Hence in his chain of equations only particle-particle correlation functions such as $g_{12}(x,p_1,p_2)$ appear, see also Kuz'menkov (1978).

In order to close the system (C.6.8) additional assumptions are needed. In plasma physics with Coulomb interactions between particles the rapid attenuation of correlations principle Bogoliubov (1946, 1962) is usually adopted. Notice that such a principle may be considered as a consequence of ergodicity of the system Smolyansky (1968). In this way the assumption of no correlation between particles

$$\mathcal{G}(x, p_1, p_2) = \mathcal{F}(x, p_1)\,\mathcal{F}(x, p_2)\,,$$
$$\mathcal{G}(x, p_1, p_2, p_3) = \mathcal{F}(x, p_1)\,\mathcal{F}(x, p_2)\,\mathcal{F}(x, p_3)\,, \tag{C.6.12}$$
$$\ldots$$

leads to the system of Vlasov-Maxwell equations

$$p^{\mu}\partial_{\mu}\mathcal{F} - \frac{q}{c}p_{\mu}F^{\mu\nu}\frac{\partial\mathcal{F}}{\partial p^{\nu}} = 0, \tag{C.6.13}$$

$$\partial_{\mu}F^{\mu\nu} = 4\pi q\int\frac{d^3p}{p^0}p^{\mu}\partial_{\mu}\mathcal{F}, \quad \varepsilon_{\mu\nu\sigma\rho}\partial^{\nu}F^{\sigma\rho} = 0. \tag{C.6.14}$$

Taking into account nonvanishing two point correlation function, but neglecting three point correlations results in the Belyaev-Budker equation Beliaev and Budker (1956). For its derivation from the BBGKY hierarchy see Klimontovich (1960b), Naumov (1981) and Polyakov (1988). The result instead of eq. (C.6.13) is

$$u^{\mu}\partial_{\mu}\mathcal{F} = -\frac{\partial K_{\mu}}{\partial p^{\mu}},$$
$$K_{\mu} = \frac{2\pi\left(qq'\right)^2\Lambda}{c^2}\int d^4p'\frac{\left(u_{\lambda}u'_{\lambda}\right)^2}{c\left[\left(u_{\lambda}u'_{\lambda}\right)^2-1\right]^{\frac{3}{2}}}B_{\mu\nu}\left(\mathcal{F}\frac{\partial\mathcal{F}'}{\partial p'_{\nu}} - \mathcal{F}'\frac{\partial\mathcal{F}}{\partial p_{\nu}}\right), \tag{C.6.15}$$
$$B_{\mu\nu} = \left\{\left[\left(u_{\lambda}u'_{\lambda}\right)^2-1\right]\delta_{\mu\nu} - u_{\mu}u_{\nu} - u'_{\mu}u'_{\nu} - u_{\lambda}u'_{\lambda}\left(u_{\mu}u'_{\nu} + u'_{\mu}u_{\nu}\right)\right\},$$

where Λ is Coulomb logarithm, see eq. (C.7.22) below, primed and unprimed values correspond to two incoming particles, and the mean field is neglected. In non-relativistic case Landau (1936, 1937) this equation reduces to

$$\frac{\partial f}{\partial t} + \mathbf{v}\frac{\partial f}{\partial \mathbf{r}} + q\left(\mathbf{E} + \frac{1}{c}\mathbf{v}\times\mathbf{B}\right)\frac{\partial f}{\partial \mathbf{p}} = -\frac{\partial s_a}{\partial p_a}, \tag{C.6.16}$$
$$s_a = 2\pi q^2\Lambda\int\left(f\frac{\partial f'}{\partial p'_b} - f'\frac{\partial f}{\partial p_b}\right)\frac{\left(\mathbf{v}-\mathbf{v}'\right)^2\delta_{ab} - \left(v_a - v'_a\right)\left(v_b - v'_b\right)}{\left(\left|\mathbf{v}-\mathbf{v}'\right|\right)^3}d^3p'.$$

Recall that in dilute plasma collisions with small momentum transfer dominate. For this reason the Coulomb collision integral in non-relativistic plasma is usually approximated by the Fokker-Planck diffusive term. Such approximation actually becomes invalid for relativistic plasma with $k_B T \gtrsim m_e c^2$, where m_e is electron mass, since at these temperatures pairs of electrons and positrons form, see Sec. C.8 below. Description of such relativistic plasma requires the full Boltzmann collision integral.

It has to be noted that both system (C.6.13), (C.6.14) and equation (C.6.15) are microscopic equations in the sense that they define one particle distribution functions for discrete sources and corresponding electromagnetic fields.

The system of particles interacting via gravitational mean field is described Zakharov (2000) by the Einstein-Vlasov system of equations

$$R^{\mu\nu} - \frac{1}{2} g^{\mu\nu} R + g^{\mu\nu}\Lambda = \frac{8\pi G}{c^4} c \int \frac{d^3 p}{p^0} p^\mu p^\nu \mathcal{F}^K \tag{C.6.17}$$

$$p^\mu \frac{\partial \mathcal{F}^K}{\partial x^\mu} - \Gamma^i_{\nu\lambda} p^\nu p^\lambda \frac{\partial \mathcal{F}^K}{\partial p^i} = 0,$$

where $\mathcal{F}^K$ is the Klimontovich DF defined by eq. (C.3.16). These equations form the basis for microscopic gravity. For mathematical aspects see recent review Andréasson (2011).

Macroscopic gravitation theory should be derived from these equations by applying the averaging procedure. Following the discussion in Sec. C.6 it is expected that correlations should appear in both equations after the averaging and represent matter-field, matter-matter and field-field correlations. An attempt to construct such equations up to the second order terms in interaction is made in Zakharov (2000).

C.7. Gases and plasmas

Having derived basic kinetic equation in Sec. C.3 and C.6 let us turn to their application. Dilute gas and plasma are traditionally considered as primary applications for KT. The generalization to relativistic case of KT for gas required mainly terminological changes Synge (1957). However, KT of plasma had to be build on relativistic basis from the beginning since Maxwell equations, being intrinsically relativistic, are necessarily a natural part of it. Besides, in relativistic domain (at relativistic temperatures) many qualitatively new phenomena occur in plasma. In order to understand these phenomena, as well as to provide the physical foundations for the derivation of the Boltzmann and Vlasov equations discussed in the previous section, it is very useful to discuss characteristic quantities in both gases and plasmas.

C.7.1. Plasma frequency

Let us start from the Maxwell equations (C.6.4) and assume that particles move collectively with velocity v given by the equation of motion

$$m\frac{\partial U^{\mu}}{\partial x^{\nu}} = -\frac{q}{c}F^{\mu}_{\nu}, \tag{C.7.1}$$

Taking 0-1 components in eq. (C.6.4) one has

$$m\frac{d\left(\gamma\beta\right)}{dt} = qE, \quad \frac{dE}{dt} = -4\pi q n \beta, \tag{C.7.2}$$

where $\beta = v/c$ and $\gamma = \left(1-\beta^2\right)^{-1/2}$. Differentiating the first equation with respect to time one gets, see e.g. Benedetti et al. (2011)

$$\frac{d^2u}{dt} + \frac{4\pi q^2 n}{m}\frac{u}{\sqrt{1+u^2}} = 0, \quad u = \gamma\beta. \tag{C.7.3}$$

This equation describes nonlinear Langmuir oscillations (reducing to harmonic ones for $v \ll c$) with the frequency given by

$$\omega_p^2 = \frac{4\pi q^2 n}{m\gamma}. \tag{C.7.4}$$

This parameter is one of the most fundamental ones and it is called *plasma frequency*.

C.7.2. Correlations in plasma

In order to determine other characteristic quantities of plasma one needs to consider the notion of correlation in plasma. It is well known that the correlation function in a medium composed of particles interacting via Coulomb potential is divergent. However, since a neutral plasma contains both positive and negative charges in equal amount, the field of a charged particle in plasma is different from the Coulomb field. In order to illustrate this point consider a charged particle at rest in the origin, see e.g. Chen (1984) and Silin (1998). The system of equations (C.6.13) and (C.6.14) simplifies for this case and there remain only two of them:

$$\mathbf{v}_i \frac{\partial f_i}{\partial \mathbf{r}} - q_i \frac{\partial \varphi}{\partial \mathbf{r}} \frac{\partial f_i}{\partial \mathbf{p}_i} = 0, \quad \Delta\varphi = -4\pi \sum_i q_i n_i - 4\pi q \delta\left(r\right), \tag{C.7.5}$$

where φ is electrostatic potential, and for clarity the DF defined in eq. (C.2.2) is used instead of $\mathcal{F}$. In order to solve these equations one has to set up the boundary conditions. Assume that the electric field vanishes at infinity, i.e. $\varphi\left(\infty\right) = 0$. Assume also that the DF far from the origin is the Maxwell-Boltzmann one (C.5.28), that is

$$f_i\left(\gamma_i\right) \propto n_i \exp\left(-\frac{\gamma_i m_i c^2 + q_i \varphi(r)}{k_B T}\right). \tag{C.7.6}$$

Then taking into account charge conservation $\sum_i q_i n_i = 0$ one can get for the potential

$$\Delta\varphi = -4\pi q \delta\left(r\right) + 4\pi \sum_i q_i n_i \left[1 - \exp\left(-\frac{q_i \varphi}{k_B T}\right)\right]. \tag{C.7.7}$$

At large radii $|q_i \varphi| \ll k_B T$ and instead of eq. (C.7.7) a linear equation is obtained

$$\Delta\varphi - \frac{1}{\lambda_D^2}\varphi = -4\pi q \delta\left(r\right), \quad \lambda_D^2 = \frac{k_B T}{\sum_i 4\pi q_i^2 n_i}. \tag{C.7.8}$$

and it gives the solution for the electric potential in equilibrium plasma

$$\varphi = \frac{q}{r} \exp\left(-\frac{r}{\lambda_D}\right). \tag{C.7.9}$$

This result implies that at large distances the Coulomb field of the point charge is screened.

Define now a two-particle *spatial* correlation function in equilibrium as

$$f_2\left(1,2\right) = f_1\left(\gamma_1\right) f_1\left(\gamma_2\right) g(r), \tag{C.7.10}$$

where the functions $f_i\left(\gamma_i\right)$ are given by eq. (C.5.29), $r = |\mathbf{x}_2 - \mathbf{x}_1|$ and $g(r)$ is called radial distribution function . Using the normalization $\int f_i(\gamma_i)\, d\gamma_i = 1$ one can introduce the *total correlation function*

$$\xi(r) = g(r) - 1 \ll 1, \qquad \text{(C.7.11)}$$

where $\xi(r)$ is zero for uncorrelated particles. For dilute plasma in a state close to equilibrium Klimontovich (1997) this function is

$$\xi(r) = -\frac{1}{k_B T}\frac{q^2}{r}\exp\left(-\frac{r}{\lambda_D}\right), \qquad \text{(C.7.12)}$$

which means that the correlation radius for this plasma is $r_{cor} \sim \lambda_D$.

C.7.3. Gravitational correlations in expanding Universe

Unlike for the electromagnetic interactions, there is no Debye screening in the gravitational interactions since there is no negative mass. In an expanding Universe it is possible, however, to introduce the gravitational correlation radius. Following Zakharov (2000) consider the Poisson-Vlasov equations in the comoving coordinates

$$\frac{\partial f}{\partial t} + \frac{\mathbf{u}}{a^2}\frac{\partial f}{\partial \mathbf{q}} - \frac{\partial \Phi}{\partial \mathbf{q}}\frac{\partial f}{\partial \mathbf{u}} = 0, \quad \Delta\Phi = \frac{4\pi G}{a}\int f d^3u - a^3\rho_0, \qquad \text{(C.7.13)}$$

where ρ_0 is the average density, Φ is gravitational potential. Here comoving coordinates $\mathbf{q}$ and velocities $\mathbf{u}$ are related to the physical ones as usual

$$\mathbf{q} = \frac{\mathbf{x}}{a(t)}, \quad \mathbf{u} = a(t)\left[\mathbf{v} - H(t)\,\mathbf{x}\right], \qquad \text{(C.7.14)}$$

where $a(t)$ is cosmological scale factor. By comparison of eqs. (C.7.13) and (C.7.5) one finds that the average density in eq. (C.7.13) plays the role of opposite charge particles. By analogy with eq. (C.7.7) considering a gravitating particle in a uniform media, insert in eq. (C.7.13) instead of $a^3\rho_0$ a new density

$$a^3\rho = a^3\rho_0 \exp\left(-\frac{m\Phi}{k_B T}\right). \qquad \text{(C.7.15)}$$

In the physical coordinates one obtains

$$\Delta\Phi = 4\pi G\rho \left[\exp\left(-\frac{m\Phi}{k_B T} \right) - 1 \right], \tag{C.7.16}$$

which is similar to eq. (C.7.7). For large distances it reduces to

$$\frac{1}{r^2}\frac{d}{dr}\left(r^2 \frac{d\Phi}{dr} \right) + \frac{4\pi G\rho_0 m}{k_B T}\Phi = 0, \tag{C.7.17}$$

which gives

$$\Phi \propto \frac{1}{r}\cos\left(\frac{r}{r_g} \right), \quad r_g^2 = \frac{k_B T}{4\pi G\rho_0 m}. \tag{C.7.18}$$

It is important that this dependence, being introduced in the correlation function

$$g_{ab} = f_{ab} - f_a f_b \propto \exp\left(\frac{\Phi\left(\mathbf{r}_1, \mathbf{r}_2\right)}{k_B T} - 1 \right). \tag{C.7.19}$$

leads to finite integrals at infinity.

C.7.4. Coulomb collisions

Consider Coulomb collision with large impact parameter and, consequently, small deflection angle ϑ, measured in the center-of-mass system. The transport cross-section in non-relativistic case Lifshitz and Pitaevskii (1981) is

$$\sigma_t = \int (1 - \cos\vartheta)\, d\sigma \simeq \frac{1}{2}\int \vartheta^2 d\sigma. \tag{C.7.20}$$

Here the differential cross section with small angles is given by the Rutherford formula

$$d\sigma = \frac{8\pi\left(qq'\right)^2}{\mu^2\left(v - v'\right)^4}\frac{d\vartheta}{\vartheta^3}, \tag{C.7.21}$$

where prime denotes the second particle. Then the total cross-section is

$$\sigma_t = \frac{4\pi\left(qq'\right)^2}{\mu^2\left(v - v'\right)^4}\Lambda, \qquad \Lambda = \log\left(L\right) = \int \frac{d\vartheta}{\vartheta}. \tag{C.7.22}$$

This result shows that in non-relativistic plasma, due to the long-range nature of the electromagnetic interactions the "collision" process occurs at large distances between particles.

Consider now *Coulomb logarithm* in relativistic plasma. Electron-electron or electron-positron collisions are then described by Møller and Bhabha cross-sections, instead of (C.7.21). In this case the Born approximation has to be used since the relative velocity v_r between particles is larger than αc and then

$$L = \frac{m \langle v\gamma \rangle}{h} \lambda_D \simeq \vartheta_{\min}^{-1}. \tag{C.7.23}$$

In thermal equilibrium, using eqs. (C.7.8) and (C.5.15) one finds

$$\left\langle \frac{v}{c}\gamma \right\rangle = 3\theta + \frac{K_1\left(\theta^{-1}\right)}{K_2\left(\theta^{-1}\right)} \underset{\theta\to\infty}{\longrightarrow} 3\theta, \tag{C.7.24}$$

so in relativistic case one has

$$\log\left(\Lambda\right) = \frac{3}{4\pi^{3/2}}\theta^{\frac{3}{2}}\left(\alpha\lambda_C^3 n\right)^{-\frac{1}{2}} \underset{\theta\to\infty}{\longrightarrow} \mathcal{O}(1), \tag{C.7.25}$$

where α is the fine structure constant. This result implies that the mean free path due to Compton scattering $l_C = \frac{1}{n\sigma_T}$and the one due to Coulomb scattering $l_C = \frac{1}{\log(\Lambda)\sigma_T}$ become equal in the ultra-relativistic case. This formula shows also that for relativistic plasmas, when $\log\left(\Lambda\right) \simeq \mathcal{O}(1)$ the momentum transfer in Coulomb collisions is no longer small, and so the Fokker-Planck approximation (C.6.15) does not hold.

C.7.5. Characteristic distances

Following Klimontovich (1983) let us compare the characteristic distances in gas and plasma: the correlation radius r_{cor}, the average distance between particles r_{av} and the mean free path l.

For dilute gas interactions between particles occur when they approach each other, so the correlation length is $r_{cor} \sim r_0$, where r_0 is the particle (atom or molecule) size. Average distance between particles is determined from particle density n as $r_{av} \sim n^{-1/3}$. The mean free path, i.e. the average distance that particles travel without interactions is $l \sim (n\sigma)^{-1} \sim \left(nr_0^2\right)^{-1}$, where in the last relation the fact that the cross-section in gas is typically $\sigma \sim r_0^2$ is used.

For dilute plasma, as discussed above, $r_{cor} \sim \lambda_D$. The mean free path is instead $l \sim \left(n\lambda_D^2\right)^{-1}$.

From these quantities it is possible to construct dimensionless parameters characterizing a given medium: for dilute plasma and gas, respectively

$$\mathfrak{g}_p = \frac{1}{n\lambda_D^3} \ll 1, \quad \mathfrak{g}_g = nr_0^3 \ll 1. \tag{C.7.26}$$

Relativistic plasma in thermal equilibrium is always dilute, see Fig. C.3. In

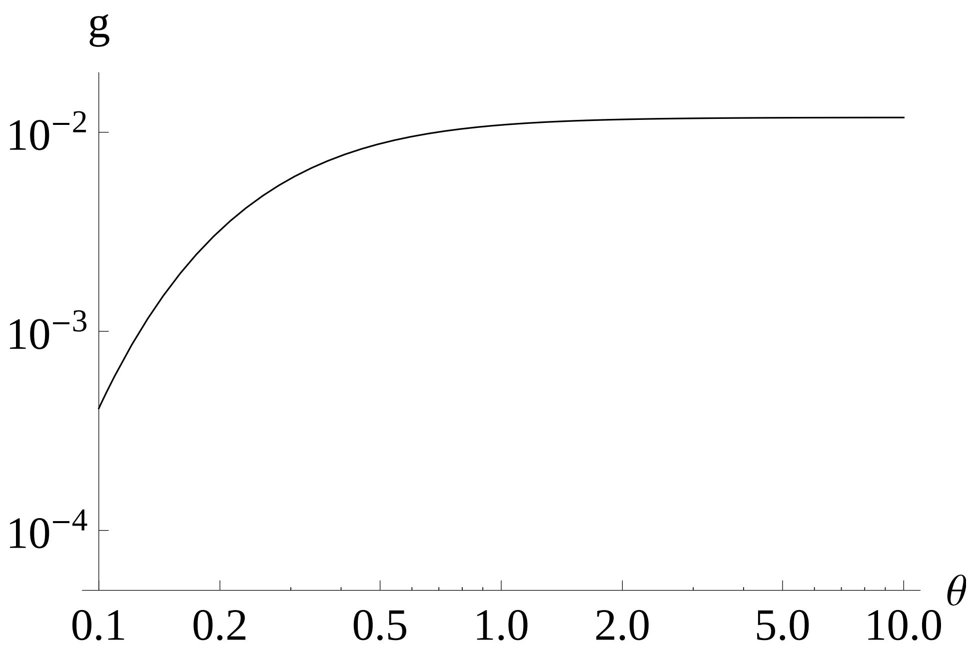

Figure C.3.: The plasma parameter of relativistic plasma in thermal equilibrium as function of dimensionless temperature.

general the following inequalities hold for gas and plasma

$$\begin{aligned} r_{cor} \ll r_{av} \ll l, &\quad \text{(gas)} \\ r_{av} \ll r_{cor} \ll l. &\quad \text{(plasma)} \end{aligned} \tag{C.7.27}$$

It is clear that in dilute gas interaction occurs only when two particles encounter or "collide" with each other. Correlations between particles may be neglected before and after the collision. In dilute plasma the situation is opposite. A given particle is interacting simultaneously with many particles located in the Debye sphere around this particle with radius λ_D. It means that particles move in the mean electromagnetic field, created by many other particles. This field has to be averaged over some volume, smaller than the Debye volume λ_D^3, but larger than the interparticle volumes r_{av}^3. The Vlasov approximation (C.6.13),(C.6.14) is valid when the rate of particle collisions is smaller than the rate of change of these averaged electromagnetic field. In other words, the relaxation lengths are much larger than the size of the system L.

Now it is possible to justify the derivation of the Boltzmann equation in Sec. C.3, where only binary interactions have been considered and interactions between three particles, four particles, and so on were neglected. Indeed, triple collisions in gas are much less probable than binary collisions, since the correlation function $C\,(1,2)$ is small, see e.g. Liboff (2003)

$$C\,(1,2) = f_2\,(1,2) - f_1\,(1)\,f_1\,(2) \sim \mathfrak{g}_g f_2\,(1,2)\,, \qquad \text{(C.7.28)}$$

where $f_2\,(1,2)$ is two particle DF, $f_1\,(1)$ and $f_1\,(2)$ stand for one particle DF of particle one and two, respectively. Analogously, $C\,(1,2,3) \sim \mathfrak{g}_g f_3\,(1,2,3)$ and so on.

From the kinetic point of view physically infinitesimally small scales should satisfy the inequalities

$$r_{ph} \ll L, \quad n r_{ph}^3 \gg 1, \qquad \text{(C.7.29)}$$

where L is the characteristic size in the problem (the size over which DF changes significantly). Then one has for such kinetic infinitesimally small scales

$$\begin{aligned} &r_K \ll l, \quad \text{(gas)} \\ &r_K \ll \lambda_D. \quad \text{(plasma)} \end{aligned} \qquad \text{(C.7.30)}$$

From the hydrodynamic point of view the relaxation scale is a function of the characteristic size L and of one of the three dissipation coefficients: diffusion D, viscosity ν and heat conductivity χ. The corresponding physically infinitesimally small scale satisfies the following inequality

$$r_{HD} \ll \frac{vL^2}{D^*}, \quad D^* = \max(D, \nu, \chi). \tag{C.7.31}$$

The transition from kinetic level of description to the hydrodynamic one is realized by the introduction of the physical *Knudsen number*

$$Kn = \frac{r_{ph}}{L} \ll 1. \tag{C.7.32}$$

The approximate methods of solutions of the Boltzmann equation (such as Hilbert, Chapman-Enskog, Grad methods, see e.g. Cercignani and Kremer (2002) and Liboff (2003)) use Kn as a small parameter for expansion of kinetic equations. The ratio of the two infinitesimally small scales (kinetic and hydrodynamic ones) is

$$\frac{r_K}{r_{HD}} \sim \mathfrak{g}_g^{3/10} Kn^{6/5} \leq 1, \tag{C.7.33}$$

where equality corresponds to the maximal Knudsen number (minimal scale L) when a common hydrodynamic and kinetic description of the system is still possible.

C.7.6. Relativistic degeneracy

If the temperature of plasma decreases for a given density of particles it may become degenerate Landau and Lifshitz (1980). The same phenomenon occurs when particle density increases, but the temperature is fixed. It is useful to construct the temperature-density diagram, see Fig. C.4.

The characteristic temperature which separates non-degenerate from degenerate systems is defined by

$$\theta_F \equiv \frac{E_F}{m_e c^2}, \tag{C.7.34}$$

where E_F is Fermi energy, corresponding to Fermi momentum

$$p_F = \left(3\pi^2 n\right)^{\frac{1}{3}} \hbar. \tag{C.7.35}$$

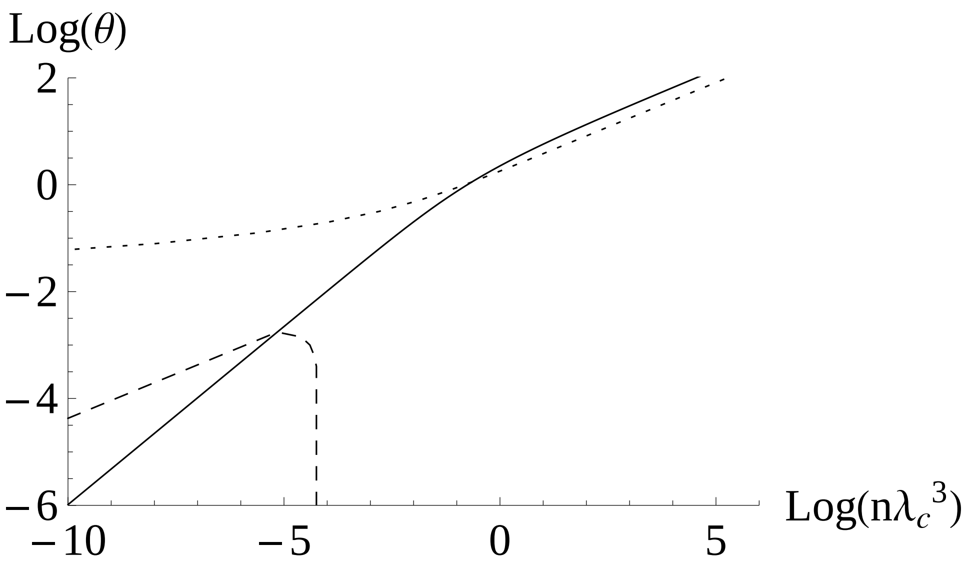

Figure C.4.: The temperature-density diagram for relativistic plasma. Solid line corresponds to the condition $\mathcal{D} = 1$. To the right of this curve $\mathcal{D} < 1$ and plasma is degenerate. Dashed curve corresponds to the condition $\mathfrak{g}_p = 1$. Above this curve $\mathfrak{g}_p < 1$ and plasma is ideal. Dotted curve corresponds to thermal electron-positron plasma.

For a relativistic gas the total energy and momentum are related $E^2 = p^2c^2 + m_e^2c^4$. Equating the kinetic energy $E - m_ec^2$ to the Fermi energy the degeneracy temperature is obtained

$$\theta_F = \left[\left(3\pi^2\right)^{\frac{4}{3}} \left(\lambda_C n^{\frac{1}{3}}\right)^2 + 1\right]^{1/2} - 1. \tag{C.7.36}$$

Define the degeneracy parameter

$$\mathcal{D} = \frac{\theta}{\theta_F}. \tag{C.7.37}$$

Note that it is related to the degeneracy parameter introduced in Groot et al. (1980) as $\mathcal{D}' = \frac{\theta^3}{n\lambda_C^3} \simeq \mathcal{D}^3$. Definition (C.7.37) takes into account both non-relativistic and ultra-relativistic asymptotics in eq. (C.7.36). As can be seen from Fig. C.4 even in thermal equilibrium relativistic plasma becomes degenerate, though this degeneracy is weak.

C.7.7. Landau damping

Following Lifshitz and Pitaevskii (1981) consider non-relativistic linear Landau damping with a simplified treatment. More details, including non-linear damping are given in the mathematical treatise Mouhot and Villani (2011), see also Klimontovich (1997). Consider a homogeneous isotropic plasma with DF $f_0(p)$. Assume that a weak electromagnetic field is present, which induces a small perturbation on DF such that $f = f_0(p) + \delta f$. In isotropic plasma magnetic field in eqs. (C.6.13),(C.6.14) is not important, then linearized eq. (C.6.13) becomes

$$\frac{\partial \delta f}{\partial t} + \mathbf{v} \cdot \nabla \delta f = q\mathbf{E}\frac{\partial f_0}{\partial \mathbf{p}}, \tag{C.7.38}$$

where δf and $\mathbf{E}$ are, respectively, DF and electric field perturbations. Assuming that $\delta f \sim \exp\left[i\left(\mathbf{kr} - \omega t\right)\right]$, $\mathbf{E} \sim \exp\left[i\left(\mathbf{kr} - \omega t\right)\right]$, the solution is

$$\delta f = \frac{q\mathbf{E}}{i\left(\mathbf{k}\cdot\mathbf{v} - \omega\right)} \cdot \frac{\partial f_0}{\partial \mathbf{p}}. \tag{C.7.39}$$

The dielectric constant, given by $4\pi\mathbf{P} = (\varepsilon - 1)\,\mathbf{E}$ can be found, observing that

$$i\mathbf{k}\cdot\mathbf{P} = -\rho = q\int \delta f d^3 p. \tag{C.7.40}$$

Since the function δf has a pole at $\omega = \mathbf{k}\cdot\mathbf{v}$ the integral above should be evaluated using the Landau rule $\omega \to \omega + i0$. The result is

$$\varepsilon = 1 - \frac{4\pi q^2}{k^2}\int \mathbf{k}\cdot\frac{\partial f_0}{\partial \mathbf{p}}\frac{d^3 p}{\left(\mathbf{k}\cdot\mathbf{v} - \omega - i0\right)}. \tag{C.7.41}$$

It means that the dielectric constant has an imaginary part. Introducing the DF along x-axis and choosing the direction of $\mathbf{k}$ along the same axis one gets

$$\mathrm{Im}\left(\varepsilon\right) = -\frac{4\pi q^2 m}{k^2}\frac{df\left(p_x\right)}{dp_x}. \tag{C.7.42}$$

Non-vanishing Im (ε) means that the electric field looses energy with the rate

$$Q = -|\mathbf{E}|^2 \frac{\pi m q^2}{2k^2} \frac{df(p_x)}{dp_x}. \tag{C.7.43}$$

This is collisionless damping of electromagnetic waves as established by Landau Landau (1946). The validity condition for this result is $\lambda_D \ll \frac{2\pi}{k} \ll L$.

Actually, the damping of electromagnetic field oscillations in non-relativistic case is exponentially weak. In contrast, in ultra relativistic case there are two possibilities: when phase velocity of the wave is smaller than the speed of light the damping is strong; in the opposite case the damping is absent Buti (1962). This result is generally confirmed for electron-positron plasma Laing and Diver (2006).

C.8. Pair plasma

In this section a special case of plasma will be considered, when both negative and positive charge carriers have equal masses: electron-positron plasma. Electron-positron plasma is of interest in many fields of physics and astrophysics. In cosmology during the lepton era ultra-relativistic electron-positron pairs contribute to the matter content of the Universe Weinberg (2008). The cosmic microwave background radiation is created at the black body photosphere Khatri and Sunyaev (2012), around the cosmic redshift $z = 10^6$.

In astrophysics comparable energy densities are expected to be reached in gamma-ray bursts sources, hence electron-positron pairs play an essential role there Piran (2005). Indications exist that the pair plasma is present also in active galactic nuclei Wardle et al. (1998), in the center of our Galaxy Churazov et al. (2005), around hypothetical quark stars Usov (1998). In the laboratory pair plasma is expected to appear in the fields of ultra intense lasers Blaschke et al. (2006), see also Benedetti et al. (2013) and Ruffini et al. (2010b) for review.

In many stationary astrophysical sources the pair plasma is thought to be in thermodynamic equilibrium. A detailed study of the relevant processes Bisnovatyi-Kogan et al. (1971), Weaver (1976), Lightman (1982), Gould (1982), Stepney and Guilbert (1983), Coppi and Blandford (1990), radiation mechanisms Lightman and Band (1981), possible equilibrium configurations

Lightman (1982), Svensson (1982a), Guilbert and Stepney (1985) and spectra Zdziarski (1984) in an optically thin pair plasma has been carried out. Particular attention has been given to collisional relaxation process Gould (1981), Stepney (1983), pair production and annihilation Svensson (1982b), relativistic bremsstrahlung Gould (1980), Haug (1985), double Compton scattering Lightman (1981), Gould (1984).

An equilibrium occurs if the sum of all reaction rates vanishes, see eq. (C.5.9) and discussion that follows. For instance, electron-positron pairs are in equilibrium when the net pair production (annihilation) rate is zero. This can be achieved by variety of ways and the corresponding condition can be represented as a system of algebraic equations Svensson (1984). However, the main assumption made in all the above mentioned works is that the plasma is assumed to obey relativistic quantum statistics. The latter is shown to be possible, in principle, in the range of temperatures up to 10 MeV Bisnovatyi-Kogan et al. (1971),Stepney (1983). It will be shown that independently of a wide set of initial conditions, thermal equilibrium forms for the phase space distribution functions are recovered during the process of thermalization by two body and three body direct and inverse particle-particle collisions. The pair plasma is assumed to be optically thick. Although moderately thick plasmas have been treated in the literature Guilbert and Stepney (1985), only qualitative description Bisnovatyi-Kogan et al. (1971),Svensson (1982a) was available for large optical depths until recently Aksenov et al. (2007),Aksenov et al. (2009).

C.8.1. Basic parameters

Consider a mildly relativistic plasma with average energy per particle $0.1 \lesssim \frac{\epsilon}{\mathrm{MeV}} \lesssim 10$. Before formulating the relativistic kinetic equations for the electron-positron plasma recall the basic plasma parameters and their typical values. The plasma parameter (C.7.26) for electron-positron plasma is typically $\mathfrak{g}_p = (n_- \lambda_D^3)^{-1} \sim 10^{-3}$, here $\lambda_D = \frac{c}{\omega}\sqrt{\theta_-}$ is the Debye length (C.7.8), $\theta_- = k_B T_- / (mc^2)$ is the dimensionless temperature, $\omega = \sqrt{4\pi q^2 n_- / m}$ is the plasma frequency, n_- is the electron number density, m is its mass. It implies that the relativistic Boltzmann equations for one particle distribution functions can be used to describe an electron-positron plasma. The classicality parameter $\varkappa = e^2/(\hbar v_r) = \alpha/\beta_r < 1$, where $v_r = \beta_r c$ is the mean relative velocity of particles. It means that in electron-positron plasma a quantum description of scattering is required. The Coulomb logarithm is $\Lambda = \mathcal{M}\lambda_D v_r \gamma_r/\hbar$, where $\mathcal{M}$ is the reduced mass. Since this expression contains the Debye length, which is defined only for a thermal plasma, the expression (C.7.25) for relativistic Coulomb logarithm will be used. As already mentioned in Sec. C.7.6 a relativistic plasma may be degenerate, but in what follows such relativistic degeneracy will be neglected.

Intensity of interaction of photons with other particles is characterized by the optical depth

$$\tau = \int_{\mathcal{L}} \sigma\,(n_- + n_+)\,dl, \tag{C.8.1}$$

where σ is the cross-section and the integral (C.8.1) is taken over the light-like worldline $\mathcal{L}$. In what follows consider the case in which plasma linear dimensions R exceed the photon mean free path $\lambda_\gamma = (n_-\sigma)^{-1}$, thus $\tau \gg 1$.

When admixture of protons and electrons is allowed it may be characterized by an additional parameter, the baryonic loading

$$B = \frac{n_p M c^2}{\rho_r}, \tag{C.8.2}$$

where M is the proton mass, ρ_r is the energy density in relativistic component (electrons, positrons and photons).

In thermal equilibrium, while e^+e^- are relativistic, with average energies $\epsilon_\pm \sim mc^2 \sim k_B T$, protons are not with kinetic energies $Mv_p^2 \sim k_B T$, and thus $\frac{v_p}{c} \sim \sqrt{\frac{m}{M}}$. Also in equilibrium with $\epsilon_\pm \geq mc^2$ one has $\rho_\pm \approx n_\pm mc^2$ and thus the density ratio between protons and pairs is $\frac{n_p}{n_\pm} \sim \frac{m}{M}B$. Since electron is subject to interaction with both electrons (positrons) and photons, one has for the ratio of mean free paths, see e.g. Groot et al. (1980)

$$\frac{\lambda_\gamma}{\lambda_\pm} = \log\left(\Lambda\right) + \frac{n_\pm + n_p}{n_\gamma}. \tag{C.8.3}$$

Note that there are two natural parameters for perturbative expansion in various expressions: the fine structure constant $\alpha \simeq 1/137$ and the ration between electron and proton masses $m/M \simeq 1/1836$.

C.8.2. Kinetic equation and collision integrals

Relativistic Boltzmann equations (C.3.9) for homogeneous isotropic plasma are

$$\frac{1}{c}\frac{\partial f_i}{\partial t} - \nabla U \frac{\partial f_i}{\partial \mathbf{p}} = \mathrm{St}\, f, \tag{C.8.4}$$

where U is a potential due to external force, $f_i(\epsilon, t)$ are distribution functions and the index i stands for electrons, positrons and photons. The second term on the LHS of eq. (C.8.4) describes the mean field produced by all particles, plus an external field. Particle collisions, including Coulomb ones, are taken into account by collision terms on the RHS. Particle motion between collisions is assumed to be subject to the mean field, which is neglected. This is an assumption, but in dense collision dominated plasma this assumption is justified, see e.g. Groot et al. (1980). Then eq. (C.8.4) reduces to a coupled system of partial-integro-differential equations

$$\frac{1}{c}\frac{\partial f_i}{\partial t} = \sum_q \left(\eta_i^q - \chi_i^q f_i\right), \tag{C.8.5}$$

where η_i^q and χ_i^q are the emission and the absorption coefficients for a given process q Mihalas and Mihalas (1984).

The elementary interactions between particles are described by the quantum field theory. In the case under consideration this is quantum electrodynamics. These coefficients have to be computed from the probability of a given process, expressed as function of the corresponding matrix element. In general, for a process involving a outgoing and b incoming particles the differential probability per unit time is ($\hbar = c = 1$)

$$dw = c(2\pi\hbar)^4 \delta^{(4)}\left(\mathfrak{p}_f - \mathfrak{p}_i\right)\left|M_{fi}\right|^2 V \left[\prod_b \frac{\hbar c}{2\epsilon_b V}\right]\left[\prod_a \frac{d\mathbf{p}'_a}{(2\pi\hbar)^3}\frac{\hbar c}{2\epsilon'_a}\right], \tag{C.8.6}$$

where $\mathbf{p}'_a$ and ϵ'_a (ϵ_b) are respectively momenta and energies of outgoing (incoming) particles, M_{fi} are the corresponding matrix elements, $\delta^{(4)}$ stands for energy-momentum conservation, V is the normalization volume. The list of processes that are relevant for optically thick electron-positron plasma is given in Tab. C.1.

The list of the leptonic processes involving protons is given in Tab. C.2.

Binary interactions	Radiative and pair producing variants
Møller and Bhabha scattering $e_1^\pm e_2^\pm \longrightarrow e_1^{\pm\prime} e_2^{\pm\prime}$ $e^\pm e^\mp \longrightarrow e^{\pm\prime} e^{\mp\prime}$	Bremsstrahlung $e_1^\pm e_2^\pm \longleftrightarrow e_1^{\pm\prime} e_2^{\pm\prime}\gamma$ $e^\pm e^\mp \longleftrightarrow e^{\pm\prime} e^{\mp\prime}\gamma$
Single Compton scattering $e^\pm\gamma \longrightarrow e^\pm\gamma'$	Double Compton scattering $e^\pm\gamma \longleftrightarrow e^{\pm\prime}\gamma'\gamma''$
Pair production and annihilation $\gamma\gamma' \longleftrightarrow e^\pm e^\mp$	Radiative pair production and three photon annihilation $\gamma\gamma' \longleftrightarrow e^\pm e^\mp \gamma''$ $e^\pm e^\mp \longleftrightarrow \gamma\gamma'\gamma''$
	$e^\pm\gamma \longleftrightarrow e^{\pm\prime} e^\mp e^{\pm\prime\prime}$

Table C.1.: Microphysical processes in the pair plasma.

Binary interactions	Radiative and pair producing variants
Coulomb scattering $p_1 p_2 \longrightarrow p_1' p_2'$ $pe^\pm \longrightarrow p' e^{\pm\prime}$	Bremsstrahlung $p_1 p_2 \longleftrightarrow p_1' p_2' \gamma$ $pe^\pm \longleftrightarrow p' e^{\pm\prime}\gamma$
	$pe_1^\pm \longleftrightarrow p' e_1^{\pm\prime} e^\pm e^\mp$
Single Compton scattering $p\gamma \longrightarrow p'\gamma'$	Double Compton scattering and radiative pair production $p\gamma \longleftrightarrow p'\gamma'\gamma''$
	$p\gamma \longleftrightarrow p' e^\pm e^\mp$

Table C.2.: Microphysical processes involving protons in the pair plasma.

Each of the above mentioned reactions is characterized by the corresponding time-scale and optical depth. For Compton scattering of an electron, for instance, one has

$$t_{\rm cs} = \frac{1}{\sigma_T n_\pm c}, \qquad \tau_{\rm cs} = \sigma_T n_\pm R, \tag{C.8.7}$$

where $\sigma_T = \frac{8\pi}{3}\alpha^2(\frac{\hbar}{mc})^2$ is the Thomson cross-section, R is the linear size of plasma. There are several time-scales in this problem that characterize the condition of detailed balance between direct and inverse reactions, namely

- Pair production, Compton and electron-electron scattering: $t_{\gamma e} \sim t_{\gamma e} \sim (\sigma_T nc)^{-1}$;
- Cooling: $t_{br} = \alpha^{-1} t_c$;
- Proton-proton: $\left(n_p t_{pp}\right)^{-1} \approx \sqrt{\frac{m}{M}}\left(n_- t_{ee}\right)^{-1}, \qquad v_p \approx \sqrt{\frac{m}{M}} v_e, \qquad v_e \approx c$;
- Electron-proton: $t_{ep}^{-1} \approx \frac{\epsilon_\pm}{Mc^2} t_{ee}^{-1}, \qquad \epsilon_\pm \ll \epsilon_p$;
- Proton Compton scattering: $\left(n_p t_{\gamma p}\right)^{-1} \approx \left(\frac{\epsilon}{Mc^2}\right)^2 \left(n_- t_{\gamma e}\right)^{-1}, \qquad \epsilon \geq mc^2$;
- Dynamical time-scale: $\qquad t_{hyd} \sim R/c$.

As example of collision integral consider the absorption coefficient for Compton scattering which is given by

$$\chi^{\rm cs} f_\gamma = \int d\mathbf{k}' d\mathbf{p} d\mathbf{p}' W_{\mathbf{k}',\mathbf{p}';\mathbf{k},\mathbf{p}} f_\gamma(\mathbf{k},t) f_\pm(\mathbf{p},t), \tag{C.8.8}$$

where $\mathfrak{p}$ and $\mathfrak{k}$ are the four-momenta of electron (positron) and photon respectively, $\mathbf{p}$ and $\mathbf{k}$ are their three-momenta, $d\mathbf{p} = d\epsilon_\pm do \epsilon_\pm^2 \beta_\pm / c^3$, $d\mathbf{k}' = d\epsilon'_\gamma \epsilon'^2_\gamma do'_\gamma / c^3$ and the transition rate $W_{\mathbf{k}',\mathbf{p}';\mathbf{k},\mathbf{p}}$ is related to the differential transition probability $dw_{\mathbf{k}',\mathbf{p}';\mathbf{k},\mathbf{p}}$ per unit time as

$$W_{\mathbf{k}',\mathbf{p}';\mathbf{k},\mathbf{p}} d\mathbf{k}' d\mathbf{p}' \equiv V dw_{\mathbf{k}',\mathbf{p}';\mathbf{k},\mathbf{p}}, \quad dw_{\mathbf{k}',\mathbf{p}';\mathbf{k},\mathbf{p}} = w_{\mathbf{k}',\mathbf{p}';\mathbf{k},\mathbf{p}} d\mathbf{k}' d\mathbf{p}'. \tag{C.8.9}$$

One integration over $d\mathbf{p}'$ as $\int d\mathbf{p}' \delta(d\mathbf{k} + d\mathbf{p} - d\mathbf{k}' - d\mathbf{p}') \to 1$ can be readily performed. Then it is necessary to take into account the momentum conservation in the next integration over $d\mathbf{k}'$, namely

$$\int d\epsilon'_\gamma \delta(\epsilon_\gamma + \epsilon_\pm - \epsilon'_\gamma - \epsilon'_\pm) \to \frac{1}{|\partial(\epsilon'_\gamma + \epsilon'_\pm)/\partial\epsilon'_\gamma|} \equiv J_{\rm cs}, \tag{C.8.10}$$

where the Jacobian of the transformation is $J_{\rm cs} = \frac{1}{1-\beta'_\pm \mathbf{b}'_\gamma \cdot \mathbf{b}'_\pm}$, where $\mathbf{b}_i = \mathbf{p}_i/p$, $\mathbf{b}'_i = \mathbf{p}'_i/p'$ and $\mathbf{b}'_\pm = (\beta_\pm\epsilon_\pm\mathbf{b}_\pm + \epsilon_\gamma\mathbf{b}_\gamma - \epsilon'_\gamma\mathbf{b}'_\gamma)/(\beta'_\pm\epsilon'_\pm)$. Finally, for the absorption coefficient one has

$$\chi^{\rm cs} f_\gamma = -\int \frac{do'_\gamma d\mathbf{p}}{(2\pi)^2} \frac{\epsilon'_\gamma |M_{fi}|^2 \hbar^2 c^2}{16\epsilon_\pm\epsilon_\gamma\epsilon'_\pm} J_{\rm cs} f_\gamma(\mathbf{k}, t) f_\pm(\mathbf{p}, t), \tag{C.8.11}$$

where the matrix element squared, see e.g. Berestetskii et al. (1982), is

$$\begin{aligned} |M_{fi}|^2 = 2^6\pi^2\alpha^2 & \left[\frac{m^2c^2}{s - m^2c^2} + \frac{m^2c^2}{u - m^2c^2} + \left(\frac{m^2c^2}{s - m^2c^2} + \frac{m^2c^2}{u - m^2c^2} \right)^2 \right. \\ & \left. - \frac{1}{4} \left(\frac{s - m^2c^2}{u - m^2c^2} + \frac{u - m^2c^2}{s - m^2c^2} \right) \right], \end{aligned} \tag{C.8.12}$$

$s = (\mathfrak{p} + \mathfrak{k})^2$ and $u = (\mathfrak{p} - \mathfrak{k}')^2$ are invariants, $\mathfrak{k} = (\epsilon_\gamma/c)(1, \mathbf{e}_\gamma)$ and $\mathfrak{p} = (\epsilon_\pm/c)(1, \beta_\pm\mathbf{e}_\pm)$ are energy-momentum four-vectors of photons and electrons, respectively, $d\mathbf{p} = d\epsilon_\pm do \epsilon_\pm^2 \beta_\pm/c^3$, $d\mathbf{k}' = d\epsilon'_\gamma \epsilon'^2_\gamma do'_\gamma/c^3$ and $do = d\mu d\phi$.

As example of triple interactions consider the relativistic bremsstrahlung

$$e_1 + e_2 \leftrightarrow e'_1 + e'_2 + \gamma'. \tag{C.8.13}$$

For the time derivative, for instance, of the distribution function f_2 in the direct and in the inverse reactions (C.8.13) one has

$$\begin{aligned} \dot{f}_2 &= \int d\mathbf{p}_1 d\mathbf{p}'_1 d\mathbf{p}'_2 d\mathbf{k}' \left[W_{\mathbf{p}'_1,\mathbf{p}'_2,\mathbf{k}';\mathbf{p}_1,\mathbf{p}_2} f'_1 f'_2 f'_k - W_{\mathbf{p}_1,\mathbf{p}_2;\mathbf{p}'_1,\mathbf{p}'_2,\mathbf{k}'} f_1 f_2 \right] = \\ &= \int d\mathbf{p}_1 d\mathbf{p}'_1 d\mathbf{p}'_2 d\mathbf{k}' \frac{c^6\hbar^3}{(2\pi)^2} \frac{\delta^{(4)}(P_f - P_i)|M_{fi}|^2}{2^5\epsilon_1\epsilon_2\epsilon'_1\epsilon'_2\epsilon'_\gamma} \left[f'_1 f'_2 f'_k - \frac{1}{(2\pi\hbar)^3} f_1 f_2 \right], \end{aligned} \tag{C.8.14}$$

$$d\mathbf{p}_1 d\mathbf{p}_2 W_{\mathbf{p}'_1,\mathbf{p}'_2,\mathbf{k}';\mathbf{p}_1,\mathbf{p}_2} \equiv V^2 dw_1, \quad d\mathbf{p}'_1 d\mathbf{p}'_2 d\mathbf{k}' W_{\mathbf{p}_1,\mathbf{p}_2;\mathbf{p}'_1,\mathbf{p}'_2,\mathbf{k}'} \equiv V dw_2,$$

A finite difference method with a computational grid in the phase space can

	Interaction	Parameters of DFs
I	e^+e^- scattering	$\theta_+ = \theta_-$, $\forall\nu_+,\nu_-$
II	$e^\pm p$ scattering	$\theta_p = \theta_\pm$, $\forall\nu_\pm,\nu_p$
III	$e^\pm\gamma$ scattering	$\theta_\gamma = \theta_\pm$, $\forall\nu_\gamma,\nu_\pm$
IV	pair production	$\nu_+ + \nu_- = 2\nu_\gamma$, if $\theta_\gamma = \theta_\pm$
V	Tripe interactions	ν_γ, $\nu_\pm = 0$, if $\theta_\gamma = \theta_\pm$

Table C.3.: Thermodynamic quantities under detailed balance conditions for a given process.

be used for numerical solution of eq. (C.8.5), see Aksenov et al. (2009). In what follows a concrete example of numerical solution of the system of relativistic Boltzmann equations (C.8.5) will be discussed. In order to interpret this solution it is necessary to introduce the notion of kinetic equilibrium Aksenov et al. (2007).

C.8.3. Kinetic and thermal equilibria

The number of conservation laws in the problem under consideration imply the existence of some relations between thermodynamic quantities in equlibrium. The following conservation laws exist: energy conservation $\frac{d}{dt}\sum_i \rho_i = 0$, particle number conservation for binary reactions $\frac{d}{dt}\sum_i n_i = 0$, baryonic number conservation $\frac{dn_p}{dt} = 0$ and charge conservation $n_- = n_+ + n_p$. The condition for the chemical potentials coming from detailed balance conditions is $\varphi_+ + \varphi_- = 2\varphi_\gamma$.

The kinetic equilibrium is defined as the state when the detailed balance condition is satisfied for any binary process. In this state distribution functions have the following form

$$f_i(\varepsilon) = \frac{2}{(2\pi\hbar)^3} \exp\left(-\frac{\varepsilon - \nu_i}{\theta_i}\right), \tag{C.8.15}$$

with chemical potential $\nu_i \equiv \frac{\phi_i}{mc^2}$ and temperature $\theta_i \equiv \frac{k_B T_i}{m_e c^2}$, where $\varepsilon \equiv \frac{\epsilon}{m_e c^2}$ is the energy of the particle. In particular, detailed balance conditions with respect to a given direct and inverse process listed in Tab. C.1 leads to the following constraints on temperatures and chemical potentials in eq. (C.8.15):

Provided conditions I-IV in Tab. C.3 are satisfied, one can obtain the relation between two couples of quantities: total the number density and the total energy density on the one hand, and temperature and the chemical potential on the other hand. In particular, for photons

$$n_\gamma = \frac{1}{V_0}\exp\left(\frac{\nu_\gamma}{\theta}\right)2\theta^3, \qquad \frac{\rho_\gamma}{n_\gamma mc^2} = 3\theta, \qquad V_0 = \frac{1}{8\pi}\left(\frac{2\pi\hbar}{mc}\right)^3. \quad \text{(C.8.16)}$$

From eqs. (C.5.15) and (C.5.19) for non-degenerate pairs

$$n_\pm = \frac{1}{V_0}\exp\left(\frac{\nu_\pm}{\theta}\right)j_1(\theta), \qquad \frac{\rho_\pm}{n_\pm mc^2} = j_2(\theta), \quad \text{(C.8.17)}$$

and for non-relativistic protons

$$n_p = \frac{1}{V_0}\sqrt{\frac{\pi}{2}}\left(\frac{M}{m}\right)^{3/2}\exp\left(\frac{\nu_p - M/m}{\theta}\right)\theta^{3/2}, \qquad \frac{\rho_p}{Mn_pc^2} = 1 + \frac{3}{2}\frac{m}{M}\theta, \quad \text{(C.8.18)}$$

where

$$\begin{aligned} j_1(\theta) &= \theta K_2(\theta^{-1}) \rightarrow \left\{ \begin{array}{ll} \sqrt{\frac{\pi}{2}}e^{-\frac{1}{\theta}}\theta^{3/2}, & \theta \rightarrow 0 \\ 2\theta^3, & \theta \rightarrow \infty \end{array} \right., \\ j_2(\theta) &= \frac{3K_3(\theta^{-1}) + K_1(\theta^{-1})}{4K_2(\theta^{-1})} \rightarrow \left\{ \begin{array}{ll} 1 + \frac{3}{2}\theta, & \theta \rightarrow 0 \\ 3\theta, & \theta \rightarrow \infty \end{array} \right. . \end{aligned} \quad \text{(C.8.19)}$$

With nonzero baryon loading (C.8.2) in kinetic equilibrium $\theta_+ = \theta_- = \theta_\gamma = \theta_\mathrm{k}$, but it may be that $\theta_p \neq \theta_\mathrm{k}$. Summing up energy densities

$$\begin{aligned} \sum_{e^+,e^-,\gamma}\rho_i = \frac{mc^2}{V_0}&\left\{\left[1 - \frac{n_pV_0}{j_1(\theta_\mathrm{k})}\exp\left(-\frac{\nu_+}{\theta_\mathrm{k}}\right)\right]^{\frac{1}{2}} \times \right. \\ &\left. \times 6\theta_\mathrm{k}^4\exp\left(\frac{\nu_+}{\theta_\mathrm{k}}\right) + \left[2j_1(\theta_k)\exp\left(\frac{\nu_+}{\theta_\mathrm{k}}\right) - n_pV_0\right]j_2(\theta_\mathrm{k})\right\}, \end{aligned} \quad \text{(C.8.20)}$$

and analogously for number densities

$$\sum_{e^+,e^-,\gamma} n_i = \frac{1}{V_0}\left\{\left[1-\frac{n_p V_0}{j_1(\theta_\mathrm{k})}\exp\left(-\frac{\nu_+}{\theta_\mathrm{k}}\right)\right]^{\frac{1}{2}} \times \right. \tag{C.8.21}$$
$$\left. \times 6\theta_\mathrm{k}^4 \exp\left(\frac{\nu_+}{\theta_\mathrm{k}}\right) + 2j_1(\theta_\mathrm{k})\exp\left(\frac{\nu_+}{\theta_\mathrm{k}}\right)\right\}.$$

Equations (C.8.20) and (C.8.21) represent the relations between (ρ, n) and $(\nu_+, \theta_\mathrm{k})$. Conservation laws allow to determine the rest of chemical potentials, obtained from the following relations

$$\exp\left(\frac{\nu_-}{\theta_\mathrm{k}}\right) = \exp\left(\frac{\nu_+}{\theta_\mathrm{k}}\right) + \frac{n_p V_0}{j_1(\theta_\mathrm{k})}, \tag{C.8.22}$$

$$\exp\left(\frac{\nu_\gamma}{\theta_\mathrm{k}}\right) = \exp\left(\frac{\nu_+}{\theta_\mathrm{k}}\right)\left[1+\frac{n_p V_0}{j_1(\theta_\mathrm{k})}\exp\left(-\frac{\nu_+}{\theta_\mathrm{k}}\right)\right]^{\frac{1}{2}}, \tag{C.8.23}$$

The temperature and chemical potential of protons can be found separately.

In thermal equilibrium ν_γ vanishes and one has

$$\nu_- = \theta_\mathrm{k}\mathrm{arcsinh}\left[\frac{n_p V_0}{2j_1(\theta_\mathrm{k})}\right], \qquad \nu_+ = -\nu_-, \tag{C.8.24}$$

which both reduce to $\nu_- = \nu_+ = 0$ for $n_p = 0$. At the same time, for $n_p > 0$ one always has $\nu_- > 0$ and $\nu_+ < 0$ in thermal equilibrium. In order to determine the Coulomb logarithm as function of particle energies, one can use the relation (C.7.23). The minimal scattering angle in thermal relativistic plasma in the center of mass system Haug (1985) is

$$\theta_{\min} = \frac{2\hbar}{\mathcal{M}cD}\frac{\gamma_r}{(\gamma_r+1)\sqrt{2(\gamma_r-1)}}, \tag{C.8.25}$$

where the maximum impact parameter (neglecting the effect of protons) is $D = \frac{c^2}{\omega}\frac{p_0}{\epsilon_{10}}$, where p_0 and ϵ_{10} are CM quantities, and the invariant Lorentz factor of relative motion is

$$\gamma_r = \frac{1}{\sqrt{1-\left(\frac{v_r}{c}\right)^2}} = \frac{\epsilon_1\epsilon_2 - \mathbf{p}_1\mathbf{p}_2 c^2}{m_1 m_2 c^4}. \tag{C.8.26}$$

The Coulomb logarithm is

$$\log(\Lambda) = \frac{1}{2} - \log\left(\sqrt{2}\sin\theta_{\min}\right). \tag{C.8.27}$$

C.8.4. Numerical example

Consider now an example of thermalization of initially non-equilibrium electron-positron plasma, following Aksenov et al. (2009). The following initial conditions are adopted: flat initial spectral energy densities $E_i(\epsilon_i) = \frac{4\pi\epsilon_i^3\beta_i f_i}{c^3} = \text{const}$, with total energy density $\rho = 10^{24}\text{erg/cm}^3$. Plasma is dominated by photons with small amount of electron-positron pairs, the ratio between energy densities in photons and in electron-positron pairs $\rho_\pm/\rho_\gamma = 10^{-5}$. Baryonic loading parameter $B = 10^{-3}$, corresponding to $\rho_p = 2.7 \times 10^{18}\text{erg/cm}^3$. The energy density in each component of plasma

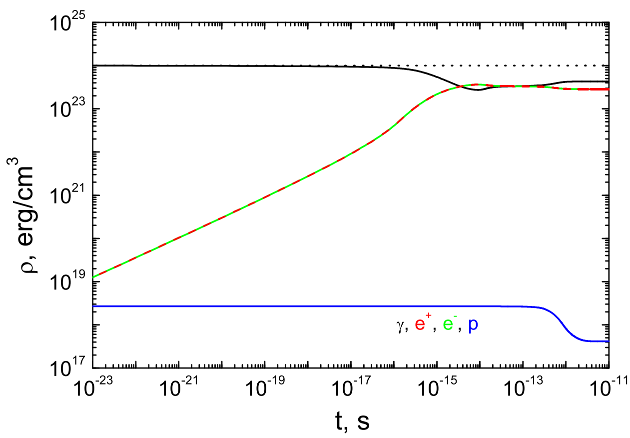

Figure C.5.: Depencence on time of energy densities of electrons (green), positrons (red), photons (black) and protons (blue) for initial conditions I. Total energy density is shown by dotted black line. Interaction between pairs and photons operates on very short time-scales up to 10^{-23} sec. Quasi-equilibrium state is established at $t_k \simeq 10^{-14}$ sec which corresponds to kinetic equilibrium for pairs and photons. Protons start to interact with then as late as at $t_{th} \simeq 10^{-13}$ sec.

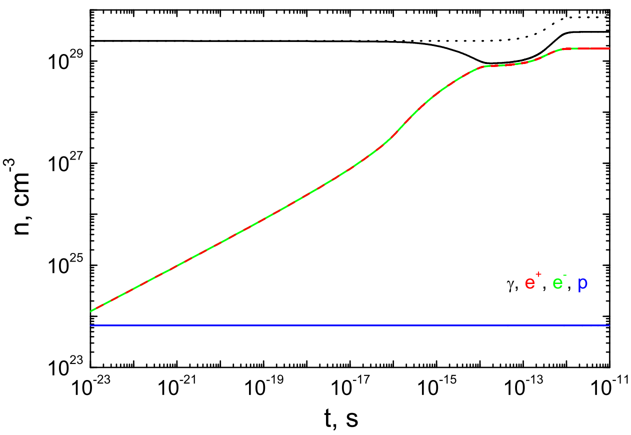

Figure C.6.: Depencence on time of concentrations of electrons (green), positrons (red), photons (black) and protons (blue) for initial conditions I. Total number density is shown by dotted black line. In this case kinetic equilibrium between electrons, positrons and photons is reached at $t_k \simeq 10^{-14}$ sec. Protons join thermal equilibrium with other particles at $t_{th} \simeq 4 \times 10^{-12}$ sec.

changes, as can be seen from Fig. C.5, keeping constant the total energy density shown by dotted line in Fig. C.5, as the energy conservation requires. As early as at 10^{-23} sec the energy starts to redistribute between electrons and positrons from the one hand and photons from the other hand essentially by the pair-creation process. This leads to equipartition of energies between these particles at 3×10^{-15} sec. Concentrations of pairs and photons equalize at 10^{-14} sec, as can be seen from Fig. C.6. From this moment temperatures and chemical potentials of electrons, positrons and photons tend to be equal, see Fig. C.7 and Fig. C.8 respectively, and it corresponds to the approach to kinetic equilibrium.

This is quasi-equilibrium state since total number of particles is still approximately conserved, as can be seen from Fig. C.6, and triple interactions are not yet efficient. At the moment $t_1 = 4 \times 10^{-14}$ sec, shown by the vertical line on the left in Fig. C.7 and Fig. C.8, the temperature of photons and pairs is $\theta_k \simeq 1.5$, while the chemical potentials of these particles are $\nu_k \simeq -7$. Concentration of protons is so small that their energy density is not affected by the presence of other components; also proton-proton collisions are inef-

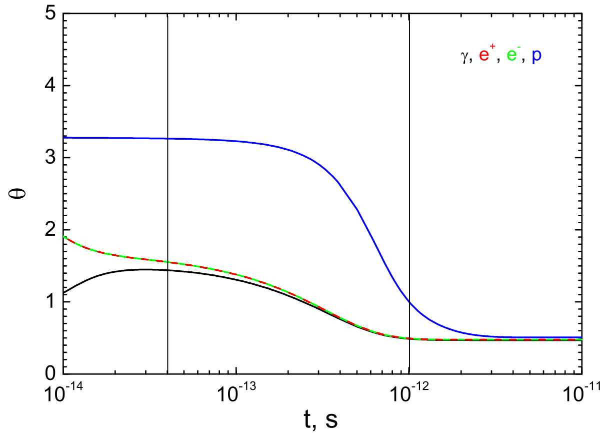

Figure C.7.: Depencence on time of dimensionless temperature of electrons (green), positrons (red), photons (black) and protons (blue) for initial conditions I. The temperature for pairs and photons acquires physical meaning only in kinetic equilibrium at $t_{\rm k} \simeq 10^{-14}$ sec. Protons are cooled by the pair-photon plasma and acquire common temperature with it as late as at $t_{\rm th} \simeq 4 \times 10^{-12}$ sec.

ficient. In other words, protons do not interact yet and their spectra are not yet of equilibrium form, see Fig. C.9. The temperature of protons start to change only at 10^{-13} sec, when proton-electron Coulomb scattering becomes efficient.

As can be seen from Fig. C.8, the chemical potentials of electrons, positrons and photons evolved by that time due to triple interactions. Since chemical potentials of electrons, positrons and photons were negative, the particles were in deficit with respect to the thermal state. This caused the total number of these particles to increase and consequently the temperature to decrease. The chemical potential of photons reaches zero at $t_2 = 10^{-12}$ sec, shown by the vertical line on the right in Fig. C.7 and Fig. C.8, which means that electrons, positrons and photons are now in thermal equilibrium. However, protons are not yet in equilibrium with other particle since their spectra are not thermal, as shown in the lower part of Fig. C.9.

Finally, the proton component thermalize with other particles at 4×10^{-12} sec, and from that moment plasma is characterized by unique temperature,

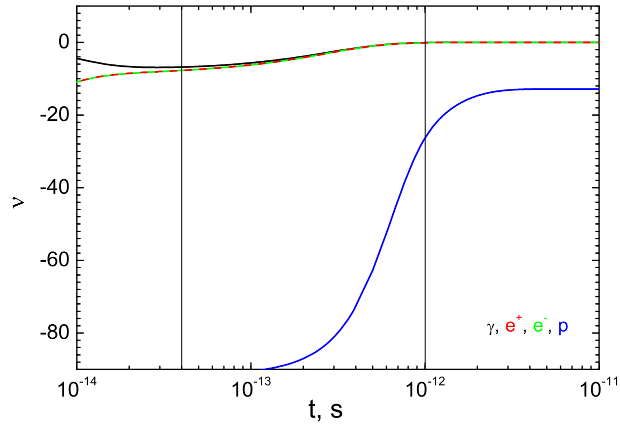

Figure C.8.: Depencence on time of dimensionless chemical potential of electrons (green), positrons (red), photons (black) and protons (blue) for initial conditions I. The chemical potential for pairs and photons acquires physical meaning only in kinetic equilibrium at $t_k \simeq 10^{-14}$ sec, while for protons this happens at $t_{th} \simeq 4 \times 10^{-12}$ sec. At this time chemical potential of photons has evolved to zero and thermal equilibrium has been already reached.

$\theta_{th} \simeq 0.48$ as Fig. C.7 clearly shows. Protons have final chemical potential $\nu_p \simeq -12.8$.

This state is characterized by thermal distribution of all particles as can be seen from Fig. C.10. There initial flat as well as final spectral densities are shown together with fits of particles spectra with the values of the common temperature and the corresponding chemical potentials in thermal equilibrium.

In this particular example relaxation time-scales towards kinetic and thermal equilibria have been determined. One can similarly determine relaxation time-scales as the function of total energy density ρ and baryon loading parameter B in wide range range of these parameters. This was done in Aksenov et al. (2010).

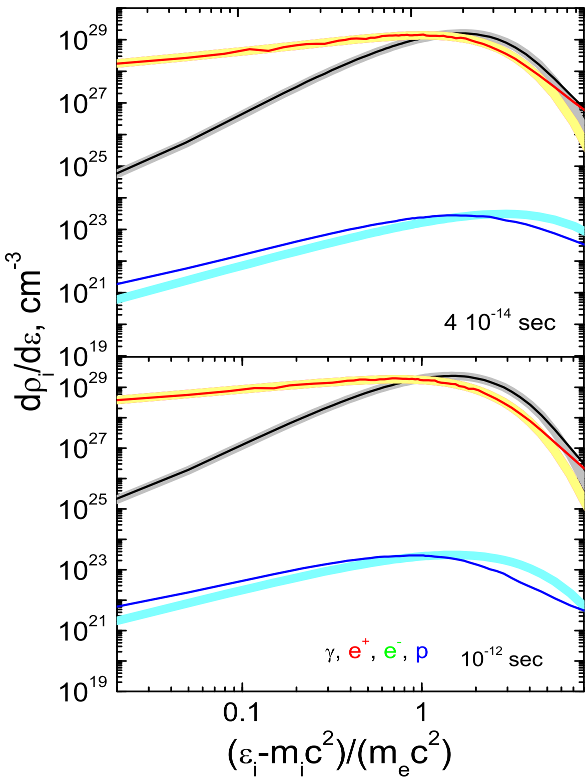

Figure C.9.: Spectral density as function of particle energy for electrons (green), positrons (red), photons (black) and protons (blue) for initial conditions I at intermediate time moments $t_1 = 4 \times 10^{-14}$ sec (upper figure) and $t_2 = 10^{-12}$ sec (lower figure). Fits of the spectra with chemical potentials and temperatures corresponding to thermal equilibrium state are also shown by yellow (electrons and positrons), grey (photons) and light blue (protons) thick lines. The upper figure shows the spectra when kinetic equilibrium is established for the first time between electrons, positrons and photons while the lower figure shows the spectra at thermal equilibrium between these particles. On both figures protons are not yet in equilibrium neither with themselves nor with other particles.

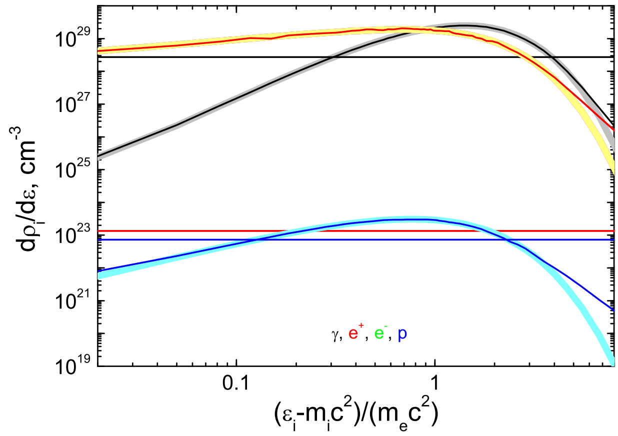

Figure C.10.: Spectral density as function of particle energy are shown as before at initial and final moments of the computations. The final photon spectrum is black body one.

C.9. Collisionless and self-gravitating systems

The kinetic approach is remarkably useful in studying collisionless systems. In such systems particle do not collide, but interact via long range forces such as gravitational and electromagnetic fields. The basic equations governing evolution of the system are, respectively, Vlasov-Einstein and Vlasov-Maxwell equations. In this Section systems interacting via electromagnetic and gravitatinal fields will be discussed.

C.9.1. Plasma instabilities

In Sec. C.7.7 damping of waves in collisionless plasma were discussed. This process suppresses the amplitude of initial perturbations thus bringing the system to an equilibrium. The opposite can happen, namely initially small perturbation can grow with time: this process is generally referred to as instability. There are many plasma instabilities occurring when different plasma flows, particles with different masses and electromagnetic fields interact Mikhailovskii (1975). The focus will be on two particular kinds, which are thought to occur in astrophysical conditions: *Weibel* and *two stream* instabilities.

The Weibel instability is a plasma instability present in homogeneous or nearly-homogeneous electromagnetic plasmas which possess an anisotropy in momentum (velocity) space. In the linear limit the instability causes exponential growth of electromagnetic fields in the plasma which helps to restore momentum space isotropy.

The two stream instability can be thought of as the inverse of Landau damping, where the existence of a greater number of particles that move slower than the wave phase velocity as compared with those that move faster, leads to an energy transfer from the wave to the particles. Again, focus will be on non-relativistic case for simplicity, see Achterberg and Wiersma (2007) for Weibel instability in relativistic plasma and Dieckmann (2005) for relativistic two-stream instability, see also Bret et al. (2008).

Following Weibel (1959) consider an electron-ion plasma, where electrons have an anisotropic DF $f_0(\mathbf{v})$. The equations for first order perturbations are obtained from the Vlasov-Maxwell equations (C.6.13),(C.6.14) as

$$\frac{\partial \delta f}{\partial t} + \mathbf{v}\cdot\frac{\partial \delta f}{\partial \mathbf{r}} + \frac{q}{m}\left[\mathbf{v}\times\mathbf{B}_0\right]\cdot\frac{\partial \delta f}{\partial \mathbf{v}} = -\frac{q}{m}\left[\mathbf{E}+\mathbf{v}\times\mathbf{B}\right]\cdot\frac{\partial f_0}{\partial \mathbf{v}}, \tag{C.9.1}$$

where magnetic field $\mathbf{B}_0$ is included for generality. In analogy with Sec. C.7.7 assume that perturbations of DF and electromagnetic fields fields are of the form $\exp\left[-i\left(\mathbf{k}\cdot\mathbf{r}-\omega t\right)\right]$. Then it follows

$$i\left(\omega+\mathbf{k}\cdot\mathbf{v}\right)\delta f - \frac{q}{m}\mathbf{B}_0\cdot\left[\mathbf{v}\times\frac{\partial \delta f}{\partial \mathbf{v}}\right] = -\frac{q}{m\omega}\left\{\omega\mathbf{E}\cdot\frac{\partial f_0}{\partial \mathbf{v}} + \left[\mathbf{k}\times\mathbf{E}\right]\cdot\left[\mathbf{v}\times\frac{\partial f_0}{\partial \mathbf{v}}\right]\right\}, \tag{C.9.2}$$

where the effect of anisotropy is seen on the RHS. Actually the external magnetic field $\mathbf{B}_0$ is not necessary for the development of instability, it is included for generality. Assume $\mathbf{k}\parallel\hat{\mathbf{z}}$, $\mathbf{E}\perp\mathbf{k}$ and consider a special case of distribution function

$$f_0 = \frac{n}{(2\pi)^{3/2}\,u_0^2 u_3}\exp\left(-\frac{v_x^2+v_y^2}{2u_0^2}-\frac{v_z^2}{2u_3^2}\right). \tag{C.9.3}$$

Now taking $\mathbf{B}_0=0$, $\omega\gg u_3 k$ it is possible to integrate the dispersion relation and get

$$\omega^4-\left(\omega_p^2+k^2\right)\omega^2-u_0^2\omega_p^2k^2=0, \tag{C.9.4}$$

where $\omega_p^2 = \frac{4\pi q^2 n}{m}$ is the usual plasma frequency. This equation has four roots

$$\omega = \pm \left\{ \frac{1}{2} \left[\omega_p^2 + k^2 \pm \sqrt{\left(\omega_p^2 + k^2\right)^2 + 4u_0^2\omega_p^2 k^2} \right] \right\}^{1/2}, \tag{C.9.5}$$

and the one corresponding to both "$-$" signs is negative imaginary. It is the source of instability. This solution is valid only when $u_0 \gg u_3$ (velocity dispersion in $\hat{\mathbf{z}}$ direction is much smaller than in other directions).

The two stream instability occurs for instance when there is a stream of particles uniformly distributed in space through a plasma at rest (counter streaming beams etc.). Consider electron-ion plasma with electron density n_e, and electrons with much smaller density n_e' stream through it with constant velocity $\mathbf{v}$ (total charge is zero).

Following the same steps as before the dispersion relation can be obtained, see e.g. Lifshitz and Pitaevskii (1981). In this case one has

$$\left(\frac{\omega_e}{\omega}\right)^2 + \left(\frac{\omega_e'}{\omega - \mathbf{k}\cdot\mathbf{v}}\right)^2 = 1, \quad \omega_e^2 = \frac{4\pi q^2 n_e}{m}, \quad \omega_e'^2 = \frac{4\pi q^2 n_e'}{m}, \tag{C.9.6}$$

and one should search for its solution of the form $\omega = \mathbf{k}\cdot\mathbf{v} + \delta$, where $\delta \ll \mathbf{k}\cdot\mathbf{v}$. The solution is

$$\delta = \pm \frac{\omega_e'}{\sqrt{1 - (\omega_e/\mathbf{k}\cdot\mathbf{v})^2}}. \tag{C.9.7}$$

For $\mathbf{k}\cdot\mathbf{v} \ll \omega_e$ purely imaginary δ is found, which again means the presence of instability. The linear analysis presented above shows that initially small perturbations grow exponentially with time. Actually, as soon as validity condition $\delta f \ll f_0$ breaks down, the non-linear character of instabilities has to be considered.

C.9.2. Collisionless shock waves

Such instabilities are present in relativistic regime as well. They may play a crucial role in the Gamma-Ray Burst phenomena, where interaction between two streams moving relativistically with respect to each other is expected Spitkovsky (2008b). Similar plasma instabilities are expected also in experiments with ultra-intense lasers Fiuza et al. (2012).

The growth rates for linear Weibel and two-stream instabilities are, respectively

$$\Gamma_W \propto \left(\frac{n'_e}{n_e}\right)^{1/2}, \quad \Gamma_{TS} \propto \left(\frac{n'_e}{n_e}\right)^{1/3}, \tag{C.9.8}$$

see e.g. Silva (2006). The typical wavelengths are similar

$$\lambda_W \simeq \frac{c}{\omega_e}, \quad \lambda_{TS} \simeq \frac{v}{\omega_e}, \tag{C.9.9}$$

where v is velocity of plasma stream. It is remarkable that currently numerical experiments in three dimensions, see e.g. Frederiksen et al. (2004),Spitkovsky (2008a), allow studying not only development of instabilities at their linear stage, but also following them on much longer time-scales, where saturation occurs and complex electromagnetic field patterns emerge.

C.9.3. Free streaming

Gas of self-gravitating particles in a flat space time is also known to be unstable Jeans (1902). Following Bisnovatyi-Kogan and Zel'Dovich (1971) consider Vlasov-Poisson equations (C.7.13) for collisionless particles in expanding Universe

$$\frac{\partial f}{\partial t} + \mathbf{v}\cdot\frac{\partial f}{\partial \mathbf{r}} - \frac{\partial \Phi}{\partial \mathbf{r}}\cdot\frac{\partial f}{\partial \mathbf{v}} = 0, \quad \Delta\Phi = 4\pi G\rho, \tag{C.9.10}$$

where $\rho = m\int f d^3\mathbf{v}$ is mass density of particles. The background solution for a Newtonian universe with zero spatial curvature is

$$\rho = \frac{1}{6\pi G t^2}, \quad \Phi = \frac{2}{3}\pi G\rho\,(t)\, r^2, \quad \frac{\partial \Phi}{\partial \mathbf{r}} = \frac{2}{9}\frac{\mathbf{r}}{t^2}. \tag{C.9.11}$$

Solving the corresponding linearized equations for a perturbed Maxwellian distribution with temperature θ by integration over characteristics the gravitational potential is found

$$\varphi\,(t) = \frac{2}{t^{2/3}}\int_0^t \varphi\,(t')\,\tau \exp\left(-\frac{9}{4}k^2\theta\tau^2\right) dt', \quad \tau = t^{-1/3} - t'^{-1/3}, \tag{C.9.12}$$

where $\Phi = \exp\,(ik\xi)\,\varphi\,(t)$.

For long waves the exponential is substituted by unity and the result is

$$\varphi(t) \propto t^{-5/3}, \quad \delta\rho/\rho \propto t^{2/3}, \tag{C.9.13}$$

which is the usual result of gravitational instability in matter dominated phase of the Universe, see e.g. Weinberg (2008). For short waves with $\frac{9}{4}k^2\theta \gg t^{1/3}$ using the method of steepest descents one finds

$$\varphi(t) \propto \exp\left[\frac{1}{9}\sqrt{\frac{2e\lambda^3}{\pi}\frac{1}{t}}\right], \quad \lambda = \frac{9}{4}k^2\theta, \tag{C.9.14}$$

which means perturbations are damped with time. This phenomenon is similar to Landau damping in plasma and is called *gravitational Landau damping* (or *free streaming*). Distribution function with two counter streams has been studied as well in Bisnovatyi-Kogan and Zel'Dovich (1971), but it was found that this does not lead to additional instability. For the formulation of the problem within General Relativity see Bond and Szalay (1983).

Note that the treatment of perturbations in hydrodynamic limit shows oscillations of perturbations at small scales, see e.g. Lattanzi et al. (2003), instead of damping. These oscillations occur due to interplay between gravity and pressure. Hence the hydrodynamic treatment does not capture an essential phenomenon in self-gravitating systems.

This result of kinetic theory is so remarkable that it has been one of the main reasons why purely hot dark matter cosmological scenarios were rejected, see e.g. White et al. (1983). In fact, light particles which decouple from primordial plasma when relativistic have the free streaming scale Padmanabhan (1993)

$$l_{FS} \simeq 0.5\left(\frac{m_{DM}}{1\,\mathrm{keV}}\right)^{-4/3}(\Omega_{DM}h^2)^{1/3}\,\mathrm{Mpc}, \tag{C.9.15}$$

where m_{DM} is particle mass, Ω_{DM} is the fraction of the dark matter in the critical density of the Universe, $H = 100h$ km/s/Mpc is the Hubble parameter. On the scale smaller than l_{FS} structures cannot form as any perturbations are exponentially suppressed. A corresponding mass scale has an order of supercluster of galaxies or even larger if the particle mass is $m_{DM} < 30\,\mathrm{eV}$, implying that dark matter cannot consist mainly of particles with such mass.

C.9.4. Phase mixing and violent relaxation

The phenomenon of phase mixing is thought to be important in formation of galaxies and large scale structure of the Universe, see e.g. Binney and Tremaine (2008). For illustration of this phenomenon let us consider an example. Assume particles are placed in a rectangular potential well and each one moves with constant velocity, see Fig. C.11. When particles

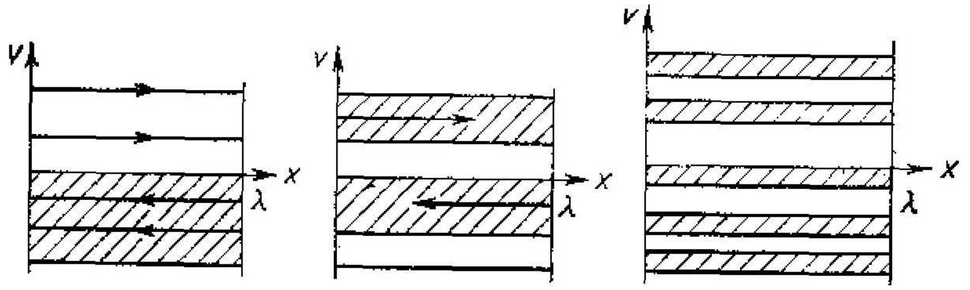

Figure C.11.: Phase space of particles moving in rectangular potential well, see Artsimovich and Sagdeev (1979), p. 80.

hit the wall they change the direction of the velocity. While in the beginning only lower half of the phase space is filled, in course of time the distribution function tends to fill all the phase space. While the *fine grained DF f* stays constant by the Liouville theorem, the *coarse grained DF* decreases. Another example of phase mixing is given in Binney and Tremaine (2008).

Relaxation mechanism related to phase mixing is found by Linden-Bell Lynden-Bell (1967). It should operate in a newly formed gravitationally bound collisionless systems such as galactic halo or cluster of galaxies. When a star moves in a fixed potential Φ its specific energy is constant $\epsilon = \frac{1}{2}v^2 + \Phi$. When the potential is time varying $\Phi(\mathbf{x}, t)$, the energy is not constant

$$\frac{d\epsilon}{dt} = \frac{1}{2}\frac{dv^2}{dt} + \frac{d\Phi}{dt} = \mathbf{v}\cdot\left(\frac{d\mathbf{v}}{dt} + \nabla\Phi\right) + \frac{\partial\Phi}{\partial t} = \left.\frac{\partial\Phi}{\partial t}\right|_{\mathbf{x}(t)}. \tag{C.9.16}$$

This is a mechanism of redistributing particles in the phase space, i.e. relaxation. It differs from particle collisions, because the energy change does not depend on mass. Linden-Bell derived also the relaxation time-scale, which is

$$t_{LB} \simeq \frac{3}{4\sqrt{2\pi G \langle \rho \rangle}} = \frac{3}{8\pi} P, \tag{C.9.17}$$

where P is the typical radial period of the orbit of a star in the galaxy.

C.9.5. Dark matter structure formation

The processes discussed above provide a mechanism to form the structure in the Universe. Almost homogeneous matter initially has small density fluctuations being subject to gravitational instability. Structures become gravitationally bound, detach from the Hubble flow, relax by phase mixing and violent relaxation, and end up as virialized equilibrium systems. The process repeats on larger and larger scales. This bottom-up picture of structure formation is called *hierarchical clustering*, and it is supported by numerical simulations. There are additional physical effects such as merging of smaller structures that influence and possibly even dominate structure formation.

The largest success of the numerical N-body simulations resulted in so called Navarro-Frenk-While profile of dark mater halos Navarro et al. (1996). The dark matter halo density profile is inferred from numerical simulations, and has a universal shape with mass density profile

$$\frac{\rho}{\rho_c} = \frac{\delta_c}{(r/r_s)\,(1 + r/r_s)^2}, \tag{C.9.18}$$

where ρ_c is the critical density, δ_c is the characteristic density, r_s is the scale radius. It should be noted that other halo profiles are suggested in the literature which may give better agreement with measurements of rotation curves of galaxies.

C.10. Conclusions

These brief lecture notes summarize the material presented during five lectures during XV Brazilian School of Cosmology and Gravitation. The idea has been to illustrate not only the theoretical progress in kinetic theory in relativistic domain, but also to acknowledge the rapid development of its applications, especially in the field of astrophysics and cosmology. Many processes in these fields can be understood on the basis of hydrodynamics. However, the study of phenomena which generally involve *non-equilibrium* processes require a different approach, based on kinetic theory.

I could only touch upon several phenomena, providing references in which interested reader could find more details. Much more phenomena remain even not mentioned: the choice is due to personal interests of the author.

Phenomena that I did not cover include, among others, reheating after inflation, cosmic recombination, cosmological nucleosynthesis, primordial magnetic fields generation, particle acceleration in shocks, Sunyaev–Zeldovich effect. I conclude with a general remark: that astrophysics and cosmology are natural fields of application of kinetic theory, since basic requirements of the theory such as large number of particles are easily satisfied.

D. Cosmic absorption of ultra high energy particles

D.1. Introduction

Observation of ultra high energy (UHE) particles, such as photons, ions and neutrinos, provides the crucial information on astrophysical systems as well as mechanisms of charged particle acceleration in these systems. Such information cannot be obtained from the study of low energy emission, which is much easier to detect.

Propagation of UHE particles on cosmological distances involves interaction with other particles, as well as with electromagnetic fields, in the case of charged particles (Aharonian, 2003). One of the most important reservoir of photons is the cosmic microwave background (CMB). Interaction with CMB imposes strong limits on propagation of UHE photons, protons, and nuclei, for a review see e.g. Bhattacharjee and Sigl (2000). Extragalactic background light (EBL), being the accumulated radiation in the Universe due to stars and active galactic nuclei, represents additional background of photons (Hauser and Dwek, 2001), which limits propagation of high energy photons. Yet another important background is cosmic neutrino background (CνB), which places a tight limit on the propagation of UHE neutrinos.

In this work, we review stringent limits on propagation of UHE particles, namely photons, protons and neutrinos, in the Universe due to their interactions with cosmic background of photons and neutrinos. We pay the particular attention to accounting for the cosmic evolution of CMB and CνB fields, being important at high redshifts. We discuss relation with previous results, as well as implications of new results, obtained in this work.

First in Sec. D.2 we discuss most important processes, responsible for interaction of UHE particles with cosmic backgrounds, as well as the corresponding cross-sections. Most of these processes are discussed in detail by Ruffini et al. (2010a). Then in Sec. D.3 we discuss the method used to compute the mean free path of UHE particles, which takes into account cosmological redshift of particle energy, as well as temperature evolution of the CMB and CνB. In Sec. D.4 the definition of the mean energy loss distance is given. We present and discuss results in Sec. D.5. Conclusions follow.

D.2. Processes

D.2.1. Processes involving photons

UHE photons are likely produced in sources of UHE cosmic rays. The most important process, responsible for intergalactic absorption of high-energy γ-rays is the Breit-Wheeler process (Breit and Wheeler, 1934) for the photon-photon pair production

$$\gamma_1 + \gamma_2 \longrightarrow e^+ + e^- \tag{D.2.1}$$

It was first discussed by Nikishov (1961) back in 1961 and then, after the discovery of CMB, by Gould and Schréder (1967).

Breit and Wheeler (1934) studied collision process (D.2.1) of two photons with energies E and $\mathcal{E}$ in the laboratory frame, producing electron and positron pair. They found the total cross-section

$$\sigma_{\gamma\gamma} = \frac{\pi}{2}\left(\frac{\alpha\hbar}{m_e\, c}\right)^2 (1-\beta^2)\left[2\beta(\beta^2-2) + (3-\beta^4)\ln\left(\frac{1+\beta}{1-\beta}\right)\right], \tag{D.2.2}$$

where

$$\beta = \sqrt{1-\frac{1}{x}}, \quad x = \frac{E\mathcal{E}}{(m_e c^2)^2}, \tag{D.2.3}$$

$\hbar$ is Planck's constant, m_e is electron mass, c is the speed of light and α is the fine structure constant. The necessary kinematic condition in order for the process (D.2.1) to take place is that the energy of two colliding photons is larger than the energetic threshold $2m_e c^2$, i.e., $x \geq 1$. Due to this kinematic condition the function (D.2.2) has a low energy cut-off at $x = 1$. The cross-section has a maximum at $x \simeq 2$, with $\sigma_{\gamma\gamma}^{\max} \simeq \sigma_T/4$, where σ_T is Thomson cross-section. At higher energies it decreases as $1/x$.

A simple estimate of the mean free path for the Breit-Wheeler absorption of high energy photon can be given as follows. Considering the actual CMB photon density $n_{CMB} \simeq 411$ cm^{-3} and taking $\sigma_T/4$ for the cross-section of the interaction, the mean free path is $\lambda_{BW} = (\sigma_T n_{CMB}/4)^{-1} \simeq 4.8$ kpc. One can refer to this distance as to a *horizon*, namely the maximal distance to the source for which the particle with the given energy can still be detected on Earth. However, owing to the energy dependence of the cross-section, and cosmic evolution of the CMB photon field the actual mean free path strongly depends on energy. The characteristic energy of UHE photons interacting with CMB, having temperature today $T_0 \approx 2.725$ K, is given by $E_{BW} = (m_e c^2)/kT_0 \simeq 1.11$ PeV. At lower energies, in the TeV range, photons interact by the Breit-Wheeler process with the EBL (Gould and Schréder, 1967; Vassiliev, 2000; Coppi and Aharonian, 1999). Hence the observation of TeV radiation from distant ($d > 100$ Mpc) extragalactic objects provides important constraints on the EBL (Aharonian et al., 2007; Meyer et al., 2012; Sinha et al., 2014).

At much higher energies the double pair production process

$$\gamma_1 + \gamma_2 \to e^+ + e^- + e^+ + e^- \tag{D.2.4}$$

dominates (Brown et al., 1973; Coppi and Aharonian, 1997). In this high-energy limit it has nearly a constant cross-section, see e.g. (Ruffini et al., 2010a)

$$\sigma_{dpp} = \frac{\alpha^2}{36\pi}\left(\frac{\alpha\hbar}{m_e\, c}\right)^2 [175\zeta(3) - 38] \sim 6.45\mu b. \tag{D.2.5}$$

Clearly, this process has a threshold with the sum of energies of photons which must exceed $4m_e c^2$. It imposes a limit for UHE photons propagation $\lambda_{dpp} = \left(\sigma_{dpp} n_{CMB}\right)^{-1} \simeq 121$ Mpc. The influence of this process on development of cascades at very high energies is discussed by Demidov and Kalashev (2009).

Besides, at energies much higher than E_{BW} the UHE photon interacts with the typical CMB photon well above the threshold. Due to large asymmetry in energy distribution between electron and positron, one of them takes almost all the energy of original UHE photon and then upscatters another CMB photon. This process of pair creation and subsequent Compton scattering creates secondary UHE photon and thus originate a cascade (Bonometto, 1971). The mean energy loss in a single pair creation episode is

$$\left\langle \frac{\Delta E}{E} \right\rangle \simeq \frac{1}{\pi\sqrt{x}}. \tag{D.2.6}$$

One also has to keep in mind the photons from the radio background, produced by normal galaxies and radio galaxies. Such background may dominate the opacity for VHE photons at $10^{19} - 10^{23}$ eV, see e.g. (Protheroe and Biermann, 1996; Coppi and Aharonian, 1997). Since the spectrum of radio background is presently not well constrained, we do not discuss the contribution of radio background to photon opacity in this work.

D.2.2. Processes involving protons

Charged UHE particles, such as protons and nuclei, are assumed to originate from extragalactic sources, which work as "cosmic accelerators" (Aharonian, 2003). Such particles interact with the CMB photons as well. In fact, the famous Greisen–Zatsepin–Kuzmin (GZK) limit (Greisen, 1966; Zatsepin and Kuz'min, 1966) was established by considering that this UHE particle interacts with the CMB photons via the pion photoproducton process

$$p + \gamma \longrightarrow \begin{pmatrix} p \\ n \end{pmatrix} + \pi. \tag{D.2.7}$$

and lose its initial energy. Due to the fact that at this process the proton loses more than half of its energy (Dermer and Atoyan, 2006), such interaction imposes a strong cut-off on energies of UHE cosmic rays. The cut-off energy is easy to estimate. Recall that the characteristic energy in the Breit-Wheeler process (D.2.1) is $E_{BW} = (m_e c^2)^2/kT_0$. When the photopion process (D.2.7) is concerned, the electron mass is exchanged with the pion mass, and an additional factor 4 comes from the reference frame transformation, giving $E_{p\gamma} = 4(m_\pi c^2)^2/kT_0 \simeq 3 \times 10^5 E_{BW} = 3.33 \times 10^{20}$ eV. More careful evaluation of the energy by comparing energy losses due to photopion (D.2.7) and photoproduction of pair (D.2.9) processes (see below) gives the value $E_{p\gamma} = 5 \times 10^{19}$ eV (Berezinskii and Grigor'eva, 1988). The cross-section of the photopion process in high energy limit is constant with the value (Dermer and Atoyan, 2006)

$$\sigma_{p\gamma} \simeq 120 \mu b. \tag{D.2.8}$$

The mean free path due to this process for energies $E > E_{p\gamma}$ is $\lambda_{p\gamma} = \left(\sigma_{p\gamma} n_{CMB}\right)^{-1} \simeq 6$ Mpc.

Another process relevant for interaction of UHE particles with CMB is the photoproduction of electron-positron pair on a nucleus, or Bethe-Heitler process (Bethe and Heitler, 1934). In the case of proton, which is the only one considered in this work, this process is

$$p + \gamma \longrightarrow p + e^+ + e^-. \tag{D.2.9}$$

It has the characteristic energy $E_{BH} = m_e m_p c^4/(2kT_0) \simeq 1.0 \times 10^{18}$ eV. This process has a threshold with photon energy in the proton rest frame $\mathcal{E}' > 2m_e c^2$. We use for its cross-section in the proton rest frame the expressions given by Chodorowski et al. (1992), namely near the threshold with $2 \leq \epsilon' \leq 4$

$$\sigma_{BH}^{thr}(\epsilon') \simeq \frac{2\pi}{3}\alpha\left(\frac{\alpha\hbar}{m_e\, c}\right)^2 \\ \left(\frac{\epsilon'-2}{\epsilon'}\right)^3\left(1+\frac{1}{2}\eta+\frac{23}{40}\eta^2+\frac{37}{120}\eta^3+\frac{61}{192}\eta^4\right), \tag{D.2.10}$$

where $\epsilon' = \mathcal{E}'/(m_e c^2)$ is photon energy in the proton rest frame and $\eta = (\epsilon'-2)\,/\,(\epsilon'+2)$. At higher energies $\epsilon' > 4$ the cross-section is

$$\sigma_{BH}^{he}(\epsilon') \simeq \alpha\left(\frac{\alpha\hbar}{m_e\, c}\right)^2\left\{\frac{28}{9}\delta-\frac{218}{27}+\left(\frac{2}{\epsilon'}\right)^2\right. \tag{D.2.11}$$
$$\times\left[6\delta-\frac{7}{2}+\frac{2}{3}\delta^3-\delta^2-\frac{\pi^2}{3}\delta+2\zeta(3)+\frac{\pi^2}{6}\right]$$
$$\left.-\left(\frac{2}{\epsilon'}\right)^4\left[\frac{3}{16}\delta+\frac{1}{8}\right]-\left(\frac{2}{\epsilon'}\right)^6\left[\frac{29}{9\times 256}\delta-\frac{77}{27\times 512}\right]\right\},$$

where $\delta = \log(2\epsilon')$. Expression (D.2.11) is logarithmically increasing at high energies, so we can take a characteristic value obtained by Bethe and Heitler $\sigma_{BH} \simeq (28/9)\alpha\left[(\alpha\hbar)/(m_e\, c)\right]^2$ in order to estimate the mean free path of UHE protons, which gives $\lambda_{BH} = (\sigma_{BH} n_{CMB})^{-1} \simeq 437$ kpc.

It is important to note that unlike the Breit-Wheeler process, leading to annihilation of UHE photons, or the pion photoproducton, where single interaction alters the energy of the UHE proton, the single Bethe-Heitler interaction does not change the proton energy significantly. Therefore, unlike all previous processes, the mean free path λ_{BH} does not correspond to a horizon. Another quantity is used for this purpose, namely the mean energy loss distance, defined as $\lambda_{BH} \sim [dE/(Ecdt)]^{-1}$, where E is the proton energy, which corresponds to the distance on which the energy of the UHE proton is reduced by a factor e due to numerous interactions with background photons (Dermer and Atoyan, 2006; Berezinskii and Grigor'eva, 1988; Stanev et al., 2000). However, it should be emphasized that single Bethe-Heitler interaction deflects the UHE proton by a small angle. This effect is discussed in detail below.

D.2.3. Processes involving neutrinos

UHE neutrinos can be produced either in astrophysical sources, or in some exotic new physics scenarios (Ringwald, 2006). Below we compute the horizon due to interaction of UHE neutrinos with cosmic neutrino background (CνB). Following Lunardini et al. (2013) we assume CνB neutrinos are in their mass states. The cross-section is composed of two parts. The resonant neutrino annihilation occurs in the s-channel:

$$\nu + \bar{\nu} \longrightarrow Z^0 \longrightarrow f + \bar{f}, \qquad \text{(D.2.12)}$$

where bar denotes antiparticle, f is a fermion. It has a typical Breit-Wigner shape and is given in the analytic form by D'Olivo et al. (2006). We take the small momentum expansion of the cross-section given by eq. (23) of D'Olivo et al. (2006) as

$$\sigma^R_{\nu\bar{\nu}} \simeq 4\sqrt{2}G_F \frac{m_\nu M_Z^2 \sqrt{\xi} E}{(M_Z^2 - 2Em_\nu)^2 + 4E^2 m_\nu^2 \xi} \mathrm{GeV}^{-2}, \qquad \text{(D.2.13)}$$

where $G_F = 1.16637 \times 10^{-5}$ GeV^{-2} is the Fermi's coupling constant, $\xi = (\Gamma/M_Z)^2$, $\Gamma = 2.495$ GeV is the width of Z^0 resonance and $M_Z = 91.1876$ GeV is the mass of Z^0 boson, m_ν is neutrino mass, E is energy of UHE neutrino in laboratory frame. Clearly, the position of the resonance scales inversely proportional to the neutrino mass. Throughout this paper we use the reference value $m_\nu = 0.08$ eV/c^2, corresponding to the recent cosmological bound from the Planck mission (Planck Collaboration et al., 2014), which gives characteristic energy $E_r = M_Z^2 c^2/2m_\nu \simeq 5.2 \times 10^{22}$ eV. The amplitude of the resonance does not depend on neutrino mass, and is given by

$$\sigma_{\nu\bar{\nu}}^{R\,\max} = 2\sqrt{2}G_F M_Z/\Gamma \simeq 0.471\mu b. \tag{D.2.14}$$

The resonant production of the Z-boson in neutrino-antineutrino annihilation (the Z-burst mechanism) has been suggested as a possible mechanism for creation of UHE particles near or above the GZK limit (Weiler, 1982). However, this mechanism requires significant clustering of light neutrinos, disfavored by the current cosmological model.

The second contribution is the non-resonant cross-section, which is adopted here in the form

$$\sigma_{\nu\bar{\nu}}^{NR} = \frac{\sigma_{\nu\bar{\nu}}^{he}}{1+(E/E_r)^{-1}}, \tag{D.2.15}$$

where $\sigma_{\nu\bar{\nu}}^{he} \simeq 8.3\times 10^{-4}\mu b$.

We assume that neutrino are non-relativistic even at sufficiently high redshift, which is a good approximation for $z < 10^2$ for $m_\nu = 0.08$ eV/c^2. Effects of non-zero momentum on the neutrino annihilation cross-section are studied by D'Olivo et al. (2006); Lunardini et al. (2013). Using the number density of relic neutrinos $n_{C\nu B} \simeq 112$ cm^{-3} and the non-resonant cross-section in the high energy limit one can estimate the horizon for UHE neutrinos at highest energies. Solving the Friedmann equation (see next section) one finds for the redshift $z_\nu \simeq 84$.

D.3. The optical depth and the mean free path

In this section we compute the optical depth for the propagation of UHE particles in the Universe. Imposing the condition that it equals unity we determine the corresponding mean free path. It should be noted that simple estimates, made in the literature, as well as in previous section, do not take into account evolution of CMB and CνB fields with time. The simplest way to account for cosmic redshift is to compare this estimate of the mean free path to the expansion scale c/H_0, where H_0 is the present day Hubble parameter, see e.g. (Berezinskii and Grigor'eva, 1988; Stanev et al., 2000). In what follows we describe more rigorous way to take into account both redshift of particle energy as well as the evolution of CMB and CνB fields with redshift.

The optical depth along the particle world line $\mathcal{L}$ is defined as

$$\tau = \int_{\mathcal{L}} \sigma j_\mu dx^\mu, \tag{D.3.1}$$

where σ is the cross-section of a given process, j^μ is the 4-current of particles, on which the UHE particle scatters, and dx^μ is the element of the UHE particle world line. We assume the Universe is homogeneous and isotropic, and the background particles are either CMB photons or CνB neutrinos. Both have thermal distribution functions, given by

$$f(\mathcal{E}/kT) = \frac{1}{e^{(\mathcal{E}-\mu)/kT} \pm 1}, \tag{D.3.2}$$

where k is the Boltzmann constant, T is the CMB or CνB temperature, the sign "$-$" is for photons while the sign "$+$" is for neutrinos, $\mathcal{E}$ and μ are the energy and the chemical potential of background particles (for photons $\mu = 0$). Then the optical depth (D.3.1) is

$$\tau(E,t) = \frac{g_s}{2\pi^2\hbar^3c^3}\int_t^0 cdt' \int_{\mathcal{E}_{tr}}^\infty \mathcal{E}^2 d\mathcal{E} f(\mathcal{E})\sigma(E,\mathcal{E},t'), \tag{D.3.3}$$

where $\mathcal{E}_{tr}$ is threshold energy in a given process, $g_s = 2$ is the number of helicity states for both protons and neutrinos. Here we assumed that UHE particles move along light-like geodesics. The integral over time can be transformed into the integral over redshift by means of the Friedmann equation. The latter for the flat Universe reads

$$\left(\frac{1}{a}\frac{da}{dt}\right)^2 = \frac{8\pi G}{3}\rho, \tag{D.3.4}$$

where a is the scale factor, ρ is energy density of the Universe, G is Newton's constant. From this equation, the definition of cosmological redshift, as well as the definition of the density parameters

$$a_0/a = 1+z, \qquad \Omega_i = \frac{\rho_i}{\rho_c}, \qquad \rho_c = \frac{3H_0^2}{8\pi G}, \tag{D.3.5}$$

where H_0 and a_0 are present time Hubble parameter and scale factor, respectively, we have

$$\int_t^0 cdt' \longrightarrow \frac{c}{H_0}\int_0^z \frac{dz'}{(1+z')\,H(z')}, \tag{D.3.6}$$

where H_0 is the Hubble parameter and the function $H(z)$ is given by

$$H(z) = [\Omega_r(1+z)^4 + \Omega_M(1+z)^3 + \Omega_\Lambda]^{1/2}, \tag{D.3.7}$$

and Ω_r, Ω_M and Ω_Λ are present densities of radiation, matter and dark energy, respectively. Then the expression (D.3.3) can be written as follows

$$\tau(E,z) = \frac{1}{\pi^2\hbar^3c^3}\frac{c}{H_0}\int_0^z \frac{dz'}{(1+z')\,H(z')} \times \int_{\mathcal{E}_{tr}}^{\infty} \mathcal{E}^2 d\mathcal{E} f(\mathcal{E})\sigma(E,\mathcal{E},z'). \tag{D.3.8}$$

Cosmic expansion results in the energy and temperature dependence on redshift

$$T = (1+z)T_0, \quad \mathcal{E} = (1+z)\mathcal{E}_0, \quad E = (1+z)E_0, \tag{D.3.9}$$

where temperature $T_{0,\gamma} \simeq 2.725$ K for photons, $T_{0,\nu} = (4/11)^{1/3} \simeq 1.95$ K for neutrinos and energies E_0, $\mathcal{E}_0$ are measured at the present time.

The second integral in (D.3.8) can be simplified, provided two conditions are fulfilled: a) the cross-section does not depend on the energy of background particle and b) there is no threshold in the given process ($\mathcal{E}_{tr} = 0$). In this case one has

$$\frac{1}{\pi^2\hbar^3c^3}\int_0^\infty \mathcal{E}^2 d\mathcal{E} f(\mathcal{E})\sigma(E,z) = \sigma(E,z)n(z) = \sigma(E,z)n_0\,(1+z)^3\,, \tag{D.3.10}$$

where n_0 is present number density and it stands for either

$$n_{0,\gamma} \approx \frac{2\zeta\,(3)}{\pi^2}\left(\frac{\hbar}{m\,c}\right)^{-3}\left(\frac{kT_0}{m_ec^2}\right)^3 \simeq 411\ \mathrm{cm}^{-3}$$

for photons, or $n_{0,\nu} = 3/4\left(T_{0,\nu}/T_{0,\gamma}\right)^3 \simeq 113\ \mathrm{cm}^{-3}$ for neutrinos. Then eq.

(D.3.3) becomes

$$\tau(E,z) = n_0 \frac{c}{H_0} \int_0^z \frac{\sigma(E,z')\,(1+z')^2\,dz'}{H(z')}. \tag{D.3.11}$$

When the cross-section is just a constant, the integral (D.3.11) can be readily performed. Assuming $\Omega_r \simeq 9.2 \times 10^{-5}$, $\Omega_M \simeq 0.315$, $\Omega_\Lambda \simeq 0.685$ and $H_0 = 67.3$ km/s/Mpc (Planck Collaboration et al., 2014) in the matter dominated epoch we have

$$\int_0^z \frac{(1+z')^2\,dz'}{[\Omega_M(1+z')^3 + \Omega_\Lambda]^{1/2}} \simeq \begin{cases} 1.045z, & z \ll 1, \\ 1.006z^{3/2}, & z \gg 1. \end{cases}$$

The mean free path is defined by the condition $\tau(E_0,z) = 1$. For the constant cross-section σ at low redshift $z \ll 1$ we get the traditional definition $\lambda = (\sigma n)^{-1}$ used above. For high redshift $z \gg 1$ one can define the redshift, corresponding to the mean free path as

$$z_\lambda = \left(\frac{n_0 \sigma c}{H_0}\right)^{-2/3} \simeq 8.9 \left(\frac{n_0}{n_{0,\gamma}} \frac{\sigma}{10^{-8}\sigma_T}\right)^{-2/3}. \tag{D.3.12}$$

Using this equation we obtain for UHE neutrinos with highest energies $z_\lambda \simeq 84$.

D.4. The mean energy loss distance

When UHE particle annihilates in a given process, such as in the case of Breit-Wheeler one (D.2.1), the mean free path correpsonds to the horizon defined above.

Another possibility is that the particle is not annihilated in a given process, but scattered, such as in the case of proton producing the pion (D.2.7). When the energy loss in single scattering corresponds to a large fraction of UHE particle energy, the situation is similar to the case of annihilation. However, UHE particle may lose only a small fraction of its energy, as in the case of Bethe-Heitler process (D.2.9). Here another relevant quantity corresponds the particle horizon defined above is the mean energy loss distance $\tilde{\lambda}$. We define it following Blumenthal (1970) as

$$\tilde{\lambda}^{-1} = \left(\frac{1}{E}\frac{dE}{cdt}\right). \tag{D.4.1}$$

Then we evaluate the quantity

$$\tilde{\tau} = \int_t^0 \frac{cdt}{\tilde{\lambda}} = \frac{c}{H_0}\int_0^z \frac{dz'}{\tilde{\lambda}\,(1+z')\,H(z')}. \tag{D.4.2}$$

It is computed below for the Bethe-Heitler process.

The propagation of ultra high energy particles on cosmological distances is usually dealt with by Monte Carlo simulations, see e.g. (Aloisio et al., 2012; Kampert et al., 2013). These codes are essentially one-dimensional and do not describe particle deflections, discussed below.

D.5. Results

Now we apply the method developed in the previous section to the computation of the mean free path for UHE photons, protons and neutrinos, as well as the mean energy loss distance for protons interacting via the Bethe-Heitler process.

D.5.1. Photons

First, we consider cosmic limits on propagation of UHE photons. In the Breit-Wheeler process (D.2.1) the cross-section depends on both energies through the definition (D.2.3). When one considers all possible orientations of CMB photons additional averaging over their angular distribution has to be performed (Nikishov, 1961; Gould and Schréder, 1967). The resulting averaged cross section differs from eq. (D.2.2). The useful approximations for this quanity can be found e.g. in (Gould and Schréder, 1967; Aharonian et al., 1983; Coppi and Blandford, 1990). We use the accurate expression given by eq. (3.23) of Aharonian (2003):

$$\bar{\sigma}_{\gamma\gamma}(x) = \frac{3}{2}\sigma_T \Sigma(x), \tag{D.5.1}$$
$$\Sigma(x) = \frac{1}{x^2}\left[\left(x + \frac{1}{2}\log x - \frac{1}{6} + \frac{1}{2x}\right) \times \right.$$
$$\left. \times \log\left(\sqrt{x} + \sqrt{x-1}\right) - \left(x + \frac{4}{9} - \frac{1}{9x}\right)\sqrt{1 - \frac{1}{x}}\right].$$

We change our variables in eq. (D.3.8) and get

$$\tau_{\gamma\gamma}(E_0, z) = \frac{A}{y_0^3}\int_0^z \frac{1}{(1+z')^4}\frac{dz'}{H(z')}\int_1^\infty \frac{x^2 dx}{\exp(x/y) - 1}\Sigma(x), \tag{D.5.2}$$

where

$$A = \frac{4\alpha^2}{\pi}\frac{c}{H_0}\left(\frac{\hbar}{m\,c}\right)^{-1}\left(\frac{kT_0}{m_e c^2}\right)^3 \approx 2.37 \times 10^6, \tag{D.5.3}$$

and

$$y = y_0(1+z)^2; \quad y_0 = \frac{E_0}{m_e c^2}\frac{kT_0}{m_e c^2}, \tag{D.5.4}$$

and y_0 is the energy E_0 in units of the critical energy $E_{BW} = \left(m_e c^2\right)^2 / kT_0 \simeq 1.11 \times 10^{15}$ eV. The intergal over energy can be evaluated numerically and we find a reasonable fit

$$F_1(y) = 0.839\left(y^{2.1} + 2 \times 10^{-8} y^{2.8}\right)\exp\left(-\frac{1.1}{y}\right). \tag{D.5.5}$$

Then eq. (D.5.2) becomes

$$\tau_{\gamma\gamma}(y_0, z) = \frac{A}{y_0^3}\int_0^z \frac{1}{(1+z')^4}\frac{dz'}{H(z')}F_1\left[y_0(1+z)^2\right]. \tag{D.5.6}$$

This integral is also evaluated numerically.

In the low energy $E \ll E_{BW}$ and high redshift $z \gg 1$ limit the integral (D.5.6) can be evaluated analytically. The redshift corresponding to the mean free path in this limit is

$$z_{\lambda,BW} \simeq 0.21 \left(\frac{E}{E_{BW}}\right)^{-1/2}. \tag{D.5.7}$$

This result is known as the Fazio-Stecker relation (Fazio and Stecker, 1970), see their eq. (9).

In addition to the Breit-Wheeler process (D.2.1), following Coppi and Aharonian (1997) we consider also the double pair production process (D.2.4) with the cross-section defined in (D.2.5). This process is relevant for the highest energies. The optical depth for this process is

$$\begin{aligned}\tau_{\gamma\gamma}^{dpp}(y_0,z) &= \frac{B}{y_0^3}\int_0^z \frac{1}{(1+z')^4}\frac{dz'}{H(z')}\int_2^\infty \sigma_{dpp}\frac{x^2dx}{\exp(x/y)-1} = \\ &= \frac{B}{y_0^3}\int_0^z \frac{1}{(1+z')^4}\frac{dz'}{H(z')}F_2\left[y_0(1+z')^2\right],\end{aligned} \tag{D.5.8}$$

where

$$\begin{aligned}F_2(y) = \frac{8}{3} - 4i\pi y - 4y\log\left[\exp\left(\frac{2}{y}\right)-1\right] - \\ - 4y^2\text{PolyLog}\left[2,\exp\left(\frac{2}{y}\right)\right] + 2y^3\text{PolyLog}\left[3,\exp\left(\frac{2}{y}\right)\right].\end{aligned} \tag{D.5.9}$$

and $B \approx 15.3$.

The condition $\tau(y_0,z) = \tau_{\gamma\gamma}(y_0,z) + \tau_{\gamma\gamma}^{dpp}(y_0,z) = 1$ in eqs. (D.5.2) and (D.5.8) determines the mean free path of UHE photons. This mean free path is shown in Fig. D.1 in megaparsecs and in Fig. D.2 in cosmological redshift by the solid curve. The region above the solid curve is opaque for high energy photons. In addition, thick black dashed line shows the boundary of transparency for EBL, according to the baseline model of Inoue et al. (2013), while dotted line in Fig. D.1 shows the cosmological horizon $z = \infty$.

For the distance smaller than a critical value of about $d_c = 6.8$ kpc, the CMB is transparent to high-energy photons with arbitrary energy. For larger distances there are two branches of solutions for the condition $\tau_{\gamma\gamma}(y_0,z) = 1$, respectively corresponding to the different energy-dependence of the average cross-section (D.5.1). This average cross-section $\bar{\sigma}_{\gamma\gamma}(x)$ increases with the center of mass energy x from the energy threshold $x = 1$ to $x \simeq 3.5$, and

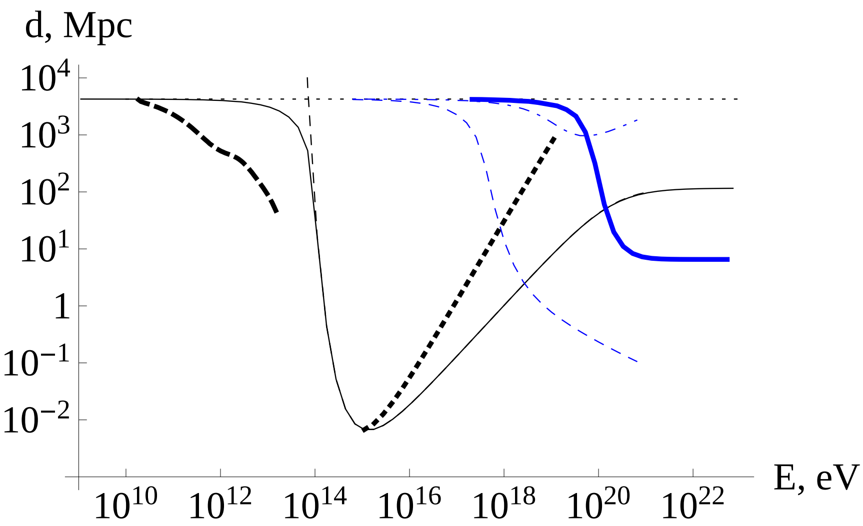

Figure D.1.: The mean free path, measured in megaparsecs as a function of energy E of UHE particles, measured in electronvolts. In the region above the curves the optical depth is larger than unity. Thin black curve shows the mean free path of UHE photons. Dashed black curve shows the photon mean free path computed without accounting for cosmological evolution (imposing $z = 0$). Thick black dashed curve shows the boundary of transparency for the EBL, according to the baseline model (Inoue et al., 2013). Thick black dotted curve shows the mean energy loss distance for photons interacting with the CMB. Thick blue curve shows the mean free path of UHE protons (GZK limit). Blue dashed (dotted-dashed) curve shows the mean free path (mean energy loss distance) for UHE protons due to Bethe-Heitler process. Dotted horizontal line shows cosmological horizon.

decreases from $x \simeq 3.5$ to $x \to \infty$. The energy of the UHE photon corresponding to the critical distance d_c is about 1.11 PeV, which separates two branches of the solution. The double pair production process (D.2.4) is relevant for the highest energies, as expected. Photons with energies above 10 PeV are absorbed by the double pair production if they are emitted at redshift above $z \simeq 0.03$ (distance about 120 Mpc). We show the mean energy loss distance by thick dotted curve which above the energy E_{BW} is a factor $\sqrt{E/E_{BW}}$ larger than the mean free path (Bonometto, 1971).

For comparison we show by the dashed curve also the mean free path computed at $z = 0$, namely neglecting cosmological expansion, see e.g.

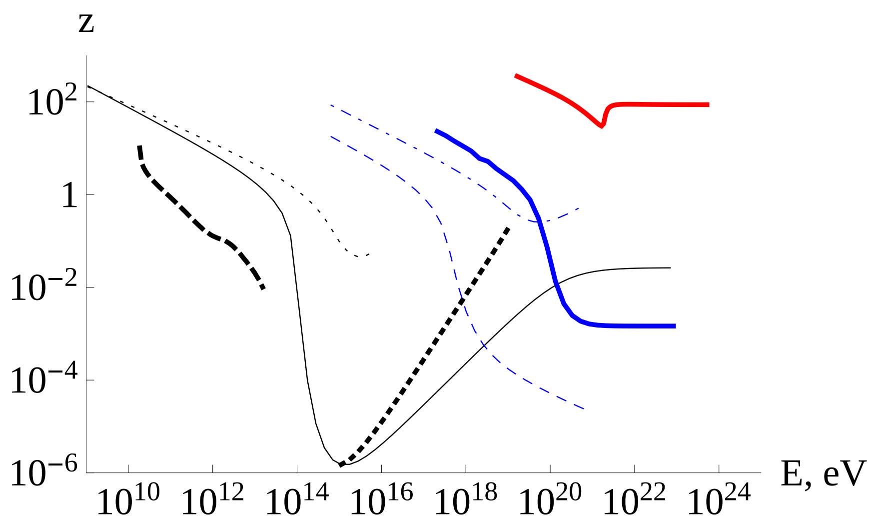

Figure D.2.: The same as in Fig. D.1 for the distance measured in cosmological redshift. Red thick curve shows the mean free path of UHE neutrinos.

(Coppi and Aharonian, 1997).

We also show in Fig. D.2 by the dotted curve the mean free path for the photon-photon scattering which follows from the Euler-Heisenberg lagrangian, see e.g. (Berestetskii et al., 1982; Ruffini et al., 2010a). This process was first discussed by Zdziarski and Svensson (1989); Svensson and Zdziarski (1990). We will discuss it in details in a separate publicationBatebi et al. (2015).

Finally, the black dotted thick curve shows the horizon of photons with energies above 20 GeV and below 100 TeV, which is determined by their interaction with the EBL. The latest EBL model (Inoue et al., 2013) is used. It is clear, that the contribution of CMB photons gives the absolute upper limit on the mean free path. In the energy range between 1 GeV and 20 GeV the propagation of high energy photons is limited only by the CMB radiation.

D.5.2. Protons

Second, we consider the propagation of UHE protons, accelerated in a source located at a cosmological distance from Earth. First, considering the photo-pion process (D.2.7) we use the method developed in the previous section and compute the GZK limit (Greisen, 1966; Zatsepin and Kuz'min, 1966). This limit applies to protons and other charged particles, leading to the existence of a cutoff in the observed spectrum of (UHE) cosmic rays at about 10^{20} eV. For the photopion process (D.2.7) one can use the simple expression (D.3.11) with the constant cross-section (D.2.8). However, we compute the optical depth in the same way as in the case of double pair production, using eq. (D.5.8) with different value of the constant $B' \approx 253$.

The mean free path due to photopion process is shown by the blue thick curve in Fig. D.1 in megaparsecs and in Fig. D.2 in cosmological redshift. From Fig. D.1 it appears that for energies well below $E_{p\gamma} \simeq 3.3 \times 10^{20}$ eV the GZK limit approaches the cosmological horizon. Instead, from Fig. D.2 it follows that the mean free path measured in redshift, below the energy $E_{p\gamma}$, increases with decreasing energy as a power law, which is a consequence of eq. (D.3.12).

Similarly to the Breit-Wheeler case, the integral (D.5.8) is evaluated analytically in the low energy $E \ll E_{p\gamma}$ and high redshift $z \gg 1$ limit, with the result

$$z_{\lambda,GZK} \simeq 0.57 \left(\frac{E}{E_{p\gamma}}\right)^{-1/2}. \tag{D.5.10}$$

We also evaluate the mean free path due to the Bethe-Heitler process (D.2.9). Since cross-sections (D.2.10) and (D.2.11) are given in the proton rest frame, one has to transform photon energy to this reference frame using

$$\mathcal{E}' = 2\Gamma\mathcal{E} = 2\frac{E\mathcal{E}}{m_p c^2}, \tag{D.5.11}$$

where the primed quantity corresponds to the proton rest frame, while unprimed quantities to laboratory reference frame. Then it is convenient to make use of the same type of variable change as before for the Breit-Wheeler process[1], with a difference that instead of electron mass squared a product of electron and proton masses arises, namely

$$\bar{x} = 2\frac{E\mathcal{E}}{m_e m_p c^4}, \qquad \bar{y}_0 = 2\frac{E_0}{m_p c^2}\frac{kT_0}{m_e c^2} = \frac{E_0}{E_{BH}}. \tag{D.5.12}$$

[1]We assume that UHE protons collide with the with CMB photons head on. More accurate calculation with average over angular distribution of the CMB photons does not change qualitatively our results.

The optical depth is computed in the laboratory frame as follows[2]

$$\tau_{p\gamma}(\bar{y}_0, z) = \frac{1}{\pi^2}\frac{c}{H_0}\left(\frac{\hbar}{m\,c}\right)^{-3}\left(\frac{kT_0}{m_e c^2}\right)^3 \times \tag{D.5.13}$$
$$\times\frac{1}{\bar{y}_0^3}\int_0^z \frac{1}{(1+z')^4}\frac{dz'}{H(z')}\int_2^\infty \frac{\bar{x}^2 d\bar{x}}{\exp(\bar{x}/\bar{y})-1}\sigma_{BH}(x).$$

The intergal over energy can be evaluated numerically and we find a reasonable fit

$$F_3(\bar{y}) = \frac{86.15\exp\left(-\frac{2}{\bar{y}}\right)}{10^{3\bar{y}-3.47}+\bar{y}^{-3}}. \tag{D.5.14}$$

Then eq. (D.5.2) becomes

$$\tau_{p\gamma}(\bar{y}_0, z) = \frac{C}{\bar{y}_0^3}\int_0^z \frac{1}{(1+z')}\frac{dz'}{H(z')}F_3\left[\bar{y}_0(1+z)^2\right], \tag{D.5.15}$$

where

$$C = \frac{2\alpha^3}{3\pi}\frac{c}{H_0}\left(\frac{\hbar}{m\,c}\right)^{-1}\left(\frac{kT_0}{m_e c^2}\right)^3 \approx 2863. \tag{D.5.16}$$

The mean free path for protons interacting via the Bethe-Heitler process is shown by blue dashed curve in Fig. D.1 in megaparsecs and in Fig. D.2 in cosmological redshift. The integral (D.5.15) is evaluated analytically in the low energy $E \ll E_{BH}$ and high redshift $z \gg 1$ limit, with the result

$$z_{\lambda,BH} \simeq 0.43\left(\frac{E}{E_{BH}}\right)^{-1/2}. \tag{D.5.17}$$

As discussed before, at energies above 10^{18} eV the mean free path is relatively small, about a few hundred kiloparsecs, and it quickly decreases with increasing energy. This is in contrast with the large mean energy loss path, which is above 1 Gpc at energies $10^{18}-10^{20}$ eV, see e.g. (Berezinskii and Grigor'eva, 1988; Stanev et al., 2000). It means, that before UHE proton starts to lose its energy, it is scattered many hundred

[2]Note that the integral over energy is not transformed to the proton rest frame, as done e.g. by Blumenthal (1970). Instead, only a change of variables is performed in the integral (D.5.13).

times (Dermer and Atoyan, 2006). At each of this scattering the proton recoils, being deflected by a small angle measured in the laboratory reference frame. From the analysis of the cross-section as the function of recoil angle (Jost et al., 1950), see also (Motz et al., 1969) in the proton rest frame, it follows that in the high energy limit the photon recoils in the plane, orthogonal to the incident photon. It implies that each scattering produces a deflection of the UHE proton in the laboratory frame by angle $\sim 1/\gamma$, where $\gamma = E/\left(m_p c^2\right)$ is proton Lorentz factor. The number of scatterings is given approximately by τ.

One can compute the mean energy loss distance defined in (D.4.1) and then evaluate the quantity (D.4.2) using eq. (18)-(20) of Blumenthal (1970) to obtain

$$\tilde{\tau} = \frac{D}{y_0^3} \int_0^z \frac{dz'}{\left(1+z'\right)^4 H(z')} \int_2^\infty \frac{d\bar{x}}{\exp(\frac{\bar{x}}{\bar{y}}) - 1} \phi\left(\bar{x}\right), \tag{D.5.18}$$

where the function $\phi\left(\bar{x}\right)$ is given in eq. (16) of (Blumenthal, 1970)

$$\phi\left(\bar{x}\right) = \bar{x}\left[-86.07 + 50.95 \log \bar{x} - 14.45 \left(\log \bar{x}\right)^2 + 2.667 \left(\log \bar{x}\right)^3\right] \tag{D.5.19}$$

and

$$D = \frac{2}{\pi^2} \alpha^3 \frac{m_e}{m_p} \frac{c}{H_0} \left(\frac{\hbar}{m\, c}\right)^{-1} \left(\frac{kT_0}{m_e c^2}\right)^3. \tag{D.5.20}$$

From the condition $\tilde{\tau} = 1$ we determine the mean energy loss distance $\tilde{\lambda}$. This distance is shown by blue dash-dotted curve in Fig. D.1 in megaparsecs and in Fig. D.2 in cosmological redshift.

We evaluate the optical depth (D.5.13) at the redshift, corresponding to $\tilde{\lambda}$ for energies in the range between 10^{15} and 10^{20} eV and find it in the range 10^4 to 10^5, see Fig. D.3. Since the deflection at each interaction is small, the average number of interactions is proportional to the optical depth. The average deflection angle is then

$$\delta \sim \frac{\sqrt{\tau\left(E\right)}}{\gamma}. \tag{D.5.21}$$

We find an average deflection angle of UHE protons as a function of proton energy for sources located at the mean energy loss distance and show it in Fig. D.4. At energies $E = 10^{16}$eV, this angle is about $\delta \sim 15''$ and it decreases

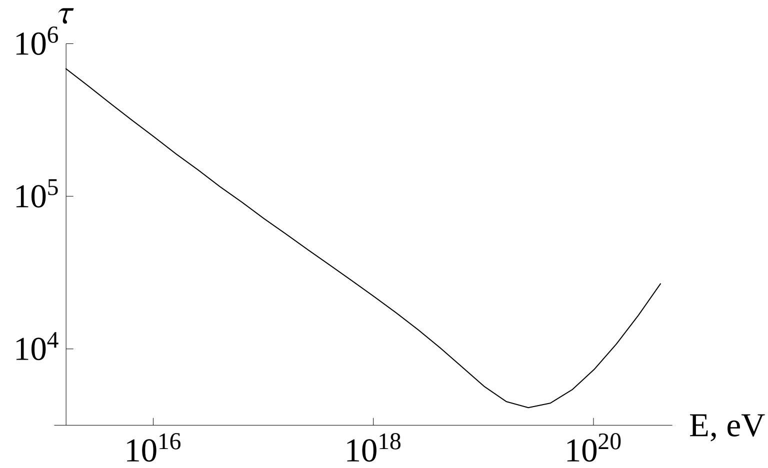

Figure D.3.: The optical depth at the mean energy distance for the Bethe-Heitler process.

down to $\delta \sim 2.4$ mas for $E = 10^{19}$eV. For $E < 10^{19}$eV we find a relation

$$\delta \simeq 7.6 \times 10^{-9} \left(\frac{E}{10^{19} eV} \right)^{-1.27} . \tag{D.5.22}$$

Such deflection, although small compared to deflection in galactic magnetic field (Medina Tanco et al., 1998), might be comparable to deflection in intergalactic magnetic fields (Dolag et al., 2005). The latter are poorly coonstrained, but their knowledge is essential for the charged particle astronomy.

D.5.3. Neutrinos

Third, we consider the propagation of UHE neutrinos. Such neutrinos can be produced in the source of UHE cosmic rays in decay of secondary pions $\pi^+ \longrightarrow \mu^+ + \nu_\mu$ or secondary neutrons $n \longrightarrow p + e^- + \bar{\nu}_e$ (Dermer and Atoyan, 2006). UHE neutrino can be produced also in some extensions of the standard model of particle physics (Ringwald, 2006). Such UHE neutrino interacts with the CνB via the process (D.2.12).

The cross-section of this process has a resonance, and it approaches a constant for highest energies. We compute the optical depth, which instead of

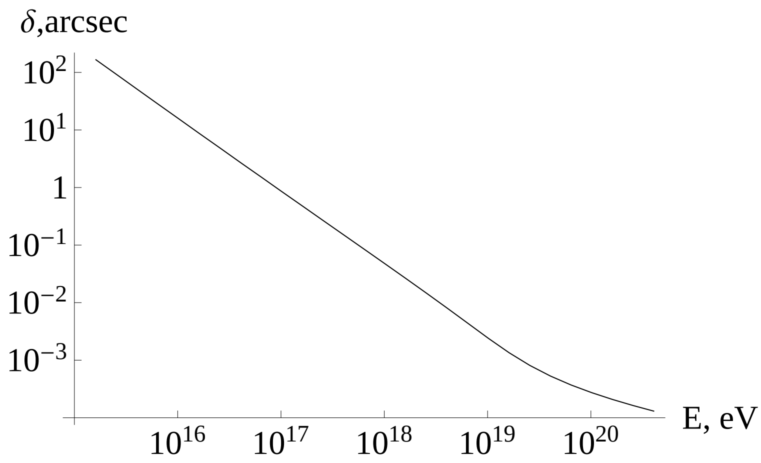

Figure D.4.: The average deflection angle of UHE protons as function of proton energy for sources located at the mean energy loss distance for the Bethe-Heitler process.

eq. (D.3.8) is given by

$$\begin{aligned}\tau_{\nu\nu}(E,z) &= \frac{1}{\pi^2\hbar^3c^3}\frac{c}{H_0}\int_0^z \frac{dz'}{(1+z')\,H(z')} \\ &\times \int_{\mathcal{E}_{tr}}^{\infty} \mathcal{E}\sqrt{\mathcal{E}^2-(m_\nu c^2)^2}d\mathcal{E}f(\mathcal{E})\sigma(E,z) \\ &\approx \frac{1}{\pi^2\hbar^3c^3}\frac{c}{H_0}n_{0,\nu}\int_0^z \frac{(1+z')^2\,dz'}{H(z')}\sigma(E(1+z\prime)),\end{aligned} \tag{D.5.23}$$

using the cross-sections given in the laboratory reference frame by eqs. (D.2.13) and (D.2.15). The mean free path for neutrinos, measured in cosmological redshift, is shown in Fig. D.2 by the thick red curve. Since the characteristic redshifts are high, this curve practically coincides with the horizon, when measured in megaparsecs, so we do not show it in Fig. D.1. It is clear that the Breit-Wigner resonance in the cross-section decreases the mean free path in a wide range of energies. The lowest redshift for $E \simeq E_r$ at which the Universe is transparent for UHE neutrinos is $z_{min} \simeq 30$. The resonance produces a dip around $E_r/(1+z_{min}) \simeq 1.7 \times 10^{21}\,(m_\nu/0.08\text{ eV})^{-1}$ eV, where $z_{min} \simeq 30$. Additional broadening of the resonance, due to thermal effect, is discussed in detail by Lunardini et al. (2013). At higher energies the corresponding redshift is $z \simeq 87$.

Similarly to the previous cases, in the low energy $E \ll E_{p\gamma}$ and high redshift $z \gg 1$ limit, we find

$$z_{\lambda,\nu} \simeq 14 \left(\frac{E}{E_r}\right)^{-2/5} . \tag{D.5.24}$$

D.6. Conclusions

We reviewed cosmic limits on propagation of ultra high energy particles such as photons, protons and neutrinos, set up by their interactions with the cosmic background of photons and neutrinos. In doing so we take into account explicitly cosmic evolution of both cosmic backgrounds, and redshift of UHE particle energy. This is in contrast with majority of the literature, where corresponding mean free paths are found at present epoch, neglecting cosmic expansion. A number of new results were obtained, in particular:

- for UHE photons the contribution of CMB photons gives the absolute upper limit on the mean free path. At high redshift, where other radiation backgrounds, such as EBL are absent, the CMB radiation limits the propagation of UHE photons at energies above GeV.

- for UHE protons the mean free path due to Bethe-Heitler process appears to be much shorter than the mean energy loss distance. This results in multiple deflections suffered by UHE protons, before they start to lose energy in the energy range $10^{16} - 10^{20}$ eV. Such deflections result in dimming of point sources of UHE protons, which makes it more difficult to detect them.

- for UHE neutrinos for the first time we compute the horizon as a function of redshift. We found that the Universe is transparent of UHE neutrinos at redshifts $z < 30$, near the Breit-Wigner resonance at $E_r \simeq 5.2 \times 10^{22} \left(m_\nu/0.08\,\mathrm{eV}\right)^{-1}$ eV, and it is transparent at redshifts $z < 87$ at higher energies.

- Remarkably, in the low energy and high redshift limit, the Fazio-Stecker relation (Fazio and Stecker, 1970) holds for all processes with exception of neutrinos, and it is given by a universal expression $z_\lambda \simeq$

$\mathcal{O}(1)\left(\frac{E}{E_{thr}}\right)^{-1/2}$, where E_{thr} is the characteristic (e.g. threshold) energy for a given process. In the case of neutrinos similar power law exists $z_\lambda \propto E^{-2/5}$.

E. Interaction of high energy photons with the background radiation in the Universe

E.1. Introduction

Cosmic ray particles permanently hit the earth. When these particles enter the atmosphere with energies up to and above $10^{18}eV$, they initiate cascades of high energetic particles moving towards the ground, called extensive air showers Torres and Anchordoqui (2004). Till now, the accurate source of the cosmic rays is unknown. However, some theories and models of particle acceleration in astrophysical sources can explain the source of these high energy particles. Also some theories predict exotic particles remaining from the big bang, which on decay might produce ultra-high energy cosmic rays Sushchov et al. (2012). Some of the possible astrophysical sources of UHE photon are Pulsars, active galactic nuclei, gamma ray bursts(GRB), quiet black holes, colliding galaxies and so on, see e.g. Stanev (2004). Interaction of Ultra High energy photons with background radiation, impose strong limits on UHE photons. some of the studied are given in Zdziarski and Svensson (1989); Svensson and Zdziarski (1990); Venters et al. (2009); Colombo and Bonometto (2003); Protheroe and Johnson (1996).

UHE photon in the presence of cosmic microwave background (CMB) interact predominantly in the ways of pair production,$\gamma\gamma \rightarrow e^-e^+$, double pair production, $\gamma\gamma \rightarrow e^-e^+e^-e^+$, photon- photon scattering, $\gamma\gamma \rightarrow \gamma\gamma$ Zdziarski and Svensson (1989); Svensson and Zdziarski (1990).

The photon-photon scattering is a special process of quantum electrodynamics (QED), which does not occur in classical electrodynamics, owing to the fact that Maxwell's equations are linear. The leading contribution to the photon-photon scattering comes from Feynman "box" diagrams of the four external photon lines, which is the leading term in the Euler-Heisenberg effective Lagrangian.

The Euler-Hesinberg effective Lagrangian is given by Heisenberg and Euler (1935):

$$£_{eff} = -\frac{1}{4}F_{\mu\nu}F^{\mu\nu} + \frac{\alpha^2}{90m_e^4}\left[(F_{\mu\nu}F^{\mu\nu})^2 + \frac{7}{4}(F_{\mu\nu}\tilde{F}^{\mu\nu})^2\right], \quad \text{(E.1.1)}$$

where the first term $\frac{1}{4}F_{\mu\nu}F^{\mu\nu}$ is the classical Maxwell Lagrangian.
Therefore, cross section of photon-photon collision $\gamma\,\gamma \to \gamma\,\gamma$ can be generalized to any arbitrary reference frame and natural unit as follows:

$$\begin{aligned} \sigma &= \frac{0.031}{8}\,\alpha^2\,r_e^2\,x^3(1-cos\theta)^3 \quad x \ll 1, \\ \sigma &= \frac{4.7}{2}\,\alpha^4\,(\frac{1}{m_e})^2\frac{1}{x\,(1-cos\theta)} \quad x \gg 1; \end{aligned} \quad \text{(E.1.2)}$$

where $x = \varepsilon E/m_e^2$ and α is the fine structure constant, r_e is the classical electron radius, ε and E are the energy of incoming photons.
Since Photon-Photon scattering is a forth- order process the cross section is of order $\alpha^2 r_e^2 \simeq 4\times10^{-30}cm$ at $x^3 \sim 1$ where at large and smaller values of $x^3 \sim 1$ the cross section is declines rapidly.

The cross section of photon photon pair production, $\gamma\gamma \to e^-e^+$, is a threshold process with condition $x > 1$. the Euler Heisenberg cross section is of the order of $\alpha^2 \sim 10^{-4}$ smaller than pair production cross section. However, photon photon scattering can be important only in threshold $x \ll 1$ lower than pair production threshold energy where pair production is forbidden.

E.2. Optical Depth

UHE photons attenuation is a function of the observed γ-ray energy E_0 and the redshift z of the emitting source. The attenuation is generally parameterized by the optical depth $\tau(E_0, z)$, which is defined as the number of e-fold reductions of the observed flux, I_{obs}, as compared with the emitted source flux, $I_{emitted}$, at redshift z:

$$I_{obs} = e^{-\tau(E0,z)}I_{emitted}. \quad \text{(E.2.1)}$$

The optical depth is calculated from physical principles. For a photon emitted at time t in the past and travelling to us at time $t = 0$ optical depth,$\tau(E0, z)$, given by:

$$\tau_{\gamma\gamma}(E, t) = \int_t^0 n(\varepsilon)\sigma(\varepsilon, E)dt; \tag{E.2.2}$$

The integral over time can be transformed into the integral over redshift as follow:

$$\int_t^0 dt' \longrightarrow \frac{1}{H_0} \int_0^z \frac{dz'}{(1+z')\,\hat{H}(z')}, \tag{E.2.3}$$

where H_0 is the Hubble parameter and the function $\hat{H}(z)$ is given by

$$\hat{H}(z) = [\Omega_r(1+z)^4 + \Omega_M(1+z)^3 + \Omega_\Lambda]^{1/2}, \tag{E.2.4}$$

and $\Omega_r \leq 10^{-4}$, $\Omega_M = 0.3$ and $\Omega_\Lambda = 0.7$ are present densities of radiation, matter and dark energy, respectively. Therefore, the optical depth of the cosmic background for a γ- ray emitted at matter and dark energy dominant redshift z is given by standard formula:

$$\tau(E, z) \quad = \quad \frac{1}{4\pi} \int_0^z \frac{dz'}{(1+z')\,H(z')} \int_{\varepsilon_{th}}^{\infty} d\varepsilon\, \frac{dn(\varepsilon)}{d\varepsilon} \int\int d\Omega(1 - cos\theta)\, \sigma(\varepsilon, E) \tag{E.2.5}$$

Where $\frac{dn}{d\varepsilon}$ is differential number density of background photons, θ and ε_{th} are scattering angle and threshold energy of the specific interaction.

E.2.1. UHE photon attenuation through CMB

In this section we describe our calculation for optical depth of UHE photon in presence of the most important cosmic background, CMB through Euler-Heisenberg lagrangian.

CMB is the thermal radiation filled the universe and predicted by Big Bang Cosmology. UHE photons attenuation through interaction with CMB. Euler-Hiesenberg cross section in lab frame, through the definition (E.1.3), depends on both energies. then optical depth is as follows:

$$\tau_{\gamma\gamma}(\omega_0, z) = \frac{C_\tau}{y_0} \int dz \frac{(1+z)^8}{H(z)} \int dx_0 \frac{dn(x_0)}{dx_0}\, x_0^3 \tag{E.2.6}$$

where we can substitute $H_0^{-1} \simeq 6.5 \times 10^32\ eV^{-1}$ and $T_0 = 2.34 \times 10^-4\ eV$, then:

$$C_\tau = \frac{0.06}{5}\alpha^4(\frac{1}{m_e})^2\frac{1}{H_0}T_0, \tag{E.2.7}$$

and $\frac{dn(\varepsilon)}{d\varepsilon} = \frac{(\frac{\varepsilon}{\pi})^2}{e^{\frac{\epsilon}{kT}}-1}$ is differential number density of CMB in dimension eV^2 in natural unit, and $x = x_0(1+z)^2, y = y_0(1+z)^2$, where

$$y_0 = \frac{E_0}{m_e}\frac{T_0}{m_e} \tag{E.2.8}$$

E_0, ε_0 and T_0, are the energy of UHE photon, background photon and CMB temperature today, respectively. one can approximate the solution of equation(E.2.6), at $z \gg 1$ and $\varepsilon \ll E_{BW}$, where $E_{BW} = m_e c^2/kT \simeq 1.11 PeV$, to obtain a cutoff energy above which γ-rays originating at a high redshift cannot reach us. The redshift corresponding to the mean free path in this limit is

$$z = 0.57(\frac{E_0}{E_{BW}})^{-2/5}\ ; \tag{E.2.9}$$

At last scattering redshift the maximum critical energy of photon is $E_C = 6.78 \times 10^{-9} eV$.

Anyway, the equation(E.2.6) can be solved analytically. Finally by considering low energy EH cross section, the exact solution to the E.2.6 is obtain as follow:

$$\tau_{\gamma\gamma_{CMB}}(E_0, z) = C'(\tau)\ y_0^3 \int_{z_C}^{z} \frac{(1+z')^8 dz'}{H(z')} \tag{E.2.10}$$

where

$$C'(\tau) = \frac{0.06}{5}\ \frac{8}{63}\ \frac{\pi^4}{H_0}\ \frac{\alpha^4}{m_e^2}\ T_0^3 \simeq 14.12 \tag{E.2.11}$$

By calculating $\tau(E_0, z) = 1$ cosmological redshift as a function of energy is given in Fig. E.1. this result is compered by critical redshift obtained by Breit-Wheeler process, $\gamma_1 + \gamma_2 \to e^+ + e^-$, studied inRuffini et al. (2015).

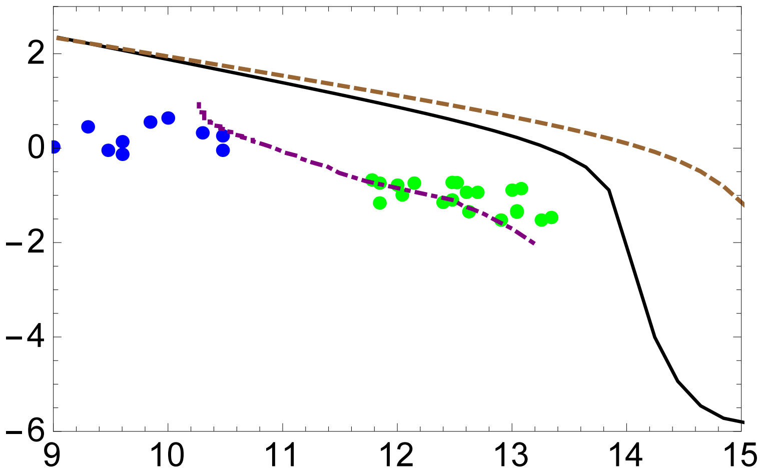

Figure E.1.: This plot shows distance measured in cosmological redshift as a function of energy E of UHE photons, in electronvolts. Thin black curve shows the of UHE photons transparency for CMB according to pair production Breit- Wheeler interactionRuffini et al. (2015). Dashed brown curve shows the UHE photons transparency for CMB according to the Euler-Heisenberg photonphoton scattering . Dotdashed purple curve shows the boundary of transparency for extragalactic background light(EBL), according to the baseline model of Inoue et al. (2013). Dark blue points and green points show GRB (Ackermann et al., 2013) and Blazar (Finke and Razzaque, 2009) photons detected recently, respectively.

E.3. Conclusion

We have studied propagation of UHE cosmic rays through the cosmic backgrounds over cosmological distances. This important calculation was done Zdziarski and Svensson (1989) previously for CMB. We updated this calculation, in doing so we considered the energy above GeV. We confirm that high energy photons interact with background photons mainly producing electron-positron pairs at high redshift. We showed the blazar and GRB datum observed recently, are consistent with the obtained result.

F. A regular and relativistic Einstein Cluster within the S2 orbit centered in SgrA*

F.1. Introduction

In 1939 Einstein Einstein (1939) provided a model of self-gravitating masses, each moving along geodesic circular orbits under the influence of the gravitational field of the rest of the particle in the system. This model allowed him to argue that 'Schwarzschild singularities' do not exist in physical reality because a cluster with a given number of masses cannot be arbitrarily concentrated. This is due to the fact that otherwise the particles constituting the cluster would reach the speed of light. Of course, this model can actually only be considered as an interesting possibility to try to provide a counterexample of a singularity within Einstein's theory of gravity, since Black Holes are a physical reality within the theory of General Relativity.

The aim of this chapter is to model the central (sub-milliparsec) region of our galaxy in terms of a dark 'Einstein Cluster' (EC) in order to provide an alternative to the Super Massive Black Hole (SMBH) of mass $M = 4.4 \times 10^6 M_\odot$ thought to be hosted at very center Ghez et al. (2008); Gillessen et al. (2009). A dark EC is understood as an EC composed by dark matter particles of mass m (regardless of its nature), and therefore no contribution to the pressure in form of radiation is assured as the cluster shrinks till relativistic regimes. The model is based on the assumption of a constant density distribution harbored inside the peri-center of the S2 star ($r_{p(S2)}$), the closest to SgrA* as observed in Gillessen et al. (2009). We will first analyze the stability condition in the specific case of a regular and relativistic energy density EC, contained marginally inside the S2 peri-center. Secondly, and for an EC with fixed particle number $\mathcal{N}$, we will explicitly show through the R vs. M relation, and for particle velocities ranging from zero up to the speed of light, up to which point an EC can be shrank before loosing its global stability.

F.2. Einstein Clusters

The full theoretical formalism of 'Einstein Clusters' and their different stability analysis has been extensively studied in Zapolsky (1968); Gilbert (1954); Hogan (1973); Florides (1974); Comer and Katz (1993); Cocco and Ruffini (1997); Böhmer and Harko (2007b); Geralico et al. (2012). We give in next a short summary of the most important outcomes of this theory, pointing out the principal formulas which will allow us to deal with the astrophysical application object of this work. Thus, consider a static spherically symmetric distribution of particles all with rest mass m which are moving along circular geodetic orbits about the center of symmetry. The associated line element ds^2 is written in terms of a Schwarzschild metric of the form $g_{\mu\nu} = \mathrm{diag}(-e^{\nu}, e^{\lambda}, r^2, r^2 \sin^2\theta)$, where ν and λ depend only on the radial coordinate r. From now and on we will work in the geometric unit system ($G = c = 1$).

The stress-energy tensor in the laboratory frame is assumed to take the form

$$T^{\mu\nu} = m\, n_0\, U^{\mu} U^{\nu}\,, \qquad U = \gamma[e_{\hat{t}} + v^{\hat{\theta}} e_{\hat{\theta}} + v^{\hat{\Phi}} e_{\hat{\phi}}]\,, \tag{F.2.1}$$

which is just the Einstein's *ansatz* Einstein (1939) (or a dust-like *ansatz*). n_0 is the proper particle number density (i.e. defined at rest w.r.t a coordinate system of special relativity), U is the particle 4-velocity satisfying the circular geodetic equations in the laboratory frame with $v^{\hat{\theta}}$ and $v^{\hat{\Phi}}$ the linear velocities along the angular directions, $\gamma = (1 - v^2)^{-1/2}$ ($v^2 = \delta_{\theta\phi} v^{\theta} v^{\Phi}$), and the unitary vectors introduced in U corresponds to the following orthonormal frame (adapted to the static observers)

$$e_{\hat{t}} = e^{-\nu/2}\partial_t\,, \qquad e_{\hat{r}} = e^{-\lambda/2}\partial_r\,, \qquad e_{\hat{\theta}} = \frac{1}{r}\partial_\theta\,, \qquad e_{\hat{\phi}} = \frac{1}{r^2 \sin\theta}\partial_\phi\,. \tag{F.2.2}$$

In the laboratory frame, and after applying the killing vector formalism to this specific spacetime (see also Geralico et al. (2012)) naturally appears the two constants of motion associated with each trajectory, the energy E and the angular momentum L which reads

$$E = m\gamma\, e^{\nu/2}, \qquad L^2 = L_\theta^2 + L_\phi^2 / \sin^2\theta = m^2\gamma^2 r^2 v^2. \tag{F.2.3}$$

The angular momentum formula in (F.2.3) together with the definition of γ directly implies $\gamma = (1 + \tilde{L}^2/r^2)^{1/2}$ which will be very useful in what follows, with $\tilde{L} = L/m$.

By writing the conserved L^2 in terms of each angular component $L_\theta = m\gamma r v_\theta$ and $L_\phi = m\gamma r v_\phi \sin\theta$ as done in (F.2.3), implies the following relation $1 = (L_\theta/L)^2 + (L_\phi/(L\sin^2\theta))^2$. This last equation further implies that the possible values of L_θ/L and $L_\phi/(L\sin^2\theta)$ lie on a circle of unit radius, and then each angular component can be written in terms of an angle α respect to the $e_{\hat{\theta}}$-axis. This decomposition allow us to make an average of the angular momentum components in the $e_{\hat{\theta}} - e_{\hat{\phi}}$ plane (i.e. around each orbit with $\alpha \in [0, 2\pi]$), as originally proposed by Einstein Einstein (1939). The averaged variables reads[1].

$$\langle L_\theta \rangle = \langle L_\phi \rangle = 0, \qquad \langle L_\theta^2 \rangle = \langle L_\phi^2 / \sin^2\theta \rangle = L^2/2\,. \tag{F.2.4}$$

The above averaging allows to express the averaged stress-energy components without any angular dependence, and reads

$$\langle T^t{}_t \rangle = -mn_0 \left(1 + \frac{\tilde{L}^2}{r^2}\right) \equiv -\rho\,, \qquad \langle T^\theta{}_\theta \rangle = \langle T^\phi{}_\phi \rangle = \frac{mn_0}{2}\frac{\tilde{L}^2}{r^2} \equiv p_t\,, \tag{F.2.5}$$

where ρ is the energy density of the system and p_t the tangential pressure. It can be easily verified that the divergence of the stress-energy tensor vanishes identically.

The relevant Einstein equations are

$$\frac{1}{r^2}[r(1 - e^{-\lambda})]' = 8\pi\rho\,, \tag{F.2.6}$$

$$\nu' = \frac{1}{r}(e^\lambda - 1)\,, \tag{F.2.7}$$

$$\frac{e^{-\lambda}}{2}\left[\nu'' + \frac{\nu'^2}{2} + \frac{\nu' - \lambda'}{r} - \frac{\nu'\lambda'}{2}\right] = 8\pi p_t\,, \tag{F.2.8}$$

where a prime denotes differentiation with respect to r. By using the standard definition of the mass function in terms of λ, $e^\lambda = (1 - 2M(r)/r)^{-1}$, the

[1]The average or mean value is defined by $2\pi\langle L_a(\alpha)\rangle = \int_0^{2\pi} L_a(\alpha)d\alpha$, with a either θ or ϕ.

system (F.2.6–F.2.8) is solved to give:

$$M(r) = 4\pi \int_0^r \rho r^2 dr, \qquad e^{\nu} = (1 - 2M/R)e^{-2\Phi(r)}, \tag{F.2.9}$$

where

$$\Phi(r) = \int_r^R \frac{v_k^2}{r} dr, \qquad v_k^2 = \frac{M(r)}{r - 2M(r)}, \qquad \tilde{L} = \gamma\, v_k\, r \tag{F.2.10}$$

where v_k is the Keplerian speed. Thus, in order to completely solve the problem we have to provide a the energy density $\rho(r)$ (or equivalently the mass profile).

Another needed relevant quantity is the total particle number $\mathcal{N}$. It can be easily shown that the averaged 4-current $\langle J^{\mu} \rangle = -n_0 \langle U^{\mu} \rangle$ is divergence-free. The associated conserved particle number is thus given by Misner and Sharp (1964)

$$\mathcal{N} = \int_{\Sigma} \langle J^{\mu} \rangle \, d\Sigma_{\mu}\,, \tag{F.2.11}$$

where Σ denotes a spacelike hypersurface with infinitesimal element $d\Sigma^{\nu} = n^{\nu} d\Sigma$ and unit timelike normal n. By choosing Σ to be a $t =$ const hypersurface with unit normal $n = e_{\hat{t}}$ and $d\Sigma = e^{\lambda/2} r^2 \sin\theta \, dr \, d\theta \, d\phi$, Eq. (F.2.11) gives

$$\mathcal{N} = 4\pi \int_0^R n_0(r) \gamma e^{\lambda/2} r^2 \, dr\,. \tag{F.2.12}$$

A constant energy density $\rho = 3M/(4\pi R^3)$ implies a radial distribution mass $M(r) = Mr^3/R^3$, and consequently through second and third Eqs. in (F.2.10), an angular momentum per unit mass $\tilde{L}$ with the corresponding number distribution of the particles mn_0 given by

$$\tilde{L} = \sqrt{\frac{M}{R}} \frac{r^2}{R} \left(1 - \frac{3Mr^2}{R^3}\right)^{-1/2}, \qquad mn_0 = \frac{3M}{4\pi R^3} \frac{R^3 - 3Mr^2}{R^3 - 2Mr^2}\,. \tag{F.2.13}$$

where $0 \leq r \leq R$. Thus, the full solution of the Einstein equations (F.2.6–F.2.8) gives for the metric functions

$$e^{\nu} = \left(1 - \frac{2M}{R}\right)^{3/2} \left(1 - \frac{2Mr^2}{R^3}\right)^{-1/2}, \qquad e^{\lambda} = \left(1 - \frac{2Mr^2}{R^3}\right)^{-1}, \quad \text{(F.2.14)}$$

The stability conditions for particles moving along a circular geodetic orbit on the equatorial plane is studied in next for the specific case of an EC of constant energy density, in terms of the effective potential $V_{eff} = e^{\nu/2}(1 + \tilde{L}^2/r^2)^{1/2}$ (see e.g. Geralico et al. (2012) for a general discussion of stability). The existence of circular orbit at r_0 is calculated through the necessary condition $V'_{eff}(r_0) = 0$, while the the necessary condition for stability is $V''_{eff}(r_0) > 0$. In general (for any given EC) both necessary conditions reads respectively

$$r > 3M(r), \qquad \frac{\mathrm{d}(\ln \mathrm{M(r)})}{\mathrm{d}(\ln \mathrm{r})} + 1 - \frac{6M(r)}{r} > 0\,, \quad \text{(F.2.15)}$$

In particular, for $\rho = 3M/(4\pi R^3)$ =const, the stability analysis directly implies that stable circular orbits exist within the cluster in the range

$$r < R\sqrt{\frac{R}{3M}}. \quad \text{(F.2.16)}$$

Note that there is no upper limit on r if $R > 3M$, implying that circular orbits are stable all the way up to the boundary of the configuration.

For outer particles $r > R$, the stability conditions in (F.2.15) makes possible to distinguish the following classes: models with $R > 6M$ and models with $3M < R < 6M$. If $R > 6M$ the cluster is said to be globally stable, because circular orbits are always stable both inside and outside the configuration (see also Fig. F.3 (a)).

If $3M < R < 6M$ all particles constituting the cluster move on stable orbits, but in the adjacent exterior region of the configuration there is a region of instability ($R < r < 6M$), so that the cluster is meta-stable (see also Fig. F.3 (b)). This stability criterion was first applied in Cocco and Ruffini (1997).

Another formal criterion which will be also used in next to classify an EC regarding the stability, is the one adopted in Zapolsky (1968) based on the behaviour of the gravitational binding energy of the system. Where the fractional binding energy of the cluster is defined by

$$E_b^f = \frac{m\mathcal{N} - M}{m\mathcal{N}}. \tag{F.2.17}$$

A regular and relativistic EC marginally inside the pericenter of the S2 star, has to fulfill the following observational constraints for its boundary R and total mass M

$$R = r_{p(S2)} = 6 \times 10^{-4}\,\mathrm{pc}, \qquad \mathrm{M} = 4.4 \times 10^{6}\,\mathrm{M}_{\odot}, \tag{F.2.18}$$

where both values are subject to some $\sim$ few % of error due to propagated error in the distance from the sun to the galactic center $R_0 \approx 8.3$ kpc (see e.g. Gillessen et al. (2009)). These constraints implies (in geometrical units) a ratio $R/M = 2840.9 \gg 6$, which safely indicates global stability, i.e. both inside and outside the cluster according with the criterion presented above with Cocco and Ruffini (1997).

In next we analyze, for an EC of constant number particles $\mathcal{N}$, up to which extent it can be shrank inside $r_{p(S2)}$ without becoming meta-stable, and moreover, what happens when the particles approach the ultra-relativistic regime. For this we first calculate the relation between M and R for fixed values of the rest mass $m\mathcal{N}$ of the system, taking the velocity $0 < v_k \leq 1$ as a parameter. By use of Eq. (F.2.12) we have

$$m\mathcal{N} = M\,[1/v_k^2 + 2]^{3/2} F(v_k)\,, \tag{F.2.19}$$

where

$$\begin{aligned} F(v_k) = {} & -3/4[\arctan{(x(v_k) - 3)^{-1/2}} \\ & + (x(v_k) - 3)^{1/2}/x(v_k)] + (3/4)^{1/2} \arctan{(3/(x(v_k) - 3))^{1/2}}, \end{aligned} \tag{F.2.20}$$

since $x(v_k) = R/M(v_k) = 1/v_k^2 + 2$. The direct relation between R/M and v_k is easily understood from the Keplerian velocity formula in (F.2.10) evaluated at $r = R$. Eq. (F.2.19) together with $x(v_k)$ automatically leads to the following total mass and radius normalized variables

$$\frac{R}{m\mathcal{N}} = \frac{1}{F(v_k)[1/v_k^2 + 2]^{1/2}}, \qquad \frac{M}{m\mathcal{N}} = \frac{1}{F(v_k)[1/v_k^2 + 2]^{3/2}}. \tag{F.2.21}$$

F.3. Results and discussion

In Fig. (F.1) we explicitly show the R vs. M relation (normalized with the constant rest mass) with v_k taken as a free parameter. Regions of stability and meta-stability are differentiated depending on the value of the rotation velocity (v_k) at the boundary of the EC (see caption for details). Instead, in Fig. (F.2) we show the behaviour of the binding energy as a function of the velocity v_k, this is, showing the fraction of the total mass that turns into binding energy when the cluster is contracted from $R \gg 1$ to a given R. After the maximum a change of stability takes place and the cluster itself becomes unstable according to this criterion (see caption for details).

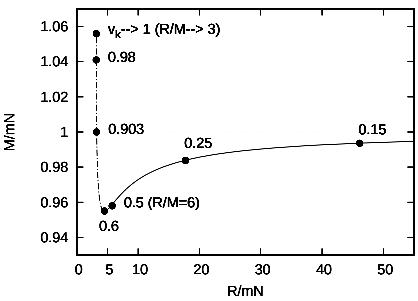

(a)

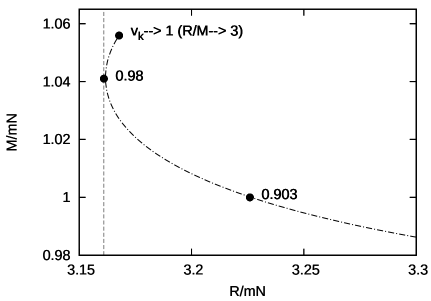

(b)

Figure F.1.: Gravitational mass vs. boundary radius relation (in units of rest mass) for an EC with constant energy density. The velocity at the boundary $0 < v_k < 1$ is taken as a parameter. In Fig. (a): for $v_k \to 0$ the total mass approaches the rest mass at $R/(mN) \to \infty$. At $v_k = 0.5$ the EC becomes meta-stable (i.e. $R/M = 6$), while $v_k = 0.6$ corresponds to the minimum in $M/(mN) = 0.955$ which further implies the maximum bounded state for the cluster (see Fig. F.2 for comparison). At $v_k = 0.903$ the gravitational mass equals the rest mass, and at $v_k = 0.98$ a turning point in the radius appears (see Fig. (b) for a zoom). Finally, the onset of instability $R/M = 3$ (according to the classification given in Cocco and Ruffini (1997)) is asymptotically approached when $v_k \to 1$.

Even though these systems reach meta-stability (according to the classification given in Cocco and Ruffini (1997)) or become unstable (according the binding energy analysis), well before the velocity v_k reaches the ultra-relativistic regime; it is interesting to note that these tangential pressure sup-

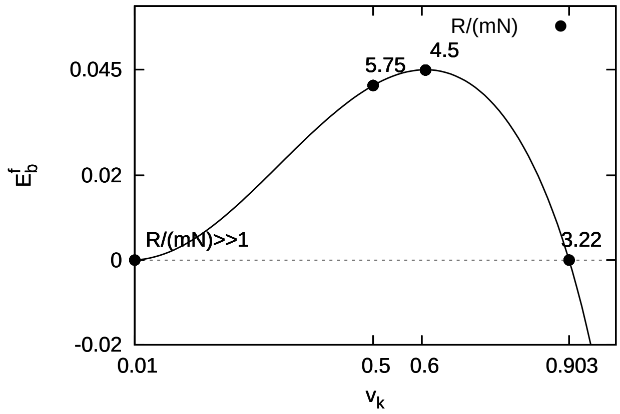

Figure F.2.: The behaviour of the fractional binding energy (F.2.17) as a function of v_k with fixed particle number. The maximum corresponds to an EC which has shrank to $R/(mN) = 4.5$ where $E_b^f \approx 0.045$. The latter vanishes at $R/(mN) = 3.22$ for a velocity $v_k = 0.903$ where the cluster is considered unstable according to this criterion. At $v_k = 0.5$ the radius of the cluster is $R/(mN) = 5.75$ implying $R/M = 6$ (see Fig. F.1 for comparison).

ported self-gravitating systems, never reaches a critical mass as in the case of radial pressure supported self-gravitating systems, being neutron stars a typical example of this last case.

In Fig. (F.3) we present two examples of constant energy density EC, the case of $R/M = 10$ (Fig. a) where circular stable orbits exist either for particles forming the EC but also for outside ones, and the case of $R/M = 3.1$ (Fig. b) where unstable orbits (i.e. a maximum in V_{eff}) appears for outer particles located in the outer vicinity of the border of the EC. In the second case the EC is called meta-stable according to the characterization given in Cocco and Ruffini (1997).

The fact of working with a fixed rest mass energy $m\mathcal{N}$ which can be calculated with the observational constraints (F.2.21), implies that the constant energy density $\rho = 3M/(4\pi R^3)$ increases more and more according the velocity v_k increases. From Eqs. (F.2.19) and ($R/M(v_k) = 1/v_k^2 + 2$) it is possible to give an explicit expression for $\rho(v_k) = 3/(4\pi)(F(v_k)/(mN))^2$, from which we can give the uppermost limits for the density of a dark EC inside SgrA*. Changing units to $M_\odot/\mathrm{pc}^3$, the first upper limit corresponds

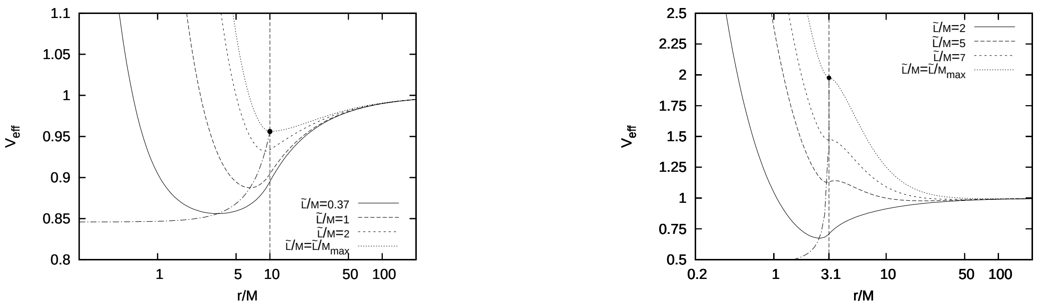

(a) (b)

Figure F.3.: Behaviour of the effective potential as a function of r/M for an EC with constant energy density. In Fig. (a) we show a globally stable cluster with $R/M = 10$, and in Fig. (b) a meta-stable one with $R/M = 3.1$. Only in Fig. (b) and for relatively high values of $\tilde{L}$ an external maximum appears showing the existence of unstable orbits in the outer vicinity of the cluster. The dots corresponds to the point a maximum angular momentum at the border of the cluster.

to $\rho(v_k = 0.5) \approx 5.5 \times 10^{23} M_\odot/\mathrm{pc}^3$, below which the EC is always globally stable. The second limit is given by $\rho(v_k = 0.6) \approx 1.1 \times 10^{24} M_\odot/\mathrm{pc}^3$, and will be considered as the uppermost limit for a regular and relativistic EC inside S2 and centered in SgrA*, due to the fact that above this velocity the value of the binding energy (F.2.17) starts to decrease from its maximum, undergoing a change of stability (see also Fig. F.2). These results are in consistency with the bound obtained in Böhmer and Harko (2007b) from a different stability analysis, based on the lose of isotropy of the fluid due to non-radial perturbations; since anisotropy serves as a source of instability (see Herrera and Santos (1997) and refs. therein).

It is important to note that this specific EC model composed by dark matter particles with $\rho = const$ provides a good alternative for the SMBH thought to be hosted in the center of SgrA*. This due to the fact that the upper limit for $\rho(v_k = 0.5)$ given above, is already about one order of magnitude higher than the lowest limit for the mass density of SgrA* as imposed in Doeleman et al. (2008) through the 1.3 mm Very Large Baseline Interferometry observations, but below the critical density required for a black hole of $4.4 \times 10^6 M_\odot$.

G. Semidegenerate Self-gravitating system of fermion as Dark Matter on galaxies I: Universality laws

Our aim here is to propose a system of self-gravitating system of fermions at a finite temperature as a unified model for galactic halos and compact objects in the center of galaxies, as an alternative to the usual black hole. This work will deal mainly with the halo part, leaving the core description to another paper Argüelles and Ruffini (2014a).

The equilibrium configurations of such systems were already studied by Gao et al. (1990) and it was found that the system is unbound and has infinite mass. In order to prevent that, a cut-off in the distribution function was used Ingrosso et al. (1992). The equations governing a spherically symmetric self-gravitating system of fermions in general relativity are the Tolman-Oppenheimer-Volkoff equations

$$\frac{dP}{dr} = -\frac{G}{c^2}\frac{(P+\rho c^2)(M_r + 4\pi\rho r^3)}{r(rc^2 - 2GM)} \tag{G.0.1}$$

$$\frac{dM_r}{dr} = 4\pi\rho r^2, \tag{G.0.2}$$

where M_r is the mass inside a radius r and $\rho(r)$ and $P(r)$ are the mass density and the pressure, respectively given by

$$\rho = m\frac{g}{h^3}\int_0^{\epsilon_c}\left(1+\frac{\epsilon}{mc^2}\right)\frac{1-e^{(\epsilon-\epsilon_c)/kT}}{e^{(\epsilon-\mu)/kT}+1}d^3p \tag{G.0.3}$$

$$P = \frac{2g}{3h^3}\int_0^{\epsilon_c}\left(1+\frac{\epsilon}{2mc^2}\right)\left(1+\frac{\epsilon}{mc^2}\right)^{-1}\frac{(1-e^{(\epsilon-\epsilon_c)/kT})\epsilon}{e^{(\epsilon-\mu)/KT}+1}d^3p. \tag{G.0.4}$$

Here $g = 2s + 1$ is the multiplicity of states, m the mass of the particle, ϵ_c is the cutoff energy and ϵ is the kinectic energy of a single particle $\epsilon = \sqrt{p^2c^2 + m^2c^4} - mc^2$. Since we are considering a system in thermodynamical equilibrium Klein (1949a).

$$(\mu + mc^2)\exp(\nu/2) = \text{constant}, \;\; T\exp(\,^\circ\,/2) = \text{constant}. \tag{G.0.5}$$

In order to solve (numerically) the system, we transform the quantities into dimensionless ones, using a characteristic length

$$\chi = \frac{\hbar}{mc}\frac{m_p}{m}\left(\frac{8\pi^3}{g}\right)^{1/2},$$

where m_p is the Planck mass. The transformed quantities are

$$\rho = \frac{c^2}{G\chi^2}\hat{\rho}, \; P = \frac{c^4}{G\chi^2}\hat{P}, \; M_r = \frac{c^2\chi}{G}\hat{M}_r, \; r = \chi\hat{r}. \tag{G.0.6}$$

Additionally we define the *d*egeneracy parameter $\theta_0 = \mu_0/kT_0$, the *t*emperature parameter $\beta = kT_0/mc^2$ and the *c*ut-off parameter $W = \epsilon_c/kT_0$, all in the center of the configuration; this, together with the mass of the particle, will serve as the free parameters of the system. However, when we turn to the dimensionless equations, the mass appears only in the definition of the characteristic length χ, and we can check the general properties of the system without specifying a mass for the particle.

Below are shown the density profile and velocity rotation curve for different values of the degeneracy parameter and the temperature parameter:

We can see that, despite the wide range of the parameters, the shape of the density profile is universal and composed of a central degenerate core, an inner halo of almost constant density and a tail that scales with r^{-2}. Also, from fig. G.1 it is clear that, for small values of θ_0 we have smaller inner halos, but the drop from the core is also smaller; and vice-versa for large values of θ_0. This means that, for small enough values, we lose the core+inner halo, being left only with the halo; inversely, for very large values of the degeneracy parameter, the drop is so sharp that the halo is practically non-existent.

The rotation curve is also universal and composed of four parts:(I) The core with constant density, where $v \propto r$; (II) The first part of the inner halo, where the mass of the core prevails over the mass of the halo and $v \propto r^{-1/2}$; (III)

Second part of the inner halo, where now the mass of the halo prevails and again $v \propto r$; (IV) The outer halo, where the velocity tends to a constant value v_0 after some oscillations of diminishing magnitude.

It is important to notice also that the velocity tends to a constant value as required by observations and it depends only on the temperature parameter at the center:

$$\log \frac{v_0}{\mathrm{km/s}} = 5.63 + 0.5 \log \beta_0. \tag{G.0.7}$$

This means we can uniquely determine β_0 for any system using only the asymptotic rotation velocity.

One important point is to compare our profile with the other existent profiles to see its validity. We choose here the phenomenological profile of Burkert (1995), the profile coming from the N-Body simulations of Navarro, Frenk and White (NFW) Navarro et al. (1996, 1997) and a simple pseudo-isothermal profile. We find that our profile is in good agreement with both NFW and Burkert profile up to a cerain radius just after the second maximum of the rotation curve.

In order to use observations to constrain our parameters, we first build a set of scaling laws for the physical properties of a given system, i.e., the core radius and mass and the halo mass and radius, where we define the radius of the core r_c as the first maximum of the rotation curve and the radius of the halo r_h as the second maximum, with respective masses:

$$\begin{aligned}
M_c &= 1.96 \times 10^{12} (\beta_0 \theta_0)^{0.75} \left(\frac{m_f}{\mathrm{kev/c^2}} \right)^{-2}, && \text{(G.0.8)}\\
r_c &= 0.180 (\beta_0 \theta_0)^{-0.25} \left(\frac{m_f}{\mathrm{kev/c^2}} \right)^{-2} && \text{(G.0.9)}\\
M_h &= 1.49 \times 10^{13} {\beta_0}^{0.75} 10^{0.16\,\theta_0} \left(\frac{m}{\mathrm{kev/c^2}} \right)^{-2}, && \text{(G.0.10)}\\
r_h &= 0.35 {\beta_0}^{-0.25} 10^{0.16\,\theta_0} \left(\frac{m}{\mathrm{kev/c^2}} \right)^{-2}. && \text{(G.0.11)}
\end{aligned}$$

where masses are in solar masses and radii in parsecs. The cutoff parameter does not influence the properties of the system and is used only to determine the size. It is interesting to note that, for the core, the important quantity is $\beta_0 \theta_0 = \mu / mc^2$, and not the parameters themselves. Also, the halo has a much stronger dependence on θ_0 than the core. This scaling laws are exact for the mass and are valid for $\log \beta_0 \in [-11, -5]$ and $\theta_0 \in [0, 200]$.

Donato et al. (2009), fitting DM halos with the Burkert profile, found out that the surface density at the Burkert radius is constant for a wide number of galaxies, with different masses and magnitudes; this implies a constant acceleration due to DM at the Burkert radius, $a_{DM}) = 3.2 \times 10^{-9} cm/s^2$. Using our scaling laws and the fact that $a_{DM} = GM_h/r_h^2$, we have the scaling law for the acceleration:

$$\log \frac{a_{DM}}{\mathrm{km^2/pc.s^2}} = 11.786 + 1.25 \log \beta_0 - 0.16\theta_0 + 2 \log \frac{m}{\mathrm{keV/c^2}}. \qquad (G.0.12)$$

Using this, with velocities 5-500 km/s, and considering a particle with a mass of 8.5 keV, we find that $\theta_0 \in [5, 40]$.

Another scaling law was found by Walker et al. (2010), now for the rotation velocity:

$$\log \frac{v}{\mathrm{km/s}} = 1.47 + 0.5 \log \frac{r}{\mathrm{kpc}}. \qquad (G.0.13)$$

We then defined an average radius where the bulk of the measurements of Walker et al. (2010) were made. With a scaling law for this radius, we can then compare our results with Eq. G.0.13 and we find a relation between two parameters:

$$\beta_0 = 2.47 \times 10^{-10+0.128\theta_0} m^{-8/5}. \qquad (G.0.14)$$

Using the velocity range 5-500 km/s and a mass of 8.5 keV, we find that $\theta_0 \in [6, 40]$, in agreement with our former result. This shows that the choice of the radius is good, since a law like Eq. G.0.13 implies a constant acceleration.

However, Boyarsky et al. (2009a), studying larger systems and using the DM column density, found that the acceleration is not constant but tend to increase for systems with $M > 10^{10} M_\odot$. Again using a scaling law for the column density, we find a slight increase for the degeneracy parameter for the same mass: $\theta_0 \in [23, 52]$.

In conclusion, we show that our model could be a viable model for DM halos and compact objects in the center of galaxies, despite still having some problems in the core (see Argüelles and Ruffini (2014a) for details). We can use observations to constrain our parameter space to two free parameters (the mass of the particle and the degeneracy parameter) and show that our model can reproduce the universality laws for a wide range of parameters.

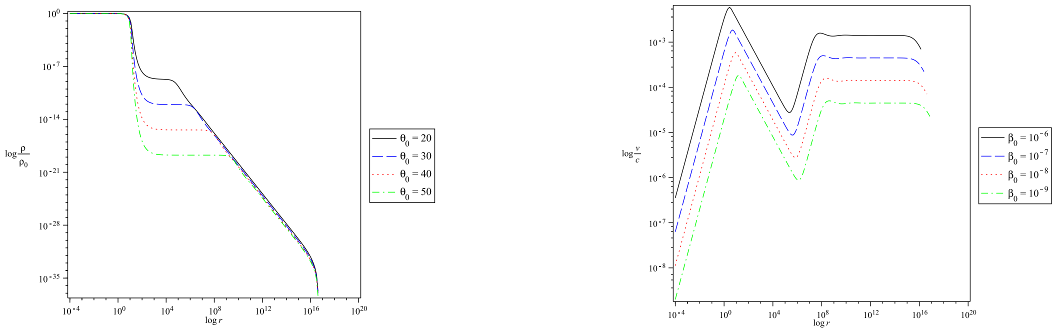

(a) (b)

Figure G.1.: (a) Density profile for different values of θ_0. (b) Rotation curve for different values of β_0.

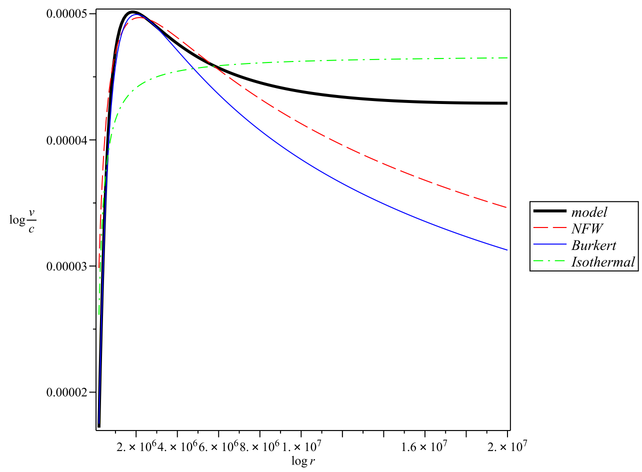

Figure G.2.: Comparison of the other profiles with our model for the best-fit parameters.

H. On the core-halo distribution of dark matter in galaxies

H.1. Introduction

The problem of identifying the masses and the fundamental interactions of the dark matter particles is currently one of the most fundamental issues in physics and astrophysics. The first astrophysical and cosmological constraints on the mass of the dark matter particle appeared in Cowsik and McClelland (1972); Weinberg (1972); Gott et al. (1974); Lee and Weinberg (1977); Tremaine and Gunn (1979). As we will show, some inferences on the dark matter particle mass can be derived from general considerations based solely on quantum statistics and gravitational interactions on galaxy scales.

An important open issue in astrophysics is the description of the dark matter in terms of collisionless massive particles. Attempts have been presented to put constraints on its phase-space density by knowing its evolution from the cosmological decoupling until the approximate time of virialization of a dark matter halo. Phenomenological attempts have been proposed in the past in terms of Maxwellian-like, Fermi-Dirac-like or Bose-Einstein-like distribution functions. Since the 80's all the way up to the present, the problem of modeling the distribution of dark matter in terms of self-gravitating quantum particles has been extensively studied and contrasted against galactic observables. In Ruffini and Stella (1983); Viollier et al. (1993); Chavanis and Sommeria (1998); Bilic et al. (2002); Chavanis (2002a); Boyanovsky et al. (2008); Argüelles et al. (2013); Ruffini et al. (2013a); Destri et al. (2013); Argüelles and Ruffini (2014b); Argüelles et al. (2014b); de Vega et al. (2014); Siutsou et al. (2015), and references therein, this problem was studied by considering Fermi-Dirac statistics in different regimes, from the fully degenerate to the dilute one, and for different fermion masses going from few eV to keV. Instead, in Sin

(1994); Hu et al. (2000); Böhmer and Harko (2007a); Boyanovsky et al. (2008); Spivey et al. (2013); Harko (2014) the same problem was analyzed in terms of Bose-Einstein condensates with particle masses from 10^{-25} eV up to few eV.

Attempts of studying galactic structures in terms of fundamental physical principles such as thermodynamics and statistical physics, has been long considered (e.g. Binney and Tremaine (2008)) since galaxies present many quasi-universal self-organized properties such as: the constant mean surface density at one-halo scale-length for luminous and dark matter (Gentile et al. (2009)); the Fundamental Plane of galaxies (Djorgovski and Davis (1987); Jorgensen et al. (1996)); or the fact that dark matter halos can be well fitted by many different but similar profiles that resemble isothermal equilibrium spheres (e.g. de Blok et al. (2008); Chemin et al. (2011); de Vega et al. (2014)). Within the statistical and thermodynamical approach, the most subtle problem is the one of understanding the complex processes of relaxation which take place before a galactic halo enters in the steady states we observe. In the context of this paper we will deal only with the (quasi) relaxed states of galaxies, and do not worry about the previous relaxation history of the halos. Nevertheless, and in order to justify in a consistent way the hypothesis we use here, the relaxation process must be certainly considered within the realm of collisionless relaxation, giving the non-interacting nature of the dark matter at halo scales. Formally speaking, this kind of relaxation process differs from the standard collisional relaxation by the fact that the last is described in terms of the Fokker-Planck equation, while the former must be described in terms of the Vlasov-Poisson equation, in order to account for the space and time variations in the overall gravitational potential, not included in the collisional approach (Binney and Tremaine (2008)). While collisional relaxation processes can be applied in globular clusters (stellar component dominant) implying relaxation times t_R of the order or less than the age of the Universe, if applied to galaxies, these processes are largely not relevant because t_R exceeds 10 Gyr by orders of magnitude (Binney and Tremaine (2008)). By the contrary, it has been extensively shown by now that the time-varying (global) gravitational potential proper of the collisionless process known as violent relaxation (Lynden-Bell (1967); Chavanis (2002b, 2006)), provides a relaxation mechanism analogous to collisions in a gas, but with an associated dynamical time-scale much shorter $t_D << t_R$; implying now an excellent opportunity to attack the problem of relaxation in galaxies. The central outcome of this theory is that within a few dynamical times t_D, the collisionless system quasi relaxes into a tremendously long lived quasi-stationary-state

(QSS), which under well mixing conditions can be described in terms of the Fermi-Dirac statistics as shown in Lynden-Bell (1967); Shu (1978); Kull et al. (1996); Chavanis (2002a,b, 2005, 2006) [1]. Even though the Fermi-Dirac distribution was first obtained in terms of a coarse-grained dynamical description (Lynden-Bell (1967)), the same statistics was also derived more fundamentally, in terms of particles, either distinguishable (i.e. stars Shu (1978)), or indistinguishable fermionic particles (Kull et al. (1996); Chavanis (2002a)), as the ones we are interested here [2].

Models based on self-gravitating fermions whose equilibrium distributions are assumed to be everywhere in a classical dilute regime (i.e. which can be well approximated by Boltzmannian distributions) as the one recently studied in de Vega et al. (2014), may have serious problems of stability when applied to galactic structures such as big spirals. Even though a model of this kind provide good fits when contrasted with observational rotation curves and density profiles (which is also the case within our model, Siutsou et al. (2015)), these profiles most likely undergo core-collapse, being this an inevitable fait of Boltzmannian-based distributions which present large density contrast between center and periphery, even in the case of collisionless particles (Padmanabhan (1990); Chavanis and Sommeria (1998); Chavanis (2002b)). By the contrary, for self-gravitating systems of collisionless particles which develop some degree of central degeneracy such that the overall dilute-regime can no longer be assumed (i.e. for $\theta_0 \gtrsim 10$ within our model), the core-collapse can be stopped, basically because the exclusion principle now present *saturates* the gravitational collapse (see Chavanis and Sommeria

[1] It has been explicitly shown that these kind of Fermi-Dirac distribution functions can be obtained from a maximization entropy principle at fixed total mass and temperature of the systems (Chavanis and Sommeria (1998); Chavanis (2002a); Bilic and Viollier (1999); Chavanis (2005)), implying therefore the necessity for these quasi-relaxed structures to be bounded in radius. This condition can be achieved, for example, by introducing a cut-off in the momentum space of the original Fermi-Dirac distribution as shown first in Ingrosso et al. (1992), and more recently in the context of the model here introduced, in Ruffini et al. (2013a); Argüelles and Ruffini (2014a). The main properties of the fermionic model relevant for the conclusions of this work do not depend on the cut-off as shown in Argüelles and Ruffini (2014a), which only set the outermost boundary radius. Therefore we will adopt for simplicity the standard Fermi-Dirac statistics throughout this paper.

[2] In any case, the (fermionic) Fermi-Dirac distribution used in this work must be always thought as the final outcome of a macroscopic *coarse-grained mixing*, such that the macroscopic entropy can increase during the complex (collisionless) relaxation processes (second law of thermodynamics) and eventually be maximized to find the final state, as in the cases mentioned in the above footnote 1.

(1998); Bilic and Viollier (1999); Chavanis (2002a,b)).

It is our opinion that in the fermionic case, a clear differentiation of a quantum degenerate core and an almost classical halo, has never been properly implemented. In particular it has been neglected the crucial role of comparing and contrasting different configurations, for fixed halo boundary conditions. As we will show, this leads to a very specific eigenvalue problem for the mass of the inos.

In this paper, and for completeness, we formulate the general problem of the dark matter distribution in galaxies based in the following assumptions: 1) that the dark matter phase-space density is described by the Fermi-Dirac statistics; 2) that the equilibrium equations for the configurations be solved within a general relativistic treatment; 3) we set the boundary condition for all dark matter profiles associated with a specific galaxy type (dwarfs, spirals, and big spirals), to have, in each case, the same value of the flat rotation curve. Having established this procedure in section H.2, we evidence in section H.3: i) the new core-halo distribution of dark matter density, which is composed by a dense compact core governed by almost degenerate quantum statistics, a semi-degenerate transition, followed by a dilute halo governed by Boltzmann classic statistics; ii) for each central degeneracy parameter we determine as an eigenvalue problem, the mass and radius of the inner quantum core, as well as the corresponding ino mass; and iii) we show that, for an ino mass of ~ 10 keV$/c^2$, there is in our model a theoretical correlation between the inner quantum core mass and the halo mass, for galaxy types from dwarf up to big spirals. From these considerations clearly follows that the determination of the ino mass is uniquely established by the properties of the inner quantum core and the asymptotic boundary conditions, and it cannot be determined in a dark matter distribution governed only by a Boltzmannian distribution, which is independent of the mass of the ino. In section H.4 we summarize and discuss our results.

H.2. Equilibrium equations and boundary conditions

Following Gao et al. (1990); Argüelles et al. (2014b), we here consider a system of general relativistic self-gravitating bare massive fermions under the approximation of thermodynamic equilibrium. As mentioned above, this approximation is well justified under the assumption of well mixing during the collisionless relaxation process, where the overall distribution function of the inos in the QSS, can be well approximated by the Fermi-Dirac distribution. No additional interactions are initially assumed for the fermions besides their fulfillment of quantum-like statistics and the relativistic gravitational equations. In particular, we do not assume weakly interacting particles as in Tremaine and Gunn (1979). We refer to this *bare* particles more generally as *inos*, leaving the possibility of additional fundamental interactions to be determined by further requirements to be fulfilled by the model. Already this treatment of bare fermions leads to a new class of equilibrium configurations and, correspondingly, to new limits to the ino mass. This is a necessary first step in view of a final treatment involving additional interactions to be treated self-consistently, as we will soon indicate here.

The density and pressure of the fermion system are given by

$$\rho = m\frac{2}{h^3}\int f(p)\left[1+\frac{\epsilon(p)}{mc^2}\right]d^3p, \tag{H.2.1}$$

$$P = \frac{1}{3}\frac{2}{h^3}\int f(p)\left[1+\frac{\epsilon(p)}{mc^2}\right]^{-1}\left[1+\frac{\epsilon(p)}{2mc^2}\right]\epsilon\, d^3p, \tag{H.2.2}$$

where the integration is over all the momentum space, $f_p = (\exp[(\epsilon - \mu)/(kT)]+1)^{-1}$ is the distribution function, $\epsilon = \sqrt{c^2p^2+m^2c^4} - mc^2$ is the particle kinetic energy, μ is the chemical potential with the particle rest-energy subtracted off, T is the temperature, k is the Boltzmann constant, h is the Planck constant, c is the speed of light, and m is the ino's particle mass. We do not include the presence of anti-fermions, i.e. we consider temperatures $T \ll mc^2/k$.

The Einstein equations for the spherically symmetric metric $g_{\mu\nu} = \mathrm{diag}(e^{\nu}, -e^{\lambda}, -r^2, -r^2\sin^2\Theta)$, being Θ the azimutal angle, where ν and λ depend only on the radial coordinate r, together with the thermodynamic equilibrium conditions of Tolman (1930), $e^{\nu/2}T =$constant, and Klein (1949b),

$e^{\nu/2}(\mu + mc^2)$ =constant, can be written as Gao et al. (1990)

$$\frac{d\hat{M}}{d\hat{r}} = 4\pi\hat{r}^2\hat{\rho}, \tag{H.2.3}$$

$$\frac{d\theta}{d\hat{r}} = -\frac{1-\beta_0(\theta-\theta_0)}{\beta_0}\frac{\hat{M}+4\pi\hat{P}\hat{r}^3}{\hat{r}^2(1-2\hat{M}/\hat{r})}, \tag{H.2.4}$$

$$\frac{d\nu}{d\hat{r}} = \frac{2(\hat{M}+4\pi\hat{P}\hat{r}^3)}{\hat{r}^2(1-2\hat{M}/\hat{r})}, \tag{H.2.5}$$

$$\beta_0 = \beta(r)e^{\frac{\nu(r)-\nu_0}{2}}. \tag{H.2.6}$$

The following dimensionless quantities were introduced: $\hat{r} = r/\chi$, $\hat{M} = GM/(c^2\chi)$, $\hat{\rho} = G\chi^2\rho/c^2$, $\hat{P} = G\chi^2 P/c^4$, where $\chi = 2\pi^{3/2}(\hbar/mc)(m_p/m)$, with $m_p = \sqrt{\hbar c/G}$ the Planck mass, and the temperature and degeneracy parameters, $\beta = kT/(mc^2)$ and $\theta = \mu/(kT)$, respectively. The constants of the Tolman and Klein conditions are evaluated at the center $r = 0$, indicated with a subscript '0'.

The system variables are $[M(r), \theta(r), \beta(r), \nu(r)]$. We integrate Eqs. (H.2.3–H.2.6) for given initial conditions at the center, $r = 0$, in order to be consistent with the observed dark matter halo mass $M(r = r_h) = M_h$ and radius r_h, defined in our model at the onset of the flat rotation curves. The so called *halo radius* (and mass) in this paper represent the one-halo scale length (and mass) associated with the fermionic model here presented, and corresponding with the turn-over of the density profiles in total analogy as other halo-scale lengths used in the literature such as r_0 or r_{-2} as shown in Fig. H.3. The circular velocity is

$$v(r) = \sqrt{\frac{GM(r)}{r - 2GM(r)/c^2}}, \tag{H.2.7}$$

which at $r = r_h$, is $v(r = r_h) = v_h$.

It is interesting that a very similar set of equations have been re-derived in Bilic et al. (2002) apparently disregarding the theoretical approach already implemented in 1990 in Gao et al. (1990). They integrated the Einstein equations fixing a fiducial mass of the ino of $m = 15$ keV$/c^2$, and they derived a family of density profiles for different values of the central degeneracy parameter at a fixed temperature consistent with an asymptotic circular velocity $v_\infty = 220$ km/s. They conclude that a self-gravitating system of such inos could offer an alternative to the interpretation of the massive black hole in the core of SgrA* (Ghez et al. (2008)). Although this result was possible at that time, it has been superseded by new constraints imposed by further observational limits on the trajectory of S-stars such as S1 and S2 (Ghez et al. (2008); Gillessen et al. (2009)).

In this paper we give special attention to the halo boundary conditions determined through the flat rotation curves. We integrate our system of equations using different boundary conditions to the ones imposed in Bilic et al. (2002) and reaching different conclusions. We first apply this model to typical spiral galaxies, similar to our own galaxy, adopting dark matter halo parameters (de Blok et al. (2008); Sofue et al. (2009)):

$$r_h = 25\ \text{kpc},\ v_h = 168\ \text{km/s},\ M_h = 1.6 \times 10^{11} M_\odot\,. \tag{H.2.8}$$

Later on we repeat the analysis also for typical dwarf spheroidal galaxies: $r_h = 0.6$ kpc; $v_h = 13$ km/s; $M_h = 2 \times 10^7 M_\odot$ (Walker et al. (2009)); as well as for typical big spiral galaxies:$r_h = 75$ kpc; $v_h = 345$ km/s; $M_h = 2 \times 10^{12} M_\odot$ (Boyarsky et al. (2009a)). The initial conditions are $M(0) = 0$, $\nu(0) = 0$, $\theta(0) = \theta_0$ and $\beta(0) = \beta_0$. We integrate Eqs. (H.2.3–H.2.6) for selected values of θ_0 and m, corresponding to different degenerate states of the gas at the center of the configuration. The value of β_0 is actually an eigenvalue which is found by a trial and error procedure until the observed values of v_h and M_h at r_h are obtained. We show in Fig. H.1 the density profiles and the rotation curves as a function of the distance for a wide range of parameters (θ_0, m), for which the boundary conditions in (H.2.8) are exactly fulfilled.

H.3. Dark matter profiles: from dwarf to big spiral galaxies

The phase-space distribution encompasses both the classical and quantum regimes. Correspondingly, the integration of the equilibrium equations leads to three marked different regimes (see Fig. H.1): a) the first consisting in a quantum core of almost degenerate fermions. These cores are characterized by having $\theta(r) > 0$. The core radius r_c is defined by the first maximum of the velocity curve. A necessary condition for the validity of this quantum treatment for the central core is that the interparticle mean-distance, l_c, be smaller or of the same order, of the thermal de Broglie wavelength of the inos,

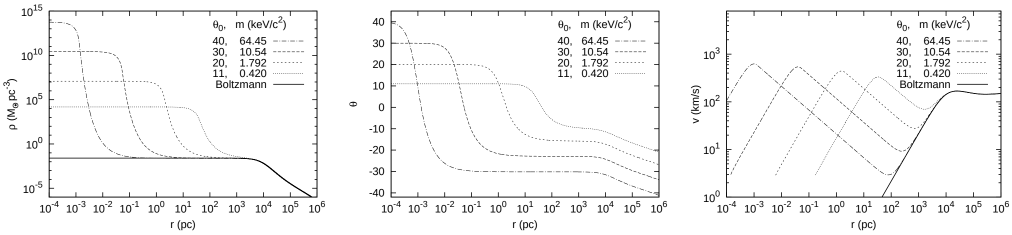

Figure H.1.: Mass density (left panel), degeneracy parameter (central panel), and rotation velocity curves (right panel) for specific ino masses m and central degeneracies θ_0 fulfilling the observational constraints (H.2.8). The density solutions are contrasted with a Boltzmannian isothermal sphere with the same halo properties. All the configurations, for any value of θ_0 and corresponding m, converge for $r \gtrsim r_h$ to the classical Boltzmannian isothermal distribution. It is clear how the Boltzmann distribution, is as it should be, independent of m. Interestingly, when the value $M_c(r \lesssim 10^{-2}$ pc)$\sim 10^6 M_\odot$ (i.e. $m \sim 10$ keV$/c^2$) is chosen as the one of more astrophysical interest, the onset of the classical Boltzmann regime takes place at distances of $r \gtrsim$ few 10^2 pc, in consistency with the observed cored nature of the innermost resolved regions in spiral galaxies as analyzed in (de Blok et al., 2008).

$\lambda_B = h/\sqrt{2\pi mkT}$. As we show below (see Fig. H.2), this indeed is fulfilled in all the cases here studied. b) A second regime where $\theta(r)$ goes from positive to negative values for $r > r_c$, all the way up to the so called classical domain where the quantum corrections become negligible. This transition region consists in a sharply decreasing density followed by an extended plateau. c) The classical regime described by Boltzmann statistics and corresponding with $\theta(r) \ll -1$ (for $r \gtrsim r_h$), in which the solution tends to the Newtonian isothermal sphere with $\rho \sim r^{-2}$, where the flat rotation curve sets in. Of course, the flat region of the velocity curve can not continue indefinitely in the case of realistic bounded systems. This can be easily achieved in the context of our model and without changing the results here presented, by introducing a cut-off in the momentum space accounting for possible dissipative and/or tidal effects as done in (Ruffini et al. (2013a); Argüelles and Ruffini (2014a)), and already explained in the footnote 1. Regarding a possible astrophysical discussion about the novel (increasing-decreasing) aspect of the inner part of the rotation curve arising before reaching the known classical behaviour, as well as the numerical implications of β_0 and θ_0, they are given at the end of

θ_0	m (keV/c^2)	r_c (pc)	$M_c(M_\odot)$	v_c (km/s)	θ_c
11	0.420	3.3×10^1	8.5×10^8	3.3×10^2	2.1
25	4.323	2.5×10^{-1}	1.4×10^7	4.9×10^2	5.5
30	10.540	4.0×10^{-2}	2.7×10^6	5.4×10^2	6.7
40	64.450	1.0×10^{-3}	8.9×10^4	6.2×10^2	8.9
58.4	2.0×10^3	9.3×10^{-7}	1.2×10^2	7.5×10^2	14.4
98.5	3.2×10^6	3.2×10^{-13}	7.2×10^{-5}	9.8×10^2	21.4

Table H.1.: Core properties for different equilibrium configurations fulfilling the halo parameters (H.2.8) of spiral galaxies.

this section.

We define the core mass, the circular velocity at r_c, and the core degeneracy as $M_c = M(r_c)$, $v_c = v(r_c)$ and $\theta_c = \theta(r_c)$, respectively. In Table H.1 we show the core properties of the equilibrium configurations in spiral galaxies, for a wide range of (θ_0, m). For any selected value of θ_0 we obtain the correspondent ino mass m to fulfill the halo properties (H.2.8), after the above eigenvalue problem of β_0 is solved.

It is clear from Table H.1 and Fig. H.1 that the mass of the core M_c is strongly dependent on the ino mass, and that the maximum space-density in the core is considerably larger than the maximum value considered in (Tremaine and Gunn, 1979) for a Maxwellian distribution. Interestingly, as can be seen from Fig. H.1, the less degenerate quantum cores in agreement with the halo observables (H.2.8), are the ones with the largest sizes, of the order of halo-distance-scales. In this limit, the fermion mass acquires a sub-keV minimum value which is larger, but comparable, than the corresponding sub-keV bound in (Tremaine and Gunn, 1979), for the same halo observables. Indeed, their formula gives a lower limit $m \approx 0.05$ keV$/c^2$ when using the proper value for the King radius, $r_K \simeq 8.5$ kpc, as obtained from $\sigma = \sqrt{2/5}v_h$ and $\rho_0 = 2.5 \times 10^{-2} M_\odot/\text{pc}^3$, which are the associated values to the Boltzmannian density profile of Fig. H.1. This small difference is formally understood by the following fact: while their conclusions are reached by adopting the maximum phase-space density, $Q^h_{max} \sim \rho^h_0 m^{-4} \sigma_h^{-3}$, at the center of a halo described by a Maxwellian distribution; in our model the maximum phase-space density is reached at the center of the dense quantum core described by Fermi-Dirac statistics, $Q^c_{max} \sim \rho^c_0 m^{-4} \sigma_c^{-3}$ (where lower and upper index c reads for the central core). An entire new family of solutions exists for larger values of central phase-space occupation numbers, always in agreement with the halo observables (see Fig. H.1). Now, since these phase-space values, by the Liouville's theorem, can never exceed the maximum primordial phase-space density at decoupling, Q^d_{max}, we have $Q^{h,c}_{max} < Q^d_{max}$. Then, considering that all our quantum solutions satisfy $Q^c_{max} > Q^h_{max}$, it directly implies larger values of our ino mass with respect to the Tremaine and Gunn limit. Nevertheless, as we have quantitatively shown above, e.g. for the case of typical spiral galaxies, the two limits become comparable for our less degenerate ($\theta_0 \approx 10$) quantum cores in agreement with the used halo observables (H.2.8).

In the case of a typical spiral galaxy, for an ino mass of $m \sim 10$ keV$/c^2$, and a temperature parameter $\beta_0 \sim 10^{-7}$, obtained from the observed halo rotation velocity v_h, the de Broglie wavelength λ_B is higher than the interparticle mean-distance in the core l_c, see Fig. H.2, safely justifying the quantum-statistical treatment applied here.

If we turn to the issue of an alternative interpretation to the black hole on SgrA*, we conclude that a compact degenerate core mass $M_c \sim 4 \times 10^6 M_\odot$ is definitely possible corresponding to an ino of $m \sim 10$ keV$/c^2$ (see Table H.1). However, the core radius of our configuration is larger by a factor $\sim 10^2$ than the one obtained with the closest observed star to Sgr A*, i.e. the S2 star (Gillessen et al. (2009)). Nevertheless, for an ino mass of $m \sim 10$ keV$/c^2$ ($\theta_0 = 30$), the very low temperature of the dense quantum core is already a small fraction of the Fermi energy (i.e. $\lambda_B > l$), where additional interactions between the inos should arise, affecting the mass and radius of the new denser core depending on the interaction adopted [3]. Indeed, we have recently applied this novel idea in Argüelles et al. (2014a), achieving now higher possible compactness for the new quantum core, in perfect agreement with the observational constraints imposed by the S2 star, and always for ino masses in the range of $m \sim 10^1$ keV$/c^2$. Moreover, the relevance of self-interactions in ultra-cold fermionic-particle collisions has been already shown in laboratory, for example, for (effective) Fermi gases, e.g. ^{6}Li, at temperatures of fractions of the Fermi energy (Giorgini et al. (2008)). There, a good agreement between experiment and theory was achieved for such a cold Fermi gas when studied in terms of a grand-canonical many-body Hamiltonian in second quantization, with a term accounting for fermion-fermion interaction, similarly as done in Argüelles et al. (2014a).

[3] This is analogous for instance to the case of neutron stars, where nuclear fermion interactions strongly influence the mass-radius relation (see, e.g., Lattimer and Prakash (2007))

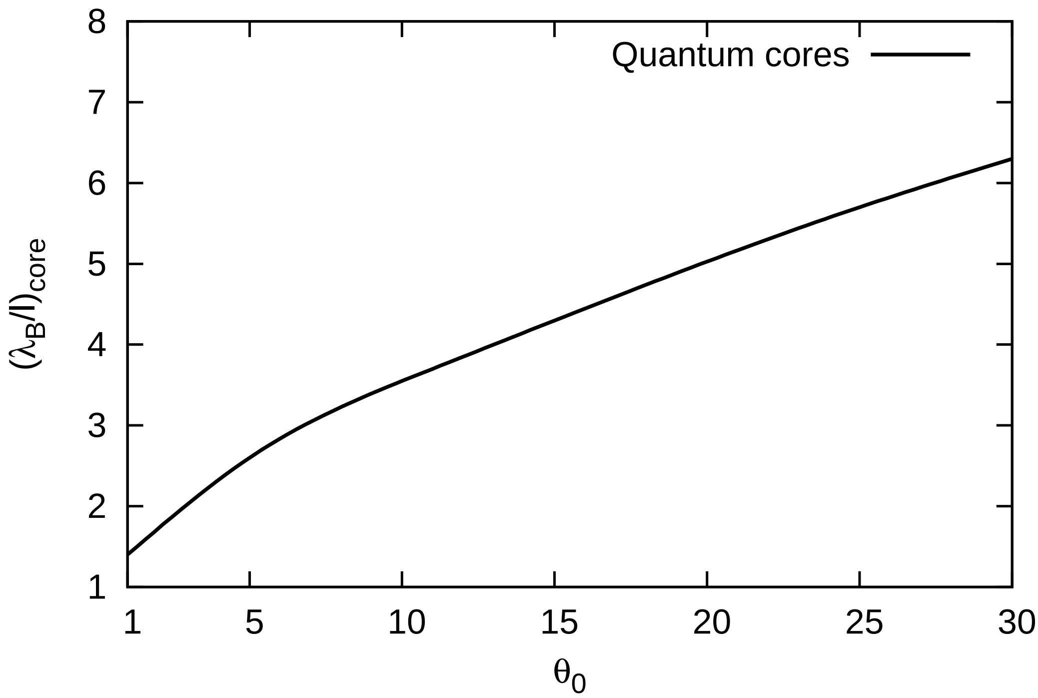

Figure H.2.: The less degenerate quantum cores in agreement with the halo observables (H.2.8) corresponds to $\theta_0 \approx 10$ ($\lambda_B \sim 3l_c$). These cores are the ones which achieve the largest sizes, of order $\sim 10^1$ pc, and implying the lowest ino masses in the sub-keV region.

We further compare and contrast in Fig. H.3 our theoretical curves of Fig. H.1 with observationally inferred ones. In order to provide a more detailed comparison, we have extensively contrasted our three-parametric fermionic model with many other dark matter parametric models resulting from N-body simulations, in terms of a formal Bayesian statistical analysis and using high resolution data samples including for baryonic components, in Siutsou et al. (2015). It is interesting that the quantum statistical treatment (including relativistic effects) considered here, is characterized by the presence of central cored structures unlike the typical *cuspy* configurations obtained from a classic non-relativistic approximation, such as the ones of numerical N-body simulations in Navarro et al. (1997). This naturally leads to a first step, in terms of a first principle physics approach, to understand the well-known core-cusp discrepancy as first shown in de Blok et al. (2001) and further confirmed for typical spiral galaxies in Chemin et al. (2011). Such a difference between the ino's core and the cuspy NFW profile, as well as the possible black hole nature of the compact source in SgrA*, will certainly reactivate the development of observational campaigns in the near future. There the interesting possibility, in view of the BlackHoleCam Project based on the largest Very Long Baseline Interferometry (VLBI) array[4], to verify the general relativistic effects expected in the surroundings of the central compact source in SgrA*. Such effects depend on whether the source is modeled in terms of the RAR model presented here (with the possible inclusion of fermion interactions, Argüelles et al. (2014a)), or as a black hole. To compare and contrast these two alternatives is an observational challenge now clearly open.

Following the analysis developed here for a typical spiral, we have also considered two new different sets of physical dark matter halos: $r_h = 0.6$ kpc; $v_h = 13$ km/s; $M_h = 2 \times 10^7 M_\odot$ for typical dwarf spheroidal galaxies, (e.g. Walker et al. (2009)); and $r_h = 75$ kpc; $v_h = 345$ km/s; $M_h = 2 \times 10^{12} M_\odot$ for big spiral galaxies, as analyzed in Boyarsky et al. (2009a). For big spirals, $\lambda_B/l_c = 5.3$, while for typical dwarfs galaxies $\lambda_B/l_c = 4.1$, justifying the quantum treatment in both cases.

A remarkable outcome of the application of our model to such a wide range of representative dark halo galaxy types, from dwarfs to big spirals, is that *for the same* ino mass, $m \sim 10$ keV$/c^2$, we obtain respectively core masses $M_c \sim 10^4 M_\odot$ and radii $r_c \sim 10^{-1}$pc for dwarf galaxies, and core masses $M_c \sim 10^7 M_\odot$ and radii $r_c \sim 10^{-2}$pc for big spirals. This leads to a possible

[4] http://horizon-magazine.eu/space

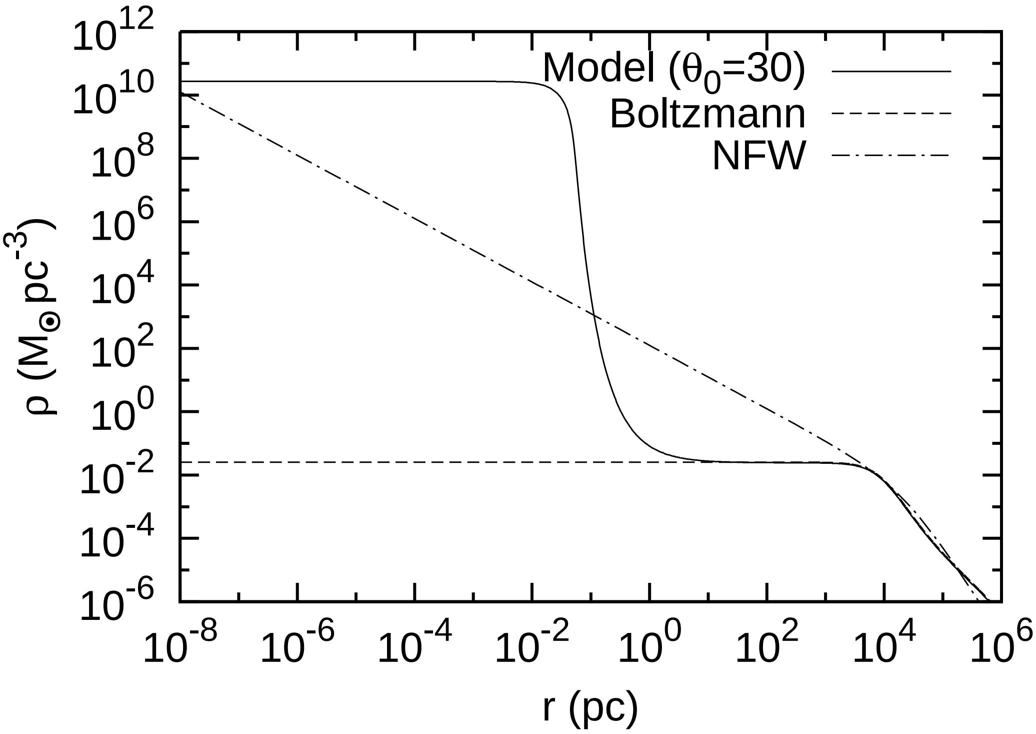

Figure H.3.: The cored behavior of the dark matter density profile from the Ruffini-Argüelles-Rueda (RAR) model is contrasted with the cuspy Navarro-Frenk-White (NFW) density profile (Navarro et al., 1997), and with a cored-like Einasto profile (Einasto, 1965; Einasto and Haud, 1989). The free parameters of the RAR model are fixed as $\beta_0 = 1.251 \times 10^{-7}$, $\theta_0 = 30$ and $m = 10.54$ keV$/c^2$. The corresponding free parameters in the NFW formula $\rho_{NFW}(r) = \rho_0 r_0/[r(1 + r/r_0)^2]$ are chosen as $\rho_0 = 5 \times 10^{-3} M_\odot$ pc^{-3} and $r_0 = 25$ kpc, and for the Einasto profile $\rho_E(r) = \rho_{-2} \exp\left[-2n(r/r_{-2})^{1/n} - 1\right]$, $\rho_{-2} = 2.4 \times 10^{-3} M_\odot$ pc^{-3}, $r_{-2} = 16.8$ kpc, and $n = 3/2$. In the last two models, the chosen free parameters are typical of spiral galaxies according to (de Blok et al., 2008; Chemin et al., 2011).

alternative to intermediate ($\sim 10^4 M_\odot$) and more massive ($\sim 10^{6-7} M_\odot$) black holes, thought to be hosted at the center of the galaxies.

Moreover, we have obtained out of first principles, a possible universal relation between the dark matter halos and the super massive dark central objects. For a fixed ino mass $m = 10$ keV$/c^2$, we found the M_c-M_h correlation law

$$\frac{M_c}{10^6 M_\odot} = 2.35 \left(\frac{M_h}{10^{11} M_\odot} \right)^{0.52}, \tag{H.3.1}$$

valid for core masses $\sim [10^4, 10^7]\, M_\odot$ (corresponding to dark matter halo masses $\sim [10^7, 10^{12}]\, M_\odot$). Regarding the observational relation between massive dark compact objects and bulge dispersion velocities in galaxies (the M_c-σ relation (Ferrarese (2002b)), it can be combined with two observationally inferred relations such as the σ-V_c and the V_c-M_h correlations, where V_c is the observed halo circular velocity and M_h a typical halo mass. This was done in Ferrarese (2002a) to find, by transitivity, a new correlation between central mass concentrations and halo dark masses (M_c-M_h). Interestingly, such a correlation matches with the one found above in Eq. (H.3.1) in the range $M_c = [10^6, 10^7]\, M_\odot$, without assuming the black hole hypothesis. The appearance of a core surrounded by a non-relativistic halo, is a key feature of the configurations presented in this paper. It cannot however be extended to quantum cores with masses of $\sim 10^9 M_\odot$. Such core masses, observed in Active Galactic Nuclei (AGN), overcome the critical mass value for gravitational collapse $M_{cr} \sim M_{pl}^3/m^2$ for keV-fermions, and therefore these cores have to be necessarily black holes (Argüelles and Ruffini (2014b)). The characteristic signatures of such supermassive black-holes, including jets and X-ray emissions, are indeed missing from the observations of the much quiet SgrA* source, or the centers of dwarf galaxies.

At this point it is relevant to discuss the qualitative and quantitative relevance of the general relativistic approach proposed here to model the distribution of dark matter in galaxies, when compared with a classical Newtonian approach. For the example analyzed here, i.e. for $m \sim 10$ keV$/c^2$ and spiral galaxies, the compactness of the quantum core is $GM_c/(r_c c^2) \sim 10^{-6}$, thus general relativistic effects are not dominant in these configurations. Under those conditions, we do expect a Newtonian approach to describe satisfactorily the configurations. Indeed, by integrating the corresponding equations of equilibrium in the Newtonian case, which are obtained in the non-relativistic weak-field limit of the treatment presented here [5], we obtain similar results to the general relativistic solution within 1% (for spiral galaxies and $m \sim 10$ keV$/c^2$), keeping the core-halo structure containing the three markedly different physical regimes from quasi-degeneracy regime in the core all the way up to Boltzmaniann one in the halo. As we have explained, such a change of regimes is due to the combination of the non-zero temperature and the changing fermion chemical potential with distance, which produces a changing degeneracy parameter with the distance. It is important to mention at this point that, if we were to model the galactic halos assuming a zero temperature, we would obtain a different behavior of the density profile (resembling our quantum core and never reaching the plateau plus Boltzmannian phase) which leads to non-flat rotation velocity curves (with a raising part, a maximum, and a Keplerian falling down region), hence inconsistent with observations.

A general relativistic treatment becomes a necessity in the case of more compact configurations approaching the critical mass for gravitational collapse, $M_{cr} \sim M_{pl}^3/m^2 \sim 10^9 M_\odot$, which as we have shown (Argüelles and Ruffini (2014b)) could be attained in the central compact cores observed in AGNs by the same dark matter candidate of $m \sim 10$ keV$/c^2$, and corresponding to different boundary conditions as contrasted with the case of normal galaxies here considered.

We turn now to briefly discuss the astrophysical implications of the full morphology of the dark matter rotation curves as well as the numerical implications of the typical temperature and degeneracy parameters found here. Indeed, the issue addressed in the present article is referred only to a pure dark matter composition while the observational data refers to the sum of the dark and baryonic (gas and stellar populations) matter. The key result presented here is that the dark matter contribution is always predominant in the inner core (at sub-pc scales), and in the outer halo region at the onset of the flat part of the given rotation curve; while in between baryonic matter prevails. We can see from the right panel of Fig. H.1 that indeed, for a Milky Way-like galaxy, our model correctly predicts both the value and flattening of the circular velocity at distances $r \gtrsim 10$ kpc. A detailed comparison of the theoretical curves analyzed here with extended astrophysical data will be soon

[5] This is obtained by taking the limit $c \to \infty$ and $e^{\nu/2} \approx 1 + \phi/c^2$, leading to thermodynamic equilibrium conditions $T =$constant, and $\mu + m\phi =$constant, with ϕ the Newtonian gravitational potential.

presented elsewhere (Argüelles et al. (2015)), including the special behavior of the circular velocity e.g. at the sub-pc scales.

Regarding the actual values of the dark matter temperatures and (effective) chemical potentials obtained out of the free parameters of the model (β_0, θ_0) consistent with the (quasi) relaxed galactic structures analyzed here, we have: for an ino mass of $m \sim 10$ keV$/c^2$, in typical dwarfs $T_d \sim 10^{-1}$ K ($\beta_0 \sim 10^{-9}$), while in spirals $T_s \sim 10^1$ K ($\beta_0 \sim 10^{-7}$). This values when combined with the central degeneracy parameters gives, for typical dwarfs $\mu_d \sim 10^{-7}$ keV ($\theta_{0,d} = 15$), and $\mu_s \sim 10^{-5}$ keV ($\theta_{0,s} = 30$) or $\mu_{bs} \sim 10^{-4}$ keV ($\theta_{0,bs} = 36$), for typical spiral or big spirals respectively[6]. The issue of the potential implications of these dark matter temperatures and chemical potentials in relation with different possible microscopic models for the dark matter candidate in cosmology, will be a subject for future works.

H.4. Conclusions

A consistent treatment of self-gravitating fermions within general relativity has been here introduced and solved with standard boundary conditions appropriate to flat rotation curves observed in galactic halos of spiral and dwarf galaxies. A new structure has been identified: 1) a core governed by quantum-like statistics; 2) a velocity of rotation at the surface of this core which is bounded independently of the mass of the particle and remarkably close to the asymptotic rotation curve; 3) a semi-degenerate region leading to an asymptotic regime described by a pure Boltzmann distribution, consistent with the flat rotation curves observed in galaxies. Interestingly it has been recently shown that quasi relaxed core-halo structures analogous as the one obtained here for the dark matter in galaxies, take part of a broader and more ubiquitous behaviour in nature, proper of long-range collisionless interacting systems including also plasmas and kinetic spin models (Levin et al. (2014)).

For $m \sim 10$ keV$/c^2$ a universal relation between the mass of the core M_c and the mass of the halo M_h has been found. This universal relation applies

[6]It is important to recall that i) due to the small general relativistic effects in the cases analyzed in this work, from the Tolman and Klein conditions the central values of T and μ given above are accurate through the overall configurations; and ii) μ is the chemical potential with the fermion rest-mass subtracted-off, therefore the (effective) chemical potentials, including the fermion rest-mass, are roughly (for all the cases with $m \sim 10$ keV$/c^2$) $\mu_{d,s,bs} + mc^2 \approx 10$ keV.

in a vast region of galactic systems, ranging from dwarf to big spiral galaxies with core masses $\sim [10^4, 10^7]\, M_\odot$ (corresponding to dark matter halo masses $\sim [10^7, 10^{12}]\, M_\odot$).

Starting from the basic treatment here introduced, of bare self-gravitating fermions, we have already examined the possibility to introduce new types of interactions (Argüelles et al. (2014a)) among the inos, considering, for example, a self-interacting picture in the context of right-handed sterile neutrinos in the minimal standard model extension (see e.g. Boyarsky et al. (2009b)), as a viable candidate for the ino particles in our new scenario. The extended approach studied in Argüelles et al. (2014a) allowed us to verify the possibility of the radius of the quantum core to become consistent with the observations of SgrA*, and so open the way to identify additional (effective) fundamental interactions in the ino physics. For this more general analysis, as well as for the model extension which allow us to deal with the very massive galactic compact cores of $M_c \sim 10^9 M_\odot$ as studied in Argüelles and Ruffini (2014b), the General Relativistic treatment here introduced for completeness, clearly becomes mandatory.

After this generalized treatment, we will further address the issue of the implications of these kev-fermions in cosmology.

I. Dark Matter Massive Fermions and Einasto Profiles in Galactic Haloes

I.1. Introduction

The problem of the distribution of Dark Matter (DM) in galaxies, as usually addressed in the literature, is mainly focused in the halo regions and associated with the galaxy rotation curves obtained from the observations, see e.g. Einasto (2013). A well-known approach used to deal with this problem is the Navarro–Frenk–White (NFW) model (Navarro et al., 1997), expected to provide a universal description of dark matter halos obtained under the following main considerations: 1) N-body simulations in Cold dark matter (CDM) and (ΛCDM) cosmologies; 2) particles each of masses of $\sim 10^9 M_\odot$ [1]; 3) classical Newtonian physics.

Despite an indicated agreement of this model with the large scale structure of the Universe, some problems remains at galactic scales, see e.g. Munshi et al. (2013). A central characteristic of the NFW dark matter density profiles, is that they show a cuspy and divergent behaviour through the center of the configuration, while empirical profiles tend to show a core of constant density, giving rise to the well-known core-cusp controversy, see e.g. de Blok (2010).

Yet another important approach developed to understand the distribution of matter in galaxies has been advanced by Einasto (1965) and Einasto and Haud (1989). This is a phenomenological approach consisting in the proposal of an empirical fitting function composed by three free pa-

[1] Modern numerical simulations can reach better resolution down to particle masses of $\sim 10^5 M_\odot$ (Gao et al., 2012).

rameters as detailed in equation (I.1.1)

$$\rho_E(r) = \rho_{-2} \exp\left(-\frac{2}{n}\left[\left(\frac{r}{r_{-2}}\right)^n - 1\right]\right), \tag{I.1.1}$$

where ρ_{-2} and r_{-2} are the density and radius at which $\rho(r) \propto r^{-2}$, and n is the Einasto index which determines the shape of the profile.

Recent N-body simulations in ΛCDM cosmology by Navarro et al. (2004) purported a novel dark matter halo model different from NFW. This model was soon realized (Merritt et al., 2006) to be the same as the Einasto one as given by equation (I.1.1).

After that, using the highest quality rotation curves available to date obtained from The HI Nearby Galaxy Survey (THINGS) (Walter et al., 2008; de Blok et al., 2008), the Einasto dark matter halo model has been proposed as the standard model for dark matter halos by Chemin et al. (2011), as it provides both cored and cusped distributions for different values of model parameters (see Fig. I.1). In that work, the fundamental core-cusp discrepancy is analyzed in detail for the whole sample of galaxies under study. It is clearly shown that for the majority of the galaxies considered in the sample, the cored halos (compatible with near unity Einasto indexes) are preferred over the cuspy ones (these instead compatible with higher Einasto indexes).

We present here a novel approach focusing on galactic structures and an underlying microphysical component of Dark Matter. The model is built upon the following general considerations: 1) the Dark Matter component is assumed to be chargeless spin-1/2 fermions; 2) the configurations are described by General Relativity; 3) the particles are assumed to be isothermal in thermodynamic equilibrium (i.e. without the need of pre-fixing any cosmological history). The theoretical fundament of this new approach is detailed in the model of semi-degenerate self-gravitating fermions first introduced by Gao et al. (1990), and more recently with applications to galactic dark matter by Argüelles et al. (2014b). Our model is based in the following main assumptions:

1. the problem of galactic cores and halos have to be addressed unitarily;

2. for definiteness we study the simplest problem of "bare" massive particles, neglecting at this stage all other interactions than the gravitational

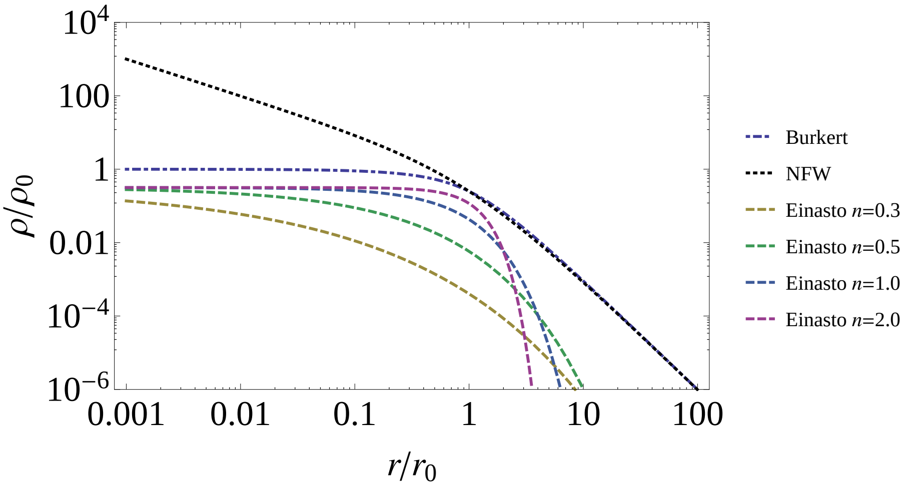

Figure I.1.: Comparison of the density profiles for different phenomenological models of dark matter distribution.

one and fulfilling only the Fermi–Dirac statistical distribution

$$f = \frac{1}{\exp\left(\frac{\epsilon-\mu}{kT}\right)+1} = \frac{1}{\exp\left(\frac{\epsilon}{\beta mc^2}-\theta\right)+1}, \tag{I.1.2}$$

where ϵ is kinetic energy of the particles, μ is chemical potential, T is the temperature, k is Boltzmann constant and c is the speed of light. The mass of the particle (m), the temperature parameter ($\beta = kT/mc^2$) and the degeneracy parameter ($\theta = \mu/kT$) at the center are the three free parameters of the model;

3. we consider zero total angular momentum and also neglect any effect of baryonic matter on the DM in the mathematical formulation.

It is shown that in any such system the density at large radii scales as r^{-2} independently of the values of the central density, providing the flat rotation curve (Gao et al., 1990; Argüelles et al., 2014b).

The dark matter halos obtained in the new dark matter approach proposed here share a common or universal feature which shed more light on the core-cusp discrepancy, while providing a new mass scale to the dark matter candidate. Our density profiles always favor a cored behaviour (without any cusp) in the observed inner halo regions, given the quantum nature of the fermionic particles. Another fundamental outcome of our model is the range of the DM particle mass, which must be $m \gtrsim 5$ keV in order to be in agreement with typical halo sizes of the observed dwarf galaxies (Argüelles et al., 2014b).

The theoretical formulation of Argüelles et al. (2014b) is based on the first principles physics and provides a physical complement to Einasto phenomenological models. It also offers the necessity to approach the Dark Matter distribution in galactic haloes with fermions with masses larger than the above mentioned bound.

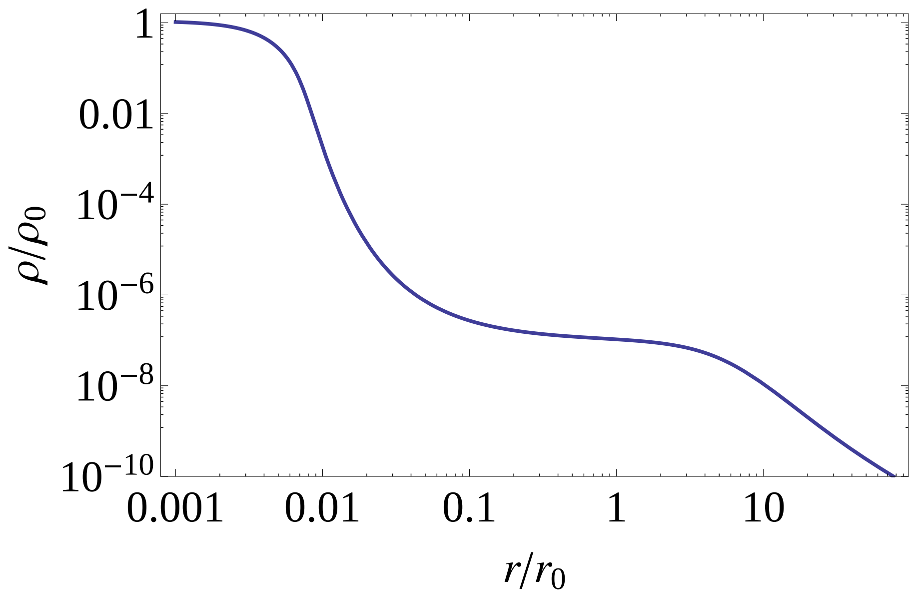

Figure I.2.: Semidegenerate density profile in dimensionless units for central degeneracy parameter $\theta_0 = 15$ and central temperature parameter $\beta_0 = 10^{-10}$.

The paper is structured as follows. We model the distribution of Dark Matter as semidegenerate fully relaxed thermal self-gravitating general relativistic fermionic solutions of Gao et al. (1990), see Sec. I.2. The resulting density profiles provide flat rotation curve at large distances, cored distribution of dark matter in the halo, and a massive degenerate core at the very center, see Sec. I.3. We describe in Sec. I.4 the actual procedure of fitting of rotation curves, and then discuss the results in Sec. I.5. Conclusions follow.

I.2. Model equations

We consider self-gravitating system of fermions in thermal equilibrium following Gao et al. (1990) with occupation numbers given by

$$f(\epsilon) = \frac{1}{e^{\frac{\epsilon-\mu}{kT}} + 1}. \tag{I.2.1}$$

Then equation of state reads

$$\rho = m\frac{g}{h^3}\int \frac{1+\epsilon/mc^2}{e^{\frac{\epsilon-\mu}{kT}} + 1}\, d^3p, \tag{I.2.2}$$

$$P = \frac{2}{3}\frac{g}{h^3}\int \frac{(1+\epsilon/mc^2)^{-1}(1+\epsilon/2mc^2)\epsilon}{e^{\frac{\epsilon-\mu}{kT}} + 1}\, d^3p, \tag{I.2.3}$$

where $g = 2s+1$, s is the spin of the particle, and integration is extended over all 3-momentum space.

The Einstein equations for the spherically symmetric metric

$$g_{\mu\nu} = \mathrm{diag}(e^{\nu}, -e^{\lambda}, -r^2, -r^2\sin^2\theta), \tag{I.2.4}$$

where ν and λ depend only on the radial coordinate r, together with the thermodynamic equilibrium conditions of Tolman (1930) and Klein (1949b)

$$e^{\nu/2}T = const\,, \qquad e^{\nu/2}(\mu + mc^2) = const, \tag{I.2.5}$$

can be written in the dimensionless form of Gao et al. (1990)

$$\frac{d\hat{M}}{d\hat{r}} = 4\pi\hat{r}^2\hat{\rho}, \tag{I.2.6}$$

$$\frac{d\theta}{d\hat{r}} = -\frac{1-\beta_0(\theta-\theta_0)}{\beta_0}\frac{\hat{M}+4\pi\hat{P}\hat{r}^3}{\hat{r}^2(1-2\hat{M}/\hat{r})}, \tag{I.2.7}$$

$$\frac{d\nu}{d\hat{r}} = \frac{\hat{M}+4\pi\hat{P}\hat{r}^3}{\hat{r}^2(1-2\hat{M}/\hat{r})}, \tag{I.2.8}$$

$$\beta_0 = \beta(r)e^{\frac{\nu(r)-\nu_0}{2}}, \tag{I.2.9}$$

$$e^{-\lambda} = 1 - \frac{2\hat{M}(\hat{r})}{\hat{r}}. \tag{I.2.10}$$

The following dimensionless quantities were introduced:

$$\hat{r} = r/\chi, \tag{I.2.11}$$

$$\hat{M} = GM/(c^2\chi), \tag{I.2.12}$$

$$\hat{\rho} = G\chi^2\rho/c^2, \tag{I.2.13}$$

$$\hat{P} = G\chi^2 P/c^4, \tag{I.2.14}$$

where $\chi = 2\pi^{3/2}(\hbar/mc)(m_p/m)$ is the characteristic length that scales as m^{-2}, with $m_p = \sqrt{\hbar c/G}$ being the Planck mass, and the temperature and degeneracy parameters, $\beta = kT/(mc^2)$ and $\theta = \mu/(kT)$, respectively. The constants of the equilibrium conditions of Tolman and Klein have been evaluated at the center $r = 0$, which we indicate with a subscript '0'.

The system of coupled differential equations (I.2.6–I.2.10) is solved for initial conditions $M(0) = \nu(0) = 0$ and given set of free parameters β_0 and θ_0, m for each galaxy under study as detailed below.

I.3. Properties of semidegenerate configurations

Galactic halos have to be necessarily composed from cold particles, so that astrophysically relevant solutions will have temperature parameters $\beta \ll 1$. In this case, the general solution for semidegenerate configurations ($\theta_0 \gtrsim 10$) present three different regions: an inner degenerate compact core, an extended low-degenerate inner halo of almost constant density and a nondegenerate outer halo with characteristic slope $\rho \propto r^{-2}$ (see Gao et al. (1990) and Fig. I.2 for additional details). The infinite mass of the configuration extended up to spatial infinity is not a problem, because in reality it is limited by tidal interactions with other galaxies, which introduce an energy cutoff into the distribution function, see e.g. Ingrosso et al. (1992). However this is not important for the inner parts of the configuration we are interested in.

In order to understand the crucial properties of this equilibrium configurations we plot the circular velocity of a test body in the metric fulfilling Eqs. (I.2.6–I.2.10) on Fig. I.3. There are indeed four regions of the solution for circular velocity, each with characteristic slope. The inner region I correspond to the degenerate core of almost constant density, so that $v_{\rm circ} \propto r$. For increasing values of radial coordinate the inner halo follows, itself composed of two different regions. In the region II the density of dark matter sharply decreases and this Keplerian region is dominated by the mass of the degenerate core, and as a result $v_{\rm circ} \propto r^{-1/2}$. For yet increasing values of the radial coordinate the density of dark matter reach an almost constant value giving rise to a plateau, see Fig. I.2. As soon as the mass of the plateau prevails over the mass of the core we have the region III where $v_{\rm circ} \propto r$. Finally in the region IV, after some oscillations the circular velocity tends to a constant independent on r, corresponding to a pure Boltzmannian regime and characteristic for the flat rotation curve of outer halo.

We define the physical characteristics of each configuration as follows:

- The characteristic radius of the core $\hat{r}_c$ is given by $\hat{v}_{\rm circ}(\hat{r}_c) = \max$ in region I.
- $\hat{M}_c$ is the mass of the core given by $\hat{M}_c = \hat{v}^2_{\rm circ}\hat{r}$ in the region II.
- The characteristic radius of the inner halo $\hat{r}_h$ correspond to $\hat{v}_{\rm circ}(\hat{r}_h) = \max$ in region III.
- The characteristic mass of the inner halo $\hat{M}_h$ is given by $\hat{M}_h = \hat{M}(\hat{r}_h)$ just between the regions III and IV.

For the parameters in the region of $\theta_0 \in [0, 200], \log\beta_0 \in [-10, -5]$ we calculate a grid of models and extracted numerically the physical characteristics mentioned above. Then we fit the obtained values by different double parametric functions and find out the best fitting formulae with the correspondent (β_0,θ_0) dependence for the range of $\theta_0 \in [20, 200]$. An interesting

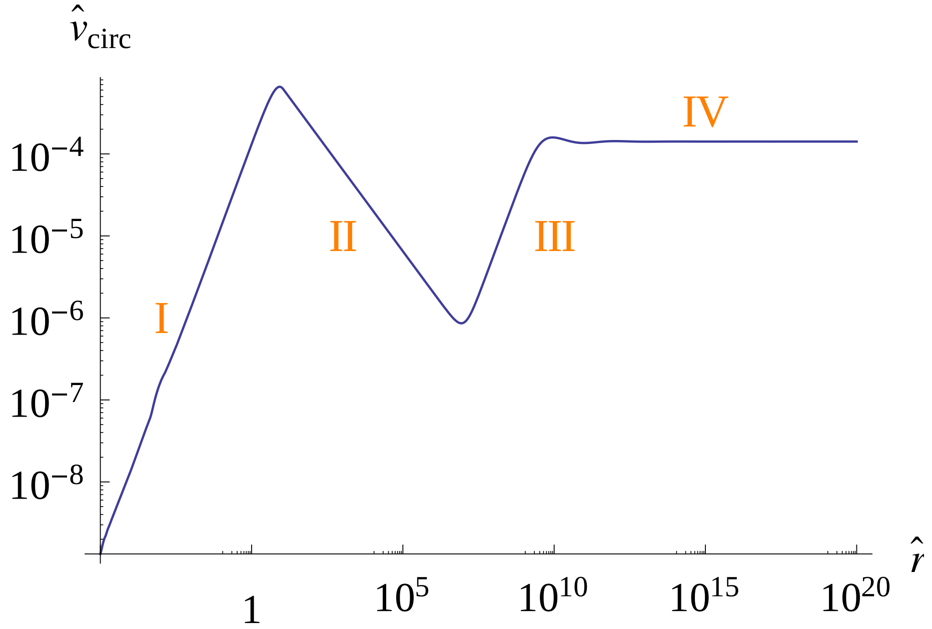

Figure I.3.: Dependence of $\hat{v}_{\rm circ} = v_{\rm circ}/c$ on dimensionless radius $\hat{r}$, $\beta = 10^{-8}$, $\theta_0 = 50$.

fact is that in our region of parameters circular velocity $v_{\rm circ}$ in the flat part of region IV (i.e. v_∞) is defined by temperature β_0 only. In the range of astrophysically relevant parameters $\theta_0 \in [10, 200], \log \beta_0 \in [-10, -5]$ the scaling relation between circular velocity and β_0 corresponds to the Boltzmannian relation between $v_{\rm circ}$ and one-dimensional dispersion velocity $\sigma = \sqrt{kT/m}$ (see e.g. Binney and Tremaine (1987))

$$\frac{v_\infty}{\rm km/s} = \sqrt{2} c \sqrt{\beta_0}. \tag{I.3.1}$$

We have here neglected general relativistic corrections which are very small in these ranges of parameters, i.e. $e^{\nu(\infty)-\nu(0)} \approx 1$, and then $\beta(\infty) \approx \beta_0$ by equation (H.2.6).

For the temperature and degeneracy free parameters in the range $\log \beta_0 \in [-10, -5]$, $\theta_0 \in [20, 200]$, respectively, we obtain the following dimensionless scaling laws for core radius and mass[2]

$$\hat{r}_c = 0.226(\beta_0 \theta_0)^{-1/4}, \tag{I.3.2}$$

$$\hat{M}_c = 0.234(\beta_0 \theta_0)^{3/4}. \tag{I.3.3}$$

However, the core region is typically very small and is not constrained by empirical data of the THINGS sample considered here. Moreover, the mass contribution of regions I and II to the total mass M_h at the end of region III is $\lesssim 10^{-2}$ in our parameter range as shown in Argüelles et al. (2014b), indicating that only regions III and IV are the relevant ones to be used in the fitting procedure against the data.

At this point it is important to emphasize that the theoretical treatment used here to fit dark matter halos applies for any core size, even for the ones which are close to its critical mass, $M_{cr} \sim 10^9 M_\odot$, as studied in Argüelles et al. (2014b), where a relativistic treatment is mandatory. Even though the regions I-II-III-IV corresponding to the sample considered here can be well explained in terms of non-relativistic physics, the general rela-

[2]For radii $r < r_c$ the configurations corresponds to region I, where $\rho(r) \approx const$ and then from (I.3.2) and (I.3.3), taking into account (I.2.11) and (I.2.12), we can write $\rho_c \propto M_c/r_c^3$ in terms of the chemical potential and particle mass ($\beta_0\theta_0 = \mu_0/mc^2$) as $\rho_c \propto \mu_0^{3/2} m^{5/2}$. This dependence is precisely the one of a fully degenerate non-relativistic Fermi gas in presence of an external gravitational field, which is further coinciding with a polytrope of index $n = 3/2$ (see e.g. Shapiro and Teukolsky (1983)).

tivistic approach has been used for formal correctness, only giving negligible corrections.

Dimensionless halo radius and mass have different scalings, they are proportional not to θ_0^α, but to α^{θ_0}

$$\hat{r}_h = 0.953\beta_0^{1/4}(1.445)^{\theta_0}, \tag{I.3.4}$$

$$\hat{M}_h = 2.454\beta_0^{3/4}(1.445)^{\theta_0}. \tag{I.3.5}$$

Formulas (I.3.4–I.3.5) represent perfect scalings in the region of parameters considered above, which involves also the scaling of the whole rotational curves in regions III and IV; formula (I.3.1) shows a perfect scaling in the flat part of the rotation curve for region IV. Moreover, the Newtonian expression for the dimensionless circular velocity $\hat{v}^2_{circ}(\hat{r}) = \hat{M}/\hat{r}$ is perfectly suitable in the physical region under consideration. The expression for maximal rotation velocity in the halo is thus obtained from (I.3.4) and (I.3.5) and reads

$$\hat{v}_h^2(\hat{r}_h(\beta_0, \theta_0)) = 2.575\beta_0^{1/2}. \tag{I.3.6}$$

In next section we explain the fitting procedure with the use of the halo scaling laws for regions III and IV obtained here.

I.4. Observed rotation curves and fitting procedure

In 2008, a sample of 34 nearby (closer than 15 Mpc) spiral and irregular galaxies (Sb to Im) were observed with The HI Nearby Galaxy Survey (THINGS) (Walter et al., 2008). These observations allowed to obtain the highest quality rotation curves available to date due to the high spatial and velocity resolution of THINGS. Then a sub-sample of these rotation curves, corresponding to 19 rotationally dominated and undisturbed galaxies, were combined with information on the distribution of gas and stars by de Blok et al. (2008) to construct mass models for the dark matter component of the sample. These models finally were used to quantify the dark matter contribution for each galaxy by using the following formula

$$V_{obs}^2 = V_{gas}^2 + \Upsilon_* V_*^2 + V_{DM}^2, \tag{I.4.1}$$

which relates the observed input curves of V_{obs}, V_{gas} and V_*, defined below, with the dark matter rotation curve V_{DM} to be determined from the known input data once the the mass-to-light ratio Υ_* is provided.

The total and gas observed rotation curves V_{obs} and V_{gas}, respectively, were both obtained from the THINGS data: the first was obtained from velocity fields analysis and the second from the neutral hydrogen (HI) distribution maps, as described in de Blok et al. (2008). Instead, each stellar (light) rotation curve V_* is obtained from the corresponding stellar distribution observed in the K band (i.e. at 3.6 μm) by the *Spitzer* Infrared Nearby Galaxy Survey (SINGS), independent of THINGS, and described in de Blok et al. (2008) and references therein. Finally, the mass-to-light ratio Υ_*^K was used to determine the rotation curve associated with the stellar mass distribution from that of the measured light.

At this point it is relevant to further emphasize the underlying hypothesis to which equation (I.4.1) is subject to. This is, each baryonic rotation velocity V_{gas} and V_* was calculated from the correspondent observed baryonic mass density distribution, and was defined as the velocity that each component would induce on a test particle in the galactic plane as if they were isolated of any external influence.

In de Blok et al. (2008) equation (I.4.1) was applied to test the cuspy Navarro-Frenk-White and cored pseudo-ISO dark matter models against data as follows: the (squared) rotation curves of the baryonic components (after appropriate scaling with Υ_*^K) were subtracted from the (squared) observed rotation curve V_{obs}^2 to apply a reduced χ^2 fitting procedure in order to find the best fitting free parameters for each dark matter model. Soon after, the same analysis was extended further to Einasto dark matter profiles by Chemin et al. (2011), concluding that the Einasto model provides the best match to the observed rotation curves when compared with NFW and pseudo-ISO models with empirical fixed values for Υ_*^K for two different stellar initial mass functions (IMFs).

Here we propose a different dark matter halo model, which is neither based on numerical N-body simulations nor on phenomenological model proposals, but relies on the underlying microphysical composition of the dark matter candidate, as explained in former sections.

Thus, analogously to de Blok et al. (2008) and Chemin et al. (2011) we use the HI high resolution observations of galaxies from THINGS survey (Walter et al., 2008). We analyze here the sample of 16 rotationally dominated and undisturbed galaxies presented both in de Blok et al. (2008) and

Chemin et al. (2011), listed below in Table 1.

Regarding the rotation curves data of the baryonic components, we consider the contributions of the gas, the stellar disk and a spherical stellar bulge V_b as given in Chemin et al. (2011). The halo rotation velocity corresponding to the spherical dark matter component is taken from the two parametric scaling, see (I.3.4–I.3.5), which we name from now on as the fermionic dark matter velocity profile $V_f(r)$.

Once each component is provided, we make use of the equation analogous to (I.4.1)

$$V_{obs}^2 = V_{gas}^2 + \Upsilon_* V_*^2 + V_b^2 + V_f^2, \tag{I.4.2}$$

With all the baryonic velocity terms (V_{gas}^2, $\Upsilon_* V_*^2$ and V_b^2) as observational inputs, we fit the HI observed rotation curve V_{obs}^2 by Levenberg–Marquardt nonlinear least-squares algorithm, in complete analogy as done in Chemin et al. (2011).

We did not take into account the contribution of molecular gas because the total gas surface densities are dominated by atomic gas for the majority of the sample, as explained in Chemin et al. (2011) and references therein. Total rotation curve was taken from de Blok et al. (2008). We have not considered models with free mass-to-light ratios, deferring it to a future paper (in preparation). Instead following Chemin et al. (2011) we have adopted the fixed mass-to-light ratios of stellar populations with a bursty star formation history with a Kroupa IMF. We choose this IMF instead of the diet-Salpeter IMF, also considered in Chemin et al. (2011) and de Blok et al. (2008), as it generally provides better agreement with observations for rotation curves (see Fig. 5 of Chemin et al. (2011)), and in some cases the Salpeter IMF leads to rotational velocities due to stellar component only already in pronounced excess over observed total rotational velocity (see, for example, cases of NGC3521 and NGC5055 at Fig. 3 of Chemin et al. (2011)).

Together with the dark matter profile of semidegenerate configurations with particle mass $m = 10$ keV$/c^2$ and varying θ_0 and β_0, and for the sake of comparison, the following profiles were also used for fitting:

- Cored profiles with central density ρ_0 and characteristic radius r_0:
  - pseudo-isothermal sphere profile

$$\rho_{DM}(r) = \rho_0 \frac{r_0^2}{r^2 + r_0^2}, \tag{I.4.3}$$

– Burkert profile

$$\rho_{DM}(r) = \rho_0 \frac{r_0^3}{(r_0 + r)(r_0^2 + r^2)}. \tag{I.4.4}$$

- Cusped profiles with characteristic radius r_{-2} where the density profile has a (logarithmic) slope of -2 (the "isothermal" value) and ρ_{-2} as the local density at that radius. In the case of Einasto profiles a third parameter is needed, the Einasto index n which determines the shape of the profile.

  – Navarro–Frenk–White profile

$$\rho_{DM}(r) = 4\rho_{-2} \frac{r_{-2}}{r} \left(\frac{r_{-2}}{r + r_{-2}} \right)^2, \tag{I.4.5}$$

  – Einasto profile[3]

$$\rho_{DM}(r) = \rho_{-2} \exp\left\{ -2n \left[\left(\frac{r}{r_{-2}} \right)^{1/n} - 1 \right] \right\}. \tag{I.4.6}$$

I.5. Results and discussion

In this section, we compare the fits of rotation curves by the different models considered in the last section. As we have to compare models with different number of parameters, which are not nested into each other, we use Bayesian Information Criterion (BIC) introduced by Schwarz (1978). It provides a penalty to models with larger number of parameters to check what of them is more likely to be correct. Model with minimum BIC value is preferred. For the models with the same number of parameters, BIC is equivalent to χ^2 criterion.

The results of fitting are presented in the Table I.1 and on Fig. I.4. Due to the scaling laws recalled in Sec. I.3 the fits obtained here for particle mass $m = 10$ keV$/c^2$ can be also transferred to another particle mass by changing

[3]The family of Einasto profiles with relatively large indices $n > 4$ are identified with cuspy halos, while low index values $n < 4$ presents a cored-like behaviour (Chemin et al., 2011). The lower the n the more cored-like the halo profile.

Table I.1.: Results of fitting

	Semidegenerate				Burkert			
Galaxy	$\beta, 10^{-8}$	θ_0^*	χ_r^2	BIC	r_0, kpc	$\rho_0,\ 10^{-3}\ M_\odot/\mathrm{pc}^3$	χ_r^2	BIC
NGC2366	0.99 ± 0.02	24.22 ± 0.08	0.10	*27*	2.2 ± 0.2	43 ± 10	0.12	35
NGC2403	7.10 ± 0.06	27.43 ± 0.07	2.7	902	4.08 ± 0.06	83 ± 3	2.3	866
NGC2841	10.8 ± 0.4	32.04 ± 0.17	2.6	*366*	20.6 ± 0.9	5.2 ± 0.5	2.7	370
NGC2903	16.33 ± 0.09	26.88 ± 0.06	0.66	*238*	2.89 ± 0.06	388 ± 18	1.1	283
NGC2976	9 ± 3	28.8 ± 0.4	0.44	*93*	20 ± 20	40 ± 150	0.49	97
NGC3031	9.7 ± 0.3	26.6 ± 0.2	3.9	470	2.63 ± 0.10	270 ± 20	3.9	468
NGC3198	7.44 ± 0.07	28.66 ± 0.08	1.06	254	6.32 ± 0.18	36 ± 2	0.99	*248*
IC2574	2.00 ± 0.06	27.96 ± 0.09	0.28	167	8.0 ± 0.6	7.2 ± 1.2	0.10	67
NGC3521	8.9 ± 0.7	28.3 ± 0.4	4.1	*437*	5.4 ± 0.4	60 ± 8	4.2	437
NGC3621	7.35 ± 0.11	28.70 ± 0.08	3.0	496	6.48 ± 0.12	34.3 ± 1.3	2.5	475
NGC4736	3.01 ± 0.13	22.4 ± 0.5	2.1	302	0.84 ± 0.07	870 ± 160	1.9	296
DDO154	0.791 ± 0.017	24.37 ± 0.10	0.84	172	2.32 ± 0.10	29 ± 3	0.62	153
NGC5055	8.35 ± 0.13	30.99 ± 0.12	1.9	708	14.3 ± 0.5	8.0 ± 0.5	2.0	719
NGC6946	8.9 ± 0.3	26.9 ± 0.2	16.4	993	3.48 ± 0.08	146 ± 7	15.7	985
NGC7331	11.7 ± 0.2	30.10 ± 0.12	0.45	226	9.7 ± 0.7	25 ± 4	0.41	214
NGC7793	4.44 ± 0.16	25.85 ± 0.13	3.7	287	2.60 ± 0.07	130 ± 8	3.5	284

	Navarro–Frenk–White				Pseudo-ISO			
Galaxy	r_{-2}, kpc	$\rho_{-2},\ 10^{-3}\ M_\odot/\mathrm{pc}^3$	χ_r^2	BIC	r_0, kpc	$\rho_0,\ 10^{-3}\ M_\odot/\mathrm{pc}^3$	χ_r^2	BIC
NGC2366	200 ± 1100	0.02 ± 0.24	1.1	117	1.29 ± 0.17	40 ± 11	0.15	42
NGC2403	11.2 ± 0.3	2.86 ± 0.17	0.7	575	1.56 ± 0.04	144 ± 8	1.2	703
NGC2841	150 ± 30	0.05 ± 0.02	3.8	402	12.5 ± 0.7	4.6 ± 0.6	2.8	374
NGC2903	4.75 ± 0.16	34 ± 2	1.8	334	0.53 ± 0.05	2300 ± 500	3.9	406
NGC2976	900 ± 40000	0.009 ± 1	2.1	158	9 ± 18	30 ± 180	0.49	98
NGC3031	4.9 ± 0.4	20 ± 3	4.0	472	0.82 ± 0.1	690 ± 170	4.3	480
NGC3198	16.5 ± 0.9	1.37 ± 0.15	2.0	306	2.7 ± 0.14	51 ± 5	1.2	266
IC2574	500 ± 1300	0.007 ± 0.045	1.5	331	5.1 ± 0.4	6.3 ± 1.1	0.11	70
NGC3521	18 ± 3	1.5 ± 0.4	5.1	457	2.4 ± 0.3	78 ± 19	4.2	439
NGC3621	123 ± 17	0.08 ± 0.02	5.9	579	2.81 ± 0.09	49 ± 3	1.1	377
NGC4736	1.25 ± 0.16	90 ± 20	1.9	296	0 ± 0.07	$0 \pm \mathrm{ND}$	2.3	311
DDO154	14 ± 2	0.35 ± 0.11	1.03	184	1.22 ± 0.07	32 ± 4	0.48	138
NGC5055	48 ± 4	0.20 ± 0.03	3.0	795	7.8 ± 0.4	7.7 ± 0.8	2.5	759
NGC6946	9.3 ± 0.4	5.3 ± 0.5	10.4	915	0.66 ± 0.03	870 ± 70	11.0	923
NGC7331	3000 ± 40000	0.004 ± 0.087	0.48	233	$5. \pm 0.5$	28 ± 6	0.32	190
NGC7793	17.0 ± 1.9	1.4 ± 0.3	4.1	294	1.47 ± 0.05	126 ± 10	4.0	293

	Einasto				
Galaxy	r_{-2}, kpc	$\rho_{-2},\ 10^{-3}\ M_\odot/\mathrm{pc}^3$	n	χ_r^2	BIC
NGC2366	2.9 ± 0.4	6.86 ± 0.04	0.9 ± 0.3	0.13	39
NGC2403	13.6 ± 1.3	1.98 ± 0.05	4.9 ± 0.4	0.6	*570*
NGC2841	24.5 ± 0.6	1.091 ± 0.006	0.54 ± 0.08	2.5	367
NGC2903	5.33 ± 0.15	28.983 ± 0.005	2.9 ± 0.2	1.6	326
NGC2976	$70000 \pm \mathrm{ND}$	$0.019 \pm \mathrm{ND}$	4.0 ± 70	0.49	100
NGC3031	4.81 ± 0.09	30.159 ± 0.002	0.56 ± 0.07	3.2	*452*
NGC3198	11.5 ± 0.4	3.029 ± 0.006	1.80 ± 0.17	1.1	257
IC2574	8.6 ± 1.2	1.57 ± 0.05	0.7 ± 0.2	0.09	*62*
NGC3521	9.3 ± 0.5	6.27 ± 0.02	1.2 ± 0.3	4.3	443
NGC3621	37 ± 10	0.3 ± 0.4	6.1 ± 0.9	0.57	*296*
NGC4736	1.73 ± 0.16	56.78 ± 0.03	2.0 ± 0.5	1.8	*295*
DDO154	4.9 ± 0.7	1.95 ± 0.03	2.0 ± 0.3	0.31	*114*
NGC5055	21.4 ± 0.4	1.464 ± 0.002	0.39 ± 0.04	1.2	*626*
NGC6946	50 ± 40	0.2 ± 4	15 ± 4	8.5	*883*
NGC7331	1000 ± 8000	0.002 ± 900	11 ± 21	0.23	*158*
NGC7793	3.65 ± 0.14	19.217 ± 0.007	0.97 ± 0.09	3.1	*279*

ND means not constrained model parameters the fitted central degeneracy parameter from θ_0^* (see Table I.1) according to the relation

$$\theta_0(m) = \theta_0^* + 12.52 \log \frac{m}{10\,\mathrm{keV}/c^2}, \tag{I.5.1}$$

provided that $\theta_0(m)$ is larger than 20 and the influence of the degenerate core on rotational velocity is negligible in the observed radial range. From the values of θ_0^* obtained for the fitting of the sample listed in Table I.1, and the lower value of $\theta_0(m)$ from which the scaling laws (I.3.2–I.3.5) are valid, it is possible to obtain from (I.5.1) a preliminary lower limit for the particle mass $m \gtrsim$ few keV$/c^2$. Nonetheless this limit should not be considered as an absolute lower limit for the fermion mass of the model because the bound $\theta_0(m) \geqslant 20$ in the formula above is a numerical limit, and no underlying physics has been specified here for it. The formal way of providing an absolute lower limit for the particle mass of our model when applied to typical spiral galaxies has been found in Argüelles et al. (2014b), and yields roughly an order of magnitude less than the one inferred here.

From the 16 galaxies analyzed, our model has minimum BIC value in 5 cases (NGC2366, NGC2841, NGC2903, NGC2976, NGC3521), Einasto model in 10 cases (NGC2403, NGC3031, IC2574, NGC3621, NGC4736, DDO154, NGC5055, NGC6946, NGC7331, NGC7793), and in the case of NGC3198 Burkert model is the best one, marginally better than ours, which in turn is marginally better than Einasto. Besides this general comparison in which apparently Einasto model is preferred against our model, there is a more relevant comparison which must be made considering that the semi-degenerate model provides cored halos only. For this, we compare the Einasto model against the semi-degenerate one for the sub-set of galaxies which are cored-like (i.e. with Einasto index $n \lesssim 4$), and then the same comparison is made for the sub-set of galaxies which are cuspy-like (i.e. with Einasto index $n > 4$). The important outcome of this new BIC comparison is that our model is *equivalently* as good as Einasto for the cored-like sub-sample, that is connected to the fact that Einasto profile with $n \sim 1$ provides rotational curves that in a wide range of radii is quite close to the one of ours at transition from region III to region IV. For cored-like galaxies in 6 cases our model has lower BIC number than Einasto model (NGC2366, NGC2841, NGC2903, NGC2976, NGC3198, NGC3521), and inversely in other 6 cases Einasto is better (NGC3031, IC2574, NGC4736, DDO154, NGC5055, NGC7793). Instead, for the cuspy-like sub-sample (NGC2403, NGC3621, NGC6946, NGC7331), in *all* the cases Einasto model has lower BIC numbers as logically one may expect due to the cored nature of the semi-degenerate halos.

If we take only the models with significant fits, i.e. with reduced χ^2 less than one at least for one fit, then our model is preferred in 3 cases (NGC2366, NGC2903, NGC2976), Einasto one in 5 cases (NGC2403, IC2574, NGC3621, DDO154, NGC7331), and Burkert fit for NGC3198 is also significant. It is remarkable that neither Navarro–Frenk–White model, nor pseudo-ISO model is preferred against others in the THINGS sample.

If we take into account only two-parametric models, then we have the same 5 aforementioned cases for our model to be the best plus the case of NGC5055, NFW model is preferred in 2 cases (NGC2403, NGC6946), pseudo-ISO one in 3 cases (NGC3621, DDO154, NGC7331), and Burkert model in 5 cases (NGC3031, NGC3198, IC2574, NGC4736, NGC7331). Taking only significant fits, we get the best performance of our model in 3 cases (NGC2366, NGC2903, NGC2976), NFW in 1 case of NGC2403, pseudo-ISO in 2 cases (DDO154, NGC7331), and Burkert in 2 cases (NGC3198, IC2574). From this we can conclude that our model is the best two-parametric model of the set considered.

It is interesting to make pair comparison of our model with Burkert profile: it is preferred statistically in 6 cases (NGC2366, NGC2841, NGC2903, NGC2976, NGC3521, NGC5055) and is disfavored in 10 cases. However, in all these cases besides IC2574 the preference is only marginal.

It should be mentioned that the velocity profile of the semidegenerate configuration used for fitting is exact only in the case of Dark Matter domination and thermal equilibrium at all radii, that can be not the case of real galaxies. However, it is especially interesting that even such a simplified model provides good correspondence to empirical rotational curves.

I.6. Conclusion

It follows from the results of fitting that the semidegenerate fermionic distributions can fit dark matter in the THINGS sample of galaxies at least as well as other profiles considered in the literature, with the important "revenue" that this profile is theoretically motivated, and is not phenomenological as most of the others. The cases when Einasto profile fits rotational curve much better than semidegenerate profile show the general cuspy behaviour of dark matter distribution, possibly representing a special class of galaxies that are still not completely relaxed.

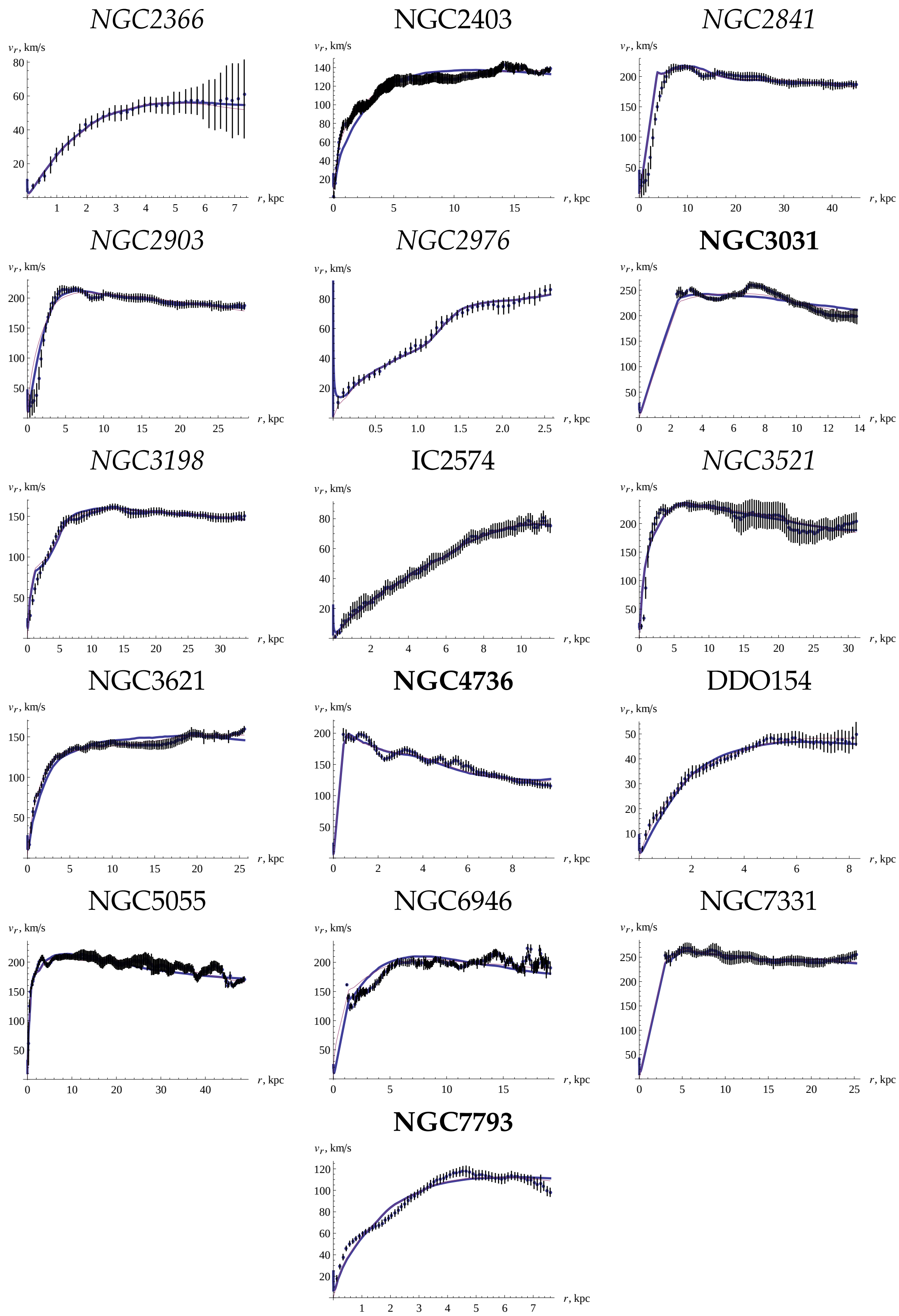

Figure I.4.: Rotational curves $v_r(r)$ for some galaxies from THINGS survey together with fits. Blue thick curves show best fits by dark matter distributions of semidegenerate configurations, while magenta thin curves show Einasto profile best fits. Galaxy names where semidegenerate profile fits rotation curves better than Einasto profile are emphasized, and names where profiles are comparable in fit quality are bolded. See digital version for colored plots.

While Einasto profile is a pure phenomenological one based on best fit of the observational and numerical simulation data, our profile is derived from the first principles and based on the General Relativistic treatment of self-gravitating neutral fermions. There is the distinct possibility that our treatment gives the conceptual physical motivation for the existence of the cored Einasto profile directly from the structure of the microphysical constituents of dark matter.

Bibliography

ACHTERBERG, A. AND WIERSMA, J.
≪The Weibel instability in relativistic plasmas. I. Linear theory≫.
A&A, **475**, pp. 1–18 (2007).

ACKERMANN, M., AJELLO, M., ASANO, K., AXELSSON, M., BALDINI, L., BALLET, J., BARBIELLINI, G., BASTIERI, D., BECHTOL, K., BELLAZZINI, R. ET AL.
≪The First Fermi-LAT Gamma-Ray Burst Catalog≫.
ApJS, **209**, 11 (2013).

AHARONIAN, F., AKHPERJANIAN, A.G., BARRES DE ALMEIDA, U., BAZER-BACHI, A.R., BEHERA, B., BEILICKE, M., BENBOW, W. AND BERNLÖHR, K.E.A.
≪New constraints on the mid-IR EBL from the HESS discovery of VHE γ-rays from 1ES 0229+200≫.
A&A, **475**, pp. L9–L13 (2007).

AHARONIAN, F.A.
Very High Energy Cosmic Gamma Radiation (World Scientific, 2003).

AHARONIAN, F.A., ATOIAN, A.M. AND NAGAPETIAN, A.M.
≪Photoproduction of electron-positron pairs in compact X-ray sources≫.
Astrofizika, **19**, pp. 323–334 (1983).

AKSENOV, A.G., RUFFINI, R. AND VERESHCHAGIN, G.V.
≪Thermalization of Nonequilibrium Electron-Positron-Photon Plasmas≫.
Phys. Rev. Lett., **99(12)**, pp. 125003–+ (2007).

AKSENOV, A.G., RUFFINI, R. AND VERESHCHAGIN, G.V.
≪Thermalization of the mildly relativistic plasma≫.
Phys. Rev. D, **79(4)**, p. 043008 (2009).

AKSENOV, A.G., RUFFINI, R. AND VERESHCHAGIN, G.V.
≪Pair plasma relaxation time scales≫.
Phys. Rev. E, **81**, p. 046401 (2010).

ALOISIO, R., BONCIOLI, D., GRILLO, A.F., PETRERA, S. AND SALAMIDA, F.
≪SimProp: a simulation code for ultra high energy cosmic ray propagation≫.
J. Cosmology Astropart. Phys., **10**, 007 (2012).

ANDRÉASSON, H.
≪The Einstein-Vlasov System/Kinetic Theory≫.
Living Reviews in Relativity, **14**, p. 4 (2011).

ARBOLINO, M.V. AND RUFFINI, R.
≪The ratio between the mass of the halo and visible matter in spiral galaxies and limits on the neutrino mass≫.
A&A, **192**, pp. 107–116 (1988).

ARGÜELLES, C., SIUTSOU, I., RUFFINI, R., RUEDA, J. AND MACHADO, B.
≪On the core-halo constituents of a semi-degenerate gas of massive fermions≫.
In *Probes of Dark Matter on Galaxy Scales*, p. 30204 (2013).

ARGÜELLES, C.R., MAVROMATOS, N., RUEDA, J.A. AND RUFFINI, R.
to be submitted (2014a).

ARGÜELLES, C.R., RUEDA, J.A. AND RUFFINI, R.
to be submitted (2015).

ARGÜELLES, C.R. AND RUFFINI, R.
≪A Regular and Relativistic Einstein Cluster within the S2 Orbit Centered in SgrA*≫.
Proceedings of The Thirteenth Marcel Grossmann Meeting, Volume B, p. 1734 (2014a).

ARGÜELLES, C.R. AND RUFFINI, R.
≪Are the most super-massive dark compact objects harbored at the center of dark matter halos?≫
International Journal of Modern Physics D, **23**, 1442020 (2014b).

ARGÜELLES, C., RUFFINI, R., SIUTSOU, I. AND FRAGA, B.M.
≪On the distribution of dark matter in galaxies: Quantum treatments≫.
Journal of the Korean Physical Society, **65(6)**, pp. 801–804 (2014b).

ARTSIMOVICH, L.A. AND SAGDEEV, R.Z.
≪Plasma physics for physicists≫.
Moscow Atomizdat (1979).

AVETISIAN, G.K., AVETISIAN, A.K. AND SEDRAKIAN, K.V.
≪The production and annihilation of electron-positron pairs in a plasma≫.
Zhurnal Eksperimentalnoi i Teoreticheskoi Fiziki, **94**, pp. 21–25, (1988).

BADJIN, D.A., BLINNIKOV, S.I. AND POSTNOV, K.A.
≪Thermal emission in gamma-ray burst afterglows≫.
Monthly Notices of the Royal Astronomical Society, **432(3)**, pp. 2454–2462 (2013).

BATEBI, S., TIZCHANG, S., RUFFINI, R., VERESHCHAGIN, G. AND XUE, S.S.
≪Euler-heisenberg interaction and opacity of the universe at high energy≫.
in preparation (2015).

BEGUE, D.
≪PhD thesis≫.
PhD thesis, University of Rome "Sapienza" (2014).

BELIAEV, S.T. AND BUDKER, G.I.
≪The Relativistic Kinetic Equation≫.
Soviet Physics Doklady, **1**, p. 218 (1956).

BENEDETTI, A., HAN, W.B., RUFFINI, R. AND VERESHCHAGIN, G.V.
≪On the frequency of oscillations in the pair plasma generated by a strong electric field≫.
Physics Letters B, **698**, pp. 75–79 (2011).

BENEDETTI, A., RUFFINI, R. AND VERESHCHAGIN, G.V.
≪Phase space evolution of pairs created in strong electric fields≫.
Physics Letters A, **377**, pp. 206–215 (2013).

BERESTETSKII, V.B., LIFSHITZ, E.M. AND PITAEVSKII, V.B.
Quantum Electrodynamics (Elsevier, 1982).

BEREZINSKII, V.S. AND GRIGOR'EVA, S.I.
≪A bump in the ultra-high energy cosmic ray spectrum≫.
A&A, **199**, pp. 1–12 (1988).

BETHE, H. AND HEITLER, W.
≪On the Stopping of Fast Particles and on the Creation of Positive Electrons≫.
Royal Society of London Proceedings Series A, **146**, pp. 83–112 (1934).

BHATTACHARJEE, P. AND SIGL, U.
≪Origin and propagation of extremely high energy cosmic rays≫.
Phys. Rep., **327**, pp. 109–247 (2000).

BILIC, N., MUNYANEZA, F., TUPPER, G.B. AND VIOLLIER, R.D.
≪The dynamics of stars near Sgr A* and dark matter at the center and in the halo of the galaxy≫.
Progress in Particle and Nuclear Physics, **48**, pp. 291–300 (2002).

BILIC, N. AND VIOLLIER, R.D.
≪General-Relativitstic Thomas-Fermi Model≫.
General Relativity and Gravitation, **31**, p. 1105 (1999).

BINNEY, J. AND TREMAINE, S.
Galactic dynamics (Princeton, NJ, Princeton University Press, 1987).

BINNEY, J. AND TREMAINE, S.
Galactic Dynamics: Second Edition (Princeton University Press, 2008).

BISNOVATYI-KOGAN, G.S., MERAFINA, M., RUFFINI, R. AND VESPERINI, E.
≪Stability of Dense Stellar Clusters against Relativistic Collapse. II. Maxwellian Distribution Functions with Different Cutoff Parameters≫.
ApJ, **500**, p. 217 (1998).

BISNOVATYI-KOGAN, G.S. AND ZEL'DOVICH, Y.B.
≪Growth of Perturbations in an Expanding Universe of Free Particles.≫
Soviet Ast., **14**, p. 758 (1971).

BISNOVATYI-KOGAN, G.S., ZEL'DOVICH, Y.B. AND SYUNYAEV, R.A.
≪Physical Processes in a Low-Density Relativistic Plasma.≫
Soviet Ast., **15**, pp. 17–+ (1971).

BISNOVATYJ-KOGAN, G.S., MERAFINA, M., RUFFINI, R. AND VESPERINI, E.
≪Stability of dense stellar clusters against relativistic collapse≫.
ApJ, **414**, pp. 187–199 (1993).

BLASCHKE, D.B., PROZORKEVICH, A.V., ROBERTS, C.D., SCHMIDT, S.M. AND SMOLYANSKY, S.A.
≪Pair Production and Optical Lasers≫.
Phys. Rev. Lett., **96(14)**, pp. 140402–+ (2006).

BLUMENTHAL, G.R.
≪Energy Loss of High-Energy Cosmic Rays in Pair-Producing Collisions with Ambient Photons≫.
Phys. Rev. D, **1**, pp. 1596–1602 (1970).

BOGOLIUBOV, N.N.
Problems of Dynamic Theory in Statistical Physics (Gostechizdat, 1946). (in Russian).

BOGOLIUBOV, N.N.
Problems of Dynamic Theory in Statistical Physics (North Holland, Amsterdam, 1962).

BÖHMER, C.G. AND HARKO, T.
≪Can dark matter be a Bose Einstein condensate?≫
J. Cosmology Astropart. Phys., **6**, 025 (2007a).

BÖHMER, C.G. AND HARKO, T.
≪On Einstein clusters as galactic dark matter haloes≫.
MNRAS, **379**, pp. 393–398 (2007b).

BOLTZMANN, L.
Lectures on Gas Theory (Dover Publications, 2011).

BOND, J.R. AND SZALAY, A.S.
≪The collisionless damping of density fluctuations in an expanding universe≫.
ApJ, **274**, pp. 443–468 (1983).

BONOMETTO, S.
≪On the transparency of extragalactic space to very-high-energy photons≫.
Lettere Al Nuovo Cimento, **1(16)**, pp. 677–680 (1971).

ISSN 0375-930X.

BOYANOVSKY, D., DE VEGA, H.J. AND SANCHEZ, N.G.
≪Constraints on dark matter particles from theory, galaxy observations, and N-body simulations≫.
Phys. Rev. D, **77(4)**, 043518 (2008).

BOYARSKY, A., RUCHAYSKIY, O., IAKUBOVSKYI, D., MACCIO', A.V. AND MALYSHEV, D.
≪New evidence for dark matter≫.
ArXiv e-prints (2009a).

BOYARSKY, A., RUCHAYSKIY, O. AND SHAPOSHNIKOV, M.
≪The Role of Sterile Neutrinos in Cosmology and Astrophysics≫.
Annual Review of Nuclear and Particle Science, **59**, pp. 191–214 (2009b).

BREIT, G. AND WHEELER, J.A.
≪Collision of Two Light Quanta≫.
Physical Review, **46**, pp. 1087–1091 (1934).

BRET, A., GREMILLET, L., BÉNISTI, D. AND LEFEBVRE, E.
≪Exact Relativistic Kinetic Theory of an Electron-Beam Plasma System: Hierarchy of the Competing Modes in the System-Parameter Space≫.
Physical Review Letters, **100(20)**, 205008 (2008).

BROWN, R.W., MIKAELIAN, K.O. AND GOULD, R.J.
≪Absorption of High-Energy Cosmic Photons through Double-Pair Production in Photon-Photon Collisions≫.
Astrophys. Lett., **14**, p. 203 (1973).

BURKERT, A.
≪The Structure of Dark Matter Halos in Dwarf Galaxies≫.
ApJ, **447**, p. L25 (1995).

BUTI, B.
≪Plasma Oscillations and Landau Damping in a Relativistic Gas≫.
Physics of Fluids, **5**, pp. 1–5 (1962).

CALZETTI, D., GIAVALISCO, M. AND RUFFINI, R.
≪The normalization of the correlation functions for extragalactic structures≫.

A&A, **198**, pp. 1–2 (1988).

CALZETTI, D., GIAVALISCO, M., RUFFINI, R., EINASTO, J. AND SAAR, E.
≪The correlation function of galaxies in the direction of the Coma cluster≫.
Ap&SS, **137**, pp. 101–106 (1987).

CERCIGNANI, C. AND KREMER, G.M.
The relativistic Boltzmann equation: theory and applications (Boston: Birkhäuser, 2002).

CHAVANIS, P.H.
≪Phase transitions in self-gravitating systems: Self-gravitating fermions and hard-sphere models≫.
Phys. Rev. E, **65(5)**, 056123 (2002a).

CHAVANIS, P.H.
≪Statistical mechanics of violent relaxation in stellar systems≫.
ArXiv Astrophysics e-prints (2002b).

CHAVANIS, P.H.
≪On the lifetime of metastable states in self-gravitating systems≫.
A&A, **432**, pp. 117–138 (2005).

CHAVANIS, P.H.
≪Quasi-stationary states and incomplete violent relaxation in systems with long-range interactions≫.
Physica A Statistical Mechanics and its Applications, **365**, pp. 102–107 (2006).

CHAVANIS, P.H. AND SOMMERIA, J.
≪Degenerate equilibrium states of collisionless stellar systems≫.
MNRAS, **296**, pp. 569–578 (1998).

CHEMIN, L., DE BLOK, W.J.G. AND MAMON, G.A.
≪Improved Modeling of the Mass Distribution of Disk Galaxies by the Einasto Halo Model≫.
AJ, **142**, 109 (2011).

CHEN, F.F.
Introduction to Plasma Physics and Controlled Fusion Volume 1: Plasma Physics (Plenum press, 1984).

CHERNIKOV, N.
≪Derivation of the equations of relativistic hydrodynamics from the relativistic transport equation≫.
Physics Letters, **5**, pp. 115–117 (1963a).

CHERNIKOV, N.A.
≪Kinetic Equation for a Relativistic Gas in an Arbitrary Gravitational Field≫.
Soviet Physics Doklady, **7**, p. 397 (1962).

CHERNIKOV, N.
≪The relativistic gas in the gravitational field≫.
Acta Physica Polonica, **23**, pp. 629–645 (1963b).

CHERNIKOV, N.
≪Equilibrium distribution of the relativistic gas≫.
Acta Physica Polonica, **26**, pp. 1069–1091 (1964a).

CHERNIKOV, N.
≪Microscopic foundation of relativistic hydrodymanics≫.
Acta Physica Polonica, **27**, pp. 465–489 (1964b).

CHLUBA, J.
Spectral Distortions of the Cosmic Microwave Background.
Ph.D. thesis, Ludwig-Maximilians-Universität München (2005).

CHODOROWSKI, M.J., ZDZIARSKI, A.A. AND SIKORA, M.
≪Reaction rate and energy-loss rate for photopair production by relativistic nuclei≫.
ApJ, **400**, pp. 181–185 (1992).

CHURAZOV, E., SUNYAEV, R., SAZONOV, S., REVNIVTSEV, M. AND VARSHALOVICH, D.
≪Positron annihilation spectrum from the Galactic Centre region observed by SPI/INTEGRAL≫.
MNRAS, **357**, pp. 1377–1386 (2005).

COCCO, V. AND RUFFINI, R.
≪On metastable Einstein's clusters.≫
Nuovo Cimento B Serie, **112**, pp. 271–287 (1997).

COLOMBO, L.P.L. AND BONOMETTO, S.A.
≪Cosmic opacity to CMB photons and polarization measurements≫.
New A, **8**, pp. 313–323 (2003).

COMER, G.L. AND KATZ, J.
≪Thick Einstein shells and their mechanical stability≫.
Classical and Quantum Gravity, **10**, pp. 1751–1765 (1993).

COPPI, P.S. AND AHARONIAN, F.A.
≪Constraints on the Very High Energy Emissivity of the Universe from the Diffuse GeV Gamma-Ray Background≫.
ApJ, **487**, pp. L9+ (1997).

COPPI, P.S. AND AHARONIAN, F.A.
≪Understanding the spectra of TeV blazars: implications for the cosmic infrared background≫.
Astroparticle Physics, **11**, pp. 35–39 (1999).

COPPI, P.S. AND BLANDFORD, R.D.
≪Reaction rates and energy distributions for elementary processes in relativistic pair plasmas≫.
MNRAS, **245**, pp. 453–507 (1990).

COWSIK, R. AND MCCLELLAND, J.
≪An Upper Limit on the Neutrino Rest Mass≫.
Physical Review Letters, **29**, pp. 669–670 (1972).

DE BLOK, W.J.G.
≪The Core-Cusp Problem≫.
Advances in Astronomy, **2010**, 789293 (2010).

DE BLOK, W.J.G., MCGAUGH, S.S. AND RUBIN, V.C.
≪High-Resolution Rotation Curves of Low Surface Brightness Galaxies. II. Mass Models≫.
AJ, **122**, pp. 2396–2427 (2001).

DE BLOK, W.J.G., WALTER, F., BRINKS, E., TRACHTERNACH, C., OH, S.H. AND KENNICUTT, JR., R.C.
≪High-Resolution Rotation Curves and Galaxy Mass Models from THINGS≫.
AJ, **136**, 2648 (2008).

DE JAGHER, P.C. AND SLUIJTER, F.W.
≪A covariant hierarchy of kinetic equations for classical particles and fields≫.
Contributions to Plasma Physics, **28**, pp. 169–183 (1988).

DE VEGA, H.J., SALUCCI, P. AND SANCHEZ, N.G.
≪Observational rotation curves and density profiles versus the Thomas-Fermi galaxy structure theory≫.
MNRAS, **442**, pp. 2717–2727 (2014).

DEBBASCH, F., RIVET, J.P. AND VAN LEEUWEN, W.A.
≪Invariance of the relativistic one-particle distribution function≫.
Physica A Statistical Mechanics and its Applications, **301**, pp. 181–195 (2001).

DEBBASCH, F. AND VAN LEEUWEN, W.A.
≪General relativistic Boltzmann equation, I: Covariant treatment≫.
Physica A Statistical Mechanics and its Applications, **388**, pp. 1079–1104 (2009a).

DEBBASCH, F. AND VAN LEEUWEN, W.A.
≪General relativistic Boltzmann equation, II: Manifestly covariant treatment≫.
Physica A Statistical Mechanics and its Applications, **388**, pp. 1818–1834 (2009b).

DEMIDOV, S.V. AND KALASHEV, O.E.
≪Double pair production by ultra-high-energy cosmic ray photons≫.
Journal of Experimental and Theoretical Physics, **108**, pp. 764–769 (2009).

DERMER, C.D. AND ATOYAN, A.
≪Ultra-high energy cosmic rays, cascade gamma rays, and high-energy neutrinos from gamma-ray bursts≫.
New Journal of Physics, **8**, p. 122 (2006).

DESTRI, C., DE VEGA, H.J. AND SANCHEZ, N.G.
≪Fermionic warm dark matter produces galaxy cores in the observed scales because of quantum mechanics≫.
New A, **22**, pp. 39–50 (2013).

DIECKMANN, M.E.

≪Particle Simulation of an Ultrarelativistic Two-Stream Instability≫.
Physical Review Letters, **94(15)**, 155001 (2005).

DJORGOVSKI, S. AND DAVIS, M.
≪Fundamental properties of elliptical galaxies≫.
ApJ, **313**, pp. 59–68 (1987).

DOELEMAN, S.S., WEINTROUB, J., ROGERS, A.E.E., PLAMBECK, R., FREUND, R., TILANUS, R.P.J., FRIBERG, P., ZIURYS, L.M., MORAN, J.M., COREY, B. ET AL.
≪Event-horizon-scale structure in the supermassive black hole candidate at the Galactic Centre≫.
Nature, **455**, pp. 78–80 (2008).

DOLAG, K., GRASSO, D., SPRINGEL, V. AND TKACHEV, I.
≪Constrained simulations of the magnetic field in the local Universe and the propagation of ultrahigh energy cosmic rays≫.
J. Cosmology Astropart. Phys., **1**, 009 (2005).

DOLGOV, A.D.
≪Neutrinos in cosmology≫.
Phys. Rep., **370**, pp. 333–535 (2002).

D'OLIVO, J.C., NELLEN, L., SAHU, S. AND VAN ELEWYCK, V.
≪UHE neutrino damping in a thermal gas of relic neutrinos≫.
Astroparticle Physics, **25**, pp. 47–56 (2006).

DONATO, F., GENTILE, G., SALUCCI, P., FRIGERIO MARTINS, C., WILKINSON, M.I., GILMORE, G., GREBEL, E.K., KOCH, A. AND WYSE, R.
≪A constant dark matter halo surface density in galaxies≫.
MNRAS, **397**, pp. 1169–1176 (2009).

ECKART, C.
≪The Thermodynamics of Irreversible Processes. III. Relativistic Theory of the Simple Fluid≫.
Physical Review, **58**, pp. 919–924 (1940).

EHLERS, J.
≪Survey of general relativity theory≫.
In *Relativity, Astrophysics and Cosmology*, pp. 1–125 (1973).

EINASTO, J.
≪On the Construction of a Composite Model for the Galaxy and on the Determination of the System of Galactic Parameters≫.
Trudy Astrofizicheskogo Instituta Alma-Ata, **5**, pp. 87–100 (1965).

EINASTO, J.
≪Dark Matter≫.
Brazilian Journal of Physics, **43**, pp. 369–374 (2013).

EINASTO, J. AND HAUD, U.
≪Galactic models with massive corona. I - Method. II - Galaxy≫.
A&A, **223**, pp. 89–106 (1989).

EINSTEIN, A.
≪On a Stationary System with Spherical Symmetry Consisting of Many Gravitating Masses≫.
Annals of Mathematics, **40**, p. 922 (1939).

EL-TAIBANY, W.F. AND MAMUN, A.A.
≪Nonlinear electromagnetic perturbations in a degenerate ultrarelativistic electron-positron plasma≫.
Phys. Rev. E, **85(2)**, 026406 (2012).

FAZIO, G.G. AND STECKER, F.W.
≪Predicted High Energy Break in the Isotropic Gamma Ray Spectrum: a Test of Cosmological Origin≫.
Nature, **226**, pp. 135–+ (1970).

FERRARESE, L.
≪Beyond the Bulge: A Fundamental Relation between Supermassive Black Holes and Dark Matter Halos≫.
ApJ, **578**, pp. 90–97 (2002a).

FERRARESE, L.
≪Black Hole Demographics≫.
In C.H. Lee and H.Y. Chang (eds.), *Current High-Energy Emission Around Black Holes*, pp. 3–24 (2002b).

FINKE, J.D. AND RAZZAQUE, S.
≪Constraints on the Extragalactic Background Light from very High Energy Gamma-Ray Observations of Blazars≫.

ApJ, **698**, pp. 1761–1766 (2009).

FIUZA, F., FONSECA, R.A., TONGE, J., MORI, W.B. AND SILVA, L.O.
≪Weibel-Instability-Mediated Collisionless Shocks in the Laboratory with Ultraintense Lasers≫.
Physical Review Letters, **108(23)**, 235004 (2012).

FLORIDES, P.S.
≪A New Interior Schwarzschild Solution≫.
Royal Society of London Proceedings Series A, **337**, pp. 529–535 (1974).

FREDERIKSEN, J.T., HEDEDAL, C.B., HAUGBØLLE, T. AND NORDLUND, Å.
≪Magnetic Field Generation in Collisionless Shocks: Pattern Growth and Transport≫.
ApJ, **608**, pp. L13–L16 (2004).

FRIIS, M. AND WATSON, D.
≪Thermal Emission in the Early X-Ray Afterglows of Gamma-Ray Bursts: Following the Prompt Phase to Late Times≫.
The Astrophysical Journal, **771(1)**, p. 15 (2013).

FRYER, C.L., RUEDA, J.A. AND RUFFINI, R.
≪Hypercritical Accretion, Induced Gravitational Collapse, and Binary-Driven Hypernovae≫.
Accepted for publication in ApJL, p. 1473 (2014).

GAO, J.G., MERAFINA, M. AND RUFFINI, R.
≪The semidegenerate configurations of a selfgravitating system of fermions≫.
A&A, **235**, pp. 1–7 (1990).

GAO, J.G. AND RUFFINI, R.
≪Relativistic limits on the masses of self-gravitating systems of degenerate neutrinos.≫
Physics Letters B, **97**, pp. 388–390 (1980).

GAO, L., NAVARRO, J.F., FRENK, C.S., JENKINS, A., SPRINGEL, V. AND WHITE, S.D.M.
≪The Phoenix Project: the dark side of rich Galaxy clusters≫.
MNRAS, **425**, pp. 2169–2186 (2012).

GENTILE, G., FAMAEY, B., ZHAO, H. AND SALUCCI, P.
≪Universality of galactic surface densities within one dark halo scale-length≫.
Nature, **461**, pp. 627–628 (2009).

GERALICO, A., POMPI, F. AND RUFFINI, R.
≪On Einstein Clusters≫.
International Journal of Modern Physics Conference Series, **12**, pp. 146–173 (2012).

GHEZ, A.M., SALIM, S., WEINBERG, N.N., LU, J.R., DO, T., DUNN, J.K., MATTHEWS, K., MORRIS, M.R., YELDA, S., BECKLIN, E.E. ET AL.
≪Measuring Distance and Properties of the Milky Way's Central Supermassive Black Hole with Stellar Orbits≫.
ApJ, **689**, pp. 1044–1062 (2008).

GHISELLINI, G., GHIRLANDA, G. AND TAVECCHIO, F.
≪Did we observe the supernova shock breakout in GRB 060218?≫
Monthly Notices of the Royal Astronomical Society: Letters, **382(1)**, pp. L77–L81 (2007).

GIAVALISCO, M.
The gravitational formation of cosmological structures.
Ph.D. thesis, University of Rome "La Sapienza" (1992).

GILBERT, C.
≪Stellar Clusters, Nebulae, Milky Way: The stability of a spherically symmetric cluster of stars describing circular orbits≫.
MNRAS, **114**, p. 628 (1954).

GILLESSEN, S., EISENHAUER, F., FRITZ, T.K., BARTKO, H., DODDS-EDEN, K., PFUHL, O., OTT, T. AND GENZEL, R.
≪The Orbit of the Star S2 Around SGR A* from Very Large Telescope and Keck Data≫.
ApJ, **707**, pp. L114–L117 (2009).

GIORGINI, S., PITAEVSKII, L.P. AND STRINGARI, S.
≪Theory of ultracold atomic Fermi gases≫.
Reviews of Modern Physics, **80**, pp. 1215–1274 (2008).

GOTT, III, J.R., GUNN, J.E., SCHRAMM, D.N. AND TINSLEY, B.M.
≪An unbound universe≫.
ApJ, **194**, pp. 543–553 (1974).

GOULD, R.J.
≪Thermal bremsstrahlung from high-temperature plasmas≫.
ApJ, **238**, pp. 1026–1033 (1980).

GOULD, R.J.
≪Kinetic theory of relativistic plasmas≫.
Physics of Fluids, **24**, pp. 102–107 (1981).

GOULD, R.J.
≪Processes in relativistic plasmas≫.
ApJ, **254**, pp. 755–766 (1982).

GOULD, R.J.
≪The cross section for double Compton scattering≫.
ApJ, **285**, pp. 275–278 (1984).

GOULD, R.J. AND SCHRÉDER, G.P.
≪Opacity of the Universe to High-Energy Photons≫.
Physical Review, **155**, pp. 1408–1411 (1967).

GREISEN, K.
≪End to the Cosmic-Ray Spectrum?≫
Physical Review Letters, **16**, pp. 748–750 (1966).

GROOT, S., LEEUWEN, W. AND WEERT, C.
Relativistic kinetic theory: principles and applications (North-Holland Pub. Co., 1980).
ISBN 9780444854537.

GUILBERT, P.W. AND STEPNEY, S.
≪Pair production, Comptonization and dynamics in astrophysical plasmas≫.
MNRAS, **212**, pp. 523–544 (1985).

HAKIM, R.
Introduction to Relativistic Statistical Mechanics: Classical and Quantum (World Scientific Publishing Company, 2011).

HALL, G. AND WATT, J.M.
Modern Numerical Methods for Ordinary Differential Equations (New York, Oxford University Press, 1976).

HARKO, T.
≪Gravitational collapse of Bose-Einstein condensate dark matter halos≫.
Phys. Rev. D, **89(8)**, 084040 (2014).

HAUG, E.
≪Electron-positron bremsstrahlung in mildly relativistic thermal plasmas≫.
A&A, **148**, pp. 386–390 (1985).

HAUG, E. AND NAKEL, W.
The Elementary Process of Bremsstrahlung (World Scientific Publishing Co., Singapore, 2004).

HAUSER, M.G. AND DWEK, E.
≪The Cosmic Infrared Background: Measurements and Implications≫.
ARA&A, **39**, pp. 249–307 (2001).

HEISENBERG, W. AND EULER, H.
≪Folgerungen aus der diracschen theorie des positrons,≫.
Zeits. Phys., **98**, pp. 714–732 (1935).

HERRERA, L. AND SANTOS, N.O.
≪Local anisotropy in self-gravitating systems≫.
Phys. Rep., **286**, pp. 53–130 (1997).

HOGAN, P.
≪≫.
Proc. R. Irish Acad., **73**, p. 91 (1973).

HU, W., BARKANA, R. AND GRUZINOV, A.
≪Fuzzy Cold Dark Matter: The Wave Properties of Ultralight Particles≫.
Physical Review Letters, **85**, p. 1158 (2000).

INGROSSO, G., MERAFINA, M., RUFFINI, R. AND STRAFELLA, F.
≪System of self-gravitating semidegenerate fermions with a cutoff of energy and angular momentum in their distribution function≫.
A&A, **258**, pp. 223–233 (1992).

INOUE, Y., INOUE, S., KOBAYASHI, M.A.R., MAKIYA, R., NIINO, Y. AND TOTANI, T.
≪Extragalactic Background Light from Hierarchical Galaxy Formation: Gamma-Ray Attenuation up to the Epoch of Cosmic Reionization and the First Stars≫.
ApJ, **768**, 197 (2013).

IZZO, L., RUFFINI, R., PENACCHIONI, A.V., BIANCO, C.L., CAITO, L., CHAKRABARTI, S.K., RUEDA, J.A., NANDI, A. AND PATRICELLI, B.
≪A double component in GRB 090618: a proto-black hole and a genuinely long gamma-ray burst≫.
Astronomy and Astrophysics, **543**, p. A10 (2012).

JAUCH, J.M. AND ROHRLICH, F.
The theory of photons and electrons. The relativistic quantum field theory of charged particles with spin one-half (Springer, New York, 1976).

JEANS, J.H.
≪The Stability of a Spherical Nebula≫.
Royal Society of London Philosophical Transactions Series A, **199**, pp. 1–53 (1902).

JORGENSEN, I., FRANX, M. AND KJAERGAARD, P.
≪The Fundamental Plane for cluster E and S0 galaxies≫.
MNRAS, **280**, pp. 167–185 (1996).

JOST, R., LUTTINGER, J.M. AND SLOTNICK, M.
≪Distribution of Recoil Nucleus in Pair Production by Photons≫.
Physical Review, **80**, pp. 189–196 (1950).

JÜTTNER, F.
≪Das Maxwellsche Gesetz der Geschwindigkeitsverteilung in der Relativtheorie≫.
Annalen der Physik, **339**, pp. 856–882 (1911).

KAMPERT, K.H., KULBARTZ, J., MACCIONE, L., NIERSTENHOEFER, N., SCHIFFER, P., SIGL, G. AND VAN VLIET, A.R.
≪CRPropa 2.0 - A public framework for propagating high energy nuclei, secondary gamma rays and neutrinos≫.
Astroparticle Physics, **42**, pp. 41–51 (2013).

KHATRI, R. AND SUNYAEV, R.A.
≪Creation of the CMB spectrum: precise analytic solutions for the blackbody photosphere≫.
J. Cosmology Astropart. Phys., **6**, 038 (2012).

KHATRI, R., SUNYAEV, R.A. AND CHLUBA, J.
≪Does Bose-Einstein condensation of CMB photons cancel μ distortions created by dissipation of sound waves in the early Universe?≫
A&A, **540**, A124 (2012).

KLEIN, O.
≪On the Thermodynamical Equilibrium of Fluids in Gravitational Fields≫.
Reviews of Modern Physics, **21**, pp. 531–533 (1949a).

KLEIN, O.
≪On the Thermodynamical Equilibrium of Fluids in Gravitational Fields≫.
Reviews of Modern Physics, **21**, pp. 531–533 (1949b).

KLIMONTOVICH, I.L.
≪The kinetic theory of electromagnetic processes≫.
Springer Verlag Springer Series on Synergetics, **10** (1983).

KLIMONTOVICH, Y.L.
≪REVIEWS OF TOPICAL PROBLEMS: Physics of collisionless plasma≫.
Physics Uspekhi, **40**, pp. 21–51 (1997).

KLIMONTOVICH, Y.L.
≪Relativistic transport equations for a plasma i≫.
Sov. Phys. JETP, **37**, pp. 524–530 (1960a).

KLIMONTOVICH, Y.L.
≪Relativistic transport equations for a plasma ii≫.
Sov. Phys. JETP, **37**, pp. 876–882 (1960b).

KULL, A., TREUMANN, R.A. AND BOEHRINGER, H.
≪Violent Relaxation of Indistinguishable Objects and Neutrino Hot Dark Matter in Clusters of Galaxies≫.
ApJ, **466**, p. L1 (1996).

KUZ'MENKOV, L.S.

≪The Bogolyubov hierarchy of equations for relativistic systems. Radiation damping of waves in a plasma≫.
Soviet Physics Doklady, **23**, pp. 469–471 (1978).

LAING, E.W. AND DIVER, D.A.
≪Relativistic Landau damping of longitudinal waves in isotropic pair plasmas≫.
Physics of Plasmas, **13(9)**, p. 092115 (2006).

LANDAU, L.D.
≪On the vibration of the electronic plasma≫.
Journal of Physics (USSR), **10**, p. 25 (1946).

LANDAU, L.D. AND LIFSHITZ, E.M.
Fluid mechanics (Oxford: Pergamon Press, 1959).

LANDAU, L.D. AND LIFSHITZ, E.M.
Statistical physics. Pt.1, Pt.2 (Oxford: PergamonPress, 1980).

LANDAU, L.D. AND LIFSHITZ, E.M.
Physical Kinetics (Elsevier, 1981).

LANDAU, L.
≪Die kinetische gleichung fur den fall coulombscher wechselwirkung≫.
Phys. Z. Sowjetunion, **10**, pp. 154–164 (1936).

LANDAU, L.
≪The kinetic equation in the case of coulomb interaction≫.
ZhETF, **7**, pp. 203–209 (1937).

LATTANZI, M., RUFFINI, R. AND VERESHCHAGIN, G.
≪On the possible role of massive neutrinos in cosmological structure formation≫.
In M. Novello and S.E. Perez Bergliaffa (eds.), *Cosmology and Gravitation*, volume 668 of *American Institute of Physics Conference Series*, pp. 263–287 (2003).

LATTANZI, M., RUFFINI, R. AND VERESHCHAGIN, G.V.
≪Joint constraints on the lepton asymmetry of the Universe and neutrino mass from the Wilkinson Microwave Anisotropy Probe≫.
Phys. Rev. D, **72(6)**, pp. 063003–+ (2005).

LATTANZI, M., RUFFINI, R. AND VERESHCHAGIN, G.V.
≪Do WMAP data constraint the lepton asymmetry of the Universe to be zero?≫
In *Albert Einstein Century International Conference*, volume 861 of *American Institute of Physics Conference Series*, pp. 912–919 (2006).

LATTIMER, J.M. AND PRAKASH, M.
≪Neutron star observations: Prognosis for equation of state constraints≫.
Physics Reports, **442**, pp. 109–165 (2007).

LEE, B.W. AND WEINBERG, S.
≪Cosmological lower bound on heavy-neutrino masses≫.
Physical Review Letters, **39**, pp. 165–168 (1977).

LEVIN, Y., PAKTER, R., RIZZATO, F.B., TELES, T.N. AND BENETTI, F.P.C.
≪Nonequilibrium statistical mechanics of systems with long-range interactions≫.
Phys. Rep., **535**, pp. 1–60 (2014).

LIBOFF, R.L.
Kinetic theory : classical, quantum, and relativistic descriptions (New York : Springer, 2003).

LIFSHITZ, E.M. AND PITAEVSKII, L.P.
Physical kinetics (Oxford: Pergamon Press, 1981).

LIGHTMAN, A.P.
≪Double Compton emission in radiation dominated thermal plasmas≫.
ApJ, **244**, pp. 392–405 (1981).

LIGHTMAN, A.P.
≪Relativistic thermal plasmas - Pair processes and equilibria≫.
ApJ, **253**, pp. 842–858 (1982).

LIGHTMAN, A.P. AND BAND, D.L.
≪Relativistic thermal plasmas - Radiation mechanisms≫.
ApJ, **251**, pp. 713–726 (1981).

LUNARDINI, C., SABANCILAR, E. AND YANG, L.
≪Ultra high energy neutrinos: absorption, thermal effects and signatures≫.
Journal of Cosmology and Astroparticle Physicsjcap, **8**, 014 (2013).

LYNDEN-BELL, D.
≪Statistical mechanics of violent relaxation in stellar systems≫.
MNRAS, **136**, p. 101 (1967).

MANDELSTAM, S.
≪Determination of the Pion-Nucleon Scattering Amplitude from Dispersion Relations and Unitarity. General Theory≫.
Physical Review, **112**, pp. 1344–1360 (1958).

MANDL, F. AND SKYRME, T.H.R.
≪The Theory of the Double Compton Effect≫.
Royal Society of London Proceedings Series A, **215**, pp. 497–507 (1952).

MEDINA TANCO, G.A., DE GOUVEIA DAL PINO, E.M. AND HORVATH, J.E.
≪Deflection of Ultra–High-Energy Cosmic Rays by the Galactic Magnetic Field: From the Sources to the Detector≫.
ApJ, **492**, pp. 200–204 (1998).

MERAFINA, M. AND RUFFINI, R.
≪Systems of selfgravitating classical particles with a cutoff in their distribution function≫.
A&A, **221**, pp. 4–19 (1989).

MERRITT, D., GRAHAM, A.W., MOORE, B., DIEMAND, J. AND TERZIĆ, B.
≪Empirical Models for Dark Matter Halos. I. Nonparametric Construction of Density Profiles and Comparison with Parametric Models≫.
AJ, **132**, pp. 2685–2700 (2006).

MEYER, M., RAUE, M., MAZIN, D. AND HORNS, D.
≪Limits on the extragalactic background light in the Fermi era≫.
A&A, **542**, A59 (2012).

MIHALAS, D. AND MIHALAS, B.W.
Foundations of Radiation Hydrodynamics (New York, Oxford University Press, 1984).

MIKHAILOVSKII, A.B.
≪Plasma instability theory. Volume 1 - Instabilities in a homogeneous plasma /2nd revised and enlarged edition/≫.
Moscow Atomizdat (1975).

MISNER, C.W. AND SHARP, D.H.
≪Relativistic Equations for Adiabatic, Spherically Symmetric Gravitational Collapse≫.
Physical Review, **136**, pp. 571–576 (1964).

MOTZ, J.W., OLSEN, H.A. AND KOCH, H.W.
≪Pair Production by Photons≫.
Reviews of Modern Physics, **41**, pp. 581–639 (1969).

MOUHOT, C. AND VILLANI, C.
≪On Landau damping≫.
Acta Mathematica, **207**, pp. 29–201 (2011).
ISSN 0001-5962.

MUNSHI, F., GOVERNATO, F., BROOKS, A.M., CHRISTENSEN, C., SHEN, S., LOEBMAN, S., MOSTER, B., QUINN, T. AND WADSLEY, J.
≪Reproducing the Stellar Mass/Halo Mass Relation in Simulated ΛCDM Galaxies: Theory versus Observational Estimates≫.
ApJ, **766**, 56 (2013).

NAUMOV, N.D.
≪Kinetic theory of a relativistic plasma≫.
Soviet Physics Journal, **24**, pp. 270–274 (1981).

NAVARRO, J.F., FRENK, C.S. AND WHITE, S.D.M.
≪The Structure of Cold Dark Matter Halos≫.
ApJ, **462**, p. 563 (1996).

NAVARRO, J.F., FRENK, C.S. AND WHITE, S.D.M.
≪A Universal Density Profile from Hierarchical Clustering≫.
ApJ, **490**, pp. 493–508 (1997).

NAVARRO, J.F., HAYASHI, E., POWER, C., JENKINS, A.R., FRENK, C.S., WHITE, S.D.M., SPRINGEL, V., STADEL, J. AND QUINN, T.R.
≪The inner structure of ΛCDM haloes - III. Universality and asymptotic slopes≫.
MNRAS, **349**, pp. 1039–1051 (2004).

NIKISHOV, A.I.
≪Absorption of high-energy photons in the universe≫.
Zhurnal Eksperimental'noi i Teoreticheskoi Fiziki, **41**, pp. 549–550 (1961).

OCHELKOV, I.P., PRILUTSKII, O.F., ROZENTAL, I.L. AND USOV, V.V.
≪Relativistic kinetics and hydrodynamics≫.
Moscow Atomizdat (1979).

PADMANABHAN, T.
≪Statistical mechanics of gravitating systems≫.
Phys. Rep., **188**, pp. 285–362 (1990).

PADMANABHAN, T.
Structure Formation in the Universe (Structure Formation in the Universe, by T. Padmanabhan, pp. 499. ISBN 0521424860. Cambridge, UK: Cambridge University Press, June 1993., 1993).

PAGE, K.L., STARLING, R.L.C., FITZPATRICK, G., PANDEY, S.B., OSBORNE, J.P., SCHADY, P., MCBREEN, S., CAMPANA, S., UKWATTA, T.N., PAGANI, C. ET AL.
≪GRB 090618: detection of thermal X-ray emission from a bright gamma-ray burst≫.
Monthly Notices of the Royal Astronomical Society, **416(3)**, pp. 2078–2089 (2011).

PE'ER, A., MESZAROS, P. AND REES, M.J.
≪Radiation from an Expanding Cocoon as an Explanation of the Steep Decay Observed in GRB Early Afterglow Light Curves≫.
The Astrophysical Journal, **652(1)**, pp. 482–489 (2006).

PILLA, R.P. AND SHAHAM, J.
≪Kinetics of Electron-Positron Pair Plasmas Using an Adaptive Monte Carlo Method≫.
ApJ, **486**, pp. 903–+ (1997).

PIRAN, T.
≪The physics of gamma-ray bursts≫.
Reviews of Modern Physics, **76**, pp. 1143–1210 (2005).

PLANCK COLLABORATION, ADE, P.A.R., AGHANIM, N., ARMITAGE-CAPLAN, C., ARNAUD, M., ASHDOWN, M., ATRIO-BARANDELA, F., AUMONT, J., BACCIGALUPI, C., BANDAY, A.J. ET AL.
≪Planck 2013 results. XVI. Cosmological parameters≫.
A&A, **571**, A16 (2014).

POLYAKOV, P.A.
≪Bogolyubov (BBGKY) hierarchy in classical relativistic electrodynamics≫.
Theoretical and Mathematical Physics, **76**, pp. 939–944 (1988).

PROTHEROE, R.J. AND BIERMANN, P.L.
≪A new estimate of the extragalactic radio background and implications for ultra-high-energy γ-ray propagation≫.
Astroparticle Physics, **6**, pp. 45–54 (1996).

PROTHEROE, R.J. AND JOHNSON, P.A.
≪Propagation of ultra high energy protons and gamma rays over cosmological distances and implications for topological defect models≫.
Astroparticle Physics, **4**, pp. 253–269 (1996).

RINGWALD, A.
≪Super-GZK neutrinos≫.
Journal of Physics Conference Series, **39**, pp. 393–399 (2006).

RUFFINI, R.
≪On the de Vaucouleurs density-radius relation and the cellular intermediate large-scale structure of the universe≫.
In H.G. Corwin Jr. and L. Bottinelli (eds.), *World of Galaxies (Le Monde des Galaxies)*, pp. 461–472 (1989).

RUFFINI, R., AKSENOV, A.G., BERNARDINI, M.G., BIANCO, C.L., CAITO, L., CHARDONNET, P., DAINOTTI, M.G., DE BARROS, G., GUIDA, R., IZZO, L. ET AL.
≪The Blackholic energy and the canonical Gamma-Ray Burst IV: the "long," "genuine short" and "fake-disguised short" GRBs≫.
In M. Novello and S. Perez (eds.), *American Institute of Physics Conference Series*, volume 1132 of *American Institute of Physics Conference Series*, pp. 199–266 (2009).

RUFFINI, R., ARGÜELLES, C.R., FRAGA, B.M.O., GERALICO, A., QUEVEDO, H., RUEDA, J.A. AND SIUTSOU, I.
≪Black Holes in Gamma Ray Bursts and Galactic Nuclei≫.
International Journal of Modern Physics D, **22**, 1360008 (2013a).

RUFFINI, R., MUCCINO, M., BIANCO, C.L., ENDERLI, M., IZZO, L., KOVACEVIC, M., PENACCHIONI, A.V., PISANI, G.B., RUEDA, J.A. AND WANG, Y.

≪On binary-driven hypernovae and their nested late X-ray emission≫.
Astronomy and Astrophysics, **565**, p. L10 (2014a).

RUFFINI, R., SIUTSOU, I.A. AND VERESHCHAGIN, G.V.
≪A Theory of Photospheric Emission from Relativistic Outflows≫.
ApJ, **772**, 11 (2013b).

RUFFINI, R., SONG, D.J. AND STELLA, L.
≪On the statistical distribution off massive fermions and bosons in a Friedmann universe≫.
A&A, **125**, pp. 265–270 (1983).

RUFFINI, R., SONG, D.J. AND TARAGLIO, S.
≪The 'ino' mass and the cellular large-scale structure of the universe≫.
A&A, **190**, pp. 1–9 (1988).

RUFFINI, R. AND STELLA, L.
≪On semi-degenerate equilibrium configurations of a collisionless self-gravitating Fermi gas≫.
A&A, **119**, pp. 35–41 (1983).

RUFFINI, R., VERESHCHAGIN, G. AND XUE, S.S.
≪Electron-positron pairs in physics and astrophysics: From heavy nuclei to black holes≫.
Phys. Rep., **487**, pp. 1–140 (2010a).

RUFFINI, R., VERESHCHAGIN, G.V. AND XUE, S.S.
≪Cosmic absorption of ultra high energy particles≫.
ArXiv e-prints (2015).

RUFFINI, R., VERESHCHAGIN, G. AND XUE, S.S.
≪Electron-positron pairs in physics and astrophysics≫.
Physics Reports, **487**, pp. 1–140 (2010b).

RUFFINI, R., WANG, Y., KOVACEVIC, M., BIANCO, C.L., ENDERLI, M., MUCCINO, M., PENACCHIONI, A.V., PISANI, G.B. AND RUEDA, J.A.
≪GRB 130427A and SN 2013cq: A Multi-wavelength Analysis of An Induced Gravitational Collapse Event≫.
Accepted for publication in ApJ, p. 5723 (2014b).

RYBICKI, G.B. AND LIGHTMAN, A.P.
Radiative processes in astrophysics (New York, Wiley-Interscience, 1979).

SADIQ, S., MAHMOOD, S., HAQUE, Q. AND ZULFIQAR ALI, M.
≪Ion Acoustic Solitons in Dense Magnetized Plasmas with Nonrelativistic and Ultrarelativistic Degenerate Electrons and Positrons≫.
ApJ, **793**, 27 (2014).

SCHWARZ, G.E.
≪Estimating the Dimension of a Model≫.
Annals of Statistics, **6**, pp. 461–464 (1978).

SHAPIRO, S.L. AND TEUKOLSKY, S.A.
Black holes, white dwarfs, and neutron stars: The physics of compact objects (Research supported by the National Science Foundation. New York, Wiley-Interscience, 1983, 663 p., 1983).

SHU, F.H.
≪On the statistical mechanics of violent relaxation≫.
ApJ, **225**, pp. 83–94 (1978).

SIGOV, Y.S.
Computing Experiment: a Bridge between the Past and Future of Plasma Physics. Selected Works (Moscow: Fizmatlit, 2001).

SILIN, V.P.
Introduction in kinetic theory of gases (Lebedev institute press, 1998).
(in Russian).

SILVA, L.O.
≪Physical Problems (Microphysics) in Relativistic Plasma Flows≫.
In P.A. Hughes and J.N. Bregman (eds.), *Relativistic Jets: The Common Physics of AGN, Microquasars, and Gamma-Ray Bursts*, volume 856 of *American Institute of Physics Conference Series*, pp. 109–128 (2006).

SIN, S.J.
≪Late-time phase transition and the galactic halo as a Bose liquid≫.
Phys. Rev. D, **50**, pp. 3650–3654 (1994).

SINHA, A., SAHAYANATHAN, S., MISRA, R., GODAMBE, S. AND ACHARYA, B.S.

≪Estimation of the Extragalactic Background Light Using TeV Observations of BL Lac Objects≫.
ApJ, **795**, 91 (2014).

SIUTSOU, I., ARGÜELLES, C.R. AND RUFFINI, R.
≪Dark matter massive fermions and Einasto profiles in galactic haloes≫.
Astronomy Reports, **59**, pp. 656–666 (2015).

SMOLYANSKY, S.A.
≪Comments on the principle of attenuation of correlation≫.
Acta Physica Academiae Scientiarum Hungaricae, **25**, pp. 147–151 (1968).

SOFUE, Y., HONMA, M. AND OMODAKA, T.
≪Unified Rotation Curve of the Galaxy – Decomposition into de Vaucouleurs Bulge, Disk, Dark Halo, and the 9-kpc Rotation Dip –≫.
PASJ, **61**, pp. 227– (2009).

SPARRE, M. AND STARLING, R.L.C.
≪A search for thermal X-ray signatures in gamma-ray bursts - II. The Swift sample≫.
Monthly Notices of the Royal Astronomical Society, **427(4)**, pp. 2965–2974 (2012).

SPITKOVSKY, A.
≪On the Structure of Relativistic Collisionless Shocks in Electron-Ion Plasmas≫.
ApJ, **673**, pp. L39–L42 (2008a).

SPITKOVSKY, A.
≪Particle Acceleration in Relativistic Collisionless Shocks: Fermi Process at Last?≫
ApJ, **682**, pp. L5–L8 (2008b).

SPIVEY, S.C., MUSIELAK, Z.E. AND FRY, J.L.
≪Astronomical constraints on quantum theories of cold dark matter - I. Einasto density profile for galactic haloes≫.
MNRAS, **428**, pp. 712–717 (2013).

STANEV, T.
≪Ultra High Energy Cosmic Rays≫.

In Z. Parsa (ed.), *Intersections of Particle and Nuclear Physics*, volume 698 of *American Institute of Physics Conference Series*, pp. 357–361 (2004).

STANEV, T., ENGEL, R., MÜCKE, A., PROTHEROE, R.J. AND RACHEN, J.P.
≪Propagation of ultrahigh energy protons in the nearby universe≫.
Phys. Rev. D, **62(9)**, 093005 (2000).

STARLING, R.L.C., PAGE, K.L., PE'ER, A., BEARDMORE, A.P. AND OSBORNE, J.P.
≪A search for thermal X-ray signatures in gamma-ray bursts - I. Swift bursts with optical supernovae≫.
Monthly Notices of the Royal Astronomical Society, **427(4)**, pp. 2950–2964 (2012).

STEPNEY, S.
≪Two-body relaxation in relativistic thermal plasmas≫.
MNRAS, **202**, pp. 467–481 (1983).

STEPNEY, S. AND GUILBERT, P.W.
≪Numerical FITS to important rates in high temperature astrophysical plasmas≫.
MNRAS, **204**, pp. 1269–1277 (1983).

SUSHCHOV, O.B., KOBZAR, O.O., HNATYK, B.I. AND MARCHENKO, V.V.
≪Search of ultra high energy cosmic rays' sources. FRI-radiogalaxy Centaurus A≫.
Kinematics and Physics of Celestial Bodies, **28**, pp. 270–279 (2012).

SVENSSON, R.
≪Electron-Positron Pair Equilibria in Relativistic Plasmas≫.
ApJ, **258**, pp. 335–+ (1982a).

SVENSSON, R.
≪The pair annihilation process in relativistic plasmas≫.
ApJ, **258**, pp. 321–334 (1982b).

SVENSSON, R.
≪Steady mildly relativistic thermal plasmas - Processes and properties≫.
MNRAS, **209**, pp. 175–208 (1984).

SVENSSON, R. AND ZDZIARSKI, A.
≪Photon-photon scattering of gamma rays at cosmological distances≫.
ApJ, **349**, pp. 415–428 (1990).

SYNGE, J.L.
The Relativistic Gas (North-Holland, 1957).

THORNE, K.S.
≪Relativistic radiative transfer - Moment formalisms≫.
MNRAS, **194**, pp. 439–473 (1981).

TOLMAN, R.C.
≪On the Weight of Heat and Thermal Equilibrium in General Relativity≫.
Physical Review, **35**, pp. 904–924 (1930).

TORRES, D.F. AND ANCHORDOQUI, L.A.
≪Astrophysical origins of ultrahigh energy cosmic rays≫.
Reports on Progress in Physics, **67**, pp. 1663–1730 (2004).

TREMAINE, S. AND GUNN, J.E.
≪Dynamical role of light neutral leptons in cosmology≫.
Physical Review Letters, **42**, pp. 407–410 (1979).

UEHLING, E.A.
≪Transport Phenomena in Einstein-Bose and Fermi-Dirac Gases. II≫.
Physical Review, **46**, pp. 917–929 (1934).

UEHLING, E.A. AND UHLENBECK, G.E.
≪Transport Phenomena in Einstein-Bose and Fermi-Dirac Gases. I≫.
Physical Review, **43**, pp. 552–561 (1933).

USOV, V.V.
≪Bare Quark Matter Surfaces of Strange Stars and e^+e^- Emission≫.
Phys. Rev. Lett., **80**, pp. 230–233 (1998).

VASSILIEV, V.V.
≪Extragalactic background light absorption signal in the TeV gamma-ray spectra of blazars.≫
Astroparticle Physics, **12**, pp. 217–238 (2000).

VENTERS, T.M., PAVLIDOU, V. AND REYES, L.C.
≪The Extragalactic Background Light Absorption Feature in the Blazar Component of the Extragalactic Gamma-ray Background≫.
ApJ, **703**, pp. 1939–1946 (2009).

VERESHCHAGIN, G.V.
≪Physics of Nondissipative Ultrarelativistic Photospheres≫.
International Journal of Modern Physics D, **23**, 1430003 (2014).

VIOLLIER, R.D., TRAUTMANN, D. AND TUPPER, G.B.
≪Supermassive neutrino stars and galactic nuclei≫.
Physics Letters B, **306**, pp. 79–85 (1993).

VLASOV, A.
≪On vibration properties of electron gas≫.
Journal of Experimental and Theoretical Physics, **8 (3)**, p. 291 (1938).
(in Russian).

WALKER, M.G., MATEO, M., OLSZEWSKI, E.W., PEÑARRUBIA, J., WYN EVANS, N. AND GILMORE, G.
≪A Universal Mass Profile for Dwarf Spheroidal Galaxies?≫
ApJ, **704**, pp. 1274–1287 (2009).

WALKER, M.G., MCGAUGH, S.S., MATEO, M., OLSZEWSKI, E.W. AND KUZIO DE NARAY, R.
≪Comparing the Dark Matter Halos of Spiral, Low Surface Brightness, and Dwarf Spheroidal Galaxies≫.
ApJ, **717**, pp. L87–L91 (2010).

WALTER, F., BRINKS, E., DE BLOK, W.J.G., BIGIEL, F., KENNICUTT, JR., R.C., THORNLEY, M.D. AND LEROY, A.
≪THINGS: The H I Nearby Galaxy Survey≫.
AJ, **136**, 2563 (2008).

WARDLE, J.F.C., HOMAN, D.C., OJHA, R. AND ROBERTS, D.H.
≪Electron-positron jets associated with the quasar 3C279≫.
Nature, **395**, pp. 457–461 (1998).

WEAVER, T.A.
≪Reaction rates in a relativistic plasma≫.
Phys. Rev. A, **13**, pp. 1563–1569 (1976).

WEIBEL, E.S.
≪Spontaneously Growing Transverse Waves in a Plasma Due to an Anisotropic Velocity Distribution≫.
Physical Review Letters, **2**, pp. 83–84 (1959).

WEILER, T.
≪Resonant Absorption of Cosmic-Ray Neutrinos by the Relic-Neutrino Background≫.
Physical Review Letters, **49**, pp. 234–237 (1982).

WEINBERG, S.
Gravitation and Cosmology: Principles and Applications of the General Theory of Relativity (Wiley-VCH, 1972).
ISBN 0-471-92567-5.

WEINBERG, S.
Cosmology (Oxford University Press, April 2008., 2008).

WHITE, S.D.M., FRENK, C.S. AND DAVIS, M.
≪Clustering in a neutrino-dominated universe≫.
ApJ, **274**, pp. L1–L5 (1983).

ZAKHAROV, A.
Macroscopic gravitation (Yanus-K, Moscow, 2000).
(in Russian).

ZAPOLSKY, H.S.
≪Can the Redshifts of Quasi-Stellar Objects BE Gravitational?≫
ApJ, **153**, p. L163 (1968).

ZATSEPIN, G.T. AND KUZ'MIN, V.A.
≪Upper Limit of the Spectrum of Cosmic Rays≫.
Soviet Journal of Experimental and Theoretical Physics Letters, **4**, p. 78 (1966).

ZDZIARSKI, A.A.
≪Spectra from pair-equilibrium plasmas≫.
ApJ, **283**, pp. 842–847 (1984).

ZDZIARSKI, A.A. AND SVENSSON, R.
≪Absorption of X-rays and gamma rays at cosmological distances≫.
ApJ, **344**, pp. 551–566 (1989).